North Sea salt marshes and their response to changing storm-climate conditions over the last century

DOROTHEA BUNZEL | Hamburg 2021

DISSERTATION

zur Erlangung des Doktorgrades der Naturwissenschaften
an der Fakultät für Mathematik, Informatik und Naturwissenschaften
Fachbereich Erdsystemwissenschaften der Universität Hamburg

North Sea salt marshes and their response to changing storm-climate conditions over the last century

Dissertation

zur Erlangung des Doktorgrades der Naturwissenschaften

an der Fakultät für Mathematik, Informatik und Naturwissenschaften

Fachbereich Erdsystemwissenschaften

der Universität Hamburg

vorgelegt von **Dorothea Bunzel**

aus Pinneberg, Deutschland

Hamburg, 2021

Als Dissertation angenommen am Fachbereich Erdsystemwissenschaften

Tag des Vollzugs der Promotion:	28.04.2021
Gutachter/Gutachterinnen:	Prof. Dr. Gerhard Schmiedl
	Prof. Dr. Christian Betzler
Vorsitzender des Fachpromotionsausschusses Erdsystemwissenschaften:	Prof. Dr. Dirk Gajewski
Dekan der Fakultät MIN:	Prof. Dr. Heinrich Graener

ABSTRACT

Twentieth-century acceleration in global and regional sea-level rise (SLR) poses an increasing risk for modern intertidal wetlands. While natural salt marshes are basically able to adapt to gradually changing sea levels with vertical and lateral growth at rates similar or higher to that of SLR, it remains uncertain to what extent human-modified marshes can withstand rising sea levels, especially if SLR rates continue to accelerate in the future. Likewise, the regional storm-surge climate is expected to be critical for low-lying coasts under future SLR, illustrating the wide range of potential flood-hazard scenarios for coastal wetlands. Sedimentary salt-marsh archives from the south-eastern North Sea coast are ideally suited to better understand how coastal ecosystems have responded to changing storm-climate conditions in the past, as they have been subjected to different degrees by human activities over the last century but experienced the same influences from natural climate effects that should have left similar regional to super-regional imprints in the depositional systems. The four salt-marsh archives studied in this respect are located in North Frisia (Bay of Tümlau and Eider estuary) and Dithmarschen (Friedrichskoog and Kaiser-Wilhelm-Koog).

For the evaluation of climate-related and non-climatic influences on the different depositional systems in the past, accurate age information is of critical importance but is challenging due to frequent sediment reworking by storm surges along the North Sea coast. To overcome this problem, chronostratigraphic control was obtained by combining different dating techniques, including radionuclides (^{210}Pb, ^{137}Cs, ^{241}Am, and ^{14}C) with trends of the industrial mercury (Hg) pollution history and XRF-based sedimentological inter-correlation for all four study sites. However, to better compare the regional contrasts with regard to the influences of human interventions, the focus was then on evaluating the sediment sequences from the un-grazed and more naturally developed salt marsh in the Bay of Tümlau and the grazed and frequently drained salt marsh in Friedrichskoog. Subsequently, the identification of lateral introduced reworked sediments within both stratified sediment sequences and evaluation of the corresponding storm-climate signals were built on different sedimentological and geochemical proxy records. These proxies provide information not only about the marine sedimentary organic matter supply itself (ln[Br/Cl] ratio) but also about the relative proportions of the marine versus terrestrial organic matter input (Br/C_{org} ratio) and the relative grain-size distribution (ln[Zr/Rb] ratio).

Rapid drops in the ln(Br/Cl) data in association with coarser sand layers imply seasonal changes in the supply and deposition of organic matter onto the marsh surfaces at both study sites so that on a local scale, sediment deposited by storm surges in winter can be differentiated from sediment deposition during generally calm weather in spring to autumn. Furthermore, both the Br/C_{org} and ln(Zr/Rb) proxy records revealed an increasing trend for both considered study sites from the mid-20th century to 1990 CE. This trend resembles the intensified North Sea storm-climate activity, taking place in the second half of the 20th century, and thus reflects

an increase in the marine influence and associated flooding frequency causing the progressing retreat of the seaward salt-marsh erosional cliffs. The environmental stress, presumably arising because of more frequent storm surges and associated flooding of the salt marshes, was evaluated considering abnormally grown tests of the agglutinated benthic foraminiferal salt-marsh indicator species *Entzia macrescens* that likewise showed highest numbers of test deformities at times of strengthening flooding. However, highest numbers occurred at the study site strongly altered by human interventions (Friedrichskoog), while comparatively less deformed tests were found at the more natural site (Bay of Tümlau), implying a higher susceptibility of the intensely human-modified salt marshes to changes in regional sea level and storm surge-induced sedimentation.

Beyond that, both the ln(Zr/Rb) and ln(Br/Cl) ratios revealed periodicities on inter-decadal timescales (10–22 years), indicating a close linkage between sediment deposition and large-scale climate oscillations. However, the inter-decadal variability of the ln(Br/Cl) ratio was lacking at Friedrichskoog, suggesting that the more intense local human interventions at this site are masking the natural climate variability. The results obtained suggest that disturbances by various human activities seem to play a critical role in local sedimentation processes as well as in the susceptibility of salt marshes to environmental stress under rising sea level and storm-climate conditions.

ZUSAMMENFASSUNG

Die im 20. Jahrhundert einsetzende Beschleunigung des globalen und regionalen Meeresspiegelanstiegs (*sea-level rise*, SLR) stellt ein zunehmendes Risiko für die Salzwiesen im Gezeitenbereich dar. Natürliche Salzwiesen sind grundsätzlich dazu in der Lage sich bis zu einem gewissen Grad an einen SLR anzupassen. Grund hierfür ist das vertikale Aufwachsen und die laterale Ausbreitung der Salzweisen mit ähnlichen oder höheren Raten als denen des aktuellen SLR. Es bleibt jedoch unklar, inwieweit anthropogen modifizierte Salzwiesen dem steigenden Meeresspiegel standhalten können. Diese Frage stellt sich insbesondere durch die Annahme, dass sich der SLR in Zukunft weiter beschleunigen wird. Hinzu kommt, dass das regionale Sturmflutniveau unter zukünftigen SLR-Bedingungen als kritisch einzuschätzen ist, was die große Bandbreite an möglichen Überflutungsgefährdungsszenarien für die niedrig gelegenen Küsten und deren Salzwiesen verdeutlicht. Um ein besseres Verständnis dafür zu erlangen, wie Salzwiesenökosysteme in der Vergangenheit auf sich ändernde Sturmflutbedingungen reagiert haben, eignen sich die sedimentären Archive der südöstlichen Nordseeküste in besonderer Weise. Diese waren im 20. Jahrhundert sowohl unterschiedlichen, vom Menschen verursachten Bewirtschaftungsmaßnahmen, als auch den Einflüssen natürlicher Klimaeffekte ausgesetzt, wobei letztere ähnliche Ablagerungsspuren in den Sedimentsequenzen hinterlassen haben sollten. Die in diesem Zusammenhang untersuchten Salzwiesenarchive erstrecken sich über Nordfriesland (Tümlauer Bucht und Grüne Insel Eiderwatt) und Dithmarschen (Friedrichskoog und Kaiser-Wilhelm-Koog).

Für die Beurteilung klimatischer und nichtklimatischer Einflüsse auf die verschiedenen Ablagerungssysteme sind genaue Altersangaben von entscheidender Bedeutung. Dies stellt sich im Bereich der Nordseeküste aufgrund der durch Sturmfluten häufig aufgearbeiteten Sedimente als besondere Herausforderung dar. Daher wurden die Aktivitäten von Radionukliden (^{210}Pb, ^{137}Cs, ^{241}Am und ^{14}C) mit Veränderungen in der industriellen Quecksilberbelastung (Hg) kombiniert und mittels XRF-basierter sedimentologischer Interkorrelation eine regionale Chronostratigraphie für alle vier Untersuchungsstandorte entwickelt. Um die größtmöglichen regionalen Kontraste hinsichtlich menschlicher Eingriffe vergleichen zu können, lag der Fokus der anschließenden Auswertungen primär auf den Salzwiesen in der Tümlauer Bucht (unbeweidet, vergleichsweise natürlich entwickelt) und von Friedrichskoog (beweidet, häufig entwässert). Die Identifikation von lateral eingeschalteten, aufgearbeiteten Sedimentschichten innerhalb der Sequenzen der Tümlauer Bucht und von Friedrichskoog sowie die Evaluierung der Sturmflutsignale erfolgte mithilfe sedimentologischer und geochemischer Proxydatensätze. Dazu gehören die mittlere Korngröße sowie die ln(Br/Cl)-, Br/C_{org}- und ln(Zr/Rb)-Verhältnisse, da diese Proxys Informationen über den sedimentären organischen Materialeintrag selbst, aber auch über die relativen Anteile des marinen

gegenüber des terrestrischen organischen Materialeintrags sowie die relative Korngrößenverteilung liefern.

Rapide Rückgänge in den ln(Br/Cl)-Verhältnissen, die zeitgleich mit gröberen Sandschichten auftreten, deuten auf saisonale Veränderungen in der Zufuhr und Ablagerung von organischem Material auf den Salzwiesenoberflächen hin. Somit kann auf lokaler Ebene zwischen Sedimenten, die durch Sturmfluten im Winter abgelagert wurden und Ablagerungen bei allgemein ruhigem Wetter im Frühjahr bis Herbst unterschieden werden. Darüber hinaus zeigen die Br/C_{org}- und ln(Zr/Rb)-Verhältnisse an beiden Untersuchungsstandorten einen ansteigenden Trend ab etwa 1950 bis 1990. Die Trends beider Datensätze reflektieren die erhöhte Aktivität des Nordsee-Sturmklimas in der zweiten Hälfte des 20. Jahrhunderts und spiegeln somit die Zunahme des marinen Einflusses und der damit einhergehenden Überflutungshäufigkeit wider, was u. a. den fortschreitenden Rückzug der seewärtigen Erosionskanten verursacht. Der Umweltstress, der vermutlich durch das häufigere Auftreten von Sturmfluten und Überflutungen der Salzwiesen entsteht, wurde anhand abnormal gewachsener Gehäuse der agglutinierten benthischen Foraminiferen-Salzwiesen-Indikatorart *Entzia macrescens* bewertet. Es konnte beobachtet werden, dass *E. macrescens* zu Zeiten häufigerer Überflutungen in einer größeren Anzahl mit Gehäusedeformationen auftritt. Die höchsten Zahlen gab es jedoch an dem durch menschliche Eingriffe stark veränderten Untersuchungsstandort (Friedrichskoog), während an dem natürlicheren Standort (Tümlauer Bucht) vergleichsweise weniger deformierte Gehäuse gefunden wurden. Dies deutet auf eine höhere Empfindlichkeit der intensiv vom Menschen veränderten Salzwiesen gegenüber Änderungen des regionalen Meeresspiegels und damit einhergehend sturmflutbedingter Sedimentation hin.

Darüber hinaus zeigten sowohl das ln(Zr/Rb)- als auch das ln(Br/Cl)-Verhältnis eine Periodizität von 10 bis 22 Jahren auf, was auf einen engen Zusammenhang zwischen der Sedimentablagerung und großräumigen Klimaschwankungen hinweist. Die interdekadische Variabilität der ln(Br/Cl)-Verhältnisse konnte jedoch nicht in Friedrichskoog beobachtet werden. Dies legt die Vermutung nahe, dass die dortigen intensiveren menschlichen Eingriffe (bspw. die Beweidung und die häufigere Instandhaltung der Entwässerungsgräben) potenzielle Signale der natürlichen großskaligen Klimavariabilität überlagern. Insgesamt zeigen die Untersuchungen, dass Störungen der Salzwiesen durch verschiedene menschliche Aktivitäten zu Zeiten des ansteigenden Meeresspiegels und häufiger auftretenden Sturmfluten offenbar eine kritische Rolle bei den lokalen Sedimentationsprozessen spielen. Folglich scheinen anthropogen modifizierte Salzwiesen anfälliger auf Umweltstress zu reagieren, welcher seit der zweiten Hälfte des 20. Jahrhunderts von den zunehmenden Klimaveränderungen und deren Folgen ausgeht.

THESIS PUBLICATIONS

This cumulative doctoral thesis builds on the content of three research articles that either are currently under review or published in different international journals with scientific quality assurance:

Bunzel, D., Milker, Y., Müller-Navarra, K., Arz, H.W., Friedrich, J., Lahajnar, N., Schmiedl, G., 2020. Integrated stratigraphy of foreland salt-marsh sediments of the south-eastern North Sea region. *Newsletters on Stratigraphy* **53**, 415–442, DOI: 10.1127/nos/2020/0540.

Bunzel, D., Milker, Y., Müller-Navarra, K., Arz, H.W., Schmiedl, G., 2021. North Sea salt-marsh archives trace past storminess and climate variability. *Global and Planetary Change* **198**, 103403, DOI: 10.1016/j.gloplacha.2020.103403.

Bunzel, D., Milker, Y., Francescangeli, F., Schmiedl, G., 2020. The response of human-modified coastal wetlands from the southeastern North Sea to amplified storm-climate conditions: indications by deformed marsh foraminifera. *Ecological Indicator*, under review.

Although each article has several authors, the first author, D. Bunzel, elaborated upon the main part of each article, including preceding fieldwork organization and implementation, data evaluation, article conceptualization and visualization, and article writing. Specific information about the respective contributions by the individual co-authors can be found in the corresponding Chapters 2–4. In order to ensure consistency and a uniform design within the present doctoral thesis, minor changes have been made to the respective articles, which may result in differences between the articles presented herein and their original formats prescribed by their respective journals. These changes are primarily related to layout but are also related to some terminologies and spellings. For instance, active voices have been changed into passive voices, *southeastern* has been consistently changed to *south-eastern*, ages in *AD* have been changed to ages in *CE*, and *storm surges* have been changed to *storm tides* (and vice versa) but only if exclusively discussing the observed water levels of the Cuxhaven tide gauge that were not corrected with respect to the full tidal cycles. The references to supplementary material, as well as the serial numbering of all Chapters and Sections, Figures and Tables, have been made consistent. However, no changes or modifications made after article submission or publication have changed the scientific content or interpretation of the data.

CONTENT

ACRONYMS

AD	Anno Domini
AMO	Atlantic Multidecadal Oscillation
AMS	Accelerator Mass Spectrometry
BC	Before Christ
BCR	Community Bureau of Reference
BP	Before Present (i.e., before 1950)
CBF	Calcareous Benthic Foraminifera
CE	Common Era
CIC	Constant Initial Concentration of unsupported ^{210}Pb
CRM	Certified Reference Material
CRS	Constant Rate of unsupported ^{210}Pb Supply
DHHN	Deutsches Haupthöhennetz
DMA	Direct Mercury Analyzer
DSPEC	Digital Signal Processing Gamma Ray Spectrometer
ESL	Extreme Sea Level
FK	Friedrichskoog
GIE	Grüne Insel Eiderwatt (Eider estuary)
GMSL	Global Mean Sea Level
HAT	Highest Astronomical Tide
HPGe	High-Purity Germanium detector
IPCC	Intergovernmental Panel on Climate Change
KWK	Kaiser-Wilhelm-Koog
LGM	Last Glacial Maximum
LIA	Little Ice Age
MAR	Mass Accumulation Rate
MBSS	Mecklenburg Bay Sediment Standard
MHW	Mean High Water
MHWS	Mean High Water Spring
MLW	Mean Low Water
MLWS	Mean Low Water Spring
MOC	Marine Organic Carbon
MSL	Mean Sea Level
MR	Managed Realignment
NAO	North Atlantic Oscillation
NHN	Normalhöhennull
NHZ1	Northern Hemisphere Zone 1
PAST	PAleontological STatistics
pMC	Percent Modern Carbon
RCC	Rapid Climate Changes
RMSL	Regional Mean Sea Level
SH	Süderheverkoog
SLR	Sea Level Rise
SPP	Special Priority Program
SR	Sedimentation Rate

SST	Sea Surface Temperature
TB	Tümlauer Bucht (Bay of Tümlau)
WoRMS	World Register of Marine Species
WSP	Wadden Sea Plan
XRF	X-Ray Fluorescence

Institutions and Authorities

BAW	Bundesanstalt für Wasserbau (Federal Waterways Engineering and Research Institute)
BSH	Bundesamts für Seeschifffahrt und Hydrographie (Federal Maritime and Hydrographic Agency of Germany)
CEN	Centrum für Erdsystemforschung und Nachhaltigkeit (Center for Earth System Research and Sustainability)
CWSS	Wattenmeersekretariat (Common Wadden Sea Secretariat)
DFG	Deutsche Forschungsgemeinschaft (German Research Foundation)
DWD	Deutscher Wetterdienst (German Meteorological Service)
ECA	Economics of Climate Adaptation
GRDC	Global Runoff Data Centre
HPA	Hamburger Hafenbehörde (Hamburg Port Authority)
HZG	Helmholtz-Zentrum Geesthacht (Helmholtz Center Geesthacht)
IOW	Leibniz-Institut für Ostseeforschung in Warnemünde (Leibniz Institute for Baltic Sea Research Warnemünde)
LARI	Labor für Radioisotope (Laboratory for Radioisotopes)
LKN.SH	Landesbetrieb für Küstenschutz, Nationalpark und Meeresschutz Schleswig-Holstein (Schleswig-Holstein Agency for Coastal Defence, National Park and Marine Conservation)
LVermGeo SH	Landesamt für Vermessung und Geoinformationen Schleswig-Holstein (State Office for Surveying and Geoinformation Schleswig-Holstein)
MELUND	Ministerium für Energiewende, Landwirtschaft, Umwelt, Natur und Digitalisierung des Landes Schleswig-Holstein (Ministry of Energy, Agriculture, the Environment, Nature and Digitalization)
MPI-M	Max-Planck-Institut für Meteorologie (Max-Planck-Institute for Meteorology)
NABU	Naturschutzbund Deutschland (Nature and Biodiversity Conservation Union)
NOAA	National Oceanic and Atmospheric Administration
SfEP	Science for Environment Policy
SICSS	School of Integrated Climate System Sciences
UNEP	United Nations Environment Programme
WSV	Wasserstraßen- und Schifffahrtsverwaltung des Bundes (Federal Waterway and Shipping Administration)

PREFACE

This doctoral thesis is part of the interdisciplinary research project called SEASTORM, which has been conducted under the umbrella of the Special Priority Program (SPP-1889), Regional Sea Level Change and Society (SeaLevel), funded by the German Research Foundation (DFG) and entitled as *"Unravelling the signals of sea level and storminess of the past millennium, southern North Sea"*. Among others, the SEASTORM project raises the hypothesis that well-stratified sedimentary salt-marsh sequences from the German North Sea coast have archived 20th-century changes in storm-surge climate and regional sea level.

To test this hypothesis, this doctoral thesis follows an integrated approach by using various detailed sedimentological, geochemical, and micropaleontological data. In doing so, this thesis represents a conceptual approach to comprehending regional storm-climate changes for the south-eastern North Sea coastal area and their impacts on intertidal systems. Based on the results, this thesis illustrates the complexity of regional storm-climate histories and their linkage to underlying super-regional climate variability affecting the coastal wetlands on different spatial and temporal scales. The comparison between anthropogenically influenced sites and more naturally developed salt marshes is further intended to contribute to a better understanding of the extent to which the respective salt-marsh systems are more resilient or vulnerable to changing climatic conditions.

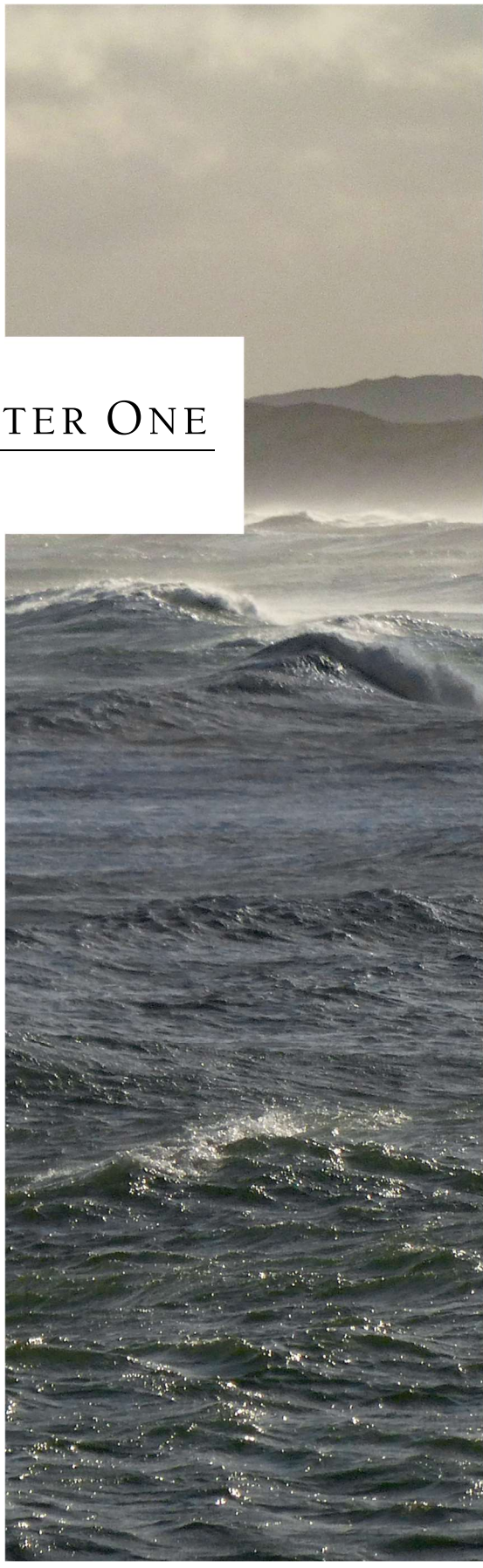

Chapter One

The critical role of intertidal wetlands: a unifying essay

> *Deus mare, Friso litora fecit –*
> *God created the sea, the Frisian the coast.*
> *[Frisian proverb]*

1.1 Introduction: climate archive salt marsh

The functioning of low-lying coastal areas is increasingly attracting attention, as global warming is expected to accelerate sea-level rise (SLR), to increase storm-surge activity, and to amplify tidal ranges by 2100 CE, posing a serious threat to coastal environments (IPCC, 2019). In north-west Europe, one of the world's largest coherent intertidal ecosystems characterizes the low-lying coasts: the Wadden Sea – comprising the tidal flats and, inseparable from them, the adjacent salt marshes but also dunes and the seawater itself, giving a total area of approximately 8000 km^2 (Wolff et al., 1994; Allen, 1997; Behrends et al., 2004; CWSS, 2010; Kabat et al., 2012). There, limited to a narrow belt, salt marshes fringe the coastline between Esbjerg (Denmark) and Den Helder (the Netherlands), thus occupying a total area of approximately 400 km^2 along the south-eastern part of the North Sea coast (Fig. 1; Dijkema, 1987; Allen, 1997; Bartholdy et al., 2004; Wolff, 2013). If, however, these low-lying coastal salt marshes do not compensate for the future rise in global or regional sea levels, they will be most vulnerable to the consequences of global warming, as SLR will initiate a large coastal retreat and continuous flooding of the previously intertidal system (Andersen et al., 2011). In this context, a sufficient sediment supply and a capable salt-marsh vegetation structure seem to be the most promising factors to enable coastal systems to adapt to SLR and increased flooding frequency and duration (Bakker et al., 1993; Allen, 2000).

Salt marshes constitute the upper part of the intertidal zone, as they are situated above the mean high water (MHW) level, but on their seaward side, they merge into the tidal flats with gradual decreasing surface elevation (Fig. 2; Allen, 1997, and references therein). As a result, salt marshes generally occur at sites where they lie within a semidiurnal tidal range of 2–4 m (mesotidal) or > 4 m (macrotidal), as found along the south-eastern North Sea coast (Allen, 1997, 2000). Accordingly, salt marshes are directly affected and strongly controlled by mean sea level (MSL), tides, storm surges, and accompanied regular flooding (Fig. 3; Wolff et al., 1994; Allen, 1997, 2000). In particular, the semidiurnal oscillating tidal currents and regular occurring storm surges during winter are responsible for the local erosion, relocation and re-deposition of sediment in the intertidal zone. This entails both the loss of marsh areas and the sufficient sediment supply, the latter being required for vertical salt-marsh growth (Allen, 1990; Temmerman et al., 2003; Schuerch et al., 2013, 2019; Müller-Navarra et al., 2019). Over time, the water masses of the regular discharging tides or storm surges cut into the salt-marsh surface morphology, creating meandering creek networks (Allen, 1997; Chirol et al., 2015). This natural tidal drainage, together with the resulting elevated salt-marsh topography alongside the creeks, is necessary for soil formation and its spatial varying aeration. This process allows for halophytic plant growth, specifically during the early stages of salt-marsh configuration, as each plant species is adapted to different aeration and flooding conditions (e.g., Armstrong et al., 1985; Bakker et al. 1993; Erchinger et al., 1996). As a result, the distribution pattern of halophytic plant species exhibits a

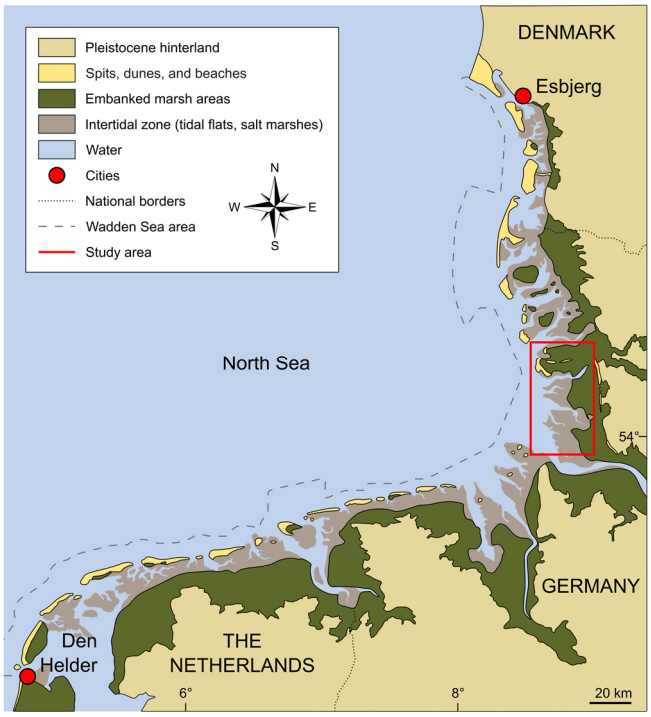

Fig. 1 | The Wadden Sea area. Overview of the south-eastern North Sea region with distribution of the intertidal systems. The individual habitat types and geological interpretation are illustrated in accordance with the Common Wadden Sea Secretariat (CWSS, 2009).

vertical zonation in relation to the tidal frame that is strongly linked to gradients in surface elevation, inundation frequency and duration and is thus controlled by in situ varying abiotic environmental factors such as pH, salinity, and substrate (Bakker et al., 1993; Silvestri et al., 2005). Concurrent with this vertical plant zonation, numerous heterotrophic protists, such as benthic foraminifera, likewise occupy different niches along the aforementioned salt-marsh gradients, revealing a similar linkage to elevation, inundation and associated changing abiotic parameters (Fig. 2; Scott and Medioli, 1978; Gehrels and Newman, 2004).

Whenever a salt marsh is exposed to wave activity during high tides or storm surges, the salt marsh's flow-resistant vegetation structure attenuates the strength of the inland pushing waves but also traps and binds reworked sediments of allochthonous origin that are introduced by the tides or surges (Allen, 1990, 1997, 2000; Andersen et al., 2011; Fagherazzi, 2014). In this manner, salt marshes provide substantial services, such as natural coastal protection measures, and are thus of critical importance in protecting the shorelines and densely populated hinterland from annual storm surges (Kirwan and Megonigal, 2013). Furthermore, the halophytic vegetation mainly contributes to sedimentary salt-marsh stratification in two different ways: first by trapping and binding reworked sediments, whereby biofilms generated by microalgae and bacteria mainly ensure that tidally introduced siliciclastic particles are retained, and second by adding organic components of indigenous origin (Allen, 2000). These components are mainly represented by sedimentary organic matter consisting of indigenous accumulated litter from marine to terrestrial primary producers, which can thus also contribute to salt-marsh stratification (Mayer et al., 1981; Allen, 1997). On this occasion, a basic distinction can be made between two different types of sediment sources, which ensure the sediment supply in either minerogenic or organogenic quality essential for the vertical growth rates and lateral extent of salt marshes (Allen, 1990; Woolnough et al., 1995). The resulting lamination of coastal salt-marsh sequences is also known as *Grodenschichtung* (e.g., Reineck, 1982; Freund and Streif, 2000).

Depending on how much minerogenic or organogenic sediment material has been deposited, conclusions may be drawn about past changes in seasonal or even long-term hydrodynamics (Allen, 1990). In fact, maximum organic matter production rates are highest during spring and summer, while maximum re-suspension of minerogenic sediment particles is highest during winter, owing to severe winter storm surges and low primary production rates (Skogen et al., 1995). At the same time, storm surges also cause the relocation of calcareous benthic foraminifera, such as *Ammonia* spp., *Cribroelphidium selseyense*, *Cribroelphidium williamsoni*, *Haynesina depressula*, and *Haynesina germanica*, which preferably inhabit tidal flats but are then re-deposited on salt-marsh surfaces and integrated into sedimentary sequences (Figs. 2, 3; Francescangeli et al., 2016, 2017; Müller-Navarra et al., 2016, 2019). Salt marshes themselves are dominated by numerous agglutinated foraminiferal species, such as *Balticammina pseudomacrescens*, *Entzia macrescens*, *Miliammina fusca*, and *Trochammina inflata* (Figs. 2, 3), whose vertical zonation with respect to the tidal frame can be used to determine past sea-level changes (Müller-Navarra et al., 2016). As opposed to halophytic plants, the fossilisable tests of benthic foraminifera within sedimentary archives have a high potential to provide information that can be used for past ecosystem reconstructions (e.g., Alve et al., 2009). Accordingly, both sediment composition and quality, together with the abundance of representative foraminiferal species within sedimentary sequences, represent ideal proxies for the reconstruction of past changes in environmental conditions and depositional processes.

The tidally and storm surge-introduced sediment budgets are thus responsible not only for the vertical accretion of salt marshes but also for that of the surrounding tidal flats, since the latter are also fed by the creeks, which carry particles in suspension with their seaward draining water during

decreasing tidal range (Allen et al., 1980; Allen, 1990, 1997). Salt-marsh accretion rates are generally able to keep pace with gradual rising sea levels, specifically at salt marshes' seaward edges that receive the highest sediment supply, finally reaching a surface elevation that is stabile relative to the shifting tidal frame but still below the storm-surge level, representing a balanced elevation response to sea-level changes (Allen, 1990; French, 1993; Andersen et al., 2011). In fact, once a salt marsh has reached a certain surface height, its vertical growth rate decreases steeply (i.e., salt-marsh maturing), as the marsh receives less minerogenic sediments with increasing surface height because it is less affected by flooding when approaching the level of the highest astronomical tide (HAT; Allen, 1990, 1997, 2000; Andersen et al., 2011). In this manner, salt-marsh accretion rates can achieve a balance with a modest SLR (Allen, 2000; Andersen et al., 2011). However, the persistence of salt marshes is only ensured when their accretion rates still exceed the relative SLR or when potential landward migration rates are more accelerated than erosion rates at the salt marshes' seaward boundary (Kirwan and Megonigal, 2013; Kirwan et al., 2016). In the latter case, the halophytic plant communities of the previous high salt marsh are then simply replaced by those of the low marsh (Bakker et al., 1993). If the sea level becomes subsequently stable or even falls and the minerogenic supply is absent, the relatively high availability of organogenic material, together with missing flooding, can then promote the formation of peat beds, initiating a shift from a saltwater- to a freshwater-dominated marsh system (Allen, 1990, 1997, 2000); see also Section 1.2. If, however, sea levels rise at an accelerated rate and sediment supply cannot keep up, this can lead to a permanent drowning of the salt marsh or increased erosion of its seaward edge, resulting in the formation of erosional cliffs that retreat further landward. Either way, it can lead to the loss of the salt-marsh areas (Andersen et al., 2011; de Groot and van Duin, 2013).

It can be concluded that both the hydrodynamic forces and the sediment supply themselves play a major role in controlling intertidal sedimentation processes (Allen et al., 1980; Allen, 2000). As intertidal wetlands are highly sensitive to hydrodynamic changes, the composition and stratification characteristics of complex sedimentary sequences represent an exceptional archive for understanding their response to past storm-surge conditions and underlying climate variability, potentially even on a long-term or super-regional scale (e.g., Davy et al., 2009; Chaumillon et al., 2017). Furthermore, the question arises of how salt marshes can cope with shifts in the frequency and intensity of storm surges – a scenario that is increasingly occurring in the course of ongoing climate change (e.g., IPCC, 2019). Accordingly, salt marshes are of considerable importance for mitigating the effects of present and future climate change as long as they keep pace with ongoing global and regional SLR.

1.2 Holocene sedimentary sequences

The Wadden Sea with its intertidal wetlands is a relatively young post-glacial formed area. During the last ice age (Weichselian glaciation), the Wadden Sea area was not covered by ice sheets, and as a result, its Pleistocene landscape was largely configurated by glacial and glaciofluvial processes, i.e., terminal moraines and outwash plains (Streif, 2004; Kabat et al., 2012). In the later stages, the Pleistocene surface was further shaped throughout the interstadial Holocene marine transgression, which started around 18 000 years BP after the Last Glacial Maximum (LGM) and with the end of the Weichselian glaciation (Streif, 1989, 2004; Behre, 2005). Initially, the melting of the glaciers caused a rapid rise in sea level (1.25 m per century; Behre, 2005), shifting the former coastline approximately 250 km inland (Streif, 1989). Although this marine intrusion created new accommodation spaces, its accelerated rise tended to prevent near-shore intertidal sedimentation processes (Kabat et al., 2012). However, this changed around 1500 cal. BC, when the rates of the Holocene relative mean SLR decelerated and, instead, increased more gradually or even temporarily stagnated, approaching more recent rates of approximately 1 mm yr^{-1} (0.11 m per century; Streif, 1989; Allen, 2000; Behre, 2003a, 2005). Based on that, the overall post-glacial SLR throughout the Holocene is usually divided into two stages: the Calais transgression (accelerated SLR) and the Dunkerque transgression (decelerated SLR; e.g., Baeteman, 1999; Behre, 2005). The deceleration of progressive SLR during the Dunkerque transgression finally allowed for intertidal sedimentation processes (Allen, 1997, 2000, and references therein). Apart from the eustatic change in sea level that was caused by increasing water volume initiated by icesheet melting, accompanying post-glacial isostatic movements due to the loss of land-ice masses designated additional changes in Holocene relative sea level (Streif, 1978; Bungenstock, 2005; Vink et al., 2007). In north-west Europe, isostatic rebound was mainly caused by the uplift of the Fennoscandian centre after the loss of its ice sheets (Vink et al., 2007).

Superimposed on the Holocene marine transgression, the last approximately 5000 years (since 3000 cal. BC) have been further characterized by high-frequency sea-level fluctuations, represented by a series of regression phases, each of which has temporarily interrupted the underlying long-term rise (Streif, 1989; Allen, 2000; Behre, 2003a, 2005). As these sea-level fluctuations could be reconstructed for the entire German North Sea coast, encompassing the

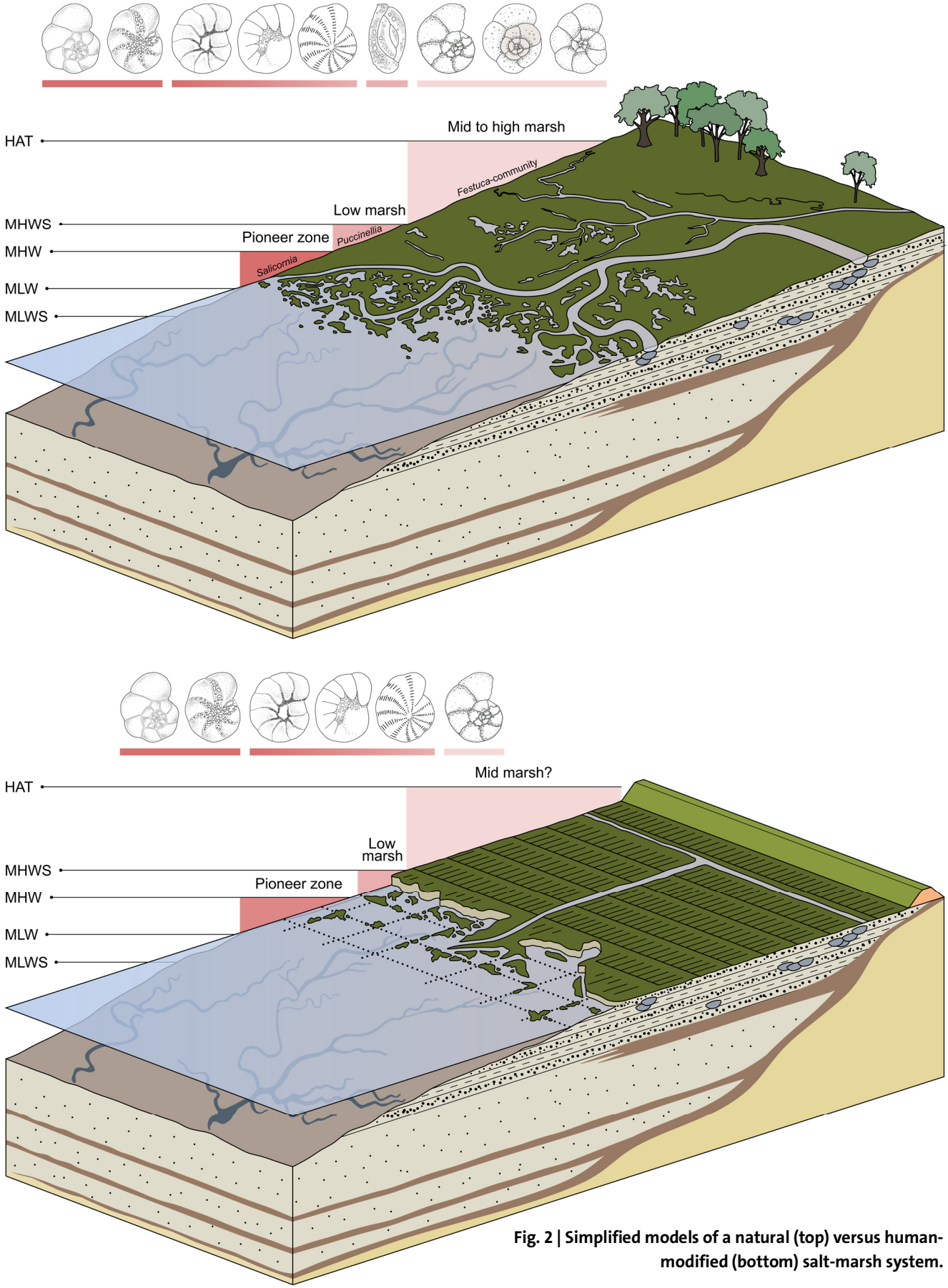

Fig. 2 | Simplified models of a natural (top) versus human-modified (bottom) salt-marsh system.

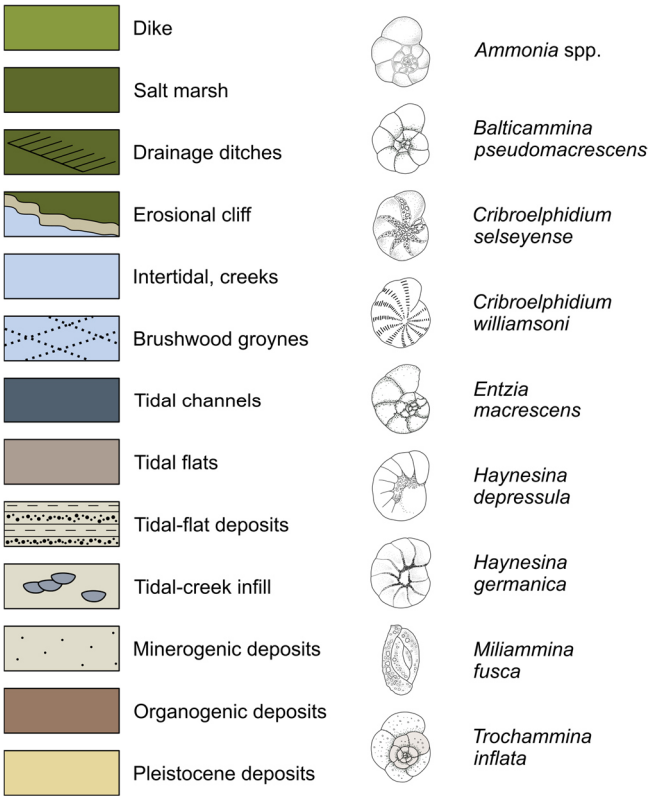

Fig. 2 | (continued). Salt-marsh models with configuration of Pleistocene deposits and basal and intercalated peat layers, demonstrating the strong linkage between the formation of the present-day Wadden Sea region and its intertidal systems to sea-level changes, as indicated by transgressive (intrusion of minerogenic deposits) and regressive overlaps (propagation of organogenic peats). The structure of natural intertidal wetlands (**upper model**) can be linked to gradients in surface elevation, inundation frequency and duration, and thus provides distinct habitats for different halophytic plant communities and benthic foraminiferal species, representing a salt-marsh zonation that can basically be subdivided into a pioneer zone, a low marsh, and a mid- to high marsh zone (note the different rose-coloured bars). In comparison, a salt marsh that is highly modified by human interventions (**lower model**), such as diking, draining, and dredging measures, lacks a clear inland surface elevation relative to the tidal frame, and thus, a distinct zonation of salt-marsh plants and benthic foraminifera is rather absent. HAT: highest astronomical tide; MHWS: mean high water spring; MHW: mean high water; MLW: mean low water; MLWS: mean low water spring. Illustrations are following Streif (1989) and Suchrow et al. (2012). Sketches are not to scale.

area between the North Frisian Islands (Schleswig-Holstein) and the Ems-Dollart estuary (Lower Saxony), it can be assumed that this oscillating pattern reflects a supra-regional signal (Bungenstock and Weerts, 2010). As glacio-isostatic movements were already largely stable in the south-eastern North Sea area during the late Holocene, it is likely that these short-term sea-level fluctuations were caused by climate variability (Behre, 2003b; Bungenstock and Weerts, 2010). In fact, the occasional regressive interruptions of post-glacial SLR may be linked to cyclic occurring rapid climate changes (RCC), during which the mid- to late Holocene climate temporarily cooled at high latitudes (Mayewski et al., 2004). Among others, these RCCs coincided with episodes of glacier expansion and highest ice-rafting activities in the subpolar North Atlantic, further including historical events such as the Little Ice Age (LIA; Bond et al., 1999; Fletcher and Zielhofer, 2013).

The stabilized conditions of the decelerated SLR since around 1500 cal. BC progressively favoured the development of pioneering, organogenic wetlands along the coastlines, while the brief regression phases fostered soil formation due to lowered marine influences and a sufficient elevated terrain surface relative to the tidal frame that is close to the HAT (Streif, 1989; Allen, 1995). These brackish-freshwater marshes mainly occurred within pre-Holocene topographic surface depressions in such a manner that the wetlands appeared sheltered between sandy barriers (the Frisian Islands) and along spits or beaches that were formed out of the eroded Weichselian moraine material, providing the required shielding for ponding (Streif, 1978; Allen, 1997). Further inland, the wetlands were bordered by the outcropping Pleistocene hinterland consisting of glacial outwash plains (Behre, 2003a; Kabat et al., 2012; MELUND, 2015a). Today, these fossil organogenic wetlands can be traced as intercalated peat layers within the Holocene sedimentary sequences along the present south-eastern North Sea coast, representing important marker horizons for the regional stratigraphy (Fig. 2; Behre, 2003a, 2003b, 2005; Bungenstock and Schäfer, 2009; Bungenstock and Weerts, 2010).

In the periods between individual regressions, when the marine influences dominated once again, coastal wetlands were over-washed by the raised water level and, as a result, subsequently overlaid by the minerogenic, i.e., clastic sediments of marine origin that propagated further inland (Fig. 2; Streif, 1989; Behre, 2003b; Bungenstock and Weerts, 2010). Based on that, the widely exposed post-glacial Holocene sedimentary sequences originating from the south-eastern North Sea coast are characterized by alternations between intercalated organogenic sediments (marsh growth during stabile or falling sea levels) and minerogenic sediments (tidal deposition during rapid SLR; Streif, 1989; Allen, 1995, 2000; Behre, 2005). The resulting cyclical facies changes in either organogenic (regressive

offlap) or minerogenic (transgressive onlap) quality and depositional structure illustrate the strong influence of sea-level changes and accompanying coastal flooding on the configuration of today's transitional environments (Fig. 2; Streif, 1989; Allen, 1995; Behre, 2003a; Bungenstock and Weerts, 2010).

1.3 Human interventions in salt marshes during early modern times

While today's tidal flats of the European Wadden Sea are considered to be rather unaffected by human interventions, as natural erosion and sedimentation processes predominate, the adjacent salt marshes have experienced massive modifications by human interventions since the last millennium (Wolff et al., 1994; Allen, 2000). These interventions are mainly due to large-scale land-claim measures for human settlement and agricultural purposes, for which the salt marshes have been increasingly defended from marine influence (Allen, 1997; Nolte et al., 2013a).

The first settlements along the south-eastern North Sea coast occurred around 900–800 cal. BC (late Bronze Age), concurrent with periods during which the regional sea level was largely stable or falling (Behre, 2005, and references therein). Human settlements finally experienced their peak during the Roman Empire, at which the buildings were initially constructed on artificial dwelling mounds (in German called *Wurth*, *Wierde* or *Warft*), as the ambient open marshes were regularly flooded, specifically during winter (e.g., Allen, 1997; Behre, 2005). However, dwelling mounds were built only along the Frisian coast, where deposited sediments are relatively incompressible and better drainable, due to their general higher minerogenic quality, than in British or French salt marshes (Allen, 1997). In medieval times (approximately 1100–1300 CE), settlers started to construct sea defences to protect themselves and their land claims from regular flooding, first as ring-shaped dikes around the dwelling mounds and later as continuous dike barriers along the mainland coast (Allen, 1997; Behre, 2003a, 2005). Specifically, in order to secure new land for further settlements or arable fields, high tidal flats or low-lying coastal salt-marsh areas were enclosed by the construction of artificial barriers; thus, these areas were permanently protected from wave action or rising water levels (Allen, 1997). Prior to the construction of barrier systems, however, brushwood groynes were built along the designated 'new' fields to trap sediments and reduce tidal and wave energy, with the fields being drained at the same time by dredged ditches (Erchinger et al., 1996; Allen, 1997; Hofstede, 2003). These measures allowed for the controlled management of sediment uptake and water drainage for the individual salt-marsh fields, which is still a common coastal protection and land conservation measure today (e.g., Erchinger et al., 1996; Suchrow et al., 2012).

Today's ditches are usually created in the form of parallel-oriented, extended trench networks with perpendicular cross-sections, giving a uniform and elongated, rectangular block-like pattern to the drained salt-marsh fields at the seaward side of the modern dikes (Fig. 2; Allen, 1997; Suchrow et al., 2012). These artificial ditches are designed not only to drain the wetlands but also to attenuate the energy of the incoming tidal currents (Reineck and Schäfer, 1956; von Lieberman et al., 1997). However, if these trenches are not regularly excavated, they quickly fill up with tidally introduced sediments (von Lieberman et al., 1997). Accordingly, in order to maintain the drainage ditches, it is necessary to regularly excavate the ditches by removing the accumulated material from the ditches and re-depositing it on the surrounding salt-marsh surfaces (in German called *Grabenräumung*; von Lieberman et al., 1997; Nolte et al., 2013a; Müller-Navarra et al., 2019; pers. comm. LKN.SH, 2020). These measures additionally raise the salt-marsh surfaces relative to the tidal frame, further promoting soil formation and vegetation growth due to improved aeration of the subsurface (Erchinger et al., 1996; Hofstede, 2003; Suchrow et al., 2012). Consequently, the evolution and growth of the modern salt marshes along the south-eastern North Sea coast have taken place mainly under human-controlled conditions (Bakker et al., 1993). With regard to the vegetation structure, the controlled conditions further include the grazing of salt marshes. Yet, the majority (> 70%) of the salt-marsh areas along the German North Sea coast have experienced moderate to intensive grazing by domestic livestock (mainly cattle and sheep; Andresen et al., 1990; Bakker et al., 1993). The resulting short-grazed turfs were originally supposed to provide increased shear strength to prevent surface erosion during severe storm surges (Bakker et al., 1993; Hofstede, 2003). It turned out, however, that intense grazing by livestock can also reduce the diversity of halophytic plant communities, and the short-grazed vegetation cover may have negative influences on sediment-accretion rates (Andresen et al., 1990; Nolte et al., 2013a). Moreover, it takes 10–20 years after abandoning grazing before a natural balance is restored in the plant community (Bakker, 1989).

The extensive disruptions of the intertidal landscape and its morphology may have led to substantial changes in the exposure of salt marshes to hydrodynamic forces (such as storm surges under 20th-century SLR) as well as the natural ecosystem functions of salt marshes (Streif, 1989; Allen, 2000; Bromberg Gedan et al., 2009). In fact, the engineered embankments and resulting cut-off of the wetlands in the hinterland from recurrent flooding ultimately led to various consequences. First, the natural sediment supply was no longer available in the hinterland, leading to a subsidence of the enclosed marshes, further promoted by the manipulation

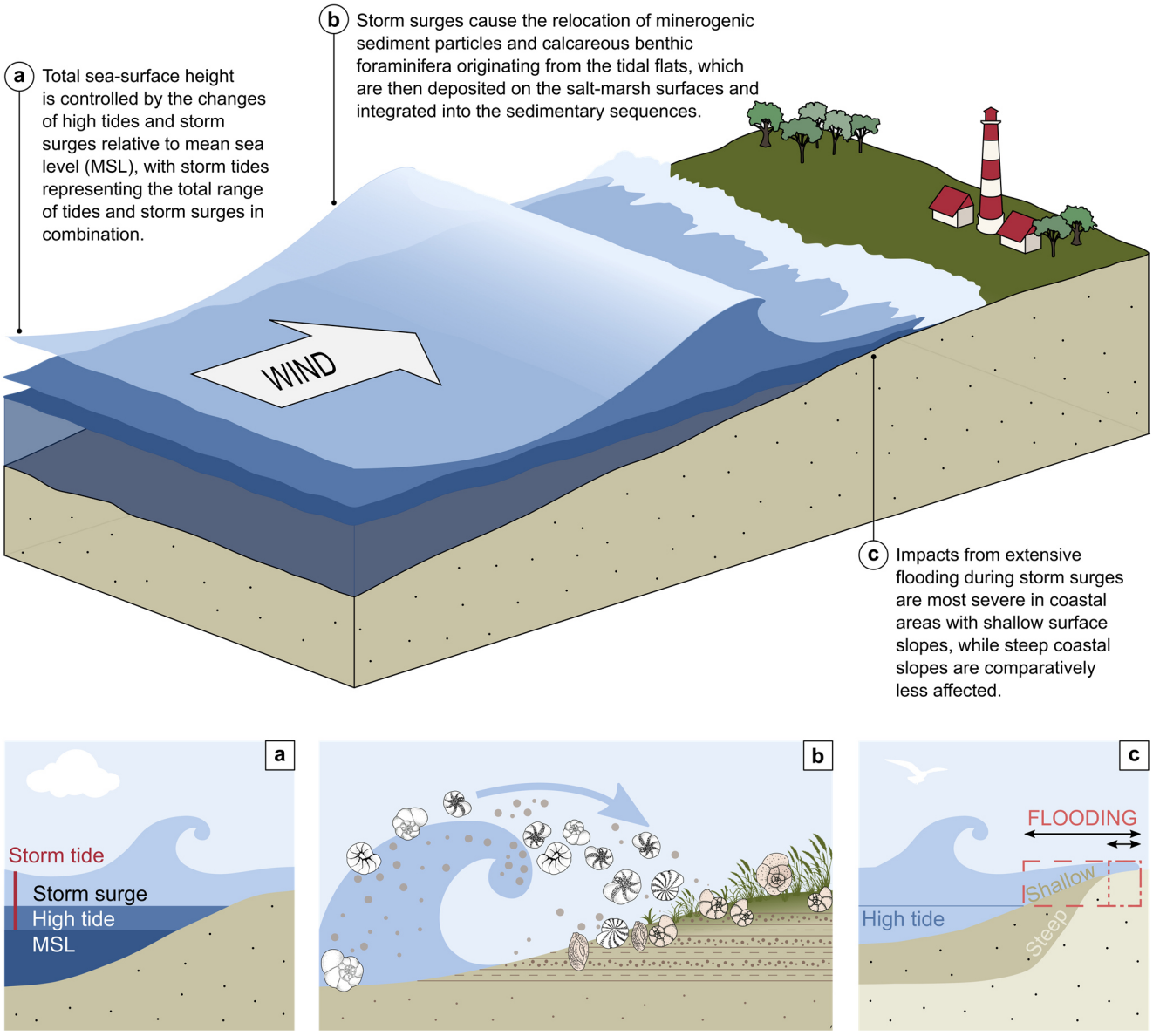

Fig. 3 | Conceptual model of how raising water levels can affect the low-lying coasts. a) Composition of the different components (mean sea level [MSL], tides, and surges) controlling changes in the total seawater level (or sea-surface height). **b**) Simplified salt-marsh model with assumed (re-)distribution pattern of calcareous tidal-flat foraminifera (white specimens) and agglutinated salt-marsh foraminifera (brown specimens) during a storm surge. **c**) Schematic showing shallow and steep coastal slopes and the associated flooding extent (arrows) during a storm surge. Illustrations (**b**, **c**) are based on the descriptions given by the National Oceanic and Atmospheric Administration (NOAA). Sketches are not to scale.

of groundwater resources (Streif, 1989; Allen, 1997, 2000; Bromberg Gedan et al., 2009). Second, the water dammed up in front of the dikes during high tides and storm surges due to the now absent flood plains, and thus rose much higher than before, leading to enhanced near-shore erosional processes (Allen, 2000; Behre, 2003b, 2005). Due to extensive coastal protection measures under accelerated SLR conditions, most of the present salt marshes are bordered by erosional cliffs at their seaward edges, which retreat further inland with increasing erosion (Fig. 2; Allen, 1989; Bakker et al., 1993; Müller-Navarra et al., 2019). However, since the storm-surge levels increased considerably with progressively rising sea levels, the dikes likewise had to be raised continuously, specifically during the second half of the 20th century (Kelletat, 1992; von Storch et al., 2008).

In 1985 CE, most of the intertidal ecosystems along the south-eastern North Sea coast, including the salt marshes, were designated as nature reserves (i.e., the Wadden Sea

National Park), as decided by nature conservation authorities. This was accompanied by the 1997 Trilateral Wadden Sea Plan (WSP), in which the Netherlands, Denmark, and Germany targeted the enhancement of the natural development of coastal salt marshes in the entire Wadden Sea area (e.g., Esselink et al., 2009). This was in contrast to the previous focus of the local farmers or coastal defence agencies, which aimed to achieve maximum sedimentation rates for the salt marshes; therefore, the salt marshes were intensely modified, and their creation promoted by human interventions (Bakker et al., 1993; Esselink et al., 2009).

1.4 Twentieth-century sea-level fluctuations: implications of global warming

Beyond the impact of non-climatic pressures in the form of direct human interventions into intertidal wetland ecosystems, low-lying coastal habitats have further been heavily stressed by shifts towards a warmer climate (IPCC, 2019). One of the most recently discussed possible consequences of ongoing climate change is the rise in global mean sea level (GMSL) in response to ocean warming, which poses a universal threat to low-lying coastal environments (Pugh, 1987; Church et al., 2008; IPCC, 2019). During the last few decades, the GMSL increase has even accelerated (Dangendorf et al., 2019). While the GMSL was rising at rates of 1.4 mm yr^{-1} during the first half of the 20th century, this changed considerably from the late 1960s onwards, and the increase finally reached about 3.2 mm yr^{-1} in 1990 CE (Dangendorf et al., 2019; IPCC, 2019). Building on this trend, climate simulations project an average SLR rate of 4–9 mm yr^{-1} to 10–20 mm yr^{-1} by the end of the 21st century, depending on whether lowest or highest greenhouse-gas emission scenarios are assumed (IPCC, 2019). This predicted SLR would substantially change and affect many coasts, as it highlights the potentially increasing exposure of low-lying and densely populated coastal regions to flood hazards (Turner et al., 1996). In fact, the need for appropriate coastal protection measures in terms of flood-risk mitigation strategies becomes evident, since more than half of the world's population lives in coastal areas today, with settlement numbers expected to rise steadily in the near future due to rising numbers in population and urbanisation (Turner et al., 1996; Small and Nicholls, 2003; UNEP, 2006).

The relative height of the sea-surface level (or sea-surface height, H) is constituted and controlled by basically three components (MSL, tides, and storm surges; Fig. 3), dependent on the time t, simplified expressed as: $H(t) = L(t) + T(t) + S(t)$. There, $L(t)$ represents the MSL long-term change, $T(t)$ is the astronomical driven tide component, and $S(t)$ is the sea level caused by meteorologically induced surges (Pugh, 1987; Weisse and von Storch, 2010). For further details, see description of the water-level components in Appendix A. If there are any rise and concomitant superposition of these components, this can dramatically increase the overall sea-level height and associated flooding risk for coastal regions, which is then referred to as extreme sea level (ESL; Flather and Williams, 2000; Horsburgh and Wilson, 2007; Weisse et al., 2012; Gregory et al., 2019; Lang et al., 2019, 2020). There is, however, a dynamic non-linear interaction between MSL, tides, and storm surges, specifically in shallow waters such as the south-eastern North Sea (Pugh, 1987; Haigh et al., 2010). Increasing water depth, such as has been observed for the North Sea during the past century due to the rising MSL, affects the bottom-friction forces and thus the amplitude of the oscillating tidal currents (Davies and Jones, 1995; Reynaud and Dalrymple, 2012; Arns et al., 2015). This, in turn, affects storm surges that tend to cluster with the rising tides, and which therefore strongly depend on local water depth and bathymetry (Fig. 3; Pugh, 1987; Horsburgh and Wilson, 2007; Gerber et al., 2016). As a result, the rising MSL and amplified tidal ranges will also lead to spatial and temporal changes in the severity of storm surges (Church et al., 2008; von Storch and Woth, 2008).

In the North Sea, ESLs appeared to outpace the rising MSL trend from the mid-1950s until 1990 CE in a non-linear progression, attributed to the concomitant and temporal changes in the tidal amplitudes and increased storm-surge activity (e.g., Mudersbach et al., 2013; Arns et al., 2015, 2017). Based on that, the expected global SLR of 0.43–0.84 m by 2100 CE (IPCC, 2019) highlights the importance of obtaining a better understanding of how this predicted sea-level change and accompanying changes of individual water-level components (such as tides or surges) affect the resilience of exposed low-lying intertidal ecosystems.

1.5 Motivation and research questions

Although the precise consequences of climate change are yet uncertain, the changes initiated will nevertheless have an impact on vulnerable intertidal ecosystems. Specifically, a more accelerated rise in sea level, which is likely to be associated with ongoing global warming, will pose a substantial threat to coastal wetlands (Bromberg Gedan et al., 2009). Moreover, a relatively well-constrained SLR may add to the risk posed by storm surges, regardless of whether the storm intensity itself changes (Church et al., 2008; von Storch and Woth, 2008; Andersen et al., 2011). In this context, it remains particularly unclear to what extent the largely human-altered coastlines can withstand more frequent and amplified storm-surge flooding in the near future. Consequently, understanding past ecosystem responses to changing climatic conditions over the course of the 20th century is of critical importance, as it provides insights about potential linkages between intertidal

sedimentation dynamics and observed climate patterns (Bartholdy et al., 2004). This can help to better assess the potential impacts of climate change in terms of how resilient or vulnerable a given habitat might be under future warming scenarios. Considering the past century, significant intensification in the storm-surge activity has already been observed for the south-eastern North Sea (e.g., Matulla et al., 2008). If, in addition, one can understand past sedimentation processes in foreland ecosystems, this might further allow for the reconstruction of past changes in the storm-surge climate far beyond observational data (Bartholdy et al., 2004; Barlow et al., 2013).

In the following, the present doctoral thesis focuses on the investigation of four sedimentary sequences, originating from different salt-marsh systems that fringe the German North Sea coast as low-lying intertidal wetlands, thus being exposed several times per year to severe storm surges (Gerber et al., 2016). The aim of this study is to assess how and to what extent these coastal wetland habitats have responded to the impacts of a changing storm climate under 20th-century rising sea level conditions. As outlined in Section 1.1, salt-marsh accretion is directly linked to the sediment supply provided by storm waves and accompanying flooding of the marshes, leading to the salt marshes' vertical growth relative to the tidal frame. This suggests that the incorporation and stratification of allochthonous sediments with minerogenic quality assurance may provide insights about past changes in flooding frequency or intensity. This raises the overarching hypothesis:

Well-stratified sedimentary salt-marsh sequences from the German North Sea coast have archived 20th-century changes in storm climate and regional sea level.

Well-stratified sedimentary salt-marsh sequences from the German North Sea coast have archived 20th-century changes in storm climate and regional sea level.

However, the sufficient accuracy of such reconstructions highly depends on the chronostratigraphic control. Yet, the extraction of such robust age information is rather challenging for modern intertidal depositional systems. On the one hand, because they are strongly controlled by complex hydrodynamic processes and human interventions, leading to the frequent re-deposition of sediments, and on the other hand, because intercalated peat layers that in principle prove to be important marker horizons for the regional Holocene stratigraphy (see Section 1.2) are absent in the younger sequences. Furthermore, the potential storm-surge layers of interest might be problematic for age dating, as the reworked material introduced by storm surges may be older than the under- and overlying sediments within the same sequence. In addition, one must be aware that certain age markers may not be found within all sedimentary salt-marsh sequences, as local differences can appear within the salt-marsh stratification due to differing intensity of human interventions (such as ditching frequency). In this context, it becomes obvious that unravelling the potential storm-climate component within the sedimentary sequences is also challenging due to the complex climate-related and non-climatic influences, and it is unclear how and to what extent specifically the intensely human-modified salt-marsh systems have archived this storm-surge signature. Finally, if it is possible to trace the storm-climate component within the sedimentary sequences, it is crucial to find out how climatic shifts towards more frequent flooding affect the different salt-marsh systems. Based on that, this thesis poses the following three research questions, and corresponding research approaches arose in order to test the overarching hypothesis outlined above:

1) How can a reliable stratigraphy be established for modern salt-marsh sediment sequences from the highly dynamic south-eastern North Sea coast?

In order to obtain the most accurate chronostratigraphic control for all four salt-marsh sequences, and to overcome the problem of possible high age uncertainties due to the frequent incorporation of reworked sediments, different dating approaches were combined and critically reviewed. This includes introduced marker horizons derived by natural and artificial radionuclides (^{241}Am, ^{14}C, ^{137}Cs, and ^{210}Pb), heavy metal contaminants (mercury, Hg), human-induced interventions (such as tidal barrier construction or fairway deepening) and changes in the salt-marsh vegetation structure documented by benthic foraminiferal indicator species, all further validated by the strong resemblance of XRF ln(Zr/Rb) records.

2) How can the changes in storm-surge frequency and intensity and possible underlying super-regional climate oscillations of the 20th-century be traced within the sedimentary sequences, although the salt marshes have experienced various anthropogenic interventions?

To answer this question, an integrated approach was followed, combining and comparing sedimentological and geochemical proxy data from two different salt-marsh sediment sequences. This includes data such as the mean

grain size, organic carbon (C_{org}), and XRF scans (Br, Cl, Rb, and Zr), further discussed in comparison with observational data (historical wind, tide gauge, and river discharge records). Only two sediment sequences were considered for subsequent analysis and evaluation, as both showed the highest contrast in terms of human interventions and modifications but at the same time consisted of sediments exhibiting the longest time series. The spectral analyses applied to selected proxy data (i.e., the ln[Br/Cl] and ln[Zr/Rb] ratios) helped to evaluate potential underlying large-scale periodic climate fluctuations.

3) How do salt-marsh ecosystems react when they are exposed to highly complex environmental stress over a long period?

Benthic salt-marsh foraminifera seem to be ideally suited to evaluating impacts by increasing stress levels, as they react very sensitively to environmental disturbances. Therefore, special focus was on the evaluation of test deformities in the agglutinated benthic foraminiferal species *E. macrescens*, which is a cosmopolitan taxon in modern salt marshes. To allow for the comparison of different impacts of human interventions during the past century, the historical foraminiferal records of the same two contrasting sedimentary salt-marsh archives addressed above were evaluated. Further, a conceptual model was created to better understand how the complexity of various impact factors (such as salinity, hydrodynamics, exposure of the salt marsh, and various human activities) led to increased environmental stress, to which large numbers of foraminifera responded with test deformation.

1.6 Synthesis and thesis outline

Based on its cumulative character, the present thesis is outlined as follows, with the central findings indicated below:

- **Chapter 2** addresses the challenge of how to establish a regional stratigraphic framework for highly dynamic depositional systems that contain sediments reworked by storm surges, as is the case for the salt marshes of the south-eastern North Sea coastal region. The combination of different dating techniques proved to be essential to compensate for lacking or uncertain age information of each method. For the analysed sediment sequences, the most promising age accuracy was achieved by integrating distinct enrichments of ^{137}Cs and ^{241}Am activities, together with human-induced pollutants (Hg) and proxy-based sedimentological inter-correlations. The reconstructed average accretion rates covering the past approximately 100 years reflected the specific exposition of the study sites to wave energy, inundation frequency, and intensity.
- The question to be answered in **Chapter 3** followes the assumption that the well-stratified salt-marsh sequences from the south-eastern North Sea provide an exceptional archive for the reconstruction and understanding of the climate variability of the last approximately 100 years, since they may capture past storm-climate signals. In fact, high-resolution geochemical and sedimentological proxy records revealed long-term increasing trends throughout the two investigated sequences, starting from the mid-20th century and continuing until recent times, resembling the observed strengthening of the regional storm-surge activity. The results implied that past regional to super-regional climate changes have been transferred into the sedimentary salt-marsh archives. The response of the studied salt marshes to different anthropogenic land-use strategies and associated exposure to flooding corroborates the importance and critical role of intertidal wetlands regarding projected future scenarios of global and regional SLR.
- As coastal salt marshes are exposed to frequent storm surges, this raises the question of how they might adapt to changing storm-climate conditions and sea levels under the influence of global warming, which is a scenario confidently predicted by the Intergovernmental Panel on Climate Change (IPCC) to occur by 2100 CE. The objectives of **Chapter 4** are to unravel and assess how coastal salt marshes respond to changes in environmental stress, as raised by the third research question. In the frame of this research, a rising number of deformed tests among the foraminiferal salt-marsh indicator species *E. macrescens* were observed at times of strengthening flooding. This indicates increasing environmental stress in the studied salt marshes towards the late 1980s, initiated by North Sea storm-climate amplification, and demonstrates the vulnerability of human-modified coastal wetlands to changing climate conditions.
- An overarching conclusion, outlining the key findings that can be drawn from the topics previously covered in Chapters 2–4, is giving in **Chapter 5**.

JOURNAL ARTICLES

The following Chapters 2–4 address the three research questions posed before, which have resulted in the present research articles:

Bunzel, D., Milker, Y., Müller-Navarra, K., Arz, H.W., Friedrich, J., Lahajnar, N., Schmiedl, G., 2020. Integrated stratigraphy of foreland salt-marsh sediments of the south-eastern North Sea region. *Newsletters on Stratigraphy* **53**, 415–442, DOI: 10.1127/nos/2020/0540.

Bunzel, D., Milker, Y., Müller-Navarra, K., Arz, H.W., Schmiedl, G., 2021. North Sea salt-marsh archives trace past storminess and climate variability. *Global and Planetary Change* **198**, 103403, DOI: 10.1016/j.gloplacha.2020.103403.

Bunzel, D., Milker, Y., Francescangeli, F., Schmiedl, G., 2020. The response of human-modified coastal wetlands from the southeastern North Sea to amplified storm-climate conditions: indications by deformed marsh foraminifera. *Ecological Indicator*, under review.

Chapter Two

The following Chapter has been published as:

Bunzel, D., Milker, Y., Müller-Navarra, K., Arz, H.W., Friedrich, J., Lahajnar, N., Schmiedl, G., 2020. Integrated stratigraphy of foreland salt-marsh sediments of the south-eastern North Sea region. *Newsletters on Stratigraphy* **53**, 415–442, DOI: 10.1127/nos/2020/0540.

Integrated stratigraphy of foreland salt-marsh sediments of the south-eastern North Sea region

D. Bunzel *et al.*

Submitted: 14 March 2019
Accepted for publication: 01 December 2019
Published online: 21 February 2020

Abstract

Depositional processes in coastal wetlands respond to a changing climate as documented in the sediment sequences of salt marshes. In this context, robust chronologies are crucial for the reconstruction of salt-marsh depositional processes in the past. However, salt-marsh sediments from the highly dynamic North Sea coast often lack a reliable stratigraphy due to the combined influences of natural processes and human activities, causing a reworking and re-deposition of the sediments. Here, a combination of absolute and relative dating methods has been applied in order to establish an integrated stratigraphic framework for active foreland salt marshes along the south-eastern North Sea coast. This stratigraphic framework is based on radionuclides (^{210}Pb, ^{137}Cs, ^{241}Am, and ^{14}C) and mercury (Hg) contaminations, together with ln(Zr/Rb) as a grain-size proxy for additional inter-correlation between the four studied sites. The studied salt marshes encompass different environmental settings concerning the inundation frequency and intensity, and anthropogenic influences. As a result, the reconstructed mean sediment-accretion rates range from 1.16 cm yr^{-1} in the anthropogenic modified and grazed coastal salt marsh at Friedrichskoog, to 1.31 cm yr^{-1} in the more sheltered and semi-enclosed salt marshes in the Bay of Tümlau, and up to 1.75 cm yr^{-1} in the dynamic open coastal salt marsh at Kaiser-Wilhelm-Koog. Similar mean high accretion rates of 1.72 cm yr^{-1} are documented for the Eider estuary until 1965 CE, before they dropped to 0.72 cm yr^{-1} after completion of the Eider tidal barrier in 1973 CE. The results highlight the advantage of combining independent dating methods for the establishment of salt-marsh chronologies, which proves to be essential to compensate for absence or blurring of distinct stratigraphic signals in highly dynamic coastal depositional settings, such as the salt-marsh systems at the south-eastern North Sea coastal region. The reconstructed sediment-accretion rates suggest a high resilience of salt-marsh systems to ongoing sea-level rise as long as sediment availability and natural flooding dynamics are maintained.

2.1 Introduction

2.1.1 Salt-marsh archives. Salt marshes represent the transition zone between marine and terrestrial environments and thus are directly affected by changes in sea level, storm-surge frequency and intensity, and sediment redistribution (Allen, 2000; Davy et al., 2009). In this context it is essential to understand how salt marshes respond to past, present-day, and future climate changes, and to which extent they can keep pace with an accelerating relative global sea-level rise, also to assess future scenarios (Schuerch et al., 2018). Rising sea levels may result in enhanced erosion of present salt marshes, however, salt-marsh plants attenuate wave energy, leading to a reduction of lateral erosion (Feagin et al., 2009). In fact, suspended sediment particles are trapped by the salt-marsh vegetation, which results in vertical salt-marsh accretion depending on the suspended sediment concentration and tidal range (Schuerch et al., 2014; Kirwan

et al. 2016). Consequently, the investigation of past and present sedimentation processes in coastal-wetland areas is crucial for the ongoing debate of coastal risk management and related adaptation strategies (e.g., Allen, 1990; Kirchner and Ehlers, 1998; Andersen et al., 2011; Kirwan et al., 2016).

For the reconstruction of past changes in coastal sedimentation processes and salt-marsh evolution, robust age information for analysed sediment sequences is of critical importance. Commonly, undisturbed continuous sedimentation is required to generate reliable age models, which is rather an exception in highly dynamic coastal areas such as the south-eastern North Sea (Nolte et al., 2013a). Moreover, sediment archives along the south-eastern North Sea coastline are influenced by sea-level changes and periodical storm surges, causing erosion, relocation and re-deposition of sediments (Redfield, 1972; Bungenstock and Schäfer, 2009; Bungenstock and Weerts, 2010; Hadler et al., 2018). The resulting stratification of allochthonous sediments together with autochthonous organogenic material reflects a variable inundation of the salt marsh and its growth in the past (Redfield, 1972; Ehlers, 1988; Ehlers et al., 1993; Müller-Navarra et al., 2019). Furthermore, first settlements along the North Sea coastline (Roman to Medieval period; Behre, 2005; Suchrow et al., 2012; Stock and Maier, 2016) were accompanied by constructing a system of parallel trench systems (ditches) in the salt marshes for agricultural purposes and land reclamation (Bromberg Gedan et al., 2009; Nolte et al., 2013a). To maintain the drainage systems, accumulated sediments within the ditches were removed regularly and deposited on top of the adjacent marsh surface (Nolte et al., 2013a; Müller-Navarra et al., 2019). Accordingly, coastal sediment sequences may also be disturbed or at least influenced by human activities, constituting another challenge in the establishment of accurate chronologies for salt-marsh archives.

2.1.2 Application of radionuclides and trace elements for sediment dating. The dating of modern sediment sequences (0–150 years) is commonly based on the decay of natural and artificial radionuclides, such as ^{210}lead (^{210}Pb), ^{137}caesium (^{137}Cs), ^{241}americium (^{241}Am), and ^{14}carbon (^{14}C; e.g., Chanton et al., 1983; Kirchner and Ehlers, 1998; Beks, 2000; Appleby, 2001; Nolte et al., 2013a, 2013b; Hadler et al., 2018). Among them, ^{210}Pb occurs naturally within the decay series of ^{238}uranium (^{238}U) with a half-life of $t_{1/2}$ = 22.3 years (Appleby, 2001). ^{210}Pb in the sediment has two main sources: the fallout from the atmosphere (unsupported ^{210}Pb; Appleby, 2001, 2008; Lubis, 2006) and the production within the sediment by in situ decay of its precursor ^{226}radium (^{226}Ra, supported ^{210}Pb; Beks, 1997; Appleby, 2001). Subsequently, the unsupported ^{210}Pb activity, which was incorporated into the sediment through atmospheric fallout and particle scavenging, decays and hence, declines continuously with time in increasing sediment depth (Lubis, 2006). This process is used in various dating models, which provide information about the sediment age. In the CIC model, constant initial concentration (CIC) of unsupported ^{210}Pb per unit dry weight in the sediment at each depth is assumed, whether or not any variations may have occurred in the rate of accumulation (Oldfield et al., 1978). This assumption requires that in undisturbed sediment sequences, unsupported ^{210}Pb concentrations should always decline monotonically with depth. The CRS model (constant rate of supply; Appleby and Oldfield, 1978), is valid when the flux of ^{210}Pb to the sediment remains constant while sedimentation rate varies.

To support the ^{210}Pb-derived ages, concentrations of the human-induced artificial radionuclides ^{137}Cs ($t_{1/2}$ = 30.2 yrs) and ^{241}Am ($t_{1/2}$ = 433 yrs) can be used as additional independent time markers (e.g., Appleby et al., 1991; Kirchner and Ehlers, 1998; Beks, 2000; Appleby, 2001, 2008). ^{241}Am is arising from the short-lived ^{241}plutonium (^{241}Pu, $t_{1/2}$ = 14.4 yrs) during decay processes (Holm and Persson, 1978; Appleby et al., 1991; Wigeland et al., 2012), while ^{137}Cs is synthesized during nuclear fission reactions from uranium isotopes (e.g., Chernorukov et al., 2015). The various decay series have been utilized for nuclear power and nuclear weapon industry, which caused a major release of ^{137}Cs and ^{241}Am into the environment in the recent past, mainly related to nuclear weapon tests or liquid discharges from nuclear reprocessing plants (Holm and Persson, 1978; Appleby et al., 1991; Beks, 2000; Appleby, 2001; Garwin, 2001; Aarkrog, 2003; Ewing, 2008; Nies et al., 2009). However, evidence for more recent nuclear power plant accidents (i.e., Chernobyl) can rather be obtained by high ^{137}Cs activities than by ^{241}Am, since ^{241}Am turned out to be rare in near surface sediments (Appleby et al., 1991). Further contributions regarding the artificial radionuclide inventories in the environment can be made by waterborne dumping of radioactive waste during the last century, i.a., from nuclear industry waste, nuclear weapons, or nuclear-powered submarines, but these contamination effects are likely negligible within the North Sea area (Aarkrog, 2003). Therefore, the main sources for artificial radionuclide accumulations in the environment are attributed to the fallout of the atmospheric nuclear bomb tests, which started in 1952 CE and significantly increased since 1954 CE, with maximum concentrations around 1963 CE, the Chernobyl nuclear power plant accident in 1986 CE, and effluent discharges from nuclear reprocessing plants, such as Sellafield (west UK) and La Hague (north France; e.g., Pennington et al., 1973; Ehlers et al., 1993; Milan et al., 1995; Callaway et al., 1996; Kirchner and Ehlers, 1998; Beks, 2000; Appleby, 2001; Aarkrog, 2003; Nies et al., 2009). Radionuclide-loaded effluent discharges took place since 1952 CE at Sellafield and since 1966 CE at La Hague

(Beks, 2000). Additionally, minor impacts were caused by distinct accidents, such as the fire at Sellafield in 1957 CE, resulting in the release of large radionuclide amounts into the atmosphere (Gallagher et al., 2005).

Another widely used dating tool is the analysis of natural and post-bomb radiocarbon (^{14}C, $t_{1/2}$ = 5730 yrs; e.g., Libby, 1961; Stuiver and Polach, 1977; Reimer et al., 2004). This method is based on the quantification of ^{14}C in inorganic or biogenic carbon, reflecting the time of mineralisation or death, when natural radiocarbon incorporation or assimilation stopped (Libby, 1961). Initially, the ^{14}C originates from cosmic radiation and related neutron releases, causing an equilibrium between atmospheric ^{14}C production and its decay (Anderson et al., 1947; Libby, 1961). However, the release of ^{14}C into the atmosphere during nuclear detonations, restricts ^{14}C dating to times older than 1950 CE (Libby, 1961; Stuiver and Polach, 1977; Enting, 1982; Hua and Barbetti, 2004). On the other hand, the specific radiocarbon increase after 1950 CE can be used to provide age information for younger deposits, in analysing their so-called post-bomb ^{14}C signature (Reimer et al., 2004). Based on that, the ^{14}C activity in the year 1950 CE is defined as $F^{14}C$ (fraction modern) = 1, representing a ^{14}C activity of 100%-Modern Carbon (pMC). Accordingly, if $F^{14}C > 1$, it is evident that the analysed carbon-bearing sample is younger than 1950 CE and vice versa (Donahue et al., 1990; Reimer et al., 2004; Larsen et al., 2017).

Further comprehensive age markers are provided by heavy metal contaminants, such as human-caused mercury (Hg) accumulations, which appear in high concentrations during industrial time (Leipe et al., 2013). There, primary anthropogenic Hg releases into the environment originated from emissions by fossil fuel combustion, metal and cement industries, chlor-alkali industries, mining, municipal waste incineration, military waste dumping, and the usage of Hg-bearing pesticides and fungicides (Travis and Hester, 1991; Pacyna and Pacyna, 2002; Hylander and Meili, 2003; Pirrone et al., 2010; SfEP, 2017), and may reveal slightly differing regional patterns. Whereas prior to human impacts, the natural Hg-background concentrations turned out to be generally very low in the Northern Hemisphere (e.g., Biester et al., 2007; Leipe et al., 2013; Moros et al., 2016). Consequently, the relative increase of the immobile Hg contaminants within a sediment sequence since ca. 1850 CE, when European industrialization started, and with peak values around ca. 1970 CE, can be used as additional and independent time marker (Norton et al., 1997; Leipe et al., 2013; Moros et al., 2016).

On a regional scale, X-ray fluorescence (XRF) element records can provide additional relative stratigraphic information through the correlation of non-dated and dated sections (Richter et al., 2006). In salt-marsh sediments, fluctuations of the ln(Zr/Rb) ratio can be interpreted as relative changes in the particle-size spectrum, since zirconium (Zr) is known to be enriched in the coarse-grained sediment fraction as detrital zircon, while rubidium (Rb) is mainly concentrated in clay minerals (e.g., Bhatia and Crook, 1986; Hoskin and Ireland, 2000; Dypvik and Harris, 2001; De Vos et al., 2006; Rothwell and Croudace, 2015). This gave the motivation to test this proxy as an additional stratigraphic tool, because XRF analyses of Zr and Rb provide high-resolution information about the chemical sediment composition, and requires little sample preparation (e.g., Richter et al., 2006).

This study aims to critically review the commonly used dating approaches in coastal wetlands, addressing their potential and biases in different depositional environments. In accordance, the above described absolute and relative dating methods were combined to date and correlate sediment sequences from coastal deposits of the south-eastern North Sea region. This enables to establish an integrated stratigraphy for modern salt-marsh sediment archives, which have experienced both natural and anthropogenic impacts during their deposition in the recent past, i.e., the last approximately 100 to 150 years. Hence, this study addresses the following research questions: (1) which impact do sedimentation processes have on the reliability of the most common radiometric dating techniques in a highly dynamic coastal environment as the salt marshes of the south-eastern North Sea region? (2) Can past human-induced pollution effects be integrated to obtain additional age information? (3) Can grain-size proxies, such as ln(Zr/Rb) ratios, be used as an additional tool for the inter-correlation of salt-marsh sequences and for further refinement of regional chronologies? (4) Which accretion rates can be derived by the integrated stratigraphic framework and how resilient are coastal salt marshes to regional sea-level rise?

2.2 Regional setting

To evaluate the salt-marsh depositional development along a N–S transect of the south-eastern North Sea coast during the last 150 years, sediment sequences from four different active salt-marsh systems have been analysed. The studied areas are located at the coasts of North Frisia and Dithmarschen (Fig. 4), which belong to the Wadden Sea National Park of Schleswig Holstein (established in 1985 CE), Germany. The investigated sites encompass different minerogenic salt-marsh systems, which have been influenced by both, anthropogenic interventions and natural processes: (1) a formerly drained and semi-enclosed coastal salt marsh (Bay of Tümlau, TB13-1, 54°21'51.07"N, 8°40'35.09"E; Müller-Navarra et al. 2019), (2) a largely natural estuarine salt marsh (the so-called Grüne Insel mit Eiderwatt, Eider estuary, GeoHH-GIE, 54°17'1.42"N, 8°53'39.58"E), (3) a drained and grazed coastal salt marsh (Friedrichskoog, GeoHH-FK, 54°2'35.02"N, 8°52'20.41"E),

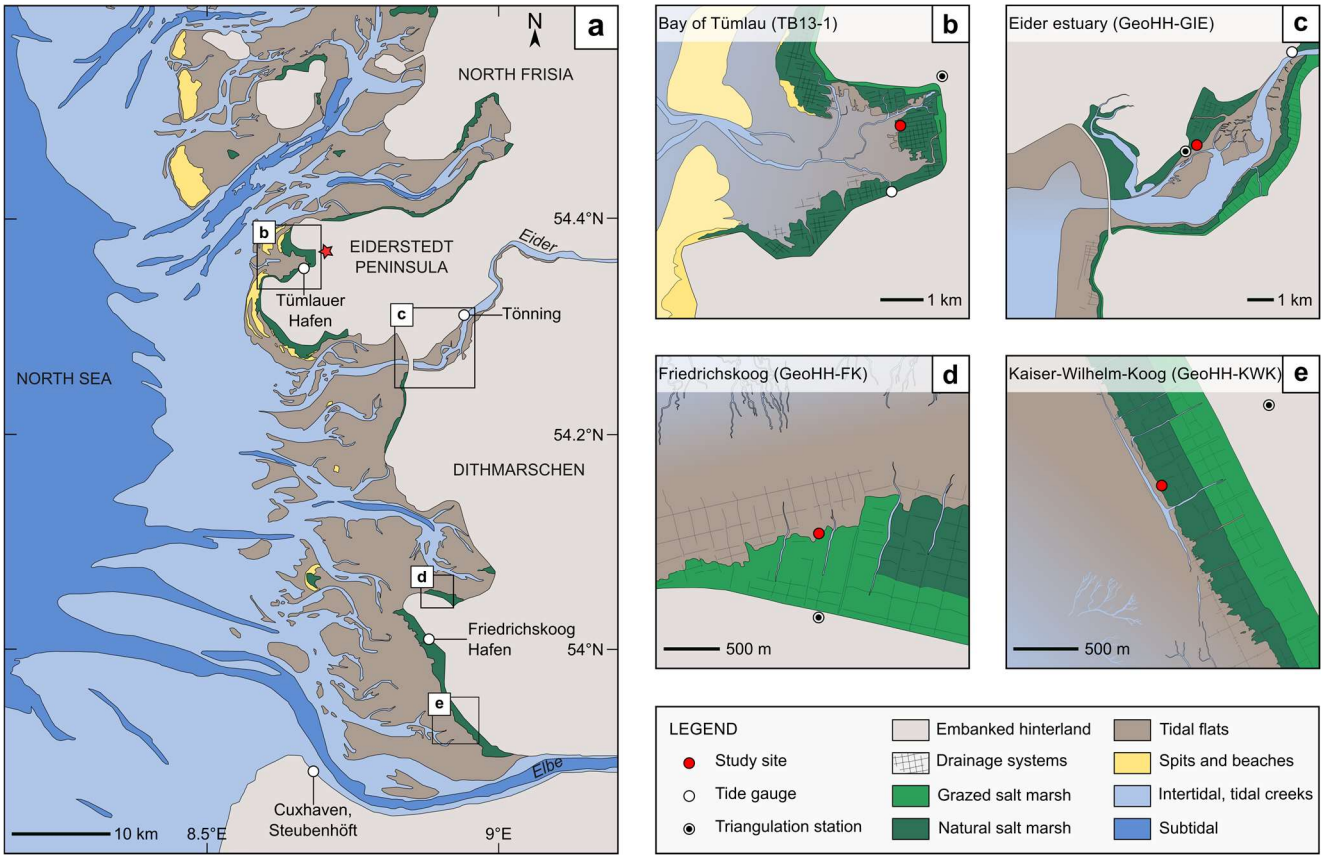

Fig. 4 | Overview of the south-eastern German North Sea coastal region. a) Location of liner core GeoHH-SH02 (red star), the tide gauges, and the study sites (**b**–**e**). The study sites (red dots) encompass different salt-marsh systems: a formerly managed and semi-enclosed coastal salt marsh (**b**; Bay of Tümlau), a semi-natural estuarine salt marsh (**c**; Eider estuary), a managed and grazed coastal salt marsh (**d**; Friedrichskoog), and a formerly managed and highly dynamic open coastal salt marsh (**e**; Kaiser-Wilhelm-Koog). Artificial drainage systems (ditches) are present in all studied salt marshes but have been stepwise abandoned, i.e., in the natural and protected salt-marsh areas after establishment of the Wadden Sea National Park in 1985 CE.

and (4) a formerly drained and highly dynamic open coastal salt marsh (Kaiser-Wilhelm-Koog, GeoHH-KWK, 53°56'4.76"N, 8°54'25.01"E). At each site, erosional cliffs are forming the coastline, in which the recent marsh surfaces vary between 2.05 to 2.90 m above NHN (*Normalhöhennull*, based on the German levelling system DHHN2016). Thus, the present salt-marsh surfaces are located 0.50 to 1.20 m above mean high water springs (MHWS; data provided by the Federal Maritime and Hydrographic Agency of Germany, BSH; Table 1), and are only flooded during storm surges when the mean high water (MHW) is exceeded by water levels ≥ 1.5 m (Gerber et al., 2016). Modern dikes were constructed in 1861 CE (Süderheverkoog) and 1933 CE (Tümlauer Koog), bordering the Bay of Tümlau, 1967–1973 CE in the Eider estuary (construction of the Eider tidal barrier called *Eidersperrwerk*), 1853 CE in Friedrichskoog, and 1873 CE in Kaiser-Wilhelm-Koog (Fischer, 1956, 1957; Ehlers, 1988; Meurer, 2000, and references therein). These embankments prevent a migration of the salt marshes further into the hinterland, likely accelerating the erosion rates at their seaward boundary with ongoing sea-level rise (Kirwan et al., 2016). These erosional cliff sites were chosen as they provide direct access to the marsh-sediment sequences deposited during the past ca. 150 years. The marsh sites themselves were selected to allow a comparison of salt-marsh systems influenced by different external conditions, i.e., exposure to wave energy and flooding dynamics. Sediment delivery at sites TB13-1, GeoHH-FK, and GeoHH-KWK is mainly linked to the anti-clockwise circulation of southern North Sea surface waters and to the Elbe river discharge (Eisma, 1981; Eisma and Kalf, 1987; Winther and Johannessen, 2006). In contrast, site GeoHH-GIE is mainly influenced by the Eider river and beyond, this location is largely cut off from storm-surge flooding since 1973 CE with completion of the Eider tidal barrier. This storm-surge barrier also reduces the natural mixing of fresh and salt waters in the estuary (Wolff et al., 2010).

2.3 Materials and methods

2.3.1 Field work. Fieldwork has been carried out at the North Frisian coast (Eider estuary, site GeoHH-GIE) and Dithmarschen (Friedrichskoog, site GeoHH-FK, and Kaiser-Wilhelm-Koog, site GeoHH-KWK) in November 2016. Salt-marsh sampling in the Bay of Tümlau was conducted by Müller-Navarra et al. (2019) in August 2013. At each site, ten plastic U-channels (with a maximum length of 130 cm, 1.75 cm width, and 2.00 cm depth) were pressed vertically into the cleaned erosional-cliff face at the seaside of the salt marsh. For illustration, see Müller-Navarra et al. (2019). The position and elevation of the salt-marsh surface was surveyed at each site with a mobile Leica Geosystems GNSS field controller (Viva Uno CS10) and referred to a nearby geodetic reference point (triangulation station). Data of the reference surveying stations were provided by the State Office for Surveying and Geoinformation Schleswig-Holstein (LVermGeo SH), comprising the triangulation stations number 1618 031 10 (Bay of Tümlau, 1.46 km distance to site TB13-1, Müller-Navarra et al. 2019), 1719 077 00 (Eider estuary, 0.34 km distance to site GeoHH-GIE), 1919 088 00 (Friedrichskoog, 0.52 km distance to site GeoHH-FK), and 2019 060 10 (Kaiser-Wilhelm-Koog, 1.12 km distance to site GeoHH-KWK; Fig. 4). Post-processing of the measured elevation heights and positions were carried out using the Leica Geo Office 8.3 software package. Standard deviation for the position uncertainty is varying between 0.2 and 0.6 mm, and for the elevation uncertainty between 0.5 and 0.9 mm after raw data processing.

The U-channels were sampled equidistantly in the laboratory, as required for the individual measurements (see Sections 2.3.2 and 2.3.3). From each site, sediments of one U-channel were sampled to measure the anthropogenic Hg concentration, organic carbon (C_{org}) content, and grain-size spectrum. Samples for radionuclide-decay measurements (^{210}Pb, ^{137}Cs) were taken from five U-channels in total, to attain the required sediment volume. Radionuclide and grain-size data together with XRF analyses of site TB13-1 were taken from Müller-Navarra et al. (2019), while Hg and organic carbon concentration levels of site TB13-1 were measured subsequently for this study.

2.3.2 Geochemical analyses. Since the approach of both natural and artificial radionuclides is a widely used method for age dating, but a rather time-consuming technique, only radionuclide analyses of sediment sequences TB13-1 and GeoHH-GIE were conducted in high resolution, while measurements for GeoHH-FK and GeoHH-KWK were performed only on a selected number of samples. For radionuclide-activity measurements, sediments from site GeoHH-GIE were sampled at 1 cm spacing between 0–73 cm depth, comprising sediment slices of 1 cm thickness each. Sediments from the bottom part of the profile (74–127 cm depth) were sampled individually between 2–10 cm spacing. There, the thickness of the single sediment slices has been increased to 2 cm below 82 cm depth. Sampling resolution was reduced, and slice thickness was increased in the lower part of the sequence, because radionuclide activities decrease while counting errors increase with depth, impeding high-resolution dating in the older part of the cores. For sites GeoHH-FK and GeoHH-KWK, sediments were sampled at 14 cm spacing (1 cm slices), resulting in a total of 8 samples

Table 1 | Tidal data at the different study sites, covering the highest astronomical tide (HAT), mean high water (MHW), mean low water (MLW), mean high water springs (MHWS), and mean tidal range. Tidal data for site GeoHH-KWK were calculated based on the average values of the nearest tide gauges Friedrichskoog Hafen and Cuxhaven Steubenhöft. All tidal data are based on the German reference level *Normalhöhennull* (NHN) and were provided by the Federal Maritime and Hydrographic Agency of Germany (BSH). Height of the marsh surface at site TB13-1 was taken from Müller-Navarra et al. (2019).

Site ID	Height [m]	Tide gauge ID	Tide gauge no.	HAT [m]	MHW [m]	MLW [m]	MHWS [m]	Tidal range [m]	Observation Period [yrs CE]
TB13-1	2.09	Tümlauer Hafen	110016	2.00	1.44	–1.73	1.59	3.17	2001–2013
GeoHH-GIE	2.05	Tönning	9520070	1.79	1.37	–1.25	1.49	2.62	1986–2018
GeoHH-FK	2.80	Friedrichskoog Hafen	110021	2.14	1.56	–0.41	1.74	1.97	1986–2018
GeoHH-KWK	2.90	Friedrichskoog Hafen/Cuxhaven Steubenhöft	110021/ 5990020	2.13	1.53	–0.95	1.71	2.48	1986–2018

for site GeoHH-FK, and 9 samples in total for site GeoHH-KWK.

All samples were dried at 38 °C and subsequently ground. Sample weights of the ground material varied between ca. 10–48 g. Each sample was filled up, mixed and homogenised with pure quartz sand accordingly, to attain the required volume of ca. 25 ml per sample (pers. comm. LARI 2017). The down-core radionuclide activities were measured at the Laboratory for Radioisotopes (LARI) of the Georg-August-University of Göttingen, using the coaxial CANBERRA's high-purity Germanium detector (HPGe) with a gamma-spectrometry analysis on energy lines 46.54 keV (^{210}Pb), 661.66 keV (^{137}Cs), 295.21 keV and 351.92 keV (^{214}lead), 609.32 keV (^{214}bismuth), a measurement time of 250 000 s per sample, and a counting rate of 1.62 counts per second. Corresponding counting errors were derived by multiplying the relative statistical counting error, which is the square root of the count rate of the sample and the background counts of the detector, with the measured activity of the sample. Before gamma counting, the samples were filled and sealed in gas-tight containers for four weeks because ^{222}radon (^{222}Rn), a gaseous precursor of ^{214}Pb and ^{214}Bi, can release from an open-air sediment sample. After four weeks (about ten times the half-life of ^{222}Rn) the radioactive equilibrium between ^{222}Rn and ^{226}Ra, and thus ^{214}Pb and ^{214}Bi has established in the sealed samples again. Then, ^{214}Pb and ^{214}Bi were counted for estimating the ^{226}Ra, which provides the supported ^{210}Pb (by ^{226}Ra decay) in the sediment. The unsupported ^{210}Pb, which represents the atmospheric fallout, was calculated by subtracting the supported ^{210}Pb (^{226}Ra) from the total ^{210}Pb activity. Post-processing has been done using the Digital Signal Processing Gamma Ray Spectrometers (DSPEC jr 2.0 and DSPEC Negge) from the ORTEC product lines, together with the gamma-spectroscopy analysis software InterWinner version 6.0. Corresponding uncertainties for the unsupported ^{210}Pb values (δu) where derived from the Gaussian error-propagation calculation, i.e.: $\delta u = \sqrt{(\delta s)^2 + (\delta t)^2}$, with the added uncertainties of the supported ^{210}Pb (δs) and total ^{210}Pb (δt) activities. However, in 21 out of the total 86 samples of site GeoHH-GIE the ^{210}Pb activity, and in 20 samples the ^{137}Cs activity, were below detection limit, and therefore not considered for further calculations. Likewise, in 4 out of the total 9 samples of the sediment sequence GeoHH-KWK the ^{137}Cs activity was below detection limit, so that the corresponding samples were not considered thereafter.

Based on the progressed decay rates since sediment recovery in the field, all radionuclide-activity measurements were decay-corrected to the time of sampling (24 October 2016, GeoHH-KWK; 18 November 2016, GeoHH-FK; 23 November 2016, GeoHH-GIE). Furthermore, and as demonstrated in previous studies (e.g., Ackermann et al., 1983; Cundy and Croudace, 1995; Milan et al., 1995; Kirchner and Ehlers, 1998), some radionuclides (i.e., unsupported ^{210}Pb and ^{137}Cs) strongly correlate with the content of organic matter and fine-grained particles (the so-called grain-size effect). Accordingly, the unsupported ^{210}Pb and ^{137}Cs down-core activities were further corrected to the corresponding sum of the organic carbon content and the portion of the sediment fraction < 20 µm, respectively, and following the previously referred literature.

The constant initial concentration (CIC) model was calculated based on the decay-corrected data only, using the function $C(x) = C(0)e^{-\lambda t}$, including $C(x)$ as present unsupported ^{210}Pb concentration at depth x (and age t), and $C(0)$ as initial unsupported ^{210}Pb concentration, with the ^{210}Pb decay constant $\lambda = 0.03114$ yr^{-1} (Appleby, 2001). The constant rate of ^{210}Pb supply (CRS) model was calculated based on the decay-corrected total and residual unsupported ^{210}Pb radioactivity using the function $A(x) = A(0)e^{-\lambda t}$ after Appleby and Oldfield (1978), assuming a constant atmospheric ^{210}Pb flux incorporated into the sediment. There, $A(0)$ is the total unsupported ^{210}Pb, $A(x)$ the residual unsupported ^{210}Pb from depth x (and age t) to the bottom of the sediment profile. Mass accumulation rates (MAR) derived by the CRS models, were calculated in accordance to: $\mathrm{MAR} = \lambda A(x)/C(x)$, and after Appleby and Oldfield (1978). By taking the cumulative dry mass (m) into account, the sedimentation rate at depth x_n is: $\mathrm{SR} = (x_n - x_{n-1})/((m_n - m_{n-1})/\mathrm{MAR}_n)$. Error estimates of the CRS ages and MAR are also calculated by the Gaussian error propagation formula, using the counting errors of the samples.

Radiocarbon dating (accelerator mass spectrometry, AMS) was carried out at the Beta Analytic Radiocarbon Dating Laboratory, Florida, on shell fragments from 145 cm depth at site GeoHH-GIE (*Limecola balthica*), as well as from 23.5–24.5 cm (mixed shell fragments) and 123 cm (*Cerastoderma edule*) depth at site GeoHH-FK. The shallow and mixed shell-fragment sample was used as a tracer for post-bomb ^{14}C activity to identify whether the shell layer was deposited prior or after atmospheric nuclear weapons testing between 1952 and 1963 CE (Hua and Barbetti, 2004; Reimer et al., 2004; Scourse et al., 2012). AMS ^{14}C ages from the base of the sediment sequences were corrected to a ΔR value of –23 (with a square root error of ±92), which is the regional reservoir-age offset between the global marine ^{14}C calibration curve (Reimer and Reimer, 2017) and the mean ^{14}C pre-bomb ages from the German Bight (54°N, 6°E) derived from *Arctica islandica* shells (Weidman, 1995). The radiocarbon calibration program CALIB (version 7.10; Stuiver and Reimer, 1993) and the calibration curve MARINE13 (Reimer et al., 2013) were used to convert the AMS ^{14}C data into calendar years. The post-bomb ^{14}C sample was calibrated for the Northern Hemisphere atmospheric ^{14}C concentration using the program CALIBomb and the NHZ1 (Northern Hemisphere zone 1) calibration curve (Reimer et al., 2004). ^{14}C activity levels of

> 1.0 were denoted as post-bomb ^{14}C level and expressed as fraction modern ($F^{14}C$), representing a ^{14}C activity of 100%-Modern Carbon (pMC) in the year 1950 CE, following Donahue et al. (1990), Reimer et al. (2004), and Larsen et al. (2017). There, the fraction modern is calculated as $F^{14}C = (^{14}C/^{13}C)_S/(^{14}C/^{13}C)_{STD}$, with the $^{14}C/^{13}C$ ratio of a sample (S) and the $^{14}C/^{13}C$ standard ratio (STD) at 1950 CE, in which both ratios are normalized to $\delta^{13}C = -25‰$ (Donahue et al., 1990; Burr et al., 2001).

Mercury (Hg) measurements were carried out at the Leibniz Institute for Baltic Sea Research Warnemünde (IOW) for all four sediment sequences (TB13-1, GeoHH-GIE, GeoHH-FK, and GeoHH-KWK) at 2 cm spacing and slices of 1 cm thickness each, using the Milestone Company's DMA-80 Direct Mercury Analyzer. Prior to analyses, the samples were freeze-dried for 48 h and ground subsequently. Sample weights for the Hg measurements were around 100 mg. To provide the accuracy of the measurements, a certified reference material (i.e., light sandy soil, Community Bureau of Reference, BCR-142R) and an internal Hg standard (Mecklenburg Bay sediment standard, MBSS-1) were measured regularly after every tenth sample. Obtained Hg maxima values were additionally tested by increasing the measurement resolution up to 1 cm spacing for the corresponding intervals. Measurements were carried out with a decomposition time of 180 s and a temperature of 750 °C for each sample. All modern Hg records were subsequently corrected to the organic carbon content, since Hg is known to be strongly adsorbed by organic matter particles (Leipe et al., 2013).

To determine the natural and preindustrial Hg-background concentration for the regional depositional environment, Hg analyses were additionally carried out on five sediment samples from 207 cm, 209 cm, 212 cm, 214 cm, and 216 cm depth in liner core GeoHH-SH02 from polder Süderheverkoog, Eiderstedt peninsula (Fig. 4a). This core comprises sediments since ca. 1000 yrs BC (Brandt, 2018), thus providing a sequence of most likely uncontaminated coastal sediments deposited prior to land reclamation and embankment, which took place there in 1862 CE (e.g., Ehlers, 1988).

Organic carbon (C_{org}) was measured for the same samples and sites, which were analysed for the ^{210}Pb, ^{137}Cs, and Hg concentrations, using an EuroVector EuroEA3000 Analyser and a measurement time of 200 s per sample. The analytical precision based on replicates was 0.05% on average. For each sample, about 5 mg of the freeze-dried and ground material was weighed into pre-combusted (550 °C) silver capsules. Prior to analysis, all samples were subsequently treated three times with 1 M hydrochloric acid (HCl, Merck Suprapure) to eliminate the inorganic carbon.

Scanning X-ray fluorescence (XRF) spectroscopy was used to generate semi-quantitative element profiles and optical images of the sediment surface for sites GeoHH-GIE, GeoHH-FK, and GeoHH-KWK. Scanning analyses were performed at the Leibniz Institute for Baltic Sea Research Warnemünde (IOW) using an ITRAX Core Scanner with a chromium X-ray source. Generator settings of 30 kV (30 mA), a step size of 1500 µm (GeoHH-GIE and GeoHH-KWK) and 500 µm (GeoHH-FK), and a measuring time of 15 s per step size were applied for the element analyses (XRF scanning).

Abundances of the immobile trace elements zirconium (Zr) and rubidium (Rb) were expressed in terms of logarithmic ratios for all four study sites, following the descriptions of Weltje and Tjallingii (2008). Lithostratigraphic tie points were derived from graphical correlation of prominent long-term trends between the single ln(Zr/Rb) records. Optical images and extracted dark/light colour-changes of the sediment sequences were used to provide further high-resolution sediment characteristics for all sites. This enables an additional correlation between the different sediment sequences, based on their internal characteristics.

2.3.3 Sedimentological and statistical analyses. For grain size measurements, one U-channel each from sites GeoHH-GIE, GeoHH-FK, and GeoHH-KWK was sampled at 0.5 cm spacing. All samples were stepwise treated with 10–30% hydrogen peroxide (H_2O_2) to remove the organic remains, as well as with 1 M acetic acid (CH_3COOH) to dissolve the carbonate components. The remaining carbonate-free material was wet-sieved over a 2000 µm screen to remove very coarse particles. Measurements were performed using a HELOS KF Magic Laser particle-size distribution analyser, covering a potential particle-size range of 0.5 to 3500 µm, in which an intern silicon carbide (SiC) standard was measured regularly after every twentieth to fiftieth sample. Grain-size quantification (i.e., mean grain size) was based on the methods described by Folk and Ward (1957) and calculated using the software GRADISTAT version 8.0 (Blott and Pye, 2001). The grain-size spectrum of each site was measured for correcting the radionuclide activity to the fine fraction (< 20 µm), and to compare the mean grain-size variability (M_G) with the ln(Zr/Rb) records, to test the reliability of this element ratio as a proxy for relative changes in the particle size.

For estimating nonparametric associations between the ln(Zr/Rb) ratios and mean grain sizes for all sediment sequences, Spearman's rank correlation coefficients (Spearman's rho) were calculated accordingly. Prior to the statistical analysis, the ln(Zr/Rb) records were rescaled with Δdepth = 1 cm (TB13-1) and Δdepth = 0.5 cm (GeoHH-GIE, GeoHH-FK, GeoHH-KWK) by using the software AnalySeries 2.0 (version 5/2005; Paillard et al., 1996). To test whether the Spearman's rho correlation of the ranked

data is significant or not, *p*-values were calculated subsequently.

2.4 Results

2.4.1 Sediment composition and description. The sediment sequences at all sites represent typical marsh soils of tidal origin, i.e., gleyic fluvisols (calcaric). They exhibit almost evenly spaced horizontal laminations, in which the single layers mainly alternate between sandy and silty sediment. There, the thickness of the single laminated layers varied between a few millimetres to several centimetres. Based on this observation, it can be assumed that each sequence has almost no disturbances caused by bioturbation, except for the uppermost interval at site GeoHH-GIE, where the thickness and horizontal extent of the single layers is rather uneven (between ca. 13–32 cm), together with a larger rooted humus horizon and soil genesis (above 13 cm; see Appendix Fig. B1). The sediment lamination at all sites is interpreted as a typical result of sediment deposition caused by a combination of periodical storm surges and tides, also known as *Grodenschichtung* (e.g., Reineck, 1982), which are responsible for a continuous sediment delivery and accumulation of reworked material from the adjacent tidal flats and salt-marsh cliffs (e.g., Turner et al., 2006; Schuerch et al., 2012, 2013, 2019). Furthermore, at site GeoHH-FK (Friedrichskoog) a single shell layer was present at around 24 cm depth below the marsh surface, mainly containing well-preserved gastropods (*Hydrobia ulvae*) and bivalve shell fragments (mainly *Cerastoderma edule*). At site GeoHH-GIE (Eider estuary), a similar layer was observed at 46 cm depth.

2.4.2 Geochemistry. Generally, the organic carbon (C_{org}) records reveal relatively low values, but with pronounced maxima in the uppermost 10 to 30 cm of all four sediment sequences (see Appendix Fig. B2). C_{org} contents vary between 0.13% to 1.96% at site TB13-1, between 0.07% and 7.44% at site GeoHH-GIE, between 0.15% and 2.30% at GeoHH-FK, and between 0.07% and 2.12% at site GeoHH-KWK.

Sediments at site TB13-1 show unsupported ^{210}Pb activity variations from approximately zero to 18.70 Bq kg^{-1} (Müller-Navarra et al., 2019), in which uncertainties vary between ±1.26 Bq kg^{-1} to ±4.49 Bq kg^{-1} of the Gaussian error-propagation estimation. In comparison, the activity levels of the unsupported ^{210}Pb decay-corrected data vary between –5.45 Bq kg^{-1} to 58.97 Bq kg^{-1} at site GeoHH-GIE, while Gaussian error-propagation estimates show uncertainties between ±6.41 Bq kg^{-1} and ±24.94 Bq kg^{-1}. Although not perfectly exponential, both sediment sequences show the expected decrease of unsupported ^{210}Pb with depth (see Appendix Fig. B3). In contrast, sites GeoHH-FK and GeoHH-KWK exhibit comparatively low activities for the unsupported ^{210}Pb. There, activity levels show variations between 1.89 Bq kg^{-1} and 20.58 Bq kg^{-1} at site GeoHH-FK, with fluctuations of the Gaussian error-propagation estimates between ±10.61 Bq kg^{-1} and ±13.77 Bq kg^{-1}. Similarly, at site GeoHH-KWK, the unsupported ^{210}Pb activities vary between 3.06 Bq kg^{-1} and 19.12 Bq kg^{-1}, with error estimates between ±9.57 Bq kg^{-1} and ±15.81 Bq kg^{-1} for the Gaussian error propagation. The selected samples of GeoHH-FK and GeoHH-KWK show only slightly decreasing trends of the unsupported ^{210}Pb activities with increasing sediment depths, comprising various outliers (see Appendix Fig. B4). After correcting the unsupported ^{210}Pb values to the sum of the fine fraction and organic carbon (C_{org}), only the corrected radionuclide data at site TB13-1 trace almost the same general downward trend as for the initial raw data (Fig. 5). As opposed to it, data correction resulted in a smoothing of the initial trend at site GeoHH-GIE, while corrected data of sites GeoHH-FK and GeoHH-KWK display a reversed downward trend relative to the initial raw data (Fig. 5).

The total ^{210}Pb activity varies between 17.13 Bq kg^{-1} and 46.72 Bq kg^{-1} at site TB13-1, with counting errors ranging from ±1.31 Bq kg^{-1} to ±4.61 Bq kg^{-1} (Müller-Navarra et al., 2019), and at site GeoHH-GIE between 12.96 Bq kg^{-1} and 73.75 Bq kg^{-1}, with counting errors between ±6.28 Bq kg^{-1} and ±24.55 Bq kg^{-1}. Both records (TB13-1, GeoHH-GIE) show decreasing activities of the total ^{210}Pb with depth (see Appendix Fig. B3). Samples of sediment sequence GeoHH-FK reveal fluctuations of the total ^{210}Pb, ranging from 38.49 Bq kg^{-1} to 57.31 Bq kg^{-1}, with uncertainties varying between ±9.22 Bq kg^{-1} and ±12.78 Bq kg^{-1}. Similar results are obtained for site GeoHH-KWK, where the total ^{210}Pb varies between 33.56 Bq kg^{-1} and 61.93 Bq kg^{-1} throughout the entire sediment sequence. There, uncertainties range between ±8.49 Bq kg^{-1} and ±14.04 Bq kg^{-1}. The total ^{210}Pb concentrations in sequences GeoHH-FK and GeoHH-KWK reveal similar patterns with slightly decreasing values with increasing depth (see Appendix Fig. B4).

The supported ^{210}Pb (^{226}Ra) slightly increases downwards with activities between 13.96 Bq kg^{-1} and 39.50 Bq kg^{-1} at site TB13-1, while counting errors range between ±0.32 Bq kg^{-1} and ±1.04 Bq kg^{-1} (Müller-Navarra et al., 2019), and between 9.01 Bq kg^{-1} and 28.40 Bq kg^{-1} at site GeoHH-GIE, with counting errors between ±1.27 Bq kg^{-1} and ±5.40 Bq kg^{-1} (see Appendix Fig. B3). In comparison, general higher supported ^{210}Pb activity levels are obtained for the other sites, showing variations between 27.65 Bq kg^{-1} and 40.48 Bq kg^{-1} at site GeoHH-FK, and between 17.15 Bq kg^{-1} and 47.46 Bq kg^{-1} at site GeoHH-KWK. Both sites show a rather weak down-core decrease of the supported ^{210}Pb (see Appendix Fig. B4). The corresponding counting errors range from ±4.74 Bq kg^{-1} to ±5.60 Bq kg^{-1} at GeoHH-FK, and from ±3.88 Bq kg^{-1} to ±7.28 Bq kg^{-1} at GeoHH-KWK.

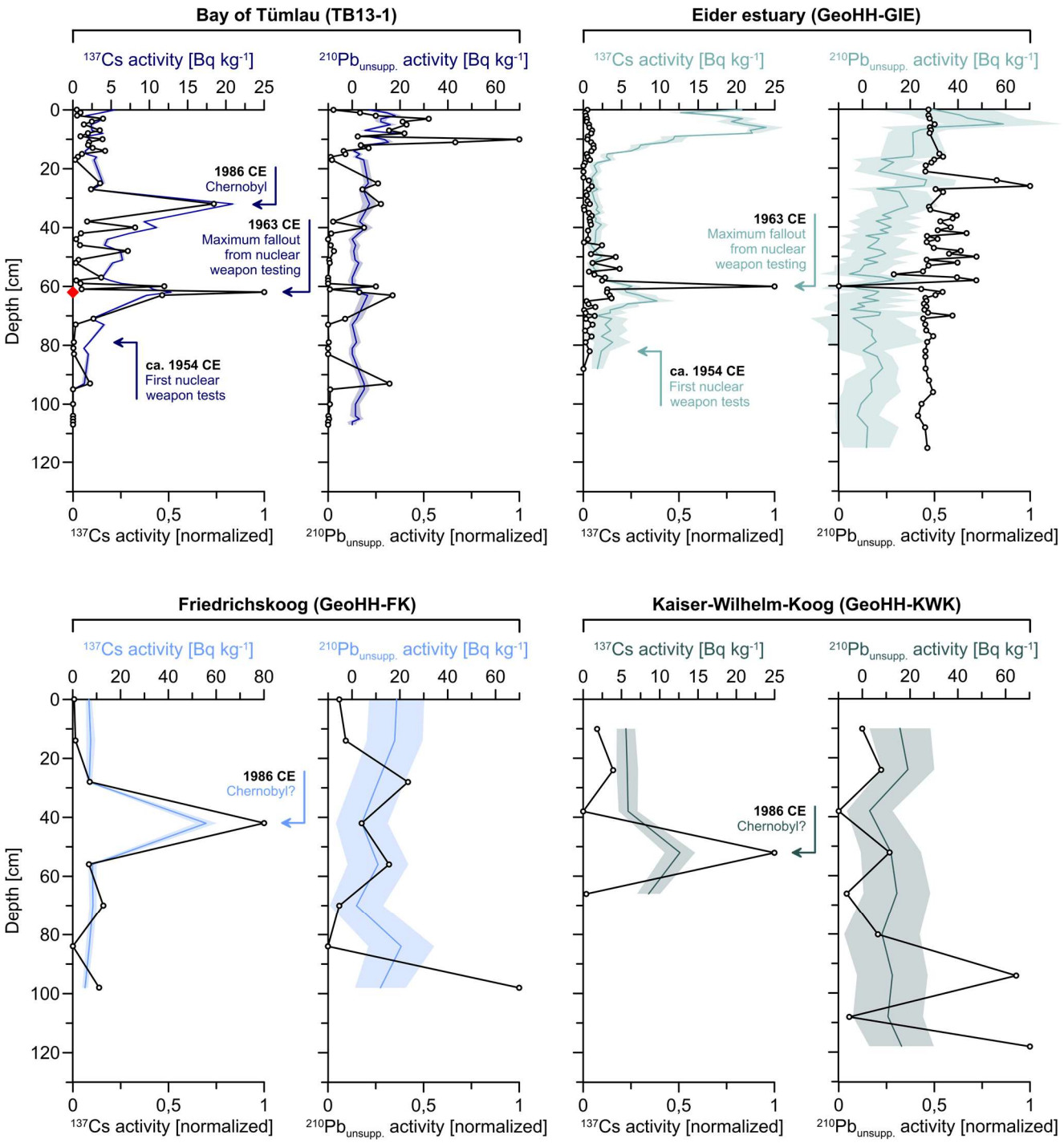

Fig. 5 | Down-core radionuclide activities. Natural (unsupported ^{210}Pb) and artificial (^{137}Cs, ^{241}Am) radionuclide activities in sediment sequences TB13-1 (Bay of Tümlau, dark blue; Müller-Navarra et al., 2019), GeoHH-GIE (Eider estuary, light green), GeoHH-FK (Friedrichskoog, light blue), and GeoHH-KWK (Kaiser-Wilhelm-Koog, dark green). Black lines represent both corrected unsupported ^{210}Pb and ^{137}Cs, i.e., normalized to the sum of organic carbon and the grain-size fraction < 20 µm. Counting errors and Gaussian error-propagation estimates for the uncorrected activities are shown as shaded areas. The red symbol denotes the distinct ^{241}Am activity peak in sediment sequence TB13-1.

For ^{137}Cs, two distinct ^{137}Cs activity maxima could be identified at 32 cm (20.90 Bq kg^{-1}) and 62 cm depths (12.83 Bq kg^{-1}) in TB13-1 (Müller-Navarra et al., 2019), and in GeoHH-GIE at 6 cm (23.88 Bq kg^{-1}) and 65 cm depths (9.63 Bq kg^{-1}; Fig. 5). In TB13-1, the deeper ^{137}Cs maximum at 62 cm depth is in line with the ^{241}Am peak (Müller-Navarra et al., 2019). Counting errors on the 661.66 keV line (^{137}Cs) reveal uncertainties ranging between ±0.17 Bq kg^{-1} and ±0.99 Bq kg^{-1} for TB13-1, and between ±0.51 Bq kg^{-1} and ±2.39 Bq kg^{-1} for GeoHH-GIE. Only one ^{137}Cs activity maximum could be identified at sites GeoHH-FK (at 42 cm depth with 55.77 Bq kg^{-1}) and GeoHH-KWK (at 52 cm depth with 12.64 Bq kg^{-1}; Fig. 5). Counting errors vary between ±1.15 Bq kg^{-1} and ±4.48 Bq kg^{-1} at GeoHH-FK, and between ±1.20 Bq kg^{-1} and ±1.99 Bq kg^{-1} at GeoHH-KWK. Due to the deviating high ^{137}Cs concentration at 42 cm depth at site GeoHH-FK, this sample has been measured twice to exclude a possible analytic error, but almost the same concentration was derived in the second run. After normalising to the fraction < 20 µm and C_{org}, the ^{137}Cs records reveal almost the same distribution patterns as for the decay-corrected activity (initial raw data). The only exception appears at site GeoHH-GIE, where the upper ^{137}Cs peak around 6 cm depth disappeared after normalisation due to the high C_{org} content (up to 7.44%) in the same interval (Fig. 5).

Both the constant initial concentration (CIC) and the constant rate of ^{210}Pb supply (CRS), as well as a composite of both models were tested to calculate sediment ages. Concerning site GeoHH-GIE, neither of the ^{210}Pb-based models could be validated against the ^{137}Cs time markers for Chernobyl (1986 CE) and to the time of highest fallout of ^{137}Cs prior to the banning of nuclear bomb testing in 1963 CE (see Appendix Fig. B5). Since both GeoHH-FK and GeoHH-KWK do not show an obvious down-core decrease of the unsupported ^{210}Pb activity, which is required for the ^{210}Pb-based age-model calculations (CIC, CRS), none of these models could be derived from the data. Accordingly, due to the substantial uncertainties of the ^{210}Pb-based models, the radiometric age models for the sediment sequences at GeoHH-FK, GeoHH-KWK, but also at GeoHH-GIE are mainly based on the ^{137}Cs time markers. The sedimentation rates (SR) obtained from the CRS-model calculations vary between 0.21 cm yr^{-1} and 11.66 cm yr^{-1} (1.84 cm yr^{-1} on average) at site GeoHH-GIE, and between 0.05 cm yr^{-1} and 14.14 cm yr^{-1} (2.17 cm yr^{-1} on average) at site TB13-1. Observed mean mass accumulation rates (MAR), which are likewise based on the CRS calculations (Appleby and Oldfield, 1978), are 2.09 g cm^{-2} yr^{-1} at site TB13-1 and about 2.20 g cm^{-2} yr^{-1} at site GeoHH-GIE (see Appendix Fig. B5).

Results of the radiocarbon analysis reveal a calibrated age of 1565 CE ±195 yrs for the base of the sequence at site GeoHH-GIE. Shell fragments from 123 cm depth in sediment sequence GeoHH-FK delivered a calibrated age of 1670 CE ±220 yrs. ^{14}C analysis of the sample from 23.5–24.5 cm depth in sequence GeoHH-FK exhibits a fraction modern value of F^{14}C = 1.2204 ±0.0046, in which the 2σ ranges give two distinct median probabilities for the post-bomb age (1960.08 CE ±0.77 yrs and 1985.21 CE ±0.91 yrs).

Despite short-term variability, the uncorrected mercury (Hg) raw data exhibit two distinct concentration maxima at all sites, with gradual decreasing values towards the top of the sequences (Fig. 6). There, Hg concentrations vary between 52.43 µg kg^{-1} and 314.65 µg kg^{-1} at TB13-1, between 13.77 µg kg^{-1} and 227.69 µg kg^{-1} at GeoHH-GIE, between 32.74 µg kg^{-1} and 324.73 µg kg^{-1} at GeoHH-FK, and between 43.00 µg kg^{-1} and 604.54 µg kg^{-1} at GeoHH-KWK. Although the maximum Hg concentration of 604.54 µg kg^{-1} at site GeoHH-KWK is found in 18 cm sediment depth, two secondary Hg concentration maxima of about 284.78 µg kg^{-1} and 308.33 µg kg^{-1} are located in the lower part of this sequence. After correcting the Hg concentration to the organic carbon content, the two bottom-most maxima are more pronounced at sites TB13-1, GeoHH-FK, and GeoHH-KWK. At site GeoHH-GIE, Hg values are generally high after normalisation to C_{org} and evenly distributed within an interval of ca. 80 cm sediment. Corrected Hg concentration maxima are observed at 50 cm and 86 cm depths in sequence TB13-1, at 60 cm and between 82 and 96 cm depths in sequence GeoHH-GIE, at 63 cm and 82 cm depths in profile GeoHH-FK, and at 92 cm and 111 cm depths in sequence GeoHH-KWK (Fig. 6). Hg concentrations of core GeoHH-SH02.2, representing pre-industrial polder sediments, exhibit natural Hg background levels between 4.02 µg kg^{-1} and 25 µg kg^{-1}.

The ln(Zr/Rb) records reveal high-frequency variability at the millimetre scale, but also quasi-periodic changes at the centimetre to decimetre scale (Fig. 7). The ln(Zr/Rb) records of sediment sequences TB13-1 and GeoHH-FK show quasi-periodic changes below 50 cm and 60 cm sediment depth, respectively, while the upper parts being characterized by rather high-frequent fluctuations (Fig. 7). At both sites, the ln(Zr/Rb) values slightly increase upwards. The ln(Zr/Rb) values of sequence GeoHH-GIE exhibit a gradual upwards increase between 127 cm and ca. 35 cm depth, with more or less regular changes at the cm to dm scale. Above ca. 30 cm depth, the ln(Zr/Rb) values abruptly drop down to around 1, remaining constantly low towards the marsh surface (Fig. 7). At site GeoHH-KWK the ln(Zr/Rb) ratio exhibits an increasing trend from the base towards the middle part, with strongest fluctuations between 50 cm and 85 cm depth. Subsequently, there is a decreasing trend towards the top of the sequence.

2.4.3 Sedimentology. The grain-size spectra of the sediment sequences at sites TB13-1 and GeoHH-FK reveal a general coarsening trend towards the marsh surface, with

bulk mean grain-size (M_G) variations between 16.58 µm to 95.30 µm in sequence TB13-1, and between 45.11 µm to 103.85 µm in sequence GeoHH-FK (Fig. 7, Appendix Fig. B6). In sequence GeoHH-GIE, the particle size distribution is rather fluctuating, with M_G ranging between 11.90 µm and 90.65 µm. At this site, a fine-grained interval with a mean grain size of 35.05 µm can be observed between 19 and 23 cm depth. The M_G spectrum varies between 37.69 µm and 84.68 µm in sequence GeoHH-KWK, lacking a consistent long-term trend (see Appendix Fig. B6).

Spearman's correlations between ln(Zr/Rb) and mean grain size exhibit a moderate to low correlation for all sites with 0.43 (TB13-1), 0.42 (GeoHH-GIE), 0.24 (GeoHH-FK) and –0.16 (GeoHH-KWK), while *p*-values of < 0.05 indicating statistical significance for all correlations.

2.5 Discussion

2.5.1 Radionuclide-based dating in coastal environments. The radionuclide-based dating of modern salt-marsh sediments has been widely used to investigate regional sediment-accumulation rates (e.g., Van Weering et al., 1987; Allen et al., 1993; Kirchner and Ehlers, 1998; Andersen et al., 2000, 2011; Pedersen and Bartholdy, 2006; Schuerch et al., 2012; Nolte et al., 2013a; Mueller et al., 2019). With respect to the ^{210}Pb-based age-model applications, deviations in the expected exponential down-core activity decline of the unsupported ^{210}Pb are commonly ascribed to variations in the sedimentation rate, following the assumptions for the CRS model (constant rate of unsupported ^{210}Pb supply; Appleby and Oldfield, 1978). Accordingly, the strong variations in the quasi-exponential unsupported ^{210}Pb decline at sites TB13-1 and GeoHH-GIE can be attributed to the periodical input of reworked sediment material, i.e., rapid sedimentation events. Similar effects of deviating low ^{210}Pb values were also described by Kirchner and Ehlers (1998) and Andersen et al. (2011), who indicated storm surges as a possible explanation for the lateral supply of re-suspended sediment particles and rapid deposition on the salt-marsh surface. Moreover, the detection of low ^{210}Pb concentrations within those sediment samples containing lateral incorporated 'older' sediments may be problematic, since most of the ^{210}Pb in this fraction may be already decayed (Kirchner, 2011). At less wave-exposed sites, as we have nowadays in the Eider estuary, the incorporation of reworked material during storm surges is expected to be low, favouring the application of radionuclide-based age reconstructions. However, the uppermost ca. 13 cm of GeoHH-GIE sediments represent an intensely rooted soil horizon, which developed a consequence of the Eider tidal barrier construction, and is characterized by high organic matter concentrations of up to 7%. This high C_{org} content likely accounts for the deviating high ^{210}Pb values in the uppermost ca. 30 cm interval of sequence GeoHH-GIE (see Appendix Fig. B1), since the atmospheric ^{210}Pb incorporated portion is well adsorbed to organic matter. Besides that, the pre-tidal barrier sequence clearly contains sediment layers rich in reworked material, thus reducing the reliability of the CRS model. Moreover, the counting errors for the 46.54 keV line (^{210}Pb) are high (24.60% to 103.80%), which is also the case for the high calculated Gaussian error-propagation estimates. Consequently, ^{210}Pb-based age estimates and corresponding sediment-accretion rates for GeoHH-GIE are associated with relatively high uncertainties. The results indicate that the application of CRS models should be used with caution in highly dynamic salt-marsh environments, considering the specific local depositional setting. CRS-based sedimentation rates of 2.17 cm yr^{-1} on average at site TB13-1 and 1.84 cm yr^{-1} at site GeoHH-GIE are, indeed, higher than those derived from integrated stratigraphic approach at the same sites (see Section 2.5.4) and also higher as reported for other sites of Dutch to German salt marshes (1.16 cm yr^{-1} on average; Nolte et al., 2013a). Observed mass accumulation rates (MAR), which are also based on the CRS calculations (Appleby and Oldfield, 1978), are 2.09 g cm^{-2} yr^{-1} at site TB13-1 and about 2.20 g cm^{-2} yr^{-1} at site GeoHH-GIE. The finding, that ^{210}Pb-derived ages are difficult in this environment, is in line with the unsupported ^{210}Pb activities at sites GeoHH-FK and GeoHH-KWK, which show rather strong fluctuations than the expected down-core decrease. In this case, it is apparently reinforced by their exposed location in a more open coastal salt-marsh setting, where the relocation of reworked sediment material might be particularly strong, at least at site GeoHH-KWK.

Distinct ^{137}Cs activity maxima could be identified at all sites, providing time markers for the stratigraphic model. The first relevant increases in the ^{137}Cs activity, starting from ca. 79 cm in TB13-1 and from ca. 82 cm depth in GeoHH-GIE, likely reflect the onset of nuclear bomb tests in 1954 CE (Fig. 5). This is in line with previous studies, documenting first significant ^{137}Cs activity levels since 1954 CE (Pennington et al., 1973; Kirchner and Ehlers, 1998; Appleby, 2001). Although a minor ^{137}Cs activity increase was already observed at 93 cm depth in TB13-1, a post-depositional migration of the ^{137}Cs in the sediment is rather likely for this section (Appleby et al., 1991), since the particle-reactive ^{137}Cs can be released from particles and diffuse with the sediment pore-water under anoxic conditions (Comans et al., 1989; Wang et al., 2017). Indications for anoxic conditions at sites TB13-1 as well as GeoHH-GIE can be derived from the greyish to blackish sediment colour in the bottom-most part of the sequences (see Appendix Fig. B1), which has been pedologically identified as reduced intervals with groundwater influence. This concerns especially the intervals below ca. 100 cm depth at site TB13-1 and below ca. 110 cm depth at site

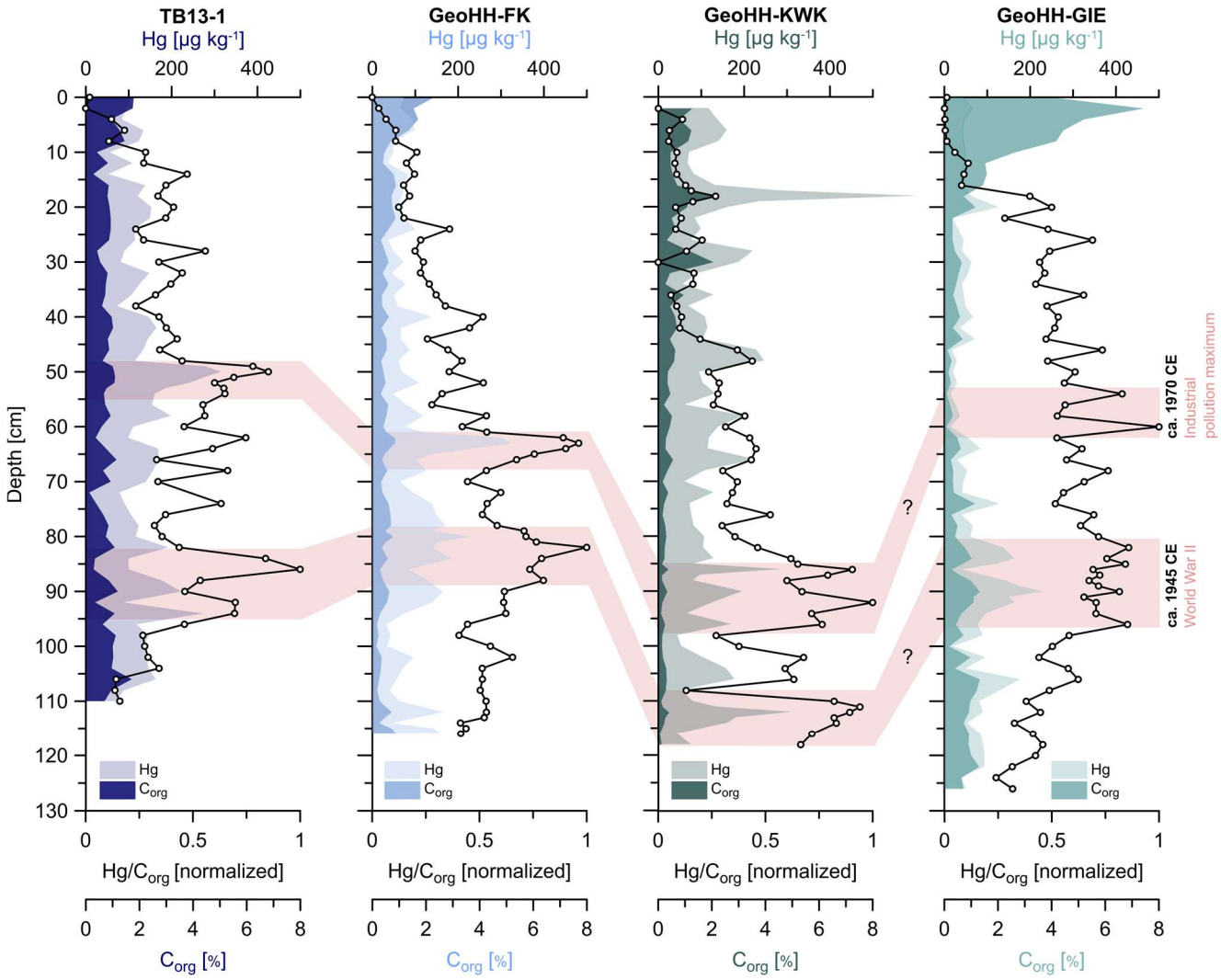

Fig. 6 | Mercury inventory of North Sea salt-marsh archives. Mercury (Hg) concentration levels corrected to organic carbon (C_{org}) changes (black lines), as well as uncorrected Hg records together with C_{org} concentrations in sediment sequences from the Bay of Tümlau (TB13-1, dark blue), Friedrichskoog (GeoHH-FK, light blue), Kaiser-Wilhelm-Koog (GeoHH-KWK, dark green), and Eider estuary (GeoHH-GIE, light green). Pale red bars indicate maximum pollution levels during industrial time and World War II (e.g., Hylander and Meili, 2003; Leipe et al., 2013; Moros et al., 2016).

GeoHH-GIE; however, the change from the oxygenated to anoxic interval is gradual and lacks a clear boundary. Accordingly, for the lower parts of both the TB13-1 and GeoHH-GIE sequences a downward migration of remobilised ^{137}Cs appears likely. Minor ^{137}Cs peaks at 73 cm (TB13-1) and 75 cm (GeoHH-GIE) depths may be attributed to the Sellafield fire in 1957 CE. In addition, authorized liquid discharges by the reprocessing plants (Sellafield and La Hague) may have contributed to a similar high ^{137}Cs contamination, entering the North Sea basin on the main pathway of the anti-clockwise circulating water masses (Kautsky, 1987; Beks, 2000; Aarkrog, 2003; Cundy et al., 2002). There, maximum discharges occurred between the 1970s and early 1980s at Sellafield (Dunster, 1998; Aarkrog, 2003), and during the early 1980s at La Hague (Cundy et al., 2002). However, minor quantities of ^{137}Cs in salt-marsh sediments from the German North Sea coast cannot be clearly attributed to either the Sellafield fire (gaseous release) or the reprocessing plant effluences (liquid discharges), and earlier evidence for the Sellafield fire in salt-marsh sediments from the island of Sylt has only been hypothesized (Ehlers et al., 1993). Moreover, Gallagher et al. (2005) described contaminations by the Sellafield fire as being overprinted by the nuclear weapon testing phase during the same time, at least for lake sediments at the Irish east coast. Instead, the lower distinct ^{137}Cs activity maxima at 62 cm (TB13-1) and 65 cm (GeoHH-GIE) depth, each around 10–13 Bq kg^{-1}, represent the maximum of atomic

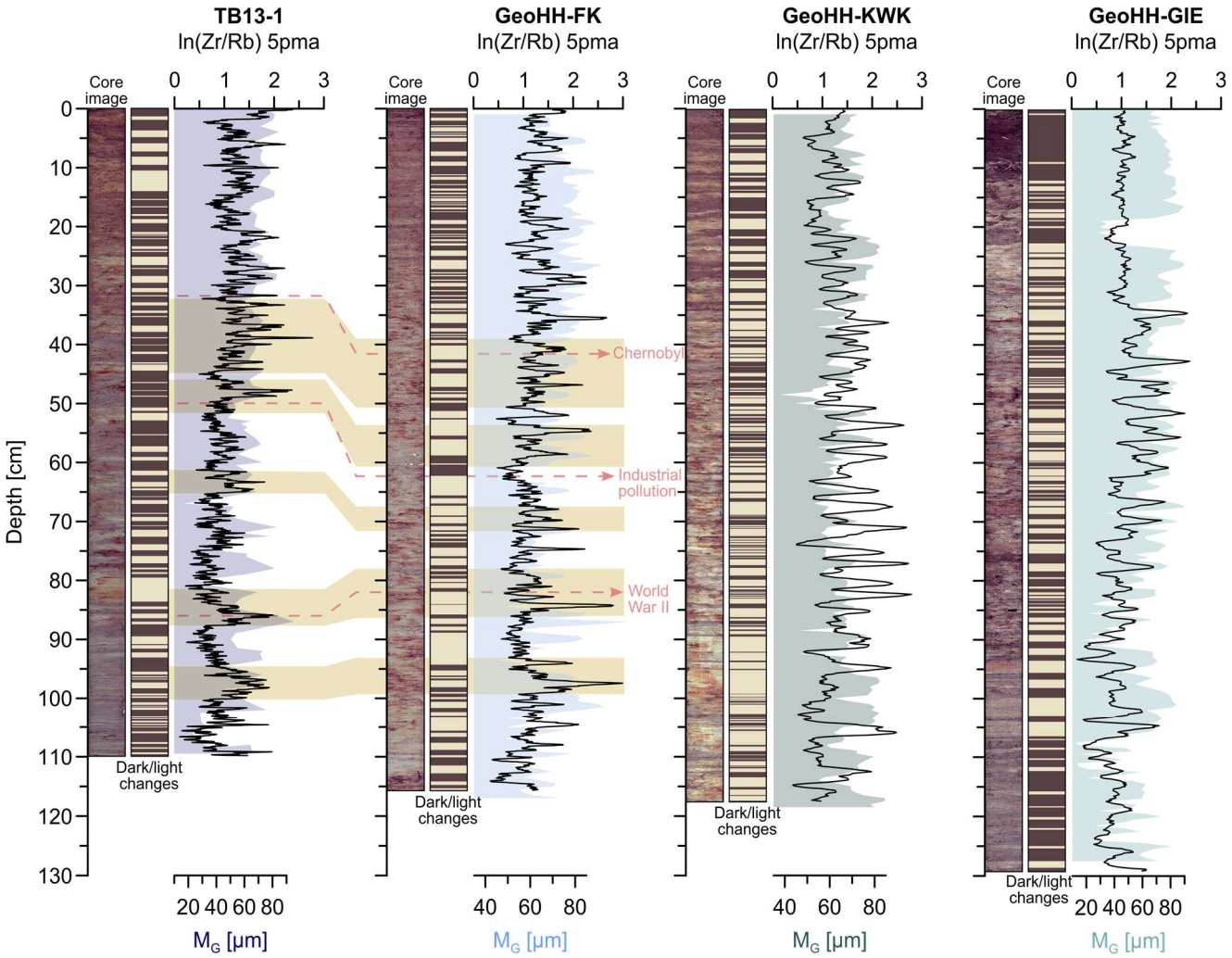

Fig. 7 | Trends in the relative grain-size composition and generalized sediment stratification. Down-core distribution of the ln(Zr/Rb) ratios at the different salt-marsh sites (black lines), together with variations in the grain-size spectrum (shaded areas in the background), optical sediment-sequence images (carried out with the ITRAX Core Scanner), and derived dark/light changes. Data of TB13-1 are from Müller-Navarra et al. (2019). Yellow bars indicate potential stratigraphic tie points for inter-correlation between sites TB13-1 and GeoHH-FK, while pale-red dashed lines represent the time markers which were documented for both sequences: two mercury (Hg) maxima, ascribable to the end of World War II in 1945 CE and the industrial pollution maximum around 1970 CE, and the nuclear power plant accident in Chernobyl 1986 CE (^{137}Cs peak). The given 5pma (5-point moving average) is averaging sediment intervals of 0.10 cm (TB13-1), 0.20 cm (GeoHH-FK), and 0.60 cm (GeoHH-KWK, GeoHH-GIE) thickness.

bomb tests in 1963 CE (e.g., Simon et al., 2006). This finding is supported by low ^{137}Cs activities, which are generally approaching zero below this initial peak at both sites. The ^{137}Cs peak at 62 cm depth at site TB13-1 also coincides with a maximum in the ^{241}Am activity, confirming the time of maximum fallout from nuclear weapon testing, since ^{241}Am is known to exhibit a less post-depositional mobility in the sediment than ^{137}Cs (Appleby et al., 1991). The identification of ^{137}Cs peaks in the sediment sequences at sites GeoHH-FK and GeoHH-KWK appears ambiguous, since the peaks are less distinct and values are slightly decreasing with depth below the peaks. In addition, both peaks are located in similar sediment depths (at 42 cm, GeoHH-FK; 52 cm, GeoHH-KWK) as at the other study sites, suggesting a relation to the maximum fallout by nuclear weapon testing. On the other hand, the maximum activity (55.77 Bq kg^{-1}) of the ^{137}Cs peak at GeoHH-FK is comparable to values measured in salt marshes of the Netherlands (around 55 Bq kg^{-1} in Noord Friesland Buitendijks), which have been linked to the Chernobyl accident in 1986 CE (Nolte et al., 2013a). Assignation of the ^{137}Cs peak at site GeoHH-FK to the Chernobyl accident would be consistent with the upper

mercury (Hg) peak at 63 cm of this site, which is appearing below the ^{137}Cs peak and can be attributed to the high pollution impacts around 1970 CE (see Section 2.5.2). The same sequence of peaks is observed at site GeoHH-KWK, in which the ^{137}Cs peak appears stratigraphically above the 1970s Hg maximum (at 92 cm), and can thus be also assigned to the Chernobyl accident. Similarly, the upper and more pronounced ^{137}Cs activity maximum, appearing at 32 cm depth at site TB13-1, can be likewise assigned to the Chernobyl accident in 1986 CE (Müller-Navarra et al., 2019). A comparable ^{137}Cs maximum of > 20 Bq kg^{-1} was also identified in surficial sediments of sequence GeoHH-GIE (at around 6–7 cm depth), but this peak vanished after correcting the ^{137}Cs data to grain size and organic carbon. Therefore, it is likely not representing the Chernobyl accident, but is rather caused by adsorption of radionuclides to organic matter in this interval (up to ca. 7% C_{org}). Again, the high organic matter content of this interval reflects the change of sedimentation processes due to the construction of the Eider tidal barrier (Eidersperrwerk) in 1967–1973 CE. After barrier construction, storm-tide impacts were purposely decreased, and water turbulence and sediment delivery to the salt marshes changed considerably in the estuary. The decrease of tidal ranges is documented at the tide gauge in Tönning, recording minimum levels around 1980 CE (Wolff et al., 2010). At site GeoHH-GIE, the corresponding change in sedimentation is also reflected by the abrupt drop of ln(Zr/Rb) values at around 30 cm depth and sustained low values above (see Section 2.5.3). The anthropogenic regime change is thus already documented at 30 cm depth at this site, while organic matter increased subsequently. In addition, soil genesis and accompanying plant root development may have disturbed the upper part of the GeoHH-GIE sequence as well. Hence, the CRS model provides plausible ages and sedimentation rates for the lower, less disturbed part of the sequence, giving an age of 1965 CE for the ^{137}Cs peak at 65 cm depth. Instead, the CRS model fails to provide reasonable ages for the upper, more disturbed part of the sediment sequence.

In intertidal environments, shells are frequently eroded from older sediments and subsequently re-deposited, and thus may provide deviant ^{14}C ages (Hadler et al., 2018). Accordingly, radiocarbon samples from the base of sequences GeoHH-GIE (1565 CE ±195 yrs) and GeoHH-FK (1670 CE ±220 yrs) reveal probably too old ages in addition to large precision errors of ±195 and ±220 yrs. In contrast, the age of the post-bomb ^{14}C sample from sequence GeoHH-FK (1985 CE ±0.91 yrs), which appears stratigraphically above the industrial Hg concentration maximum (at 63 cm depth, ca. 1970 CE), appears more reliable. Based on the Hg contamination history, the second median probability result of about 1960 CE ±0.77 yrs can be excluded. However, since the shell layer at site GeoHH-FK appeared 18 cm above the ^{137}Cs activity maximum (at 42 cm depth), which was related to the nuclear power plant accident in Chernobyl in 1986 CE, the 'older' ^{14}C age of 1985 CE at a shallower depth is likewise questionable. The shell layer at site GeoHH-FK was probably deposited during one of the extreme North Sea storm surges of the late last century, in which the corresponding mollusc specimens were already dead and deposited in the tidal flat for some time before they became reworked and re-deposited. Since the shell layer contains a high concentration of well-preserved and fragile bivalve and gastropod shells, it indicates deposition during a single event and rapid burial by subsequent sediments rather than accumulation over a longer time interval, which would have resulted in fragmentation and dissolution. A similar explanation can be assumed for the shell layer at ca. 46 cm depth of site GeoHH-GIE. However, since this layer is stratigraphically framed by the deeper ^{137}Cs bomb peak (at 65 cm depth) and the shallower abrupt drop of ln(Zr/Rb) values (at around 30 cm depth), it was likely deposited during one of the extreme storm-surge events in the late 1960s before the Eider tidal barrier was completed in 1973 CE. In summary, the application of both pre-bomb and post-bomb ^{14}C dating in highly dynamic coastal wetlands appears problematic but still useful for general age assessments. It would further profit from improvement of regional ΔR calibration data sets. Furthermore, radiocarbon dating of plant-macrofossil remains, as advised by Kemp et al. (2013), may provide a refined accuracy and precision to overcome this problematic of lateral incorporated 'older' shell fragments.

2.5.2 Mercury pollution history. Mercury concentrations of about 4–25 µg kg^{-1} in sediment core GeoHH-SH02, which contains sediments deposited long before land reclamation and embankment in 1862 CE (Ehlers, 1988; Brandt, 2018), indicate similar but slightly lower preindustrial background levels as documented for coastal and offshore Baltic Sea sediments (20–40 µg kg^{-1}; Leipe et al., 2013) or Northern Hemisphere lake sediments (5-times below industrial deposition rates; Biester et al., 2007). Since industrialization started in northern Europe around 1850 CE (Leipe et al., 2013), anthropogenic Hg emissions increased globally by at least 50%, causing an accumulation of highly contaminated Hg deposits in many ecosystems (Bergan et al., 1999; Martínez-Cortizas et al., 1999; Hylander and Meili, 2003). Accordingly, the two pronounced and stratigraphically separated peaks of the modern Hg-concentration profiles in sediment sequences TB13-1, GeoHH-FK and GeoHH-KWK, most likely represent the maximum Hg pollution in the mid-20th century (Fig. 6). Average concentration maxima along the south-eastern North Sea coastline are about 293.85 µg kg^{-1}, which are comparable to contemporaneous values of up to ca. 300 µg kg^{-1} documented in southern Baltic Sea sediments (Leipe et al., 2013). Moreover, the measured

down-core Hg concentration levels are substantially higher than the estimated natural background values (i.e., 4–25 µg kg^{-1}) in all sequences. This suggests that the analysed sediments were deposited after the mid-late 19th century.

The first Hg peak in each of the three sediment sequences (TB13-1, GeoHH-FK, and GeoHH-KWK) can likely be attributed to the impacts of World War II (e.g., Hylander and Meili, 2003), as Hg compounds were used for bomb detonators, and at the end of World War II, about 170 000 t of German military waste was dumped into the North Sea basin (Böttcher et al., 2011, 2017). The second peak of the Hg-concentration profiles can be interpreted as industrial pollution maximum between 1960 and 1970 CE, since Hg-bearing products were widely used in different industries during the mid to late 20th century (Biester et al., 2007; Leipe et al., 2013; Moros et al., 2016). Further contribution to the global Hg contamination by the Vietnam War in 1970 CE has also been mentioned (Hylander and Meili, 2003), but the pollution pattern in the sediment sequences is more likely dominated by regional sources. The upward decrease of the Hg-concentration levels within all three sequences is in line with previous studies, which described the reduction of industrial Hg usage and release to the environment after 1970 CE (Hylander and Meili, 2003; Lepland et al., 2010; Leipe et al., 2013). In the south-eastern North Sea, natural background concentrations of various heavy metals, such as copper, zinc, and nickel were reached until 2002 CE, while Hg concentrations are recently still higher than background levels (Wolff et al., 2010).

In contrast to the above described sites, sediments from the Eider estuary (site GeoHH-GIE) reveal generally elevated Hg concentrations for the entire sediment sequence with no distinct maxima as for the other sites. This general pattern reflects the Hg contamination of the Eider-river catchment, which is on average 10-times higher than the natural background of around 20 µg kg^{-1} (MELUND, 2014, 2015b). The elevated modern Hg pollution levels in the Eider estuary are caused by the combined impacts of local industries (e.g., fossil fuel combustion), and the remobilisation of 'older' Hg-polluted river deposits, which are regularly eroded by the river discharges.

The observed short-term fluctuations of the individual Hg-concentration records were likely caused by both seasonal (higher concentrations during enhanced river-runoff in winter; Wilken and Hintelmann, 1991), and re-depositional effects (lower concentrations in preindustrial sediment deposits; Leipe et al., 2013). In this context, river discharges contribute to a high level of contamination by transporting suspended pollutants from near-shore industries and harbours into the North Sea and adjacent coastal ecosystems (Bryan and Langston, 1992; Lepland et al., 2010; Wolff et al., 2010; Leipe et al., 2013). Consequently, the pronounced Hg-concentration maximum of 604.54 µg kg^{-1} in conjunction with relatively high C_{org} values at 18 cm depth at site GeoHH-KWK reflects its proximity to the Elbe estuary (see Appendix Fig. B2). Until at least 1990 CE, the Elbe river was one of the most Hg-contaminated rivers in the world (Banat et al., 1972; Wilken and Hintelmann, 1991). The observed abrupt increases of C_{org} and Hg concentrations likely document the last fairway deepening between 1997 and 2000 CE (Federal Waterway and Shipping Administration, WSV, and Hamburg Port Authority, HPA, 2011). Indeed, C_{org} measurements along a SE–NW transect from the Elbe river to the island of Sylt, revealed highest C_{org} contents for sediments within the Elbe estuary (Deek, 2011). Similar recent remobilisation effects of other contaminants in the Elbe river were also documented in environmental monitoring studies between 1996 and 1998 CE (Broeg et al., 2002). Alternatively, single Hg and other contaminant outliers could also be induced by the high frequent ship traffic in the Elbe river and estuary, causing local propeller-induced erosion and remobilisation of 'older' riverbed sediments (Lepland et al., 2010).

2.5.3 Grain-size characteristics and sedimentation dynamics. The mean grain size (M_G) records display similar general trends at the investigated sites, with an overall coarsening upward and considerable short-term variability (Fig. 7, Appendix Fig. B6). This pattern likely reflects the combined impacts of sea-level rise, landward retreat of salt-marsh cliffs, and climate variability (Kirwan et al., 2016; Müller-Navarra et al., 2019). There, the retreating cliffs are a result of lateral erosion at the seaward edge of the salt marshes, when vertical accretion and subsequent elevation growth rates are ensured (Schuerch et al., 2019), but inland migration rates of the marshes with increasing sea-level rise are prevented by modern dikes (Flemming and Nyandwi, 1994; Kirwan et al., 2016; Müller-Navarra et al., 2019). At the study sites, vertical erosion is rather absent since the salt-marsh surfaces are covered by dense root mats of typical salt-marsh plants, which bind the sediment particles and stabilise the upper parts of a sediment sequence (see also: Allen, 1989). Accordingly, the studied sediment sequences lack marked granulometric shifts, i.e., deviations from the general grain-size trends, suggesting the absence of vertical erosion and corresponding hiatuses. Commonly, the mean grain size depends on the general energy level during deposition of sediments on the salt-marsh surface, and may thus be attributed to extreme sea levels and corresponding storm-surge intensity and frequency changes in north-western Europe during the last century (Matulla et al., 2008; Weisse et al., 2012). Specifically, wind-induced wave activity during storm surges is crucial for the main sediment supply, and thus vertical accretion on the salt marshes (Morton, 1981; Stumpf, 1983; Turner et al., 2006; Schuerch et al., 2012, 2013). Grain-size characteristics of salt-marsh deposits are,

however, also dependent on the regional sediment source, the local coastal structure, the duration of submergence, and vegetation cover (e.g., Allen, 2000; Pedersen and Bartholdy, 2006; Müller-Navarra et al., 2019). Specifically, Schuerch et al. (2019) have shown that the suspended sediments, which are deposited onto the marsh surfaces, mainly originate from eroded marsh cliffs and adjacent tidal mudflats. The protection of the salt marshes after establishment of the Wadden Sea National Park in 1985 CE led to a stepwise return and maturing of the natural vegetation, likely resulting in reduced submergence and decline in sediment-accumulation rates in the southern North Sea coastal region. This is illustrated by the recently established high-marsh vegetation in the Bay of Tümlau since around 2001 CE (Stock et al., 2005; Müller-Navarra et al., 2019).

The incompatible trace elements zirconium (Zr) and rubidium (Rb) are useful for determining relative particle-size variations in intertidal sediments, because Zr is enriched in the coarse-grained sediment fraction as detrital zircon, while Rb is enriched in clay minerals, i.e., the fine fraction of the sediment (Bhatia and Crook, 1986; Fralick and Kronberg, 1997; Dypvik and Harris, 2001; Rothwell et al., 2006). The long-term ln(Zr/Rb) trends confirm the general coarsening of the sediment as reflected by the mean grain size and may deliver additional stratigraphic tie points for correlation between sequences, at least for those sequences which accumulated under a similar energy regime (Fig. 7). Discrete and single layers of coarser material are not considered for correlation purposes, since the artificial drainage ditches of the salt marshes were periodically dredged in the past, leading to potential sediment displacement. Therefore, corresponding discrete signals in the grain-size spectrum cannot be undoubtedly attributed to either specific anthropogenic or natural storm-induced sedimentation events (Müller-Navarra et al., 2019). Instead, stratigraphic tie points are rather derived from graphical correlation of prominent long-term trends between the ln(Zr/Rb) records, where grain-size variations exhibit a general coarsening of the material.

The ln(Zr/Rb) records from the more sheltered salt marshes in the Bay of Tümlau (TB13-1) and Friedrichskoog (GeoHH-FK) reveal the closest correspondence, suggesting comparable sedimentation dynamics with mean accretion rates between 1.2–1.3 cm yr^{-1} during the past ca. 100 years (Fig. 8). Due to its location in a more dynamic open coastal salt marsh close to the Elbe estuary, sediment supply is probably much higher at site GeoHH-KWK. A detailed correlation of the ln(Zr/Rb) record of GeoHH-KWK appears difficult, but the interpretation of enhanced accretion rates is further indicated by the Hg concentration maxima at greater depths and wider sediment layers on average (up to ca. 4 cm thickness) when compared to the other sites. Accordingly, ln(Zr/Rb) variability reflects a rather short time interval at

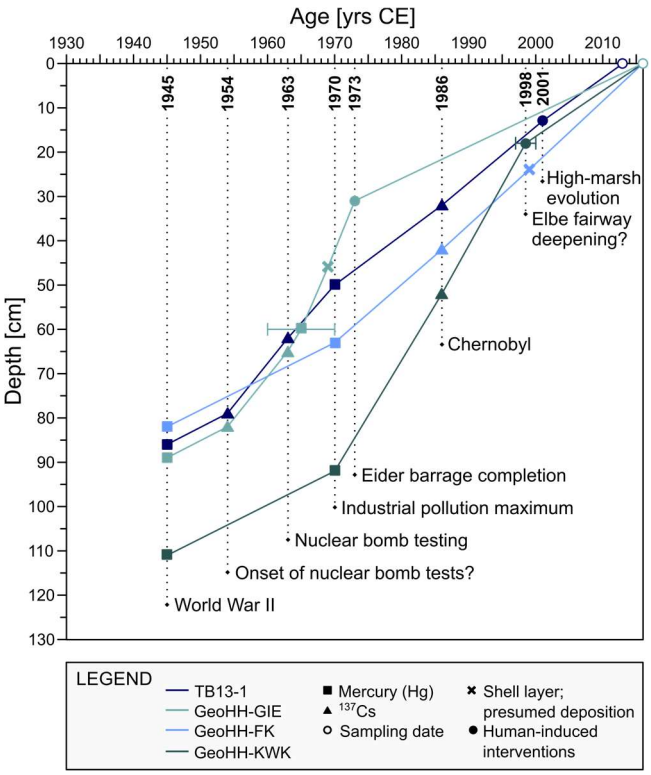

Fig. 8 | Stratigraphic frameworks for each of the sediment sequences, established by integrating different methodologies and considering the specific local depositional settings. Age-depth plot with indication of distinct time markers of artificial radionuclides (^{137}Cs), and anthropogenic mercury (Hg) pollution. Further indicated are regional human-induced interventions, including the tidal barrier construction in the Eider estuary (represented by the ln[Zr/Rb] drop), the fairway deepening of the Elbe river proximate to the Kaiser-Wilhelm-Koog (Hg, C_{org} spikes), and the return of natural conditions after abandonment of grazing and draining in the Bay of Tümlau, as indicated by the appearance of the high-marsh marker species *Balticammina pseudomacrescens* (Müller-Navarra et al., 2019).

site GeoHH-KWK, comprising sediments of the last ca. 70 years (Fig. 8). Sediments from the Eider estuary, at site GeoHH-GIE, reflect the complex interplay between estuarine and marine processes together with human interventions impeding the alignment of its ln(Zr/Rb) record with those of the other sequences. Particularly, the Eider tidal barrier completion in 1973 CE led to a change in submergence dynamics by shielding the estuarine marshes from storm surges. The reduced tidal submergence, flow velocities, and wave energy resulted in the deposition of fine-grained sediment (Allen, 2000), primarily linked to river discharge. This change in sedimentation is indicated by the abrupt drop of the ln(Zr/Rb) values at around 30 cm depth

providing a confident age marker (Fig. 8). In comparison, the ln(Zr/Rb) and M_G data series reveals deviating patterns for the uppermost ca. 30 cm of the sediment sequence at site GeoHH-GIE, i.e., low ln(Zr/Rb) but high M_G values. Despite treating the samples with H_2O_2 to remove organic remains for subsequent grain size measurements of the siliciclastic component, not all refractory organic particles could be removed from the densely rooted soil horizon, thus distorting the grain-size measurements. Such organic particles in the upper interval of GeoHH-GIE were identified under the microscope, but not further quantified. As a consequence, the ln(Zr/Rb) ratio indeed reflects the change in the sediment composition itself, i.e., a relative increase of the fine-grained clastic particles (Rb) within the soil horizon, while the presence of refractory remains result in an overestimation of the particle sizes. This bias is restricted to the estuarine core location GeoHH-GIE, but can be excluded for the active salt marshes, where frequent sediment delivery from the surrounding tidal flats is preventing comparable soil genesis.

2.5.4 Integrated stratigraphy of salt-marsh deposits. The combination of different dating approaches and further inter-correlation of the sediment sequences allowed the establishment of an integrated stratigraphic framework for the studied salt-marsh sediments (Fig. 8). Mean accretion rates are 1.31 cm yr^{-1} at the Bay of Tümlau (TB13-1), 1.90 cm yr^{-1} at the Eider estuary (GeoHH-GIE), 1.16 cm yr^{-1} at Friedrichskoog (GeoHH-FK), and 1.75 cm yr^{-1} at Kaiser-Wilhelm-Koog (GeoHH-KWK); see Table 2. The effects of autocompaction were not considered, since the mean grain size is about 66 µm on average at all sites and because coastal sediment sequences are mainly affected by autocompaction when consisting of finer-grained sediments (i.e., silty clay) together with a moderate organic matter content, while coarse grains are rather incompressible (Allen, 2000; Bartholdy et al., 2010). Mean sedimentation rates, which are based on the CRS calculations (Appleby and Oldfield, 1978), are 2.17 cm yr^{-1} at site TB13-1 and about 1.84 cm yr^{-1} at site GeoHH-GIE. Observed mass accumulation rates (MAR) are 2.09 g cm^{-2} yr^{-1} at site TB13-1 and about 2.20 g cm^{-2} yr^{-1} at site GeoHH-GIE. However, in highly dynamic coastal environments, the ^{210}Pb-based age models contain high uncertainties and errors (Andersen et al., 2011; Müller-Navarra et al., 2019), restricting their applicability as an exact stratigraphic tool. Therefore, age models in salt-marsh environments and inferred accretion rates should rely on various independent time markers, such as ^{137}Cs, ^{241}Am, and Hg, together with sedimentological characteristics in order to minimize the effects of reworking and compensate for blurring of distinct stratigraphic signals. The stratigraphic framework can be further supported by XRF records, which represent useful information for correlation of salt-marsh sequences as long as they were deposited under a similar regional setting.

The recorded accretion rates of 1.16 to 1.90 cm yr^{-1} are comparable to those reported from other salt marshes along the mainland of the south-eastern North Sea coastline (1.16 cm yr^{-1} on average; Nolte et al., 2013a), while the CRS-derived sedimentation rates of 1.84 cm yr^{-1} to 2.17 cm yr^{-1} are slightly higher. In summary, the documented accretion rates derived from this study are much higher than in those salt marshes developed at the lee side of offshore islands, as the island of Sylt, where Schuerch et al. (2012) documented accretion rates between 0.10 to 0.28 cm yr^{-1}. This is in line with previous studies, which indicated that the suspended sediment concentration in the incoming inundation wave, and subsequent sediment accretion, is directly linked to the inundation height and storm-surge intensity (Temmerman et al., 2003; Schuerch et al., 2012). Therefore, the exposition of a salt marsh (open coastal versus sheltered) is crucial for its growth rate and resilience to the regional sea-level rise of 2.4 ±0.1 mm yr^{-1} (Dangendorf et al., 2013a). Among those sites influenced by tidal currents (TB13-1, GeoHH-FK, and GeoHH-KWK), site GeoHH-FK exhibits the lowest average accretion rates. Since this site is intensively treated by livestock grazing, the vegetation cover at the seaside of the marsh is dominated by grasses, such as *Festuca rubra* and *Puccinellia maritima* (Stock et al., 2005). This vegetation likely reduced the amount of sediment, which usually would be trapped in a natural-developed vegetation of an un-grazed salt marsh (e.g., Nolte et al., 2013a). Moderate accretion rates at site TB13-1 can be attributed to its semi-enclosed position in the Bay of Tümlau, shielding the salt marsh from high-energy conditions during storm surges (Müller-Navarra et al., 2019). The sediment sequence at Kaiser-Wilhelm-Koog (GeoHH-KWK) reveal a higher average accretion rate due to its more open coastal exposition. Particularly, Kaiser-Wilhelm-Koog is directly exposed to westerly winds and waves, and is further influenced by suspension load of the Elbe estuary (Fig. 4), explaining the relatively higher accretion rates there. Despite these local differences, accretion rates decreased at all three sites during recent decades (Fig. 8), reflecting decreased inundation frequencies due to increased elevations with maturing of the salt marshes (Allen, 2000; Bartholdy et al., 2004).

With 1.90 cm yr^{-1} in total, highest average accretion rates were documented for the salt marsh in the Eider estuary (GeoHH-GIE), based on the integrated stratigraphy. There, maximum values of 3.63 cm yr^{-1} were observed for the period around 1965 to 1973 CE, concurrent to the onset of the Eider tidal barrier construction in 1967 CE (Lehmann and Heinz, 2008). During the construction phase, plenty of sediment material was likely mobilized and re-distributed in the estuary. Apart from this accretion maximum, average pre-barrier accretion rates of 1.72 cm yr^{-1} (from 1945–1965 CE) dropped to modern values of 0.72 cm yr^{-1}, in which the

Table 2 | Time markers that has been used for compiling the integrated stratigraphy together with derived mean accretion rates for sites TB13-1 (Bay of Tümlau), GeoHH-GIE (Eider estuary), GeoHH-FK (Friedrichskoog), and GeoHH-KWK (Kaiser-Wilhelm-Koog). *Bm* = *Balticammina pseudomacrescens*.

Site ID	Depth [cm]	Age [yrs CE]	Mean sediment accretion rate [cm yr^{-1}]	Time marker	Indication
TB13-1	0	2013		Sampling date	
	13	2001	1.08	Occurrence of *Bm*	Return of a natural vegetation
	32	1986	1.27	Cs-137 peak	Chernobyl
	50	1970	1.13	Hg peak	Industrial pollution maximum
	62	1963	1.71	Cs-137, Am-241 peaks	Nuclear weapon testing
	79	1954	1.89	Cs-137 increase	First nuclear weapon tests
	86	1945	0.78	Hg peak	World War II
GeoHH-GIE	0	2016		Sampling date	
	31	1973	0.72	ln(Zr/Rb) drop	Eider tidal barrier completion
	60	1965	3.63	Hg peak	Industrial pollution maximum
	65	1963	2.50	Cs-137 peak	Nuclear weapon testing
	82	1954	1.89	Cs-137 increase	First nuclear weapon tests
	89	1945	0.78	Hg peak	World War II
GeoHH-FK	0	2016		Sampling date	
	42	1986	1.40	Cs-137 peak	Chernobyl
	63	1970	1.31	Hg peak	Industrial pollution maximum
	82	1945	0.76	Hg peak	World War II
GeoHH-KWK	0	2016		Sampling date	
	18	1998.5	1.03	C_{org} and Hg spikes	Fairway deepening
	52	1986	2.72	Cs-137 peak	Chernobyl
	92	1970	2.50	Hg peak	Industrial pollution maximum
	111	1945	0.76	Hg peak	World War II

latter one reflects the widely absence of storm-tide inundation.

2.6 Conclusions

Salt marshes are sensitive indicators of environmental changes, and hence, robust chronologies are crucial to reconstruct their depositional processes in the past, which may then help to assess future climate scenarios. The combination of different age-dating techniques proves essential for the establishment of reliable stratigraphies in highly dynamic coastal depositional settings, such as the salt-marsh systems at the south-eastern North Sea. However, most of the commonly used dating techniques, which were discussed herein, are associated with high uncertainties in such highly dynamic environments, and subsequent age assessments can be rather inaccurate. The establishment of an integrated regional stratigraphic framework in combining radionuclides (i.e., ^{210}Pb, ^{137}Cs, and ^{241}Am) with human-induced pollutants (Hg), and proxy-based sedimentological inter-correlations compensates for absence or blurring of distinct stratigraphic signals. Assessing the various dating methods and based on the research questions raised in the introduction, the following main conclusions can be drawn:

(1) Since fluctuations in the unsupported ^{210}Pb are probably a result of reworked sediment horizons, the ^{210}Pb-based age models (CIC, CRS) are associated with high uncertainties and should be used as general stratigraphic orientation rather than for extracting precise age dates

and sedimentation rates. In contrast, distinct ^{137}Cs and ^{241}Am activity peaks are preserved in the salt-marsh sequences and reflect the atmospheric fallout history of nuclear weapon tests between 1954 and 1963 CE, and the Chernobyl accident in 1986 CE. The distribution of ^{137}Cs provided accurate age markers for active salt-marshes in the Bay of Tümlau (TB13-1) and Eider estuary (GeoHH-GIE).

(2) The heavy metal-pollution history of North German rivers and coastal areas is documented in elevated Hg concentrations in salt-marsh sediments during the middle of the 20th century. Distinct pollution peaks can be attributed to the aftermaths of World War II and the industrial pollution maximum between 1960 and 1970 CE. The characteristic double peak could be identified at all studied sites providing reliable stratigraphic information. In the Eider estuary, Hg concentrations remain high after 1970 CE likely reflecting the local pollution history of the river catchment and the redistribution of polluted river sediments.

(3) The ln(Zr/Rb) ratio delivers information on the relative grain-size composition of the salt-marsh sediments in high temporal resolution. This proxy proved useful for the inter-correlation of salt-marsh sediment sequences as long as they were deposited under similar environmental conditions. Specifically, the ln(Zr/Rb) records from the Bay of Tümlau (TB13-1) and Friedrichskoog (GeoHH-FK) may have experienced comparable natural and human influences, while contrasting signals at Kaiser-Wilhelm-Koog (GeoHH-KWK) and the Eider estuary (GeoHH-GIE) suggest strongly different depositional processes and energy regimes impeding the extraction of additional stratigraphic information.

(4) The integrated stratigraphic framework provides the basis for the investigation of coastal wetland responses to changes in sea level, storm surges, and human impacts. The reconstructed average accretion rates range from 1.16 cm yr^{-1} to 1.90 cm yr^{-1}, reflecting the specific exposition to wave energy, inundation frequency and intensity, as well as coastal management. Relatively lower accretion rates are documented for the sheltered salt marshes in the Bay of Tümlau (TB13-1) and Friedrichskoog (GeoHH-FK). In contrast, relatively higher accretion rates are documented for Kaiser-Wilhelm-Koog (GeoHH-KWK), which is exposed to westerly winds and related storm surges, and for the pre-barrier Eider estuary (GeoHH-GIE), which is additionally characterized by riverine sediment delivery. In summary, the investigated salt marshes provide a high potential in keeping pace with ongoing sea-level rise, while impacts by grazing livestock and/or active drainage systems did not significantly reduce the salt-marsh accretion rate during the past ca. 100 years. In contrast, present-day salt marshes in the Eider estuary are excluded from natural flooding dynamics, diminishing their function in coastal defence and management strategies.

Acknowledgements

This study was supported by grants SCHM1180/19 and MI1508/4 from the German Research Foundation (DFG) as part of the Priority Program (SPP-1889) Regional Sea Level Change and Society (SeaLevel) and within the research project SEASTORM. We acknowledge the State Office for Surveying and Geoinformation Schleswig-Holstein (LVermGeo SH) for providing information about the triangulation station, and the Federal Maritime and Hydrographic Agency of Germany (BSH) for providing tide-gauge data for the German North Sea coast. Christian Wiedemann and Martin Stock, National Park of the Schleswig-Holstein Wadden Sea, are especially thanked for assigning the permissions to work in the protected areas of the active salt marshes in Dithmarschen and North Frisia. Amalie Cordua and Sebastian Lindhorst (Universität Hamburg) are thanked for providing the sediment samples of core GeoHH-SH02.2 to test the natural mercury background level and for discussions. Matthias Moros (IOW, Warnemünde) and Helmut Fischer (University of Bremen) are thanked for helpful discussions about radionuclide age models. We thank Jutta Richarz and Marc Metzke (Universität Hamburg), Thomas Leipe, Ines Scherf, and Sascha Plewe (IOW, Warnemünde), Bernd Kopka, Ronny Thoms, and Rainer Schulz (LARI, University of Göttingen) for many helpful discussions and technical support during laboratory analyses. We greatly acknowledge the critical reviews of four anonymous reviewers, which significantly improved the quality of the manuscript.

Author contributions

Sample preparation and most of the laboratory analyses (grain size and mercury measurements, as well as XRF scanning) were carried out by D.B., who also designed the study and wrote the article. K.M.N. provided most of the required data for sediment sequence TB13-1, comprising radionuclides and grain-size data (published in Müller-Navarra et al., 2019). The processing of the XRF scans and Hg measurements was supervised by H.W.A, who also contributed to the corresponding data evaluations. J.F. conducted the ^{210}Pb-based CRS model calculations and related MARs and SRs and helped to technically discuss all radionuclide data. Measurements of the organic carbon content for all sediment sequences were carried out by N.L., who further contributed to subsequent data interpretations. Y.M. and G.S. contributed to all data discussions by providing helpful advice, comments, and revisions during the article preparation phase.

Data availability

All measured data used and discussed in this article are available at:
https://doi.pangaea.de/10.1594/PANGAEA.905240.

CHAPTER THREE

The following Chapter has been published as:

Bunzel, D., Milker, Y., Müller-Navarra, K., Arz, H.W., Schmiedl, G., 2021. North Sea salt-marsh archives trace past storminess and climate variability. *Global and Planetary Change* **198**, 103403,
DOI: 10.1016/j.gloplacha.2020.103403.

North Sea salt-marsh archives trace past storminess and climate variability

D. Bunzel *et al.*

Submitted: 23 July 2020
Accepted for publication: 18 December 2020
Published online: 23 December 2020

Abstract

Intertidal coastal wetlands are regularly exposed to storm surges and associated flooding, resulting in the recurrent accretion of reworked sediments on the salt-marsh surfaces. In this context, well-stratified salt-marsh sediment sequences provide an exceptional archive to evaluate the response of coastal wetlands to past storm-climate variability. Hence, this study focusses on the investigation of two sedimentary salt-marsh sequences from the south-eastern German North Sea coast (Bay of Tümlau and Friedrichskoog) to understand how and to which extent changes in the storm-surge climate are transferred into the sediment archive. This objective is particularly challenging as German mainland salt marshes have been greatly altered by human activities over the last century. To overcome this problem, this study combines different sedimentological and geochemical proxy data, using mean grain sizes together with ln(Br/Cl), Br/C_{org}, and ln(Zr/Rb) ratios, to allow for the identification of storm-surge layers. Local changes in the sedimentary organic matter supply are reflected by the ln(Br/Cl) ratio. There, abrupt drops in the ln(Br/Cl) data coincide with relatively coarser textured sand layers, indicating impacts by regional storm surges during winter, while intervals of comparable higher ln(Br/Cl) values may represent deposition during spring to fall. The Br/C_{org} record reflects the marine versus terrestrial organic matter input and reveals a long-term increase starting during the first half of the 20th century towards recent times, resembling the observed amplification in North Sea storminess. A similar trend is reflected by the ln(Zr/Rb) ratio (since 1950 CE), which can be used as a proxy for the grain-size distribution. Periodic fluctuations in the ln(Zr/Rb) ratio at inter-decadal timescales (10–19 years) suggest a close linkage between local sediment accretion and large-scale atmosphere-ocean climate oscillations over the North Atlantic and Europe, and thus related storm-surge frequency and intensity. Periodic variability on decadal scales was also identified in the ln(Br/Cl) record at the less human-modified and more naturally developed salt marsh at the Bay of Tümlau (12–22 years), likewise indicating a relation between North Sea storminess and associated shifts in the seasonal signal of the primary production and sediment texture to oscillations in the atmosphere-ocean system. On the contrary, similar periodicities are lacking for the intense modified salt marsh at Friedrichskoog. Apparently, the salt-marsh depositional system in the Bay of Tümlau reacts more sensitively to super-regional climatic changes, respectively, the natural depositional processes in the salt marsh at Friedrichskoog are superimposed by the more intense local human activities.

3.1 Introduction

Sedimentation in active salt marshes is mainly controlled by the complex dynamics of mean sea level (MSL), tides, and storm surges (e.g., Allen, 2000; Davy et al., 2009; Stevenson and Kearney, 2009; Haigh et al., 2010). These hydrodynamic processes are responsible for the local erosion, relocation, and re-deposition of sediments, and can therefore lead to the loss of salt marshes at some places, but at the same time provide the required sediment supply for the growth of salt marshes at other sites (Allen 1990; Temmerman et al., 2003; Mariotti and Fagherazzi, 2010; Andersen et al., 2011; Schuerch et al., 2013, 2019; Kirwan et al., 2016). The mobilisation of sediments further depends on the exposure of a salt marsh to wave energy, and its geomorphology (e.g., Allen, 2000; Mariotti and Fagherazzi, 2010). The composition of the reworked suspended sediments, which are introduced onto the salt marsh by recurrent floods, and thereby contribute to their vertical growth, reflects the availability of material originating from the adjacent tidal flats and eroded marshes (Müller-Navarra et al., 2019; Schuerch et al., 2019; Bunzel et al., 2020), as well as from rivers (Eisma and Irion, 1988). The accretion of sediments on top of the marsh surface finally depends on the vegetation cover and structure (Nolte et al. 2013a; Mariotti and Fagherazzi, 2010; Fagherazzi, 2014; Möller et al., 2014). Similar processes are also active along the North Sea coast, where specifically the recurrent flooding during storm surges results in the accumulation of well-stratified salt-marsh sequences, providing a potential high-resolution archive of past storm-surge dynamics and climate changes.

The North Sea coastline is exposed to annual storm surges, specifically during winter times (e.g., Gerber et al., 2016). The surge heights are either raised by local wind stress pushing the water towards the coastline (Weisse and von Storch, 2010), or by strong atmospheric low-pressure centres that are formed over the North Atlantic and then move across the North Sea (e.g., Müller-Navarra and Giese, 1999). During the last century, storm surges were additionally influenced by the long-term increase of regional MSL (2.4 ±0.1 mm yr^{-1} between 1871 to 2008 CE) under the influence of global warming (Dangendorf et al., 2013a). Particularly in shallow coastal areas, such as the south-eastern North Sea, a rising MSL has significant impacts on the associated bottom-friction forces, which then change with increasing water depth (Davies and Jones, 1995). Accordingly, model simulations for the German Bight documented an amplification in the intensity and range of the oscillating tidal currents during the past decades (Arns et al., 2015). It remains unclear, however, to which extend a rising MSL affects the height and impact of storm surges. Generally, the depth-limited storm-surge waves are attenuated with increasing water depth (Arns et al., 2017), but the surge generation itself preferentially occurs concomitant with rising tides (Horsburgh and Wilson, 2007). Consequently, rising MSL and amplified tidal ranges likely result in a higher variability of storm-surge heights, complicating the associated flood-risk assessment (Familkhalili and Talke, 2016). The assumed amplification in the storm-surge climate signature over the curse of the 20th century, however, can be tested in the well-stratified sediment sequences of modern foreland salt marshes along the German North Sea coast. Given the expected global sea-level rise (SLR) of 0.43–0.84 m by 2100 CE (IPCC, 2019), it further highlights the importance to obtain a better understanding on how changes in sea level and storminess affect the resilience of coastal salt marshes under ongoing global warming.

Salt-marsh sedimentation along the south-eastern North Sea coast is further influenced by local human impacts such as drainage measures, land reclamations, and shoreline modifications (Davy et al., 2009). As evaluated by Esselink et al. (2009), between 80% (Lower Saxony) and 90% (Schleswig-Holstein) of the mainland salt marshes that fringe the German North Sea coastline have been intensely modified during the past decades, specifically, by the construction and dredging of drainage ditches. Consequently, most of today's salt marshes are of anthropogenic origin, as their development has been favoured by the artificial drainage systems and their frequent upkeep (Esselink et al., 2009, 2017). Although human-modified salt marshes represent nowadays the majority of the intertidal wetlands along the German North Sea coast, they have undergone different land-use histories and degrees of modification (e.g., regarding the frequency of upkeep of the drainage ditches). Accordingly, each salt-marsh sediment sequences should reflect the specific management histories, whereas the natural influence of long-term climate changes and associated storm-surge statistics should leave a similar depositional imprint along the entire coast.

Hence, the overarching hypothesis of this study is that sedimentary salt-marsh sequences along the German North Sea coast archive past storm-climate signals, despite the influence of human coastal management. In order to test this hypothesis, this study explores how the present human-modified salt marshes have responded to climate changes during the past century, how the storm-climate signal is transferred into the sediment sequences, and how this signal can be distinguished from the anthropogenic signals. Commonly, discrete storm-surge layers are described as being dominated by siliciclastic coarser-grained sediments (e.g., Ehlers et al., 1993; Chaumillon et al., 2017), but vary in thickness and composition, often impeding a detailed evaluation based on classical sedimentological analyses. In this context, geochemical analyses by high-resolution X-ray fluorescence (XRF) scanning may add detailed information on salt-marsh sedimentation dynamics on short timescales

and may provide additional proxies for the identification of storm-surge layers. Based on that, this study follows an integrated approach by evaluating different sedimentological and geochemical proxy data, including grain size, organic carbon, and XRF scanning data (Br, Cl, Rb, and Zr). These data were obtained from two sediment sequences originating from different salt-marsh environments at the south-eastern German North Sea coast and have undergone similar natural climate processes but experienced different degrees of anthropogenic interventions during the last century. The extracted climate component is used to explore the complexity of the regional storm-surge history and its linkage to underlying super-regional climate oscillations.

3.2 Regional setting

At present, coastal salt marshes of the Wadden Sea region extend from Denmark to the Netherlands, covering an area of around 400 km^2 along the south-eastern North Sea (Dijkema, 1987; Bartholdy et al., 2004; Nolte et al., 2013a; Wolff, 2013). To promote land reclamation, these salt marshes and adjacent tidal flats were intensely managed during the last centuries, so that their development mainly occurred under human influences (Dijkema, 1987; Davy et al., 2009; Esselink et al., 2009, 2000). In order to restore and sustain the natural ecosystem services of coastal salt marshes and instead promote their natural development, they are protected since 1985 CE as part of the Wadden Sea National Park. As a consequence, coastal management and land reclamation, i.e., draining and grazing was reduced or stopped in most salt marshes during the recent past (e.g., Esselink et al., 2009; Nolte et al., 2013a; Wolff, 2013; and literature therein).

The studied sites comprise two different salt-marsh systems (Fig. 9), which both were modified to different degrees by human activities during the past century. These alterations include networks of parallel trench systems, which were recurrently renewed and dredged every two to three (Friedrichskoog, Dithmarschen) and every three to seven years (Bay of Tümlau, Eiderstedt peninsula; pers. comm. Schleswig-Holstein Agency for Coastal Defence, National Park and Marine Conservation, LKN.SH, 2017, 2020). However, since foundation of the Wadden Sea National Park, the northern site (Bay of Tümlau) belongs to a protected and restored salt-marsh area that is now dominated by natural processes, while the southern site (Friedrichskoog) is located in an area that is still intensely managed and influenced by anthropogenic interventions. Since the introduction of national nature protection measures, a return of a higher-diverse salt-marsh vegetation was documented for the Bay of Tümlau at least since 2001 CE, favouring plant-communities consisting of, i.a., the *Atriplex portulacoides*/*Artemisia*-type, *Atriplex portulacoides*/*Puccinella*-type and *Festuca rubra* (Stock et al., 2005). In contrast, draining measures and intensive grazing by sheep stock resulted in a short-grazed vegetation cover dominated by only a few grass species such as *Festuca rubra* and *Puccinellia maritima* together with few patches of *Salicornia europaea* at Friedrichskoog (Stock et al., 2005; Bunzel et al., 2020). Nowadays, the Bay of Tümlau is fringed by several modern dikes, which were constructed in 1861 CE and 1933 CE, while Friedrichskoog was diked in 1853 CE (Fischer, 1956, 1957; Ehlers, 1988). The constructed embankments are defending the populated hinterland from frequently occurring storm surges (Esselink et al., 2009; Davy et al., 2009), but they also prevent a natural landward migration of the salt marshes under rising sea level (Kirwan et al., 2016; Müller-Navarra et al., 2019; Bunzel et al., 2020). As a consequence of the embankments, both salt-marsh systems are exposed to lateral erosion at the seaward side of the dike during high tides or storm surges, and thus fringed by erosional cliffs between the tidal margins and the seaward edge of the marshes (Müller-Navarra et al., 2019; Bunzel et al., 2020). These cliffs were chosen for sediment sampling, generating sediment sequences TB13-1 (Bay of Tümlau, 54°21'51.07"N, 8°40'35.09"E; Müller-Navarra et al., 2019) and GeoHH-FK (Friedrichskoog, 54°2'35.02"N, 8°52'20.41"E; Bunzel et al., 2020).

3.3 Materials and methods

3.3.1 Field work. Fieldwork was carried out in Dithmarschen (Friedrichskoog, site GeoHH-FK) in November 2016, while sediments of the Eiderstedt peninsula (Bay of Tümlau, site TB13-01) were recovered in August 2013 (Müller-Navarra et al., 2019). The marsh surfaces at the erosional cliffs are situated 2.09 m (TB13-1) to 2.80 m (GeoHH-FK) above NHN (*Normalhöhennull*), thus exceeding the local mean high water spring (MHWS) levels by 0.50 m (TB13-1) and 1.06 m (GeoHH-FK). As a result, the investigated salt-marsh systems are only flooded during times of extreme water levels that are exceeding the mean high water (MHW) by ≥ 1.5 m (Gerber et al., 2016). Tidal data were provided by the Federal Maritime and Hydrographic Agency of Germany (BSH), and are based on the nearest tide gauges named Tümlauer Hafen (observation period: 2001–2013 CE) and Friedrichskoog Hafen (observation period: 1986–2018 CE).

The sediment sequences at both sites were sampled by 10–15 U-channels, which were pressed vertically into the previously cleaned erosional cliff face. Each U-channel has a maximum dimension of 1.75 cm width, 2.00 cm depth, and 200 cm length, and is open at one long side. Cliff-surface elevation and position was surveyed by using a Leica Geosystems GNSS field controller (Viva Uno CS10) and referred to triangulation stations number 1618 031 10 (Bay of Tümlau) and 1919 088 00 (Friedrichskoog). For further details, see Müller-Navarra et al. (2019) and Bunzel et al.

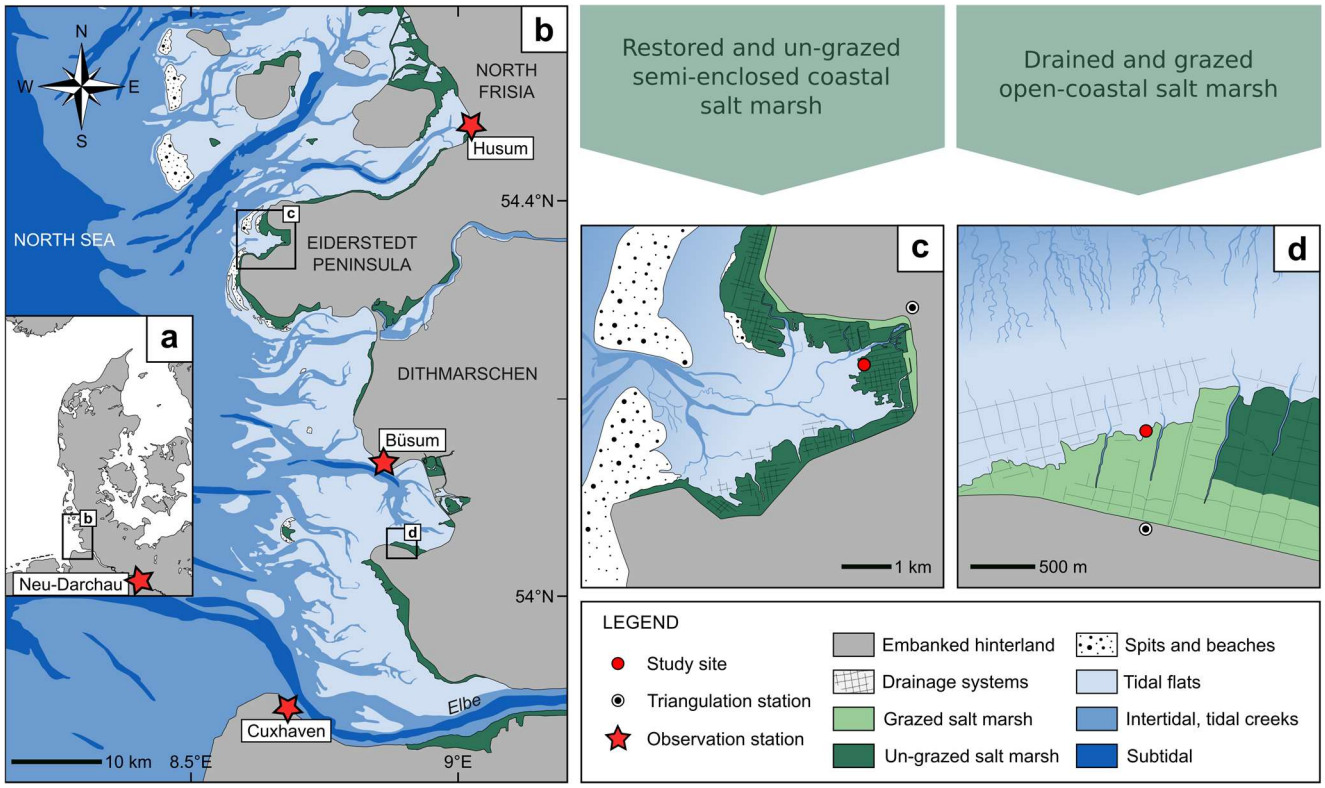

Fig. 9 | South-eastern North Sea coast and overview of the studied salt-marsh areas devoted to pasture. a, **b**) Overview of the German North Sea coastline with the location of the considered wind-signal stations (Husum, Büsum, and Cuxhaven), the Cuxhaven tide gauge, and the monitoring station for Elbe River discharges at Neu-Darchau (red stars), together with the present-day regional setting of the investigated sites at the Bay of Tümlau (**c**; TB13-1), and at Friedrichskoog (**d**; GeoHH-FK).

(2020). Data for the triangulation stations were provided by the State Office for Surveying and Geoinformation Schleswig-Holstein (LVermGeo SH). Subsequent processing of the surveyed data was conducted with the Leica Geo Office 8.3 software.

3.3.2 Historical wind, tidal, and discharge data, and simulated water level extremes. To assess past salt-marsh responses to natural climate variability during the last century, historical wind and tide-gauge observation data, as well as river runoff data for the Elbe river were evaluated. Since long-term wind-observation data recorded at different signal stations along the German North Sea coast are often incomplete due to partly lacking high-resolution records, specifically during the first half of the 20th century, data of three stations near the two study sites were taken and compared, to compensate for times of sparse meteorological observations. From north to south, the stations comprise: Husum, Büsum, and Cuxhaven (Schleswig-Holstein and Lower Saxony; Fig. 9). Data were provided by the German Meteorological Service (DWD). In order to take only severe wind conditions into account, which are directly facing the coastline, the daily means of winds with prevailing wind directions from ≥ 180° to 360° azimuth (westerly winds) and with a wind strength of ≥ 7 Beaufort (Bft), that equals a minimum wind speed of 13.9–17.1 m s^{-1} (e.g., DWD), were used for subsequent analyses. Historical water levels are based on the tide gauge in Cuxhaven, which covers the longest time period and provides the most complete data record for the south-eastern North Sea region (data were provided by the BSH). For subsequent analyses, only tidal data with MHW ≥ 1.5 m were considered hereafter, which is the classification of the minimum water-level height for storm tides (Gerber et al., 2016). Yearly mean discharge data of the Elbe river were provided by the Global Runoff Data Centre (GRDC) for the monitoring station Neu-Darchau (Lower Saxony), which is the northern-most station close to the Elbe estuary (Fig. 9).

To further compare the salt-marsh sediment sequences with large-scale climate states, simulated extreme sea levels (ESL) and their long-term variability in the German Bight were considered in addition (data were provided by Lang and Mikolajewicz, 2019). Extreme sea level indices were characterized by considering only the annual sea-level maxima. The ESL setup relies on a coupled high-resolution regional atmospheric model (REMO, Jacob and Podzun,

1997) and a global ocean model (MPIOM, Marsland et al., 2004; Jungclaus et al., 2013), which enables an integration of both regional and super-regional signals (for further details, see Lang and Mikolajewicz, 2019).

3.3.3 Sedimentological and geochemical analyses. Grain-size measurements on the siliciclastic sediment components were conducted choosing a 0.5 cm resolution for the sediment sequence at site GeoHH-FK. Data for TB13-1 were provided at a 1.0 cm resolution by Müller-Navarra et al. (2019). To remove the organic and inorganic carbon from the samples, they were treated with 10–30% H_2O_2 and 1 M CH_3COOH successively. Subsequent grain-size measurements were carried out on a HELOS KF Magic Laser particle-size distribution analyser. The accuracy of the analysis was achieved by measuring an intern silicon carbide (SiC) standard, which was regularly tested after every twentieth to fiftieth sample. Grain-size quantification was conducted by using the software GRADISTAT version 8.0 (Blott and Pye, 2001), which is based on the applications described by Folk and Ward (1957).

Scanning X-ray fluorescence (XRF) spectroscopy was performed at an ITRAX Core Scanner with a chromium tube applying a generator setting of 30 kV (30 mA), step sizes of 260 µm (TB13-1) and 500 µm (GeoHH-FK), and a counting time of 15 seconds per step. The scanning uncertainty for element intensities is generally better than 5% (Jarvis et al., 2015). Further, the accuracy of the XRF scanning performance was regularly tested and confirmed by analysing a certified reference material (CRM), before and after the scanning procedure. Analyses were carried out at the Leibniz Institute for Baltic Sea Research Warnemünde (IOW). Relative changes in the down-core distribution of element intensities (i.e., bromine, Br; chloride, Cl; rubidium, Rb; zirconium, Zr) within sediment sequences TB13-1 and GeoHH-FK were expressed as logarithmic ratios, and used for environmental interpretations following Dypvik and Harris (2001), Thomson et al. (2006), and Weltje and Tjallingii (2008). The ln(Br/Cl) ratio was considered to provide information about local changes in the marine organic matter (MOC) supply. As bromine is comparatively sparse in terrestrial organic matter, the Br/Corg ratio was then used to reflect the relative proportions of marine and terrestrial organic matter in the sediment, independent from the sediment texture (Mayer et al., 2007; Ziegler et al., 2008). In contrast, the ln(Zr/Rb) ratio was used as a high-resolution proxy for the relative grain-size distribution, since zirconium (Zr) is enriched in the coarse-grained sediment fraction in form of zircon, while rubidium (Rb) is mainly concentrated in clay minerals (e.g., Dypvik and Harris, 2001; Weltje and Tjallingii, 2008; Rothwell and Croudace, 2015). Internal sedimentological down-core characteristics were generalized and expressed as light and dark layers, based on previously generated optical and x-ray images (Bunzel et al., 2020).

Organic carbon (C_{org}) was measured by using a EuroVector EuroEA3000 Analyser and a measurement time of 200 s per sample. Prior to the instrumental analysis, one sediment-filled U-channel per sites TB13-1 and GeoHH-FK was sampled at 1–2 cm spacing. Five mg sediment material per sample were separated, subsequently freeze-dried, ground, and three times acidified with 1 M hydrochloric acid (HCl) Merck Suprapure. The accuracy of the method is 0.05%, based on the averaged standard deviations of the analysed replicates after every tenth sample.

In a previous study, individual age models were generated for each sediment sequence based on the combination of different independent dating methods commonly used to date modern sedimentary deposits (Bunzel et al., 2020). This strategy enabled the establishment of an integrated stratigraphic framework for each site. Specifically, the down-core activity of natural (^{210}Pb) and artificial (^{137}Cs) radionuclides, together with the mercury (Hg) concentration was evaluated for both study sites, whereas artificial ^{241}Am was only measured in the Bay of Tümlau (see Appendix Fig. C1). Radionuclide data of TB13-1 (comprising the decay-corrected ^{210}Pb, ^{137}Cs, and ^{241}Am data only; see description below) were taken from Müller-Navarra et al. (2019). Analyses for GeoHH-FK were conducted with the CANBERRA's high-purity Germanium detector (HPGe) with a gamma-spectrometry analysis at the Laboratory for Radioisotopes (LARI), Georg-August-University of Göttingen. Uncertainties (counting errors of ^{210}Pb, ^{137}Cs, and ^{241}Am) were derived from the relative statistical counting error and the measured activity; however, uncertainties of the unsupported ^{210}Pb were calculated by applying the Gaussian-error propagation formula on the previously obtained ^{210}Pb counting errors. For further details, see Bunzel et al. (2020). Furthermore, radionuclide data were corrected to the time of sampling (decay-correction), from which the unsupported ^{210}Pb and ^{137}Cs were further corrected to the sum of organic carbon and portion of the < 20 µm sediment fraction (Ackermann et al., 1983; Cundy and Croudace, 1995; Milan et al., 1995; Kirchner and Ehlers, 1998). At the Leibniz Institute for Baltic Sea Research Warnemünde (IOW), Hg measurements were conducted by using a Milestone Company's DMA-80 Direct Mercury Analyzer; for further details, see Bunzel et al. (2020). There, precision of the Hg analyses was controlled by the recurrent measurement of a certified reference material (light sandy soil, Community Bureau of Reference, BCR-142R) and an intern Hg standard (Mecklenburg Bay sediment standard, MBSS-1) after every tenth sample. For further details, see Bunzel et al. (2020), and the description of the stratigraphic framework in Appendix C.

3.3.4 Spectral analyses. For the evaluation of periodic signals in the proxy records, spectral analyses were carried out on the unevenly spaced time series of the ln(Br/Cl) and ln(Zr/Rb) records of sites TB13-1 and GeoHH-FK. The ln(Br/Cl) and ln(Zr/Rb) records were chosen for spectral analysis, since they provide the highest resolution of data points. Statistical significance is expressed with the χ^2 95% and χ^2 99% red-noise levels; however, subsequent data interpretation will build on the power spectra exceeding χ^2 99% as well as periods > 2.5 years only. Spectral analyses were performed with the PAleontological STatistics (PAST) software package version 4.02 (Hammer et al., 2001), using the integrated REDFIT module with a Welch window (Schulz and Mudelsee, 2002).

3.4 Results

3.4.1 Sediment composition and description. The total sediment recovery with the U-channels varied between 110 cm (TB13-1) and 116 cm (GeoHH-FK). Concerning the organic and inorganic carbon free sediment fraction, the investigated sediment sequences mainly consist of fine sand and silt, i.e., on average 55% sand and 43% silt for TB13-1, and between 61% sand and 38% silt for GeoHH-FK. The clay content can be neglected with low values ranging between 2% (TB13-1) and 0.5% (GeoHH-FK) on average (Fig. 10). The average mean grain size is 63.33 µm for TB13-1 and 70.84 µm for GeoHH-FK (Bunzel et al., 2020). The organic carbon (C_{org}) content is generally very low at both sites, showing mean values of 0.86% for TB13-1, and 0.57% for GeoHH-FK, however, maximum values occurred

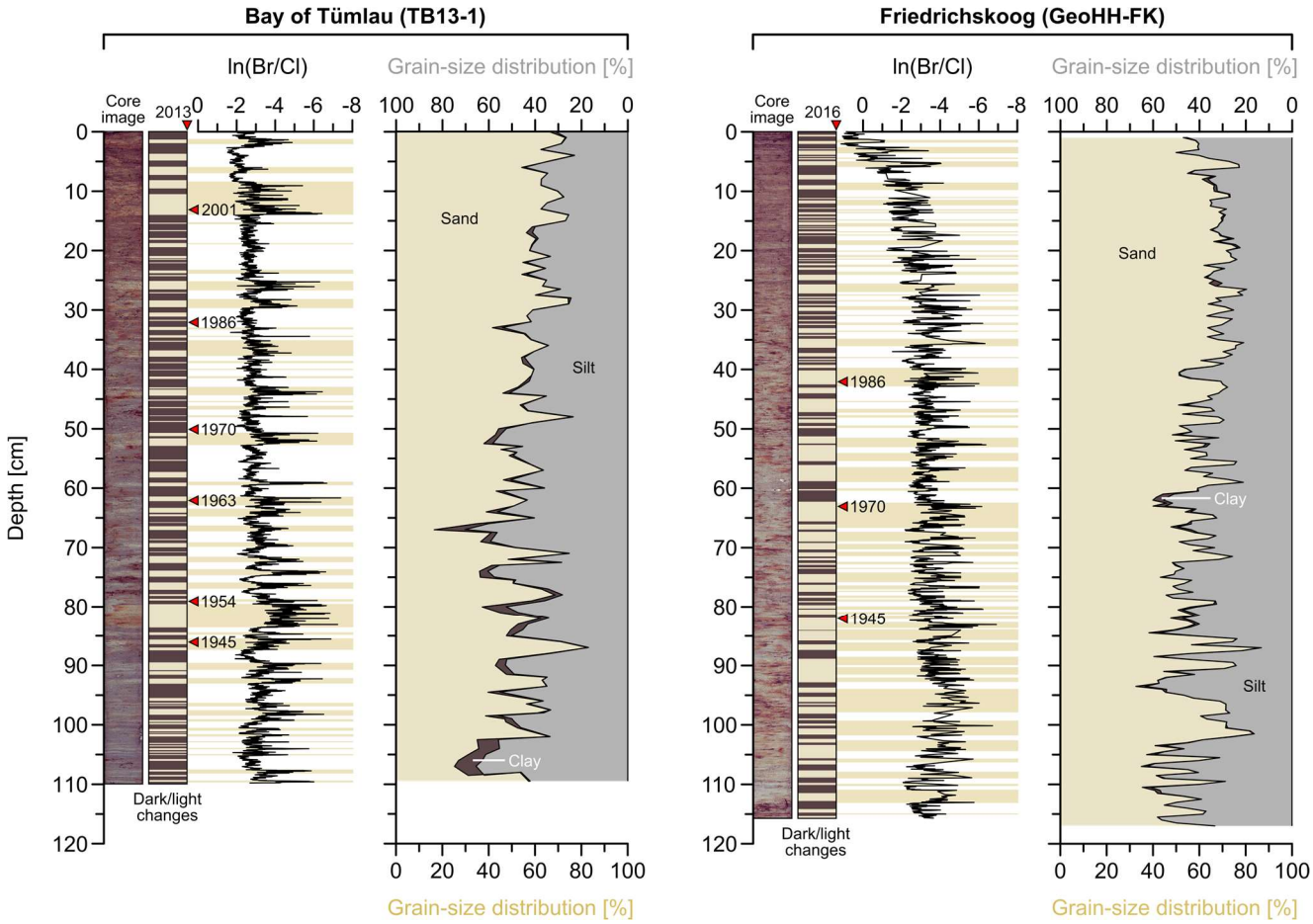

Fig. 10 | Generalized sediment stratification in association with changes in the deposition of sedimentary organic matter (ln[Br/Cl] ratio) – indications for seasonal supply? Optical images of the two sediment sequences TB13-1 and GeoHH-FK together with simplified dark/light brown colour changes, representing the dark reddish-grey to light greenish-grey sediment colours, and reliable age markers given in years CE (red triangles; Bunzel et al., 2020). Prominent drops in the ln(Br/Cl) records are highlighted with light brown shaded bars. The relative sediment composition comprises the fractions sand (light brown), silt (grey), and clay (dark brown); note the inversely oriented x-axes.

in the uppermost sediments. Furthermore, both sediment sequences are characterized by a prominent horizontal lamination of alternating light (greenish-grey) and dark (reddish-grey) coloured layers (Fig. 10; Müller-Navarra et al., 2019; Bunzel et al., 2020). The light colour is likely caused by a reduced proportion of organic components being incorporated in the sediment matrix (Müller-Navarra et al., 2019). The thickness of the individual layers in the sediment sequences ranges from around one millimetre to a few centimetres, in which the layers are slightly thickening upward, accompanied by a gradual upward coarsening trend at both sites (Fig. 10). At site GeoHH-FK, a horizontal shell layer was observed in a depth of 24 cm, which could be continuously traced along the entire erosional cliff face (see Appendix Fig. C2). The bottommost intervals at both sites were defined as reduced horizons (below ca. 100 cm at site TB13-1 and below ca. 110 cm at site GeoHH-FK), which are temporarily to permanently affected by ground water, revealing a dark greyish to blackish sediment colour (Bunzel et al., 2020).

3.4.2 Geochemical and spectral analyses. Both ln(Br/Cl) records are characterized by strong and high-frequency fluctuations with the recurrent occurrence of sharp drops, which can be attributed either to bromine (Br) decreases or chloride (Cl) increases (Fig. 10). These drops clearly coincide with the light greenish-grey coloured sandy sediment intervals. At site TB13-1, the distinct drops in the ln(Br/Cl) record are displaying variations on multi-decadal to inter-decadal timescales with strong power at periods of 131.5, 21.9, and 12.0 years at the > 99% χ^2 confidence level, as well as at periods of 6.6, 5.7, and 3.2 years (Fig. 11). In comparison, the ln(Br/Cl) record of site GeoHH-FK lacks any significant periodic variability, instead, this record is characterized by a prominent long-term increase towards today (Figs. 10, 11).

The ln(Zr/Rb) records reveal a variability on inter-decadal timescales with generally higher values occurring around 1930 CE (at ca. 98 cm depth) and between 1940 and 1950 CE (ca. 86 cm; see Appendix Figs. C3, C4). From 1950 CE onwards, the decadal variability is superposed by a long-term increasing trend. At site TB13-1, the ln(Zr/Rb) record exhibits significant power (> 99% χ^2 confidence level) centred at periods of 65.8, 16.4, 10.1, 6.9, and 4.5 years. At site GeoHH-FK, the ln(Zr/Rb) record shows significant power at the > 99% χ^2 confidence level, centred at periods of 76.9 and 19.2, respectively (Fig. 11).

For the total recorded time span (1914–2013 CE), the Br/C_{org} ratio of sediments at site TB13-1 exhibits an overall increasing trend, with maximum values around the late 2010s (within the top 10 cm depth), and a transient depletion during the 1950s (ca. 80 cm; see Appendix Figs. C3, C4). The Br/C_{org} record at GeoHH-FK partly resembles that of TB13-1, however, with lowest values around the early 1930s (at around 90 cm depth) and a subsequent increase, finally peaking around 1990 CE (ca. 35 cm). After 1990 CE, the Br/C_{org} ratio returns to low values, similar to those between 1930 and 1940 CE (see Appendix Figs. C3, C4).

3.5 Discussion

3.5.1 Salt-marsh depositional systems and their regional variations in sediment characteristics. The sediment sequences of the present study are generally dominated by fine sand (> 63 µm; on average 55% at the Bay of Tümlau and 61% at Friedrichskoog) and silt (< 63 µm; on average 43% at the Bay of Tümlau and 38% at Friedrichskoog), with rather moderate down-core variations (Fig. 10). The coarsening trends were observed by both the measured grain-size spectrum and the ln(Zr/Rb) ratio. In both sequences, however, changes in the sediment characteristics are indicated by a clearly distinct fine-scale stratification and lamination, which can be attributed to the recurrent influence of the hydrodynamic interaction between storm surges and tides (e.g., Reineck, 1982). If, however, the allocation criteria are solely based on the grain-size spectrum of the different sediment layers, storm-surge events cannot be clearly discriminated within the studied salt-marsh deposits. In fact, sedimentation dynamics in coastal salt-marsh environments are rather highly complex. For this reason, there is often inconsistency about the characteristic composition of sediment particles transported onto the salt-marsh surface during a storm surge. In various German, Dutch, and UK salt marshes, the deposition of relatively coarse-grained layers, containing sand grains and/or shell fragments, have been associated with severe storm surges (e.g., Ehlers et al., 1993; de Groot et al., 2011; Schuerch et al., 2012; Swindles et al., 2018). In contrast, Eisma and Irion (1988) and Bartholdy (2000) related the deposition of fine-grained material (< 63 µm) originating from the North Sea basin to storm surges. There, the mud of the adjacent tidal flats represents a mobile layer, which is re-suspended during the increasing shear stress of a storm event (Bartholdy and Aagaard, 2001).

Correspondingly, the high-resolution ln(Br/Cl) records from the Bay of Tümlau and Friedrichskoog were used for a more detailed reconstruction of regional storm-surge impacts and the assessment of differences in sediment accretion in a high-frequently dredged and grazed versus a less-frequently dredged and un-grazed salt marsh. Since the light greenish-grey coloured and more sandy sediment intervals clearly coincide with abrupt drops in the ln(Br/Cl) values (Fig. 10), this coincidence suggests a loss of bromine and/or supply of chloride during deposition of the siliciclastic coarser-grained sediments, which may be directly related to single storm surges (Swindles et al., 2018). In intertidal coastal wetlands, bromine is known to be incorporated by various marine

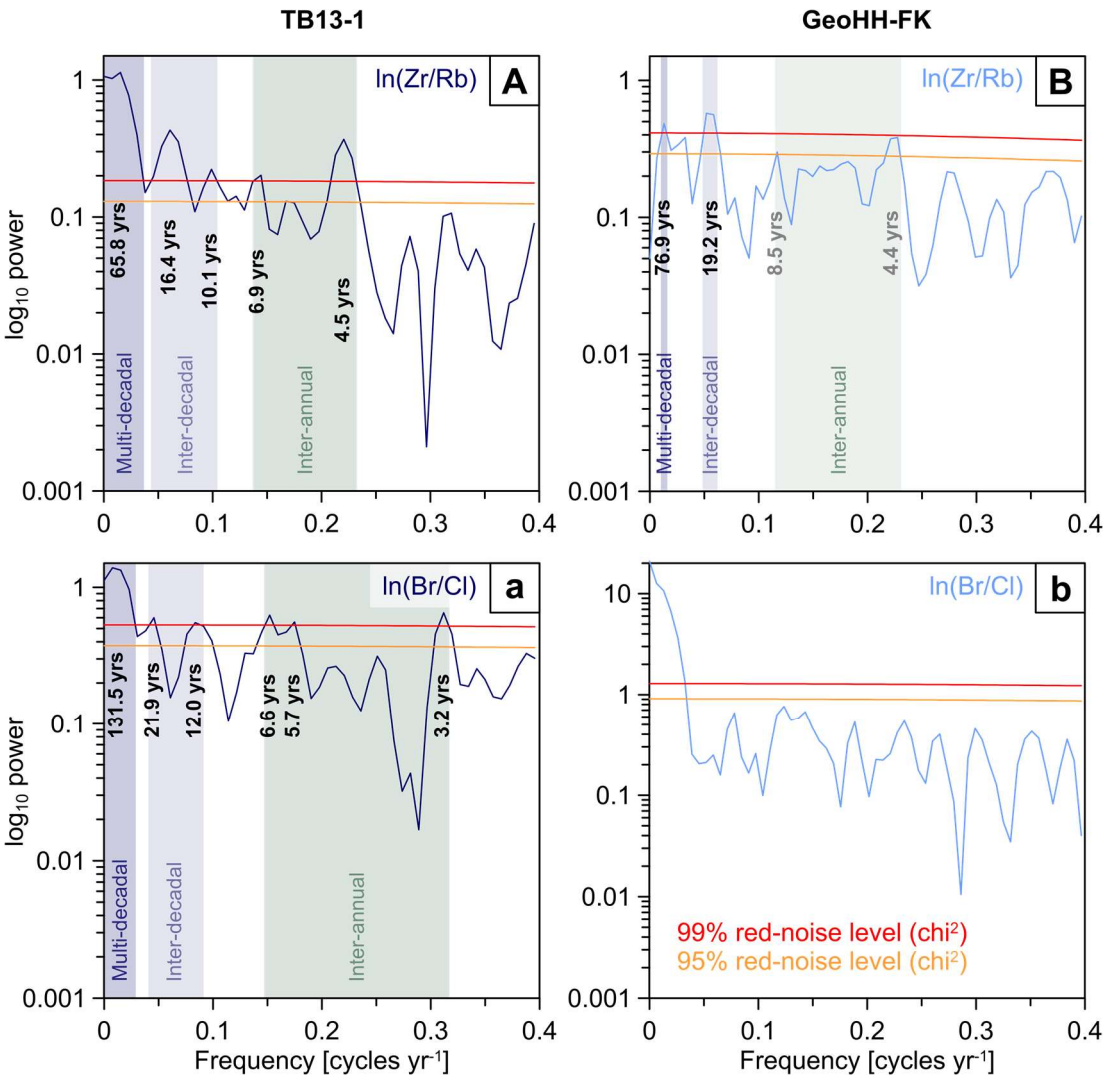

Fig. 11 | Spectral analysis characterises periodic fluctuations in the sedimentological and geochemical proxy data. REDFIT power spectra with 95% and 99% red-noise confidence levels (chi²) of the ln(Zr/Rb) and ln(Br/Cl) ratios at sites TB13-1 (**A**, **a**; dark blue line) and GeoHH-FK (**B**, **b**; light blue line), using a Welch window. Black numbers indicate periods in which the corresponding power spectra is > 99% red-noise level, grey numbers indicate periods which are significant at > 95%. Shaded bands denote the relevant time intervals.

primary producers such as phytoplankton, macroalgae, and seagrass, thus representing the marine organic carbon (MOC; Mayer et al., 1981, 2007, and references therein). In addition, bromine can indicate high sediment porosity accompanied by a high seawater content in the pore spaces (Thomson et al., 2006; Ziegler et al., 2008). In contrast, enrichments in chloride are only found in the sedimentary pore water (Thomson et al., 2006), remaining almost constant with increasing sediment depth (Beck et al., 2008). Consequently, the ln(Br/Cl) ratio can provide information about changes in the marine organic matter supply. An enhanced transport of re-suspended material from the surrounding tidal flats during a storm-surge event (e.g., Eisma and Irion, 1988), may then result in a concomitant increase of the MOC deposition on the adjacent salt marshes. However, North Sea ecosystems are characterized by strong seasonal contrasts in primary production and storm surge induced suspension, with maximum production rates during spring and summer, but maximum re-suspension of the sediment particles during winter (Skogen et al., 1995). These seasonally differing impacts seems to be archived by the stratified salt-marsh sequences, which show regular alternations between clayey-silty (dark reddish-grey coloured) and silty-sandy (light greenish-grey coloured) sediment layers across the depths. Accordingly, the stratification presumably reflects the different influences of

storm surge-induced sediment accretion (Redfield, 1972; Behre and Streif, 1980; Ehlers et al., 1993; Chaumillon et al., 2017), in dependence of that times at which the suspended material of the water columns contains more MOC and finer-grained sediments, respectively, less MOC and coarser-grained sediments (e.g., Bartholdy and Anthony, 1998). Based on these observations, the abrupt drops in the ln(Br/Cl) records in connection with the light greenish-grey coloured and more silty-sandy sediment intervals, particularly evident throughout the sediment sequence at the Bay of Tümlau, likely represent deposits evoked by regional storm surges in winter time. During winter, the MOC content of the total suspended matter is ≤ 20% (Eisma and Irion, 1988), and the high sedimentary pore volume in the sand layers promotes an enrichment of chloride (Thomson et al., 2006). Hence, pronounced drops in the ln(Br/Cl) ratio further represent the dilution of the re-suspended MOC by the concomitant high proportion of siliciclastic coarser-textured particles. Conversely, clayey-silty intervals revealing comparably higher ln(Br/Cl) values may then represent re-suspension in spring to fall under generally calm weather conditions with less intense storms, when the suspended material encompasses highest MOC contents together with finer-grained particles. This is in line with studies by Bartholdy and Anthony (1998), who documented the highest import of fine-grained sediments from the open North Sea to the Wadden Sea coast at times of fair weather conditions.

At Friedrichskoog, the observed small-scale variability in the ln(Br/Cl) ratio is less pronounced and rather superposed by the overall increasing values towards the sediment surface. Inspection of the XRF raw data reveals that this long-term ln(Br/Cl) increase is mainly caused by a concomitant decrease of the chloride counts. Since the salt-marsh surface at Friedrichskoog is situated 2.80 m above NHN (1.06 m above mean high water spring, MHWS), while the salt marsh in the Bay of Tümlau is situated only 2.09 m above NHN (0.50 m above MHWS), the seawater induced chloride supply likely decreased with increasing height of the salt-marsh surface at Friedrichskoog. This would be compatible with a long-term decrease in submergence time and frequency responding to the gradual elevation of the salt-marsh surface at Friedrichskoog during recent times. There, the increase in surface level was probably artificially promoted by the frequent dredging measures. As a consequence, the top soils at the more elevated erosional cliff became partly dehydrated (e.g., de Jong et al., 1994). In contrast, the more sheltered location of the lower salt marshes in the Bay of Tümlau favoured a more sensitive and persistent response of short-term depositional processes to seasonal changes in storminess. At this site, the response of the salt-marsh system to regional climate variability was further enhanced by a return of natural conditions when grazing and draining was persistently stopped after National Park foundation (Müller-Navarra et al., 2019).

When further taking the obtained mean accretion rates into consideration, slightly lower average accretion rates (1.16 cm yr^{-1}) appeared in the grazed and ditched salt marsh at Friedrichskoog when comparing to the less modified and more naturally developed salt marsh in the Bay of Tümlau (1.31 cm yr^{-1}; Bunzel et al., 2020). This result is surprising since the salt-marsh surface at Friedrichskoog is much higher with 2.80 m NHN, and at this more wave-exposed open coastal site the general net transport and deposition of re-suspended sediments during storm surges should be expected to be higher than in the semi-enclosed salt marsh in the Bay of Tümlau. Apparently, the contrasting accretion rates can be partly attributed to the different anthropogenic land-use histories, including the establishment of different vegetation types. Particularly, interventions by intense grazing management affect the heterogeneity of the salt-marsh plant communities (Bakker et al., 2019). Consequently, a monotonous short-grazed sward cover (mainly consisting of *Puccinellia maritima*), as it is found at Friedrichskoog, can diminish the process of capturing suspended sediments from incoming waves during submergence (Kiehl et al., 1996; Nolte et al., 2013a). In comparison, the development of a more natural vegetation in the Bay of Tümlau enhanced the accretion rate of sediment particles during storm surges (Schuerch et al. 2012; Möller et al., 2014; Leonardi et al., 2018; Müller-Navarra et al., 2019). However, due to the semi-enclosed position of the bay, storm-surge waves are attenuated and sediment deposition on the salt marsh occurs under relatively low-energy conditions (Müller-Navarra et al., 2019). This is underlined by the absence of shell fragments within the potential silty-sandy storm layers, but the occurrence of allochthonous calcareous foraminiferal tests originating from the surrounding tidal flats (Müller-Navarra et al., 2019). This finding is in accordance with results from sheltered Dutch salt marshes, where the deposition of sediments was associated with low-energy conditions of tides and waves (de Jong et al., 1994). Further, the estimated accretion rates at the Bay of Tümlau slightly decreased in recent times, which implies a naturally advanced stage of maturity of the local marsh system. In contrast, the potential storm layers deposited at Friedrichskoog contain comparatively more coarse particles, occasionally even larger shell fragments. This suggests an exposition of the studied salt-marsh sequence to rather high-energy conditions during a storm surge. Nevertheless, the overall sediment-accretion rate is lower at Friedrichskoog due to the combined effects of an altered vegetation by grazing, and a rather flat salt-marsh morphology, which is at the same time artificially elevated due to the intense dredging and drainage measures (e.g., de Jong et al., 1994; Müller-Navarra et al., 2016).

3.5.2 Salt-marsh archive of changes in storminess and regional sea level. The effects of changing extreme water levels on salt-marsh depositional processes were further evaluated by considering the sedimentary Br/C_{org} ratio. The similar appearing long-term trends in both Br/C_{org} records from the Bay of Tümlau and Friedrichskoog reveal lowest Br/C_{org} values during the first half of the 20th century, suggesting that the marine influence was likewise comparatively low during this time. Whereas, the subsequent increase in Br/C_{org} values from the mid-century towards recent times, with highest values occurring between 1990 CE (Friedrichskoog) and 2010 CE (Bay of Tümlau), reflect an increase in the marine contribution towards recent times (Fig. 12). Consequently, both Br/C_{org} records are resembling the trends in North Sea storminess, which is reflected by the historical wind observation and tide-gauge data at Husum, Büsum, and Cuxhaven showing a gradual amplification in the wind strength and water-level height around 1920 CE and towards the 1990s (Fig. 12). In fact, North Sea storminess varies on timescales of decades and longer, in which periods of enhanced storminess mainly coincide with the beginning and the end of the 20th century, while a period of reduced storminess occurs during the mid-century centred around 1960 CE (Matulla et al., 2008; Weisse et al., 2012; Dangendorf et al., 2014). It remains unclear, however, why the highest Br/C_{org} values at the different sites appear with an offset of about 20 years, i.e., 20 years earlier at Friedrichskoog (1990 CE) than in the Bay of Tümlau (2010 CE). These contrasts may likewise reflect the land-use histories of the two salt marshes with differences in morphology, elevation, and corresponding vegetation communities affecting the local submergence frequencies. Furthermore, the different and highly dynamic depositional environments at the North Sea coast may, most likely, account for ageing uncertainties within the salt-marsh stratigraphy, although the obtained age models appear relatively robust for the past ~70 years (Bunzel et al., 2020). Moreover, both Br/C_{org} records imply a storminess strengthening already starting in the first half of the 20th century, while the increasing coarsening of the sediments (as suggested by the ln[Zr/Rb] ratio) started to be decoupled from the previously prevailing inter-decadal variability since around 1950 CE, which is in line with model simulations (e.g., Matulla et al., 2008). However, the upward coarsening trends at both sites reflect rather indirectly the increase in marine influences, as the seaward edges of the salt marshes are progressively under erosion when sea level rises, leading to a retreat of the marsh-edge cliffs and increasingly proximal depositional conditions (e.g., Allen, 1989; Ehlers et al., 1993).

The modern extreme water levels, and associated risks by flooding, started to increase from the mid-20th century onwards, outpacing the rate of regional sea-level rise (SLR; e.g., Mudersbach et al., 2013; Arns et al., 2017). The reason is that mean sea level (MSL) and extreme sea levels rather seem to represent a non-linear feedback, i.e., a regional long-term MSL rise does not necessarily result in a comparable linear rise in extreme high-water levels (e.g., Dangendorf et al., 2013b; Mudersbach et al., 2013; Arns et al., 2015; and references therein). Indeed, the climate mechanisms being responsible for variations in the extreme water level and accompanied flooding likely differ from those causing background sea-level variations (Lang and Mikolajewicz, 2019). Consequently, the North Sea storminess itself lacks a clear long-term trend (Weisse et al., 2012), as it was observed for the MSL (2.4 ±0.1 mm yr^{-1}; Dangendorf et al., 2013a).

Commonly, shallow coastal environments are considered extremely vulnerable to the impacts of an accelerating SLR and possible changes in storminess (Dangendorf et al., 2013b; Arns et al., 2017). Assuming a maximum SLR scenario of 84 cm by 2100 CE (IPCC, 2019), up to 45% of the salt-marsh areas may vanish, at least along the south-eastern U.S. coast (Craft et al., 2009). Although those salt-marsh areas that receive high amounts of minerogenic sediment supplies may compensate for the SLR-evoked loss of coastal wetland habitats (French, 2006; Stevenson and Kearney, 2009). Accordingly, the recorded sediment-accretion rates of 1.16–1.31 cm yr^{-1} in Friedrichskoog and the Bay of Tümlau suggest that the different salt-marsh systems at the south-eastern North Sea coast are currently able to outpace the ongoing SLR, as long as the required sediment import and flooding dynamics are ensured (Bunzel et al., 2020). In addition to the direct consequences of climate-induced SLR and concomitant differences between MSL and extreme sea levels, coastal protection measures may have also contributed to a change in the storm-surge signal (Dangendorf et al., 2013b). Since there was no need to maintain the heights and efficiency of dikes between 1855 and 1962 CE, due to the period of reduced storminess, the severe storm-surge event in 1962 CE caused many dike failures, and thus a wide range of damages and casualties along the German North Sea coast (von Storch et al., 2008). As a consequence, extensive investments were subsequently initiated to improve coastal protection measures, i.a., by improving the dike bases and rising the dike levels up to 7.20 m above NHN, entailing persistent ecological and morphological impacts on the coastal ecosystems (Kelletat, 1992; von Storch et al., 2008; Dangendorf et al., 2013b). Hence, the establishment and observed retreat of the erosional salt-marsh cliffs and accompanied coarsening trends, as mentioned above, likely have been further accelerated due to intensified coastal protection measures, as the dikes in the hinterland prevent a landward migration of the salt marshes with SLR.

3.5.3 North Atlantic climate control on salt-marsh sedimentation in the German Bight. The investigated sediment archives cover approximately the last 100 years. A similar long-term variability in both ln(Zr/Rb) records suggest comparable depositional processes in the Bay of Tümlau (TB13-1) and Friedrichskoog (GeoHH-FK), although the different exposures and land-use histories account for site-specific differences. The relative alternation of coarser- and finer-grained material on inter-decadal timescales, i.e., at periods of 10.1 and 16.4 years (TB13-1), and 19.2 years (GeoHH-FK), is particularly pronounced during the early 20th century until 1950 CE (Fig. 12). In comparison, the ln(Br/Cl) record of site TB13-1 exhibits similar variability with significant periods centred at 12.0–21.9 years, while site GeoHH-FK lacks comparable periodicities at the > 99% confidence level (Fig. 11). Hence, the observed periodicities of the ln(Zr/Rb) and ln(Br/Cl) records suggest a close linkage of sediment accretion, changes in flooding dynamics, and related shifts in the primary production to super-regional oscillations in the atmosphere-ocean system. One of the major modes, forcing a recurrent atmospheric circulation pattern in the Northern Hemisphere, is the North Atlantic Oscillation (NAO; Hurrell, 1995; Hurrell et al., 2003), which exhibits an 11–25 year period related to the solar Hale cycles (Fairbridge and Krebs, 1961; Raspopov et al., 2004). The NAO dipole anomalies between the Arctic and subtropical Atlantic are responsible for a variety of climate changes concerning wind speed and direction, precipitation, and temperature (Hurrell, 1995; Hurrell et al., 2003; Wakelin et al., 2003; Ionita et al., 2011). The occurrence of oscillating climate patterns on inter- to multi-decadal timescales is, however, often discussed as being the result of various interfering climatic teleconnections (e.g., Comas-Bru and McDermott, 2014). Consequently, the observed periodic changes in salt-marsh sedimentation dynamics may be likewise the product of interfering decadal-scale shifts in the climate system.

Regional environmental responses to interfering climate modes were further postulated by Ionita et al. (2011) and Zanchettin et al. (2019), who documented periodic inter-decadal fluctuations in the discharge of the Elbe river, centred at a period of 14.2 years. As discussed above, salt-marsh sediments along the south-eastern North Sea coast mainly originate from the surrounded tidal flats and/or adjacent eroded salt marshes (Schuerch et al., 2019), in which the prevailing anti-clockwise sea-surface circulation and tidal currents are responsible for the required erosion, transportation, and deposition of the sediments (Postma, 1981; Eisma and Kalf, 1987; Eisma and Irion, 1988; Winther and Johannessen, 2006). Additionally, ~4.8 × 10^6 t yr^{-1} of suspended particulate matter are remobilised by the rivers and transported into the North Sea basin (Eisma and Kalf, 1987; Eisma and Irion, 1988; Allen, 1990; Wolfstein and Kies, 1999). Based on that, the sediment sequence at Friedrichskoog is likely affected by both tidal currents and the Elbe river discharge, due to its exposed location in an open coastal salt-marsh setting and its proximity to the Elbe estuary (Bunzel et al., 2020). In contrast, the more sheltered salt marsh in the Bay of Tümlau located further north is expected to be less influenced by the latter, although its ln(Zr/Rb) record is similar to that at Friedrichskoog. Accordingly, high ln(Zr/Rb) values may at least partly reflect the enhanced availability of suspended material in the Wadden Sea during times of high river discharges, that are alternating on similar inter-decadal timescales.

Changes in the atmosphere-ocean climate oscillation over the North Atlantic and Europe are further generating shifts in the wind speed and direction, and corresponding MSL (e.g., Wahl et al., 2011; Dangendorf et al., 2013a), which may also have contributed to the observed changes on inter-decadal timescales in both ln(Zr/Rb) records (Fig. 12a). Specifically, dipole anomalies towards a positive NAO phase are associated with recurrent north-westerly winds and extreme sea-level high-stands in the German Bight (Lang and Mikolajewicz, 2019). These conditions may have fostered the deposition of coarser textured particles in the salt marshes under high-energy conditions. The observed long-term increase of both ln(Zr/Rb) records and sand contents since 1950 CE onwards (Fig. 12a), which is partly superimposed on the decadal trends, corresponds to the concomitant increase in North Sea storminess (Fig. 12d), and is also reflected by the gradual Br/C_{org} increase (Fig. 12b). Apparently, the ln(Zr/Rb) and Br/C_{org} records specifically reflect the period of strengthened North Sea storminess since the mid-1950s towards recent times, when the long-term increase in rates of extreme water levels is decoupled from the MSL, as related to changes in the tidal regime (Mudersbach et al., 2013; Arns et al., 2015, 2017). While a direct comparison between individual recorded storm tides, extreme sea-level simulations from model experiments (Fig. 12c; Lang and Mikolajewicz, 2019), and sedimentary proxy records may reveal inconsistencies, their long-term trends show similar variations on various timescales (Fig. 12), as described above. Accordingly, salt-marsh deposition along the south-eastern North Sea is likely driven by interfering large-scale climate variabilities and the combined effects of storminess and Elbe river discharge, and associated suspended matter availability.

In the ln(Zr/Rb) record originating from the Bay of Tümlau, strong spectral power was further observed for a period of 65.8 years, as well as for a period of 76.9 at Friedrichskoog. Despite the comparatively low statistical significance of these long periodicities, they may reflect a relation of sedimentation processes to the Altantic Multidecadal Oscillation (AMO), coinciding with changes in the North Atlantic sea-surface temperature (SST) on periods

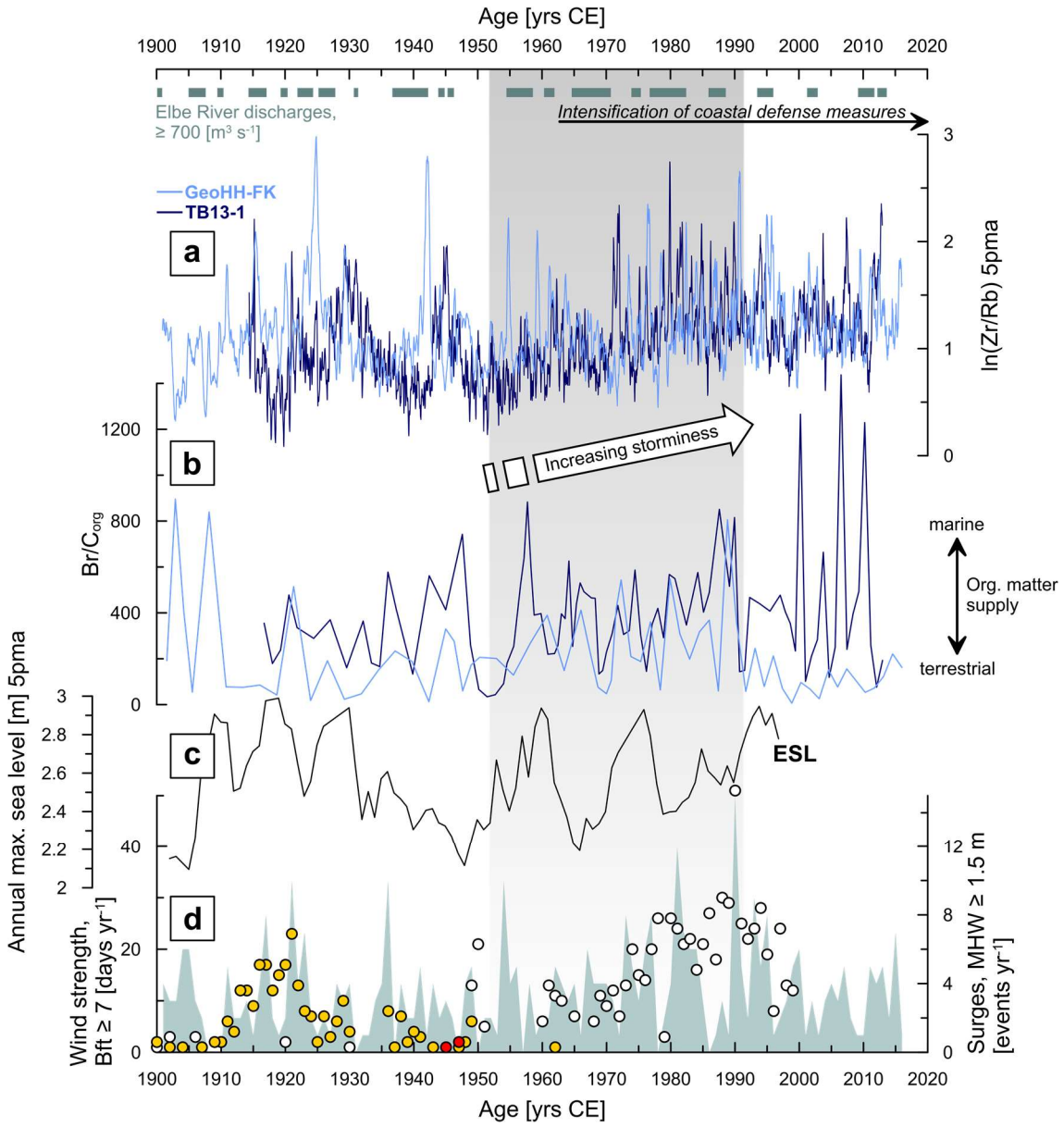

Fig. 12 | Twentieth-century changes of North Sea storminess. a, **b**) Distribution patterns of the ln(Zr/Rb) ratios as a proxy for grain-size fluctuations at the Bay of Tümlau (TB13-1; dark blue) and Friedrichskoog (GeoHH-FK; light blue), and Br/C_{org} ratios as indicator for changes in the marine organic matter supply. **c**) Simulated times series of extreme sea levels (ESL) at Cuxhaven; data were provided by Lang and Mikolajewicz (2019). **d**) Yearly number of recorded storm-surge days, which are exceeding the mean high water (MHW) with ≥ 1.5 m at the Cuxhaven tide gauge (light blue green), and number of days with westerly winds exceeding ≥ 7 Beaufort (Bft) at Husum (yellow circles), Büsum (white circles), and Cuxhaven (red circles). The grey band marks the period of general amplified storm-climate conditions and concomitant increased flooding of the salt marshes. Dark green bars at the top show observed Elbe River discharges at Neu-Darchau, when the annual mean discharges are exceeding the total mean discharges of 700 $m^3 s^{-1}$. 5pma = 5-point moving average.

of 50–90 years (Enfield and Cid-Serrano, 2010). Accordingly, the complex interaction of NAO and AMO and superposition of various periodicities in driving European hydroclimate (e.g., Enfield et al., 2001; Sutton and Dong, 2012; Zanchettin et al., 2019), may account for a comparable long-term periodicity archived by sediments of salt marshes in the Bay of Tümlau and Friedrichskoog. However, any long-term fluctuations cannot be confidently proven, as data of the corresponding sediment sequences are limited by covering only the last ca. 100 years.

Variability on shorter timescales, comprising significant periods between 3.2 to 6.9 years (> χ^2 99%), as documented by the ln(Br/Cl) and ln(Zr/Rb) records in the Bay of Tümlau, and periods with comparatively weak power (> χ^2 95%) between 4.4 and 8.5 years at Friedrichskoog (Fig. 11), cannot be clearly linked to any climate modes either, as they are likely impacted by coastal management activities. Specifically, these small-scale changes may be attributed to human-induced dredging activities, in which the drainage systems are recurrently renewed by removing the previously accumulated sediments from the drainage trenches and by replacing the material onto the surrounding salt-marsh surfaces (Nolte et al., 2013a; Müller-Navarra et al., 2019; Bunzel et al., 2020). Close to the Elbe estuary, these measures are carried out every two to three years, while the time intervals for dredging activities are increased further north (every three to seven years). This strategy considers the northward decrease in the amount of suspended particles in the water column, leading to a reduction of accumulated sediments in the drainage trenches of salt marshes in the North (pers. comm. Schleswig-Holstein Agency for Coastal Defence, National Park and Marine Conservation, LKN.SH, 2017, 2020). This management strategy was carried out in most salt-marsh systems of the south-eastern North Sea, before it was successively abandoned with establishment of the Wadden Sea National Park in 1985 CE in many areas, including the Bay of Tümlau (Nolte et al., 2013a; Müller-Navarra et al., 2019). Nowadays, these dredging activities are mainly restricted to salt-marshes, which are still grazed, such as Friedrichskoog, accounting for the observed differences in the disturbance of the sediment sequences.

3.6 Conclusions

High-resolution geochemical and sedimentological proxy records from two different salt marshes of the south-eastern German North Sea coast document variations in regional storm-climate conditions and potential links to North Atlantic climate conditions during the past century. The studied salt marshes include the more naturally developed salt-marsh at the Bay of Tümlau and the intensely anthropogenically modified salt marsh at Friedrichskoog. Despite different human management histories of ditching and grazing, storm-surge signals are archived in the sediment archive of both studied salt marshes. The main conclusions of this study are summarized below:

(1) Contrasting sediment-accretion rates in the Bay of Tümlau and Friedrichskoog reflect different anthropogenic land-use histories, which are accompanied by the establishment of deviating vegetation types. The less modified and more naturally developed salt-marsh vegetation in the Bay of Tümlau fostered sediment accumulation during storm surges, although the deposition on the salt marsh occurs under relatively low-energy conditions within the semi-enclosed position of the bay. In contrast, at the more wave-exposed open coastal salt marsh at Friedrichskoog, the deposited storm layers contain coarser particles, however, the overall sediment-accretion rate is lower due to the altered vegetation by grazing. Pronounced drops in the ln(Br/Cl) records together with the occurrence of sandy sediment layers are likely owed by storm surges in winter, when extreme water levels and subsequent inland propagating storm waves are more frequent and intense. The associated suspended material contains less marine organic carbon (MOC), and the enhanced sediment porosity in the sand layers allows for an enrichment of chloride. Hence, variations in the ln(Br/Cl) ratio are interpreted to reflect the seasonal differences in the effects of storm surges, but the specific exposure and land-use history of a salt-marsh system determines how well the signal is archived in the deposited sediments.

(2) Both salt-marsh sequences exhibit lowest Br/C_{org} values during the first half of the 20th century, suggesting that the marine influence was comparatively low during this time. The Br/C_{org} ratios started to increase from the mid-20th century towards recent times, with highest values occurring between 1990 and 2010 CE. This trend is accompanied by a concurrent increase of the ln(Zr/Rb) ratios, resembling the period of strengthened North Sea storminess since the mid-1950s onwards, when the long-term increase in rates of extreme water levels is decoupled from the MSL. The general coarsening-upward trends in the ln(Zr/Rb) ratios can then be attributed to the combined effects of the retreating erosional cliff face, increasing flooding frequency due to enhanced storminess, but also intensified coastal protection measures.

(3) The salt-marsh successions reflect changes in the regional storm climate, revealed by the ln(Zr/Rb) records alternating on inter-decadal (10–19 years) timescales at both study sites. In comparison, the ln(Br/Cl) record from the Bay of Tümlau varies on timescales of 12–22 years, while similar periodicities are lacking at Friedrichskoog. These periodicities suggest a close linkage of the North Sea storminess and associated shifts in the primary production to oscillations in the atmosphere-ocean system. The corresponding large-scale atmospheric circulation anomalies are the main drivers of European hydroclimate, generating (multi-) decadal variability of precipitation and related river runoff, westerly winds and extreme water levels in the German Bight. Apparently, the salt-marsh depositional systems in the sheltered Bay of Tümlau responded particularly sensitive to super-regional climatic impacts.

Acknowledgements

This study was conducted within the research project SEASTORM, which is part of the Priority Program (SPP-1889) Regional Sea Level Change and Society (SeaLevel). Financial support was provided by grants SCHM1180/19 and MI1508/4 from the German Research Foundation (Deutsche Forschungsgemeinschaft, DFG). We acknowledge the State Office for Surveying and Geoinformation Schleswig-Holstein (Landesamt für Vermessung und Geoinformation Schleswig-Holstein, LVermGeo SH) for providing information of the trigonometric points, the German Meteorological Service (Deutscher Wetterdienst, DWD) for delivering historical wind-observation data, and the Federal Maritime and Hydrographic Agency of Germany (Bundesamt für Seeschifffahrt und Hydrographie, BSH) for providing tide-gauge data of the German North Sea coast. The Global Runoff Data Centre (GRDC) is thanked for providing Elbe river discharge data. Christian Wiedemann and Martin Stock, National Park of the Schleswig-Holstein Wadden Sea (Nationalpark Schleswig-Holsteinisches Wattenmeer), are thanked for providing permissions to work in the restored salt marshes. The manuscript profited from the comments and suggestions of two anonymous reviewers. Andreas Lang and Uwe Mikolajewicz are thanked for providing simulated extreme sea-level data of the German Bight and for many discussions. We also thank Jutta Richarz, Sascha Plewe and Niko Lahajnar for technical support during XRF scanning and laboratory analyses. Bastian Vennemann and Pavel Reich developed the Python scripts and R packages to manage the large amounts of historical wind and tide-gauge data.

Author contributions

Sample preparation and laboratory analyses were carried out by D.B., who also designed the study and wrote the article. K.M.N. provided the required data for sediment sequence TB13-1, comprising the grain-size data (published in Müller-Navarra et al., 2019) and XRF scans (unpublished). H.W.A. supervised the processing and data discussion of all XRF scans. Y.M. and G.S. contributed to all data discussions by providing helpful advice, comments, and revisions during the article preparation phase.

Data availability

All measured data used and discussed in this article are available at:
https://doi.pangaea.de/10.1594/PANGAEA.927307.

Chapter Four

The content of the following Chapter is based on the submitted article entitled:

Bunzel, D., Milker, Y., Francescangeli, F., Schmiedl, G., 2020. The response of human-modified coastal wetlands from the southeastern North Sea to amplified storm-climate conditions: indications by deformed marsh foraminifera. *Ecological Indicator*, under review.

The response of human-modified coastal wetlands from the south-eastern North Sea to amplified storm-climate conditions: indications by deformed marsh foraminifera

D. Bunzel *et al.*

Submitted: 12 November 2020

Abstract

Intertidal wetlands are sensitive ecosystems that are subject to frequent storm surges and the progressing sea-level rise (SLR). Intact salt marshes are of substantial importance for the adaptation of coastal regions to impacts by ongoing and future climate changes, as they diminish the energy of the incoming storm-surge waves and capture the sediments brought by floods. It remains ambiguous, however, how human-modified salt marshes respond to more frequent storm-climate extremes and accompanied flooding. To address this question, the historical foraminiferal record of a sedimentary archive from the salt marsh at Friedrichskoog (south-eastern North Sea coast) was investigated, which has been intensely altered by human interventions during the past century due to draining and grazing measures. Increasing numbers of deformed tests of the salt-marsh indicator species *Entzia macrescens* between ~1950 CE and the late 1980s reflect the concomitant increasing environmental stress caused by frequent disturbances. These impacts can be linked to the observed North Sea storm-climate amplification. Comparison with results of a historical foraminiferal record of a less altered salt marsh in the vicinity, which exhibits comparatively less numbers of deformed specimens, indicates a particularly high vulnerability of intensely human-modified coastal wetland ecosystems to amplified storm-climate conditions.

4.1 Introduction

Most of today's foreland salt marshes along the German North Sea coast are of anthropogenic origin, as their development has been largely encouraged by artificially created drainage ditches and their regular upkeep. During the past century, the majority of these salt-marsh areas have been widely used for various agricultural activities such as livestock grazing (Esselink et al., 2009, 2017). Although grazing and drainage measures have been reduced since the Wadden Sea National Park was founded in 1985 CE, and are nowadays mainly restricted to areas close to the dike base, coastal salt marshes are still in urgent need of protection (Esselink et al., 2009). In fact, coastal ecosystems are projected to be more frequently and intensively exposed to impacts by extreme high sea levels (ESL) under the influence of global warming by 2100 CE (Arns et al., 2015, 2017; IPCC, 2019; Lang and Mikolajewicz, 2020). However, as salt marshes offer various natural ecosystem services, they need to be preserved (Bromberg Gedan et al., 2009). For instance, active salt marshes represent an efficient natural carbon sink due to primary productivity and the incorporation of organic carbon-rich suspended matter induced by submergences at high tides and storm surges (Kathilankal et al., 2008; Mcleod et al., 2011; Kirwan and Mudd, 2012; Müller et al., 2018). In principle, massive dikes, which are fringing the south-eastern North Sea coastline, represent the most common coastal protection measure in northern Germany (Kelletat et al., 1992). At the seaward side of the dikes, however, salt marshes act as a buffer zone and provide additional services by attenuating the energy of extreme storm-surge floods, and thus likewise substantially contribute to coastal protection by shielding the populated

hinterland from annual storm surges (Feagin et al., 2009; Kirwan and Megonigal, 2013; Möller et al., 2014). The resilience of salt marshes depends basically on their ability to grow vertically by incorporating suspended particles introduced by recurrent floods, thus, ensuring sediment-accretion rates that are higher than the sea-level rise (SLR), and their potential to migrate laterally further inland as SLR (Allen, 1990; Andersen et al., 2011; Kirwan and Megonigal, 2013; Kirwan et al., 2016). It remains unclear, however, how and to which extent anthropogenically modified coastlines and their ecosystems can withstand more frequently and intensively occurring ESLs and accompanied submergences during storm surges, which is a confident scenario by 2100 CE (IPCC, 2019). The resilience of human-modified salt marshes at the south-eastern North Sea coast is particularly questionable, as their original characteristic and natural features are no longer present. This includes the lacking landward increasing surface elevation or the absence of highly diverse halophytic plant communities, and most importantly, massive dikes prevent a spatial expansion of the marshes in the course of SLR. Accordingly, today's artificial salt marshes along the German North Sea coast are suspected to be particularly vulnerable to changes in regional sea level and storm surge-induced sedimentation.

Abundant benthic foraminifera that are occupying different tidal flat and salt-marsh habitats are increasingly used to assess the response of coastal intertidal ecosystems to changing environmental conditions, as they are sensitive to certain ambient ecological parameters (e.g., Alve, 1995; De Rijk and Troelstra, 1997; Geslin et al., 2000; Schönfeld et al., 2012; Francescangeli et al., 2016). In natural salt marshes, the occurrence of modern benthic foraminifera reflects their different species-specific sensitivity and tolerance ranges towards gradients in salinity, pH, substrate, or surface elevation, which are mainly controlled by the tidal exposure (e.g., Gehrels and Newman, 2004; Horton and Edwards, 2006; Kemp et al., 2009). Such observations allow for the assessment of modern in situ conditions in salt marshes, but also for the reconstruction of past environmental changes, e.g., initiated by changing sea levels and concomitant alterations of submergences at high tides and storm surges (Horton et al., 1999; Horton and Edwards, 2006; Scheder et al., 2019). By contrast, the human-modified salt marshes along the German North Sea coast lack a pronounced natural landward increase of surface elevation, and thus distinct vertical foraminiferal zones are absent (Müller-Navarra et al., 2016). Accordingly, the question arises how past environmental changes and related responses of coastal ecosystem can be reconstructed and assessed. In particular, if it has to be assumed that although it is possible to roughly differentiate between tidal influences (calcareous tidal-flat foraminifera) and marsh development (agglutinated salt-marsh foraminifera), this does not allow further validation of possible processes that have impacted the ecosystem. As concluded by previous studies, extreme abnormalities in the test morphology of benthic foraminifera can also provide information about ecosystem changes, apart from the occurrence of specific environmental indicator species (e.g., Geslin et al., 2000, 2002; Polovodova and Schönfeld, 2008; Brunner et al., 2013). Usually, calcareous benthic foraminifera are evaluated (e.g., species belonging to *Ammonia* or (*Cribro*-)*Elphidium*), whereby the quantity of deformed species may provide insights into environmental changes that are initiated, for instance, by heavy-metal pollution (Frontalini et al., 2009; Martínez-Colón et al., 2009, 2018). There, the incorporation of alien elements (heavy metals) into the calcareous test microstructure during certain ontogenetic stages can account for deformities (Frontalini et al., 2009). In comparison, and concerning agglutinated benthic foraminifera, highest numbers of deformities were found for the typical high-marsh indicator species *Balticammina pseudomacrescens* at salt-marsh sites heavily contaminated by oil (Brunner et al., 2013).

Here, the historical benthic foraminiferal record of a sedimentary salt-marsh archive from the south-eastern North Sea coast was evaluated that has been intensely modified by human activities due to land reclamation (draining) and agricultural land use (grazing) during the past ca. 100 years. The results are discussed in comparison with foraminiferal data from a less intense modified salt-marsh archive in the vicinity. This study builds on the investigation of irregularities in the agglutinated benthic foraminiferal species *Entzia macrescens*, which dominates in the distorted salt marshes where a distinct foraminiferal zonation is absent (Müller-Navarra et al., 2016). The aim is to assess how human-modified coastal wetlands have responded to the increasing exposure to more frequent and severe flooding during the last century under the influence of a rising mean sea level (MSL).

4.2 Regional setting

Since 1985 CE, German intertidal systems are under national nature protection and belong to the Wadden Sea National Park (Stock, 2003; Esselink et al., 2009). As a measure, parts of the existing salt marshes were substantially restored through de-embankments of summer polders, abandonment of the maintenance of artificial drainage ditches and pasture farming in order to preserve their ecosystem services including coastal protection and carbon sequestration (Esselink et al., 2009). However, the investigated coastal salt marsh north of the embanked polder Friedrichskoog (Fig. 13), northern Germany, is still actively modified by human interventions including draining measures and grazing by sheep stock (Bunzel et al., 2020). Thus, the ~6 km^2 territory in the northern part of the polder is characterized by a short-grazed monotonous vegetation

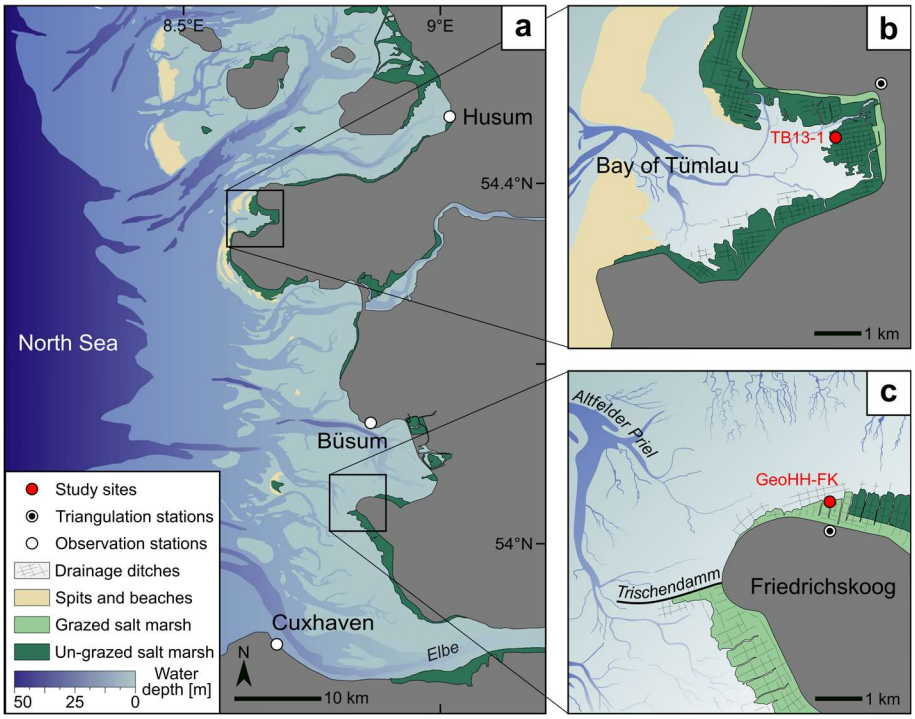

Fig. 13 | North German coastline with the studied sites at the south-eastern North Sea. a) Location map of the observational wind and tide gauge stations, and the present setting of the evaluated salt marshes at the Bay of Tümlau (**b**; TB13-1) and Friedrichskoog (**c**; GeoHH-FK). Data of TB13-1 were taken from Müller-Navarra et al. (2019).

consisting of few grass species (i.a., *Festuca rubra* and *Puccinellia maritime*) and a flat surface morphology lacking the typical and naturally pronounced landward surface increase (Stock et al., 2005; Bunzel et al., 2020). As the salt marsh is bordered to the south by a dike, the seaward marsh edge is further characterized by a striking erosional cliff. Due to its proximity to the Elbe river estuary, the coastal waters contain high amounts of suspended particles, causing a rapid filling of the local artificial drainage ditches at the adjacent salt marshes during high tides or storm surges. Consequently, the network of parallel ditches is dredged regularly every two to three years at Friedrichskoog (pers. comm. Schleswig-Holstein Agency for Coastal Defence, National Park and Marine Conservation, LKN.SH, 2020). The average tide levels recorded at the nearby tide gauge (Friedrichskoog Hafen, no. 110021) for the observation period 1986–2018 CE are the following (from highest to lowest level): highest astronomical tide (HAT): 2.14 m above NHN (Normal Null datum level); mean high water spring (MHWS): 1.74 m NHN; mean high water (MHW): 1.56 m NHN; mean low water (MLW): –0.41 m NHN; and mean low water spring (MLWS): –0.26 m NHN. The Federal Maritime and Hydrographic Agency of Germany (BSH) provided the tidal data. As the modern salt-marsh surface at Friedrichskoog is located 2.8 m NHN, it is therefore only flooded when the water level is raised, exceeding MHW by 1.5 m, and pushed ashore by severe storms (Gerber et al., 2016).

4.3 Materials and methods

4.3.1 Field work. This study builds on the investigation of the 1.16 m long sediment-filled U-channel named GeoHH-FK that was retrieved from the erosional cliff face at the seaward side of the salt marsh at Friedrichskoog in November 2016 CE (54°2'35.02"N, 8°52'20.41"E; Fig. 13); for further details see Bunzel et al. (2020). Surface elevation and position of the sampled erosional cliff were surveyed with the Leica Geosystems GNSS field controller (Viva Uno CS10) equipment with a vertical precision of 0.5 mm and a horizontal precision of 0.2 mm. The surveyed data were referred to a nearby triangulation station (no. 1919 088 00), and post-processing was realised with the Leica Geo Office 8.3 software package. Details for the triangulation station were provided by the State Office for Surveying and Geoinformation Schleswig-Holstein (LVermGeo SH).

4.3.2 Foraminiferal analyses. The obtained sediment sequence was sampled at 0.5 cm spacing, in which every second sample was considered for foraminiferal analyses, giving 116 samples in total with a sediment volume of ~1.75 cm^3 each. After sampling took place, all samples were preserved in 96% ethanol to avoid degradation of the organic components and buffered with a carbonate solution to prevent dissolution of the calcareous components. Counting of foraminiferal individuals was carried out on subsamples (splits) from the wet-sieved 63–500 µm size fraction. The splits were obtained by means of a wet-splitter (Scott and

Hermelin, 1993), into which each sample was placed for at least one hour to allow the sediment to fully and evenly settle down, producing eight equal splits per sample. The number of splits that need to be counted for their foraminiferal content depends on the minimum number of total individuals, which should be at least 300 per split according to the protocol for foraminiferal biomonitoring (Schönfeld et al., 2012). In the North Sea coastal marshes, however, the number of benthic foraminiferal species is rather low: 13 species in total, which in their average proportion throughout the sediment sequence GeoHH-FK account for > 1% of the total fauna. Therefore, foraminiferal analyses within this study are based on a target value of approximately 100 individuals per split, since a number of 100 counted foraminiferal individuals is sufficient to provide statistical reliability, which is at least valid for those species making up > 5% of the total fauna (Fatela and Taborda, 2002). Taxonomical identification was mainly following the illustrations of Feyling-Hanssen (1972), Wright et al. (2011), Milker et al. (2015), Müller-Navarra et al. (2016), and Schönfeld (2018). As the analysed sediments are rich in different genera whose individuals were often poorly preserved and seemed to be reworked, identification up to species level has often been impossible. Hence, corresponding individuals were grouped by genus, from which most genera making up less than 1% of the total fauna, while the total sum of this group accounted for 3% on average. This concerns, among others, genera such as *Bolivinita*, *Bulimina*, *Cibicides*, and *Cibicidoides*. Based on the observations of Müller-Navarra et al. (2017), who identified irregular tests of *E. macrescens* in active salt marshes on the island of Sylt, normal and irregular tests of *E. macrescens* were also distinguished in this study. In order to avoid the quantitative integration of potential intra-specific morphological variations, only severe test irregularities were counted for this study, following Alve (1991). High-resolution images of *E. macrescens*$_{\text{irregular}}$ originating from Friedrichskoog were generated by using a Keyence VHX-6000 microscope. For comparison, historical foraminiferal counts of *E. macrescens* and *E. macrescens*$_{\text{irregular}}$, as well as the sum of calcareous benthic tidal-flat foraminifera of a sediment archive from a less anthropogenically modified salt marsh (Bay of Tümlau, Eiderstedt Peninsula, site TB13-1; Fig. 13) were taken from Müller-Navarra et al. (2019). For both sites (Friedrichskoog and Bay of Tümlau), cross correlations were calculated between the absolute abundances of *E. macrescens*$_{\text{irregular}}$ and the storm-tide frequency in the German Bight, to test, if there is a delay between abundant deformed tests and years with more frequently occurring storm-tide events as recorded at the Cuxhaven tide gauge. Cross-correlation analyses were performed by using the PAleontological STatistics (PAST) software, version 4.02 (Hammer et al., 2001) and on the previously resampled records (Δt = 1 yr) by applying a simple linear interpolation processed with the AnalySeries software 2.0, version 05/2005 (Paillard et al., 1996). Required age-model compilations for the sediment successions (GeoHH-FK and TB13-1) build on the establishment of an integrated stratigraphic framework for active foreland salt marshes, in which age markers were mainly obtained by radionuclides (^{137}Cs) and the human-induced mercury (Hg) pollution history (for further details see Bunzel et al., 2020).

4.3.3 Observed wind and sea-level data. The German Meteorological Service (DWD) supplied historical wind data (stations Husum, Büsum, and Cuxhaven), and the BSH seawater-level observations (Cuxhaven tide gauge; Fig. 13). All data records were filtered in order to consider only severe wind conditions (hereafter referred to as storminess) and high seawater levels (hereafter referred to as storm tides) within this study. This includes daily means of westerly winds (≥ 180° to 360° azimuth) with wind speeds of ≥ 7 Beaufort (Bft), and the yearly number of extreme sea-level highstands, at which the observed seawater level exceeds the mean high water (MHW) by ≥ 1.5 m (Gerber et al., 2016). A correction with respect to the tidal predictions (subtractions of the full tidal cycles from the observed seawater level; Pugh, 1987) was not carried out for the Cuxhaven tide-gauge record, because the tide-surge interaction is rather complex and the generation of surges is associated with rising tides (Horsburgh and Wilson, 2007). Accordingly, the high seawater levels shown and discussed in here are the result of both storm surges and tides, i.e., storm tides.

4.4 Results and discussion

Within the sediment sequence GeoHH-FK at Friedrichskoog, 27 taxa have been identified on the genus level and additional 21 taxa on the species level. There, the majority belongs to calcareous benthic tidal-flat foraminifera (on average ~71%), mainly consisting of *Ammonia* spp., *Cribroelphidium selseyense*, and *Haynesina germanica* (see Appendix D, Plate 1), which are common taxa in tidal flat and lowermost salt-marsh habitats (Müller-Navarra et al., 2016; Francescangeli et al., 2017). In comparison, agglutinated benthic salt-marsh foraminifera were less abundant (on average ~20%). Among them, *E. macrescens* is the most dominant species (see Appendix D, Plate 2), which is a cosmopolitan taxon usually appearing in the upper intertidal marsh zone between mean high water (MHW) and highest astronomical tide (HAT; Haslett et al., 1997; Horton, 1999; Lal et al., 2020). In addition, few planktonic foraminiferal genera were distinguished (constituting on average ~5% of the total fauna), belonging to an extinct group of Cretaceous foraminifera (i.a., *Guembelitria*, *Hedbergella*, and *Planoheterohelix*; see Appendix D,

Plate 2), and few organic linings that can be neglected (on average ~0.2%). Since this study builds on the evaluation of irregularities in the agglutinated benthic foraminiferal species *E. macrescens*, the occurrence and down-core distribution pattern of single calcareous species will not be discussed in here. Instead, the results of the absolute abundance of irregular grown *E. macrescens* specimens are compared with absolute numbers of regular grown *E. macrescens* specimens as well as with the total sum of the calcareous benthic tidal-flat foraminifera.

Since completion of the polder embankment at Friedrichskoog between 1852–1854 CE (Fischer, 1957), the tidal wetlands in front of the dikes got more and more eroded, due to their exposure to amplified storm surges (Röhrs, 1938), which were comparatively strengthened at the end of the 19th and beginning of the 20th century (Dangendorf et al., 2014). As favoured by the salt-marsh loss, a nearby narrow channel (Altfelder Priel) progressively migrated towards the coast, and as a result, additionally contributed to accelerated erosional processes in front of the dike (Röhrs, 1938). The enhanced marine influence is reflected by high abundances of calcareous benthic tidal-flat foraminifera from 1900 CE until the mid-1930s that are well preserved in the sedimentary record at Friedrichskoog (GeoHH-FK; Fig. 14a). The group of calcareous taxa, mainly consisting of *Ammonia* spp., *C. selseyense*, and *H. germanica* (see Appendix D, Plate 1), indicates a period of dynamic depositional processes in an unvegetated tidal flat to shallow sub-tidal environment (Francescangeli et al., 2018). As a countermeasure to the increasing loss of land and accompanied flood risk, a 2200 m long W–E oriented dam (Trischendamm; Fig. 13c) was build and completed in 1934–1936 CE (Röhrs, 1938). The resulting truncation and diversion of the channel called *Altfelder Priel* and its previously southwards flowing currents during low tide prevented a progressive erosion, and instead favoured the intended near-shore sedimentation processes, as the previously prevailing high current velocities were now attenuated (Lorenzen, 1960). As a result, the amount of calcareous tidal-flat foraminifera is comparatively low since the mid-1930s until today (Fig. 14a). A similar pattern was observed for the total recovered time span (~1920–2013 CE) of the sedimentary salt-marsh record at the Bay of Tümlau (TB13-1; Müller-Navarra et al., 2019). Accordingly, the beginning of this record is likewise dominated by common calcareous benthic tidal-flat foraminifera, indicating a depositional period that occurred under marine influences until around 1940 CE, and again temporarily between the late 1940s to mid-1950s (Fig. 14a; Müller-Navarra et al., 2019). As a result of the polder embankment in 1935 CE (Tümlauer Koog) and the subsequent draining measures of the reclaimed land on the seaward side of the new dike, the marine influence was mitigated, fostering a progressive salt-marsh evolution at the Bay of Tümlau as seen by the gradual increase of the cosmopolitan salt-marsh species *E. macrescens* (Müller-Navarra et al., 2019). The embankment of this polder has been promoted due to the political situation at this time (Amenda, 2005). The end of World War II might have led to the abandonment of the salt-marsh conservation (draining measures), as many people that were previously responsible for these measures moved away (Amenda, 2005). The reduced drainage of the salt marsh might be indicated by the temporal increase of the calcareous tidal-flat foraminifera between the late 1940s and mid-1950s (Fig. 14a; Müller-Navarra et al., 2019). After this period, the low amount of tidal-flat foraminifera is comparable to that at Friedrichskoog (Fig. 14a). Nowadays, draining and grazing in the Bay of Tümlau has been largely stopped through the foundation of the Wadden Sea National Park, and a re-establishment of natural high-marsh conditions could be observed from 2001 CE at the latest (Stock et al., 2005; Müller-Navarra et al., 2019).

Similar to that of the Bay of Tümlau, the evolution of the salt-marsh system at Friedrichskoog is reflected by the occurrence of agglutinated salt-marsh foraminifera (mainly *E. macrescens*) from the mid-1930s onwards (Fig. 14b). This epifaunal to infaunal living species is described as being adapted to survive in extreme marginal marine environments, and preferably occurs in sediments of the middle to high marsh zone that are rich in organic carbon (Armynot du Châtelet et al., 2009; Milker et al., 2015; Francescangeli et al., 2017). In fact, *E. macrescens* seems to be able to withstand long periods of subaerial exposure (on average ~90% of the day; Francescangeli et al. 2017). Furthermore, *E. macrescens* exhibits an epiphytal life cycle related to salt-marsh plants of the *Carex acuta* type (Alve and Murray, 1999). At Friedrichskoog, the development of a local salt marsh was most likely fostered by the completion of the nearby dam that attenuated the current velocities of the Altfelder Priel, and thus favoured the coastal sedimentation processes under lowered depositional energy conditions considerably. In addition, salt-marsh accretion profited from the availability of suspended material that is generally transported and deposited on top of the marsh surface during submergence. At both locations, however, there is also a prominent increase in the number of irregularly grown tests of *E. macrescens* specimens (hereafter referred to as *E. macrescens*$_{\text{irregular}}$; see Appendix D, Plate 2), revealing conspicuous deformed chambers together with abnormal twisted tests (Figs. 15, 16b). At Friedrichskoog, the proportion of *E. macrescens*$_{\text{irregular}}$ started to increase gradually from the mid-century onwards, reaching highest numbers during the late 1980s, and then returning back to low values after 1990 CE. At the Bay of Tümlau, the abundance of *E. macrescens*$_{\text{irregular}}$ showed a similar distribution pattern as at Friedrichskoog, i.e., a gradual

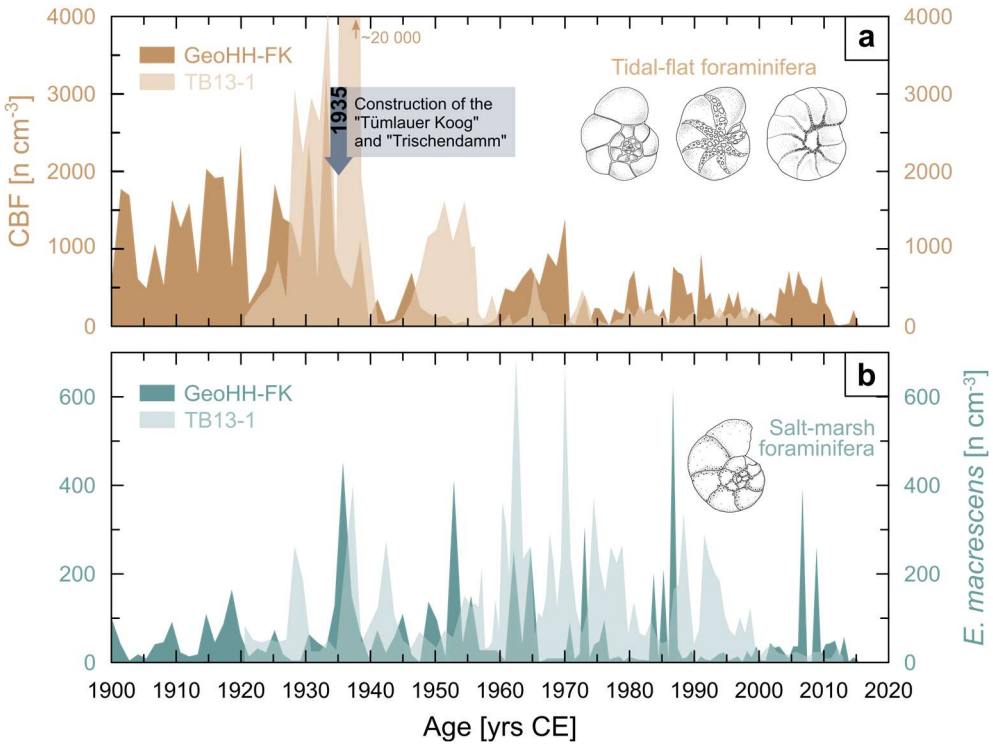

Fig. 14 | Benthic foraminiferal abundances. a) Absolute abundance (numbers per cm^3) of calcareous benthic foraminifera (CBF), mainly comprising common tidal-flat taxa such as *Ammonia* spp., *Cribroelphidium selseyense*, and *Haynesina germanica* (sketches are not to scale), displaying a general decrease after the embankment of the polder called *Tümlauer Koog* at the Bay of Tümlau in 1935 CE, and the construction of the dam called *Trischendamm* at Friedrichskoog between 1934 and 1936 CE. **b**) Salt-marsh evolution at Friedrichskoog (GeoHH-FK, dark green) and the Bay of Tümlau (TB13-1, light green) during the past century, represented by the abundance of the salt-marsh indicator species *Entzia macrescens*. Data from the Bay of Tümlau were taken from Müller-Navarra et al. (2019).

increase of deformed tests, which reached its maximum in the late 1980s, followed by relatively low values towards today. On the contrary, *E. macrescens*$_{irregular}$ initially appeared somewhat later at the Bay of Tümlau, namely during the mid-1960s, while significant numbers already increased in the first half of the 20th century at Friedrichskoog. Beyond that, the most remarkable difference between the two sites is, however, that the number of deformed tests was much lower in the sedimentary salt-marsh record at the Bay of Tümlau (up to 30 specimens cm^{-3}, i.e., 9% of the total fauna) than at Friedrichskoog (up to 250 specimens cm^{-3}, i.e., > 30% of the total fauna), considering their absolute maximum occurrences at the end of the 1980s. Nevertheless, both *E. macrescens*$_{irregular}$ records imply a gradual increase of deformed tests towards the late 1980s. As foraminifera usually respond very quickly to any kind of environmental changes due to their short-life cycle (Schönfeld et al., 2012), *E. macrescens* seemed to have reacted directly to highly variable environmental disturbances at both sites with rising numbers of deformed grown tests. In modern environments, the appearance of specifically extreme deformed calcareous foraminiferal specimens is often assumed as being evoked by human-induced environmental pollution, such as heavy metal pollution (Yanko et al., 1998; Frontalini and Coccioni, 2008; Elshanawan y et al., 2011; Martínez-Colón et al., 2018), although irregularly grown calcareous tests can also occur to a small extent (~1–3%) in less contaminated environments (Alve, 1991, 1995). If considering *E. macrescens*$_{irregular}$, however, heavy metal pollution alone as the cause for the observed increasing numbers of deformities at the two investigated salt-marsh sites seems rather unlikely. Though, previous studies documented similar heavy metal pollution levels for both Friedrichskoog and the Bay of Tümlau that were consistently well above the natural background levels (i.e., modern mercury concentrations > 100 µg kg^{-1} on average), but lacked a distinct increasing trend towards the late 1980s (Bunzel et al., 2020). If further focussing on environmental pollution as a trigger for the occurrence of deformed agglutinated species, Brunner et al. (2013)

Fig. 15 | Foraminiferal test deformities. Light microscope images of *Entzia macrescens*$_{irregular}$ (spiral view) showing different degrees of test deformation. The individuals were derived from 24 cm (**a**), 25 cm (**b**), and 44 cm (**c**) sediment depth of the sediment sequence GeoHH-FK at Friedrichskoog. Scale bars = 100 µm.

documented the highest numbers of deformities for a typical high-marsh indicator species (*B. pseudomacrescens*) at heavily oil-polluted salt-marsh sites along the Mississippi Sound and Barataria Bay (Mississippi and Louisiana, U.S.). In fact, with the increase of maritime traffic and the growing demand and use of heavy fuel oil, the number of oil spills and illegal dumping of oil residuals at sea has increased in the southern North Sea area, specifically between 1969 and 1991 CE (Fleet and Reineking, 2000; Ferraro et al., 2009; Camphuysen and Vollaard, 2015). Consequently, it leads to the assumption that the studied salt marshes might have been increasingly affected by polluted water masses during times of submergences. However, this coincidence between increasing deformities of *E. macrescens* and marine crude-oil pollution cannot be confidentially proven as studies focusing on North Sea oil pollution are often build on discoveries of oiled seabirds (Dahlmann et al., 1994), hence, the numbers may be biased because they possibly do not fully include specimens that move seasonally and perish elsewhere (non-wintering birds). Instead, it can be supposed that the complexity of various natural and human impacts might have exerted stress on the studied environments, which led to the temporal increasing irregularities of *E. macrescens*.

The course of both *E. macrescens*$_{irregular}$ records bear a strong conformity to changes in the storm-climate conditions at the south-eastern North Sea (Fig. 16). In fact, regional climate-model simulations and historical observations revealed a remarkable increasing storminess together with more frequently occurring storm-tide events for the North Sea area, starting from the 1960s towards peak values around 1990 CE, and returning to comparatively low levels after 1990 CE (Fig. 16a; e.g., Matulla et al., 2008; Weisse et al., 2012). In principle, annual occurring storm surges, which temporarily inundate the marshes, are necessary for the required sediment supply that allows the salt marshes to grow vertically (Allen 1990; Temmerman et al., 2003; Bungenstock and Schäfer, 2009), and also laterally as a function of changing sea levels (Balke et al., 2016). Indeed, the established coastal salt marshes at Friedrichskoog and the Bay of Tümlau were basically able to keep pace with the rising of mean sea level (MSL) through their vertical growth during the past century. These findings are documented by local sediment accretion rates of 1.16 cm yr^{-1} (GeoHH-FK) and 1.31 cm yr^{-1} (TB13-1) on average (Bunzel et al., 2020), exceeding the regional MSL of 2.4 ±0.1 mm yr^{-1} at all times over the 20th century (Dangendorf et al., 2013a). At the same time, however, extensive dike improvements that were initiated as a result of the severe storm surge in 1962 CE (von Storch et al., 2008), may have exerted additional stress on the salt-marsh ecosystems since the mid-1960s onwards. These dike raising and stabilisation measures along the North Sea coast hampered the natural capacity of the coastal wetlands to expand laterally and migrate further inland as MSL rises (Kelletat, 1992; Dangendorf et al., 2013b). Accordingly, the seaward sides of the salt marshes are more and more under erosion as they are increasingly exposed to storm surges and tides, indicated by the presence of their erosional cliffs (Schuerch et al., 2013; Müller-Navarra et al., 2019; Bunzel et al., 2020). Based on that, it can be assumed that the superposition of a rising MSL and storm-climate amplification has in fact a strong impact on the salt marshes at Friedrichskoog and the Bay of Tümlau. Apparently, the beneficial effects of storm-tide events in terms of sediment delivery and vertical salt-marsh growth coincide with increased stress levels due to more frequent high-energy disturbances of the salt-marsh surface. Interestingly, the *E. macrescens*$_{irregular}$ records lag three (Bay of Tümlau;

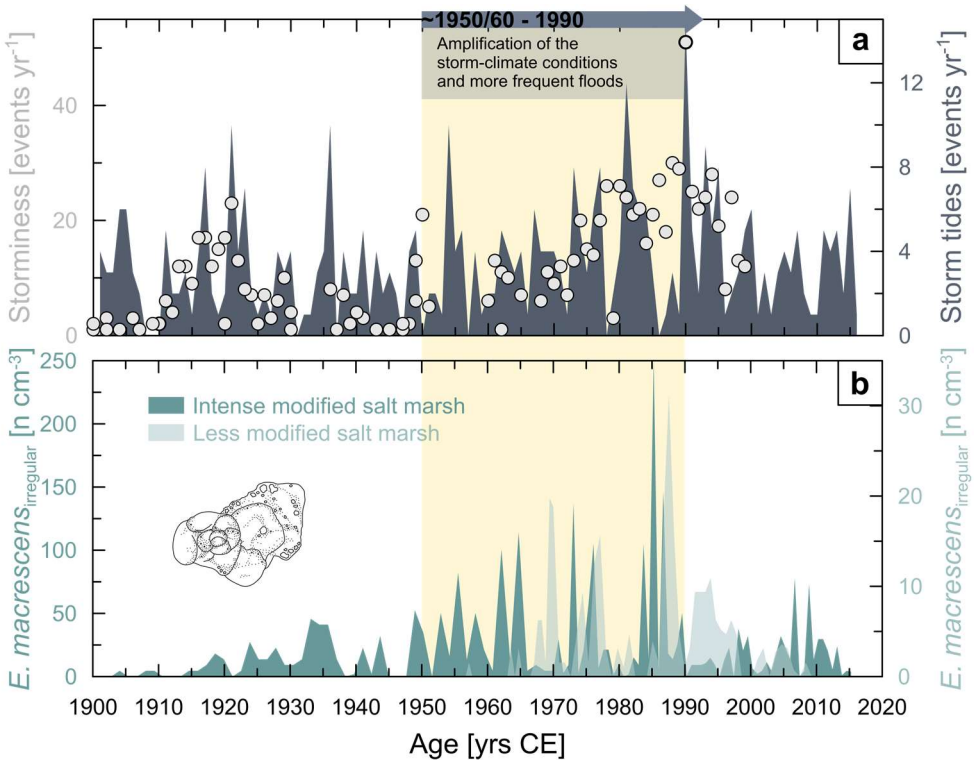

Fig. 16 | Time series of storm-climate observations with response of foraminiferal deformation quantities. a) Number of observed storm-tide events per year (dark grey), when the seawater level exceeds the mean high water (MHW) by ≥ 1.5 m at the Cuxhaven tide gauge, and number of storm days observed at Husum, Büsum, and Cuxhaven (light grey circles), when westerly winds exceed ≥ 7 Bft. **b**) Abundances (numbers per cm³) of abnormal grown tests of *Entzia macrescens* specimens at the intense human-modified salt marsh at Friedrichskoog (GeoHH-FK, dark green) and at the comparatively less modified salt marsh at the Bay of Tümlau (TB13-1, light green); note the different y-axes scaling. Foraminiferal sketch is not to scale. Data from the Bay of Tümlau were taken from Müller-Navarra et al. (2019).

p-value = 0.005) to five years (Friedrichskoog; *p*-value = 0.001) behind those years, in which severe storm-tide events were more frequent, suggesting that it takes a few years for a salt-marsh system to respond and then to rebuild again. However, these time lags may also have been caused by the uncertainties of the age models (Bunzel et al., 2020).

As storm surges can be owed by strong atmospheric low-pressure systems over the North Atlantic, which move across the North Sea, this often also results in high precipitation rates (e.g., Müller-Navarra and Giese, 1999; Svensson and Jones, 2002). As a result, the salt-marsh pore-water salinity can decrease to extreme low values, initiated by both those times when storm surges do not submerge the marshes, but evaporation is rather weak, and because of the increased precipitation associated with the storm tracks. These salinity extremes and/or strong variations are often discussed as being the critical natural environmental stressor to which foraminifera react with test deformation, which might be valid for both calcareous (Geslin et al., 2000, 2002; Polovodova and Schönfeld, 2008; Martínez-Colón et al., 2009) and agglutinated species (Müller-Navarra et al., 2017). Specifically strong fluctuations in salinity can lead to disturbances that cause numerous test deformities, if these disturbances occur during the early ontogenetic development phase of a species (Stouff et al., 1999). As shown by De Rijk (1995), *E. macrescens* can generally resist to large salinity ranges, but highest specimen numbers occur preferentially at high salinity levels (R = 0.56). It can therefore be assumed that the salinity gradients at the salt-marsh surfaces became more pronounced between ~1950 and 1990 CE. These fluctuations have likely been triggered by more frequently occurring storm-tides events towards the 1990s, which induced more drastic changes between very high and very low salinity levels at ever shorter time intervals. In addition, amplifications in the storm-tide hydrodynamics towards the 1990s may have also contributed to enhanced turbulences and sediment re-deposition. It is likely that this effect also has caused damages to the tests of living specimens of *E. macrescens*, so that deformations occurred in their later growth cycle due to regeneration phenomena, as it has been reported for calcareous tidal-flat foraminifera (Geslin et al., 2002). The contrasting number of deformed specimens at the

two salt-marsh locations might be owed by their different land-use histories and accompanied extent of human interventions, as well as their exposition facing high (open coast at Friedrichskoog) or low (semi-enclosed Bay of Tümlau) energy conditions during extreme floods that are evoked by enhanced storminess and storm tides. The combination of various disturbances to the salt marsh at Friedrichskoog, including the frequent upkeep of the artificial drainage ditches, the intensive sheep grazing that resulted in a short and less diverse vegetation cover and the unsheltered exposure to impacts by the storm climate, probably led to the enhanced susceptibility of the ecosystem to environmental stress. In addition, the salt-marsh plant species belonging to the *Carex* type, on which *E. macrescens* preferentially occurs during its epiphytic life cycle (Alve and Murray, 1999), is increasingly at risk along the North Sea area due to extensive salt-marsh management measures (Mierwald and Romahn, 2006). Accordingly, this can also bring *E. macrescens* under pressure. In comparison, and prior to the foundation of the National Park, artificial drainage ditches in the salt marshes at the sheltered Bay of Tümlau have been less frequently renewed and dredged (every three to seven years; pers. comm. LKN.SH, 2017). This is also reflected in the higher absolute abundance of non-deformed *E. macrescens* specimens in the salt marsh of the Bay of Tümlau during the last century (around 130 specimens cm^{-3} on average; Fig. 14b). This confirms the reduced ecological impact of storm tides in the sheltered bay under rather low-energy conditions. In addition, salt-marsh ecosystems in the Bay of Tümlau and the associated foraminiferal fauna profited from the return of more natural conditions with foundation of the Wadden Sea National Park in 1985 CE, abandonment of ditching, and realisation of restoration measures around 2001 CE (Müller-Navarra et al., 2019). The number of non-deformed *E. macrescens* specimens at the Friedrichskoog salt marsh is considerably lower (around 60 specimens cm–3 on average).

To summarize, pronounced changes in individual factors (salinity, hydrodynamics, exposure, and various human activities) are within the species' tolerance range, but in combination, environmental disturbances exceeded the ecological limit (threshold), at which *E. macrescens* reacted with enhanced deformation (Fig. 17a). Based on that, it can be suspected that the increased test-deformation rates of *E. macrescens* are thus likely caused by both natural and human-induced environmental stress. This finding is consistent with other studies that concluded that abrupt and highly variable natural environmental changes are more likely to be the main cause for abnormal grown foraminiferal tests, rather than merely the effects of environmental pollution alone (e.g., Geslin et al., 2002; Polovodova and Schönfeld, 2008; Martínez-Colón et al., 2009). In fact,

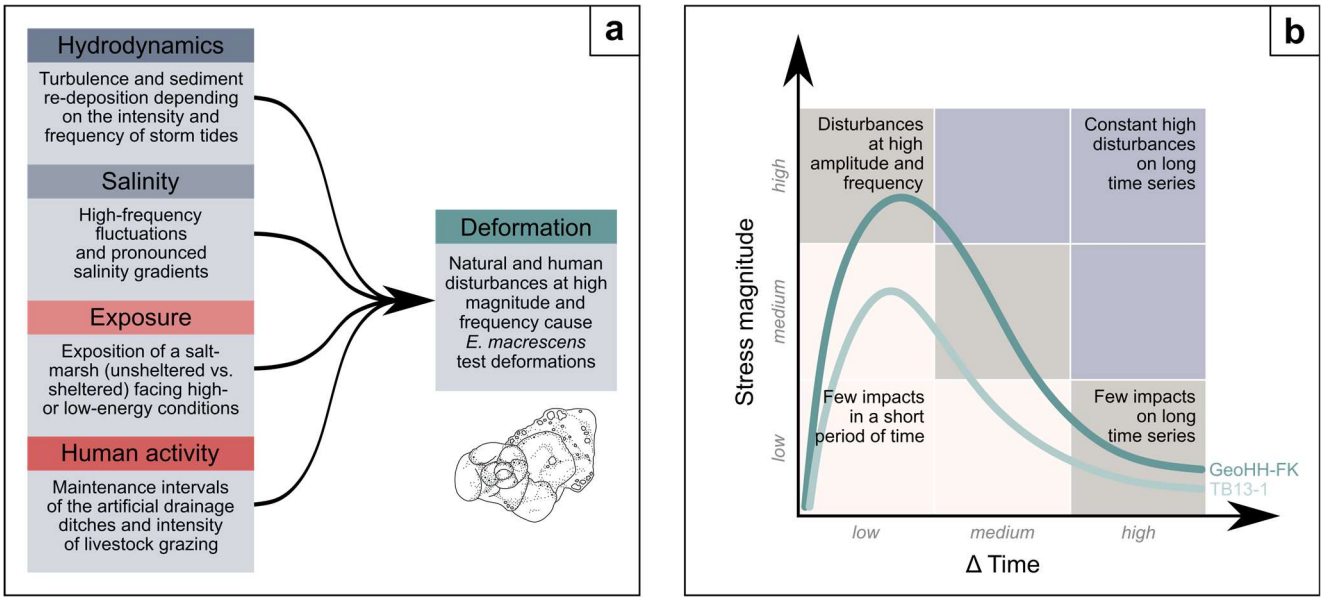

Fig. 17 | Conceptual links between environmental stressors and foraminiferal test deformities. a) Simplified impact diagram demonstrating the various natural and human-induced environmental-stress factors on test deformations of *Entzia macrescens*. **b**) Conceptual model outlining the increased deformation rates of *E. macrescens* (green lines) in relation to the combined influence of environmental-stress factors, particularly when disturbances occur at increasingly higher frequency and amplitude. The nine-field portfolio denotes different scenarios of low to high stress levels in dependence on the time intervals considered, and corresponding effects on the number of deformed foraminifera. Illustrations are not to scale.

variable test deformations and partly strong deformed tests of another typical high-marsh species (*Trochamminita irregularis*) have also been observed in naturally developed estuarine salt marshes at the Pacific coast (Oregon, U.S.; Milker, pers. observ.). This supports the assumption that test deformations are possibly due to environmental disturbances, which means that the foraminifera may reach their upper tolerance range where they can still live, but react more stressed (e.g., Martínez-Colón and Hallock, 2010). To provide a simplified overview, a conceptual model has been outlined, thereby partly following the portfolio analysis of McKinsey & Company (e.g., ECA, 2009). The two dimensions of the matrix represent the environmental stress magnitude and time between the impacts (Δ time) and allow for assessing the influence of disturbances at varying frequency and amplitude on the deformation rates of *E. macrescens* (Fig. 17b). Accordingly, morphological anomalies of typical and widespread salt-marsh foraminifera may provide a useful biomonitoring tool to assess the extent of environmental stressors on coastal wetlands.

4.5 Conclusions

This study shows that the intensely human-modified salt marsh at Friedrichskoog includes highest numbers of deformed salt-marsh foraminifera (*E. macrescens*$_{\text{irregular}}$) at times of increased storminess and storm tides from the middle of the 20$^{\text{th}}$ century until the late 1980s. In the less frequent modified salt marsh of the Bay of Tümlau, the same species exhibited comparatively less numbers of deformed tests during the same time interval of intensified storm-climate conditions. The results suggest that the intensively human-modified salt-marsh ecosystems of the south-eastern North Sea are more susceptible to the impacts of increased storm tide and submergence frequencies causing enhanced stress to the ecosystem. Accordingly, combined environmental disturbances arising from salinity, hydrodynamics, exposure, and various human activities (e.g., draining, grazing, and pollution) occurring at high magnitude and frequency caused deformities of *E. macrescens*. It therefore makes this species to be a useful indicator for assessing or reconstructing environmental stress impacts on coastal wetlands. To conclude, the results illustrate the ecological sensitivity and vulnerability of human-modified coastal salt marshes from the south-eastern North Sea to more frequent and amplified storm-climate conditions, although the marshes themselves currently still seem to be able to cope with the ongoing climate changes.

Acknowledgements

This study was financially supported by grants SCHM1180/19 and MI1508/4 from the German Research Foundation (DFG) through the Special Priority Program (SPP-1889) Regional Sea Level Change and Society (SeaLevel) under the SEASTORM project. We thank the State Office for Surveying and Geoinformation Schleswig-Holstein (LVermGeo SH), the German Meteorological Service (DWD), the Agency for Coastal Defence, National Park and Marine Conservation (LKN.SH), and the Federal Maritime and Hydrographic Agency of Germany (BSH) for providing historical observation data and for discussions. We also thank Christian Wiedemann and Martin Stock (National Park of the Schleswig-Holstein Wadden Sea) for the authorisation to work in the coastal salt marsh at Friedrichskoog.

Author contributions

Sample preparation and foraminiferal analyses were conducted by D.B., who also designed the study and wrote the article. F.F. helped to discuss the foraminiferal data. Y.M. and G.S. contributed to all data discussions by providing helpful advice, comments, and revisions during the article preparation phase.

Data availability

All measured data used and discussed in this article are available at:
https://doi.pangaea.de/10.1594/PANGAEA.927336.

Chapter Five

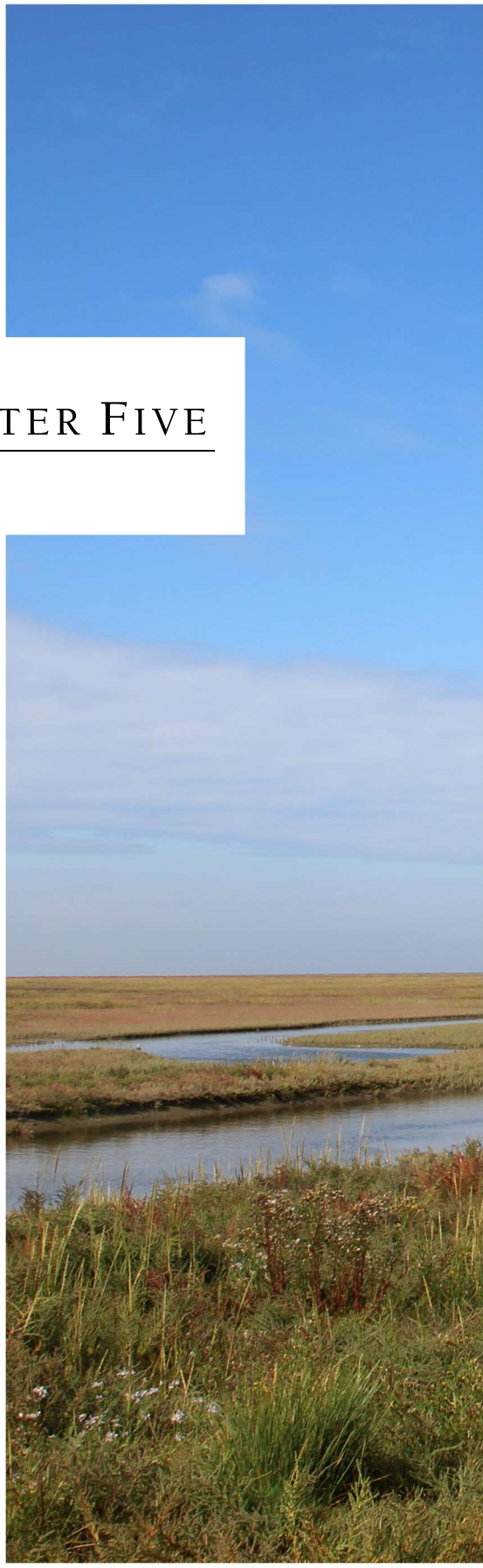

Conclusion & outlook

5.1 Key findings

Active salt marshes provide essential services that include carbon sequestration and protection of the densely populated hinterland by buffering the wave energy during inundation at high tide and storm surges, and by incorporating organic carbon-rich suspended matter (e.g., Kirwan and Megonigal, 2013; Fagherazzi, 2014; IPCC, 2019). At the same time, however, salt marshes are also vulnerable to environmental changes (Davy et al., 2009). As such, the resilience of coastal wetlands is critical to preserve their ecosystem services through withstanding predicted extreme water levels and associated flooding under a fairly warmer climate, which is a probable future scenario. The consideration of intertidal sedimentation dynamics under the influence of global warming in the 20th-century thus provides insights into possible links between salt-marsh adaptation strategies and observed climate patterns, such as the storm-climate component. However, in addition to climate-induced environmental changes, German salt marshes are further highly affected by non-climatic impacts due to various human interventions such as grazing and draining measures. To allow for the comparison between regionally different salt-marsh systems that have experienced diverse non-climatic but similar natural climate-related influences, four salt-marsh archives were analysed. They include the sites, from north to south: the Bay of Tümlau (TB13-1), the Eider estuary (GeoHH-GIE), Friedrichskoog (GeoHH-FK), and Kaiser-Wilhelm-Koog (GeoHH-KWK). As this doctoral thesis aimed to test the hypothesis that sedimentary salt-marsh sequences from the German North Sea coast archived 20th-century changes in storm climate and regional sea level, the following conclusions can be drawn based on the previously raised research questions in Section 1.5:

How can a reliable stratigraphy be established for modern salt-marsh sediment sequences from the highly dynamic south-eastern North Sea coast?

In order to reconstruct past sedimentation processes and test for possible archived storm-climate components under the influences of different climatic and non-climatic forces, it was crucial to obtain an accurate chronostratigraphic control for each analysed sedimentary salt-marsh sequence. As salt-marsh sediment sequences from the highly dynamic south-eastern North Sea coast often lack robust age information due to frequent incorporation of reworked sediments by storm surges, different independent dating techniques were combined to compensate for challenging stratigraphic signals. The resulting integrated stratigraphic approach mainly included radionuclides (^{210}Pb, ^{137}Cs, ^{241}Am, and ^{14}C) and trends of the industrial mercury (Hg) pollution history, as well as a XRF-based sedimentological inter-correlation (ln[Zr/Rb] ratio). It was found that pre-bomb and post-bomb ^{14}C dating approaches using shell material appeared problematic in highly dynamic intertidal systems, as the revealed ages seemed to be too old with too large precision errors. Similarly, the ^{210}Pb-based dating approach, most used for dating modern sedimentary sequences, also showed high uncertainties. Consequently, the ^{210}Pb-derived age models (CIC, CRS) failed to reproduce accurate age information. Nevertheless, both approaches (^{14}C and ^{210}Pb) provided a general age orientation. In contrast, more accurate age information was obtained by distinct ^{137}Cs and ^{241}Am activity peaks within the sediment sequences, attributable to nuclear bomb tests in 1963 CE and the Chernobyl power plant accident in 1986 CE. Artificial radionuclide activities could be further constrained by the area's heavy metal-pollution history as documented by elevated Hg concentrations, in which distinct enrichments within the sediment were ascribable to the aftermaths of World War II in 1945 CE and the European industrialization peak between 1960 CE and 1970 CE.

Based on the establishment of this integrated regional stratigraphic framework, average accretion rates were reconstructed for all four sedimentary salt-marsh sequences, ranging from 1.16 cm yr^{-1} to 1.90 cm yr^{-1}. There, the highest accretion rates were found close to the Elbe estuary, at Kaiser-Wilhelm-Koog (GeoHH-KWK), and in the Eider estuary (GeoHH-GIE), indicating additional riverine sediment delivery. In addition, the construction of the Eider tidal barrier in 1973 CE caused a considerable change in local depositional processes due to the decrease in storm surge-induced sediment supply in the Eider estuary. Accordingly, the following evaluations with respect to

potentially archived storm-climate signals focused on the sediment sequences obtained from Friedrichskoog (GeoHH-FK) and the Bay of Tümlau (TB13-1).

How can the changes in storm-surge frequency and intensity and possible underlying super-regional climate oscillations of the 20th-century be traced within the sedimentary sequences, although the salt marshes have experienced various anthropogenic interventions?

Despite different human-induced salt-marsh management strategies during the past century, regional storm-surge signals could be documented in the sediment archives of both studied salt marshes in Friedrichskoog and the Bay of Tümlau. Local changes in the sediment supply of either minerogenic or organogenic quality were evaluated using the ln(Br/Cl) ratio, revealing a marked decrease in the values occurring in the relatively coarser siliciclastic layers. This indicates that these layers were likely deposited during regional winter storm surges, when the suspended material of the water columns usually contains less marine organic carbon, and less bromine is consequently available. At the same time, the pore volume of the coarser layers can cause a simultaneous influx of the seawater-induced chloride. Beyond these seasonal effects, concomitant increasing trends were documented in the relative proportions of the marine versus terrestrial organic matter content (Br/C_{org} ratio) as well as in the relative sediment coarsening (ln[Zr/Rb] ratio) from the mid-20th century to 1990 CE. These increasing trends during the second half of the 20th century are comparable to the intensified North Sea storm climate as recorded by historical wind stations and tide gauges. The results obtained indicate an increasing marine influence and associated flooding frequency, which in turn lead to enhanced erosion and retreat of the seaward salt-marsh cliffs. In addition, underlying oscillations on inter-decadal timescales, as traced for both study sites by the ln(Zr/Rb) ratio (periodicities of 10–19 years) and for the Bay of Tümlau by the ln(Br/Cl) ratio (periodicities of 12–22 years), suggest that sediment deposition was further driven by large-scale atmosphere-ocean climate variabilities. At Friedrichskoog, however, the inter-decadal variability was absent from the ln(Br/Cl) record, likely due to natural climate oscillations being masked by the more intense local human activities at this site.

How do salt-marsh ecosystems react when they are exposed to highly complex environmental stress over a long period?

The local differences between the sedimentary salt-marsh sequences at Friedrichskoog and the Bay of Tümlau with regard to their historic benthic foraminiferal records illustrate the considerable stress arising from intensive human interventions. Consequently, in the sediment sequence at Friedrichskoog, a site that has been strongly altered by human interventions in the last century, a rising number of the foraminiferal salt-marsh indicator species *E. macrescens* were found to have deformed tests at times of more frequent flooding, the latter being documented by water-level observations at the Cuxhaven tide gauge for the last century. The same trend of deformed *E. macrescens* tests was also observed in the Bay of Tümlau but with considerably lower numbers, presumably as this site has been less frequently affected by human activities. These observations indicate increasing environmental stress towards the late 1980s, initiated by the North Sea storm-climate amplification and further reinforced by different intense human activities, to which the foraminifera reacted with test deformation. In fact, the more environmental disturbances occur at ever shorter time intervals, the higher the number of deformed *E. macrescens*.

To conclude, the present doctoral thesis has demonstrated that sedimentary salt-marsh sequences from the south-eastern North Sea coast do bear a storm-surge climate component, corroborating the hypothesis put forward in this thesis. Furthermore, the reconstructed sediment-accretion rates suggest that vertical salt-marsh growth rates have largely been able to outpace SLR rates over the past century, despite, or possibly because of, the occurrence of more frequent and intense regional storm surges. However, it was also found that salt marshes, which have been particularly affected by management measures, react most stressed and are thus more vulnerable to changing climatic conditions.

5.2 Coastal conservation strategies and implications for future research approaches

The most serious threat to intertidal salt-marsh systems could come from non-climatic influences in the form of direct human interventions associated with the impact of accelerated climate change and related rise in sea level and storm flood frequency. In fact, measures such as the construction of a tidal barrier (at site GeoHH-GIE) or intensive grazing (at site GeoHH-FK) appeared to reduce the incorporation of minerogenic sediments, although sufficient sediment availability was basically ensured, as shown at those sites less influenced by human activities (e.g., sites

GeoHH-KWK and TB13-1). Consequently, and based on the results of this thesis, the urgent need to further protect and preserve active foreland salt marshes and to further reduce human-induced disturbances is evident. Initiated by the Trilateral Wadden Sea Plan (WSP) adopted in 1997 CE, its policy and management plan aims to restore and – in the best case – enlarge the salt-marsh areas along the south-eastern North Sea coast and promote their development towards a more natural vegetation structure. In this context, measures have already been taken in recent decades, including the de-embankment of summer polders and implementation of regulations regarding local adjustments of grazing and draining intensities and frequencies (e.g., Esselink et al., 2009). Nevertheless, global and regional SLR will continue to pose a persistent threat to coastal salt marshes, whose lateral expansion is mainly impeded by near-shore dikes or seawalls, leading to increased erosion of salt-marsh edges – and, in the worst case, to their loss. In this context, and with regard to promoting nature-based strategies of salt-marsh adaptation to SLR and improving their ecosystem services for coastal protection without completely abandoning the dikes, different seawall managed realignment (MR) scenarios have been simulated for the Freiston Shore in the UK on the south-western North Sea coast (Kiesel et al., 2020). These MRs suggest that breaching dikes in varying numbers and sizes to create new accommodation spaces for tidal flats and salt marshes in the hinterland results in a better wave-energy attenuation during high tides and storm surges, thus helping to restore the natural function of coastal wetlands as flood plains. The re-configuration of present dikes and seawalls could be a measure also feasible for the German coastline; however, such MR projects require adequate long-term monitoring, including accompanying documentation of both the development of a more natural salt-marsh vegetation structure and sediment-accretion rates, as Kiesel et al. (2020) have already advised. MRs would work contrastingly to the present installed sluices (*Siele*) that prevent dynamic propagation of salt marshes and are closed during storm surges (Krause and Wolter, 1970). Again, sluice design invades natural sedimentation dynamics and promotes the development of freshwater- instead of saltwater-dominated wetlands, as found, for example, at the Wöhrdener Loch in Dithmarschen (NABU, 2019).

However, – and this could be the ideal starting point for future interdisciplinary projects, such as micropaleontological investigations in conjunction with in situ botanical analyses – the monitoring of the development and current state of salt marshes belonging to the Wadden Sea area largely relies on the evaluation of aerial images with regard to the distribution of different vegetation zones (Esselink et al., 2009), which can lack information on the in situ state of various salt-marsh systems. As presented in Chapter 4 of this thesis, the cosmopolitan foraminiferal species *E. macrescens* reacts very sensitively to environmental disturbances, especially at sites exposed to intensive human interference. With regard to future research strategies, it would thus be of great interest and substantial importance to monitor the occurrence of deformed foraminiferal salt-marsh indicator species, such as *E. macrescens*, during potential MR project-implementation measures. Additionally, the more salt-marsh sites would be analysed in terms of past (dead/fossil specimens) and present (living specimens) occurrences of *E. macrescens*$_{\text{irregular}}$ (or other deformed foraminifera), the better this could allow for a more accurate assessment and early detection of any kind of environmental stress. Specifically, if it would be possible to identify a kind of tipping point (e.g., how many *E. macrescens*$_{\text{irregular}}$ must occur before a salt-marsh ecosystem enters a non-reversible endangered status), monitoring of benthic foraminifera could counteract potential threats to the intertidal systems in a timely manner.

REFERENCES

Aarkrog, A., 2003. Input of anthropogenic radionuclides into the World Ocean. *Deep-Sea Research II* **50**, 2597–2606.

Ackermann, F., Bergmann, H., Schleichert, U., 1983. Monitoring of heavy metals in coastal and estuarine sediments – a question of grain-size: < 20 µm versus < 60 µm. *Environmental Technology* **4**, 317–328.

Allen, J.R.L., 1989. Evolution of salt-marsh cliffs in muddy and sandy systems: a qualitative comparison of British west-coast estuaries. *Earth Surface Processes and Landforms* **14**, 85–92.

Allen, J.R.L., 1990. Salt-marsh growth and stratification: a numerical model with special reference to the Severn Estuary, southwest Britain. *Marine Geology* **95**, 77–96.

Allen, J.R.L., 1995. Salt-marsh growth and fluctuating sea level: implications of a simulation model for Flandrian coastal stratigraphy and peat-based sea-level curves. *Sedimentary Geology* **100**, 21–45.

Allen, J.R.L., 1997. The geoarchaeology of land-claim in coastal wetlands: a sketch from Britain and the north-west European Atlantic – North Sea coasts. *Archaeological Journal* **154**, 1–54.

Allen, J.R.L., 2000. Morphodynamics of Holocene salt marshes: a review sketch from the Atlantic and Southern North Sea coasts of Europe. *Quaternary Science Reviews* **19**, 1155–1231.

Allen, G.P., Salomon, J.C., Bassoullet, P., Du Penhoat, Y., de Grandpré, C., 1980. Effects of tides on mixing and suspended sediment transport in macrotidal estuaries. *Sedimentary Geology* **26**, 69–70.

Allen, J.R.L., Rae, J.E., Longworth, G., Hasler, S.E., Ivanovich, M., 1993. A comparison of the ^{210}Pb dating technique with three other independent dating methods in an oxic estuarine salt-marsh sequence. *Estuaries* **16**, 670–677.

Alve, E. 1991. Benthic foraminifera in sediment cores reflecting heavy metal pollution in Soerfjord, western Norway. *Journal of Foraminiferal Research* **21**, 1–19.

Alve, E., 1995. Benthic foraminiferal responses to estuarine pollution: a review. *Journal of Foraminiferal Research* **25**, 190–203.

Alve, E., Murray, J.W., 1999. Marginal marine environments of the Skagerrak and Kattegat: a baseline study of living (stained) benthic foraminiferal ecology. *Palaeogeography, Palaeoclimatology, Palaeoecology* **146**, 171–193.

Alve, E., Lepland, A., Magnusson, J., Backer-Owe, K., 2009. Monitoring strategies for re-establishment of ecological reference conditions: possibilities and limitations. *Marine Pollution Bulletin* **59**, 297–310.

Amenda, L., 2005. Volk ohne Raum Schafft Raum – Rassenpolitik und Propaganda im nationalsozialistischen Landgewinnungsprojekt an der schleswig-holsteinischen Westküste. Informationen zur Schleswig-Holsteinischen Zeitgeschichte (Kiel) **45**, 4–31.

Andersen, T.J., Mikkelsen, O.A., Møller, A.L., Pejrup, M., 2000. Deposition and mixing depths on some European intertidal mudflats based on ^{210}Pb and ^{137}Cs activities. *Continental Shelf Research* **20**, 1569–1591.

Andersen, T.J., Svinth, S., Pejrup, M., 2011. Temporal variation of accumulation rates on a natural salt marsh in the 20th century – the impact of sea level rise and increased inundation frequency. *Marine Geology* **279**, 178–187.

Anderson, E.C., Libby, W.F., Weinhouse, S., Reid, A.F., Kirshenbaum, A.D., Grosse, A.V., 1947. Radiocarbon from cosmic radiation. *Science* **105**, 576–577.

Andresen, H., Bakker, J.P., Brongers, M., Heydemann, B., Irmler, U., 1990. Long-term changes of salt marsh communities by cattle grazing. *Vegetatio* **89**, 137–148.

Appleby, P.G., 2001. Chronostratigraphic techniques in recent sediments. In: Last, W.M., Smol, J.P. (Eds.), Tracking environmental change using lake sediments. Vol. 1: basin analysis, coring, and chronological techniques. Kluwer Academic Publishers, Springer, Dordrecht, the Netherlands, 171–203.

Appleby, P.G., 2008. Three decades of dating recent sediments by fallout radionuclides: a review. *The Holocene* **18**, 83–93.

Appleby, P.G., Oldfield, F., 1978. The calculation of lead-210 dates assuming a constant rate of supply of unsupported ^{210}Pb to the sediment. *Catena* **5**, 1–8.

Appleby, P.G., Richardson, N., Nolan, P.J., 1991. ^{241}Am dating of lake sediments. *Hydrobiologia* **214**, 35–42.

Armstrong, W., Wright, E.J., Lythe, S., Gaynard, T.J., 1985. Plant zonation and the effects of the spring-neap tidal cycle on soil aeration in a Humber salt marsh. *Journal of Ecology* **73**, 323–339.

Armynot du Châtelet, É., Bout-Roumazeilles, V., Riboulleau, A., Trentesaux, A., 2009. Sediment (grain size and clay mineralogy) and organic matter quality control on living benthic foraminifera. *Revue de micropaléontologie* **52**, 75–84.

Arns, A., Wahl, T., Dangendorf, S., Jensen, J., 2015. The impact of sea level rise on storm surge water levels in the northern part of the German Bight. *Coastal Engineering* **96**, 118–131.

Arns, A., Dangendorf, S., Jensen, J., Talke, S., Bender, J., Pattiaratchi, C., 2017. Sea-level rise induced amplification of coastal protection design heights. *Scientific Reports* **7**, 40171.

Baeteman, C., 1999. The Holocene depositional history of the Ijzer palaeo-valley (western Belgian coastal plain) with reference to the factors controlling the formation of intercalated peat beds. *Geologica Belgica* **2**, 39–72.

Bakker, J.P., 1989. Nature management by grazing and cutting. Kluwer Academic Publishers, Dordrecht, 400 p.

Bakker, J.P., de Leeuw, J., Dijkema, K.S., Leendertse P.C., Prins, H.H.T., Rozema, J., 1993. Salt marshes along the coast of The Netherlands. *Hydrobiologia* **265**, 73–95.

Bakker, J.P., Schrama, M., Esselink, P., Daniels, P., Bhola, N., de Vries, Y., Veeneklaas, R.M., Stock, M., 2019. Long-term effects of sheep grazing in various densities on marsh properties and vegetation dynamics in two different salt-marsh zones. *Estuaries and Coasts* **43**, 298–315.

Balke, T., Stock, M., Jensen, K., Bouma, T.J., Kleyer, M., 2016. A global analysis of the seaward salt marsh extent: the importance of tidal range. *Water Resources Research* **52**, 3775–3786.

Banat, K., Förstner, U., Müller, G., 1972. Schwermetalle in Sedimenten von Donau, Rhein, Ems, Weser und Elbe im Bereich der Bundesrepublik Deutschland. *Die Naturwissenschaften* **59**, 525–528.

Barlow, N.L.M., Shennan, I., Long, A.J., Gehrels, W.R., Saher, M.H., Woodroffe, S.A., Hillier, C., 2013. Salt marshes as late Holocene tide gauges. *Global and Planetary Change* **106**, 90–110.

Bartholdy, J., 2000. Processes controlling import of fine-grained sediment to tidal areas: a simulation model. In: Pye, K., Allen, J.R.L. (Eds.), Coastal and estuarine environments: sedimentology, geomorphology and geoarchaeology. *Geological Society, London, Special Publications* **175**, 13–29.

Bartholdy, J., Anthony, D., 1998. Tidal dynamics and seasonal dependent import and export of fine-grained sediment through a back-barrier tidal channel of the Danish Wadden Sea. In: Alexander, C., Davis, R.A., Henry, V.J. (Eds.), Tidalities: processes and products. *Society for Sedimentary Geology (SEPM), Special Publication* **61**, 43–52.

Bartholdy, J., Aagaard, T., 2001. Storm surge effects on a back-barrier tidal flat of the Danish Wadden Sea. *Geo-Marine Letters* **20**, 133–141.

Bartholdy, J., Christiansen, C., Kunzendorf, H., 2004. Long term variations in backbarrier salt marsh deposition on the Skallingen peninsula – the Danish Wadden Sea. *Marine Geology* **203**, 1–21.

Bartholdy, J., Pedersen, J.B.T., Bartholdy, A.T., 2010. Autocompaction of shallow silty salt marsh clay. *Sedimentary Geology* **223**, 310–319.

Beck, M., Dellwig, O., Liebezeit, G., Schnetger, B., Brumsack, H.-J., 2008. Spatial and seasonal variations of sulphate, dissolved organic carbon, and nutrients in deep pore waters of intertidal flat sediments. *Estuarine, Coastal and Shelf Science* **79**, 307–316.

Behre, K.-E., 2003a. Nacheiszeitliche Küstenentwicklung an der Nordsee. In: Liedtke, H., Mäusbacher, R., Schmidt, K.-H. (Eds.), Nationalatlas der Bundesrepublik Deutschland, Band 2, Natur und Umwelt I: Relief, Boden und Wasser, 76–77.

Behre, K.-E., 2003b. Eine neue Meeresspiegelkurve für die südliche Nordsee, Transgressionen und Regressionen in den letzten 10 000 Jahren. *Probleme der Küstenforschung im südlichen Nordseegebiet* **28**, 9–63.

Behre, K.-E., 2005. Meeresspiegelanstieg, Marschentwicklung, Küstenlinien. Die letzten 10 000 Jahre an der deutschen Nordseeküste im Zeitraffer. In: Fansa, M. (Ed.), Kulturlandschaft Marsch. Natur, Geschichte, Gegenwart. Vorträge anlässlich des Symposiums in Oldenburg vom 3. bis 5. Juni 2004. Schriftenreihe des Landesmuseums für Natur und Mensch, Heft 33. Isensee-Verlag, Oldenburg, 25–36.

Behre, K.-E., Streif, H., 1980. Kriterien zu Meeresspiegel- und darauf bezogene Grundwasserabsenkungen. *Eiszeitalter und Gegenwart* **30**, 153–160.

Behrends, B., Dittmann, S., Liebezeit, G., Kaiser, M., Knoke, V., Petri, G., Rahmel, J., Roy, M., Scheiffarth, G., Wilhelmsen, U., 2004. Gesamtsynthese Ökosystemforschung Wattenmeer – Zusammenfassender Bericht zu Forschungsergebnissen und Systemschutz im deutschen Wattenmeer. Umweltforschungsplan des Bundesministeriums für Umwelt, Naturschutz und Reaktorsicherheit, Forschungsbericht 296 85 905, UBA-FB 000190, 481 p.

Beks, J.P., 1997. The ^{210}Pb budget of the North Sea – atmospheric input versus sediment flux. In: Germain, P., Guary, J.C., Guéguéniat, P., Métivier, H. (Eds.), Radioprotection, radionuclides in the oceans, RADOC 96–97, proceedings part 1, inventories, behaviour, and processes. *Radioprotection* **32**, 219–224.

Beks, J.P., 2000. Storage and distribution of plutonium, ^{241}Am, ^{137}Cs and ^{210}Pbxs in North Sea sediments. *Continental Shelf Research* **20**, 1941–1964.

Bergan, T., Gallardo, L., Rodhe, H., 1999. Mercury in the global troposphere: a three-dimensional model study. *Atmospheric Environment* **33**, 1575–1585.

Bhatia, M.R., Crook, K.A.W., 1986. Trace element characteristics of graywackes and tectonic setting discrimination of sedimentary basins. *Contributions to Mineralogy and Petrology* **92**, 181–193.

Biester, H., Bindler, R., Martínez-Cortizas, A., Engstrom, D.R., 2007. Modeling the past atmospheric deposition of mercury using natural archives. *Environmental Science and Technology* **41**, 4851–4860.

Blott, S.J., Pye, K., 2001. GRADISTAT: a grain size distribution and statistics package for the analysis of unconsolidated sediments. *Earth Surface Processes and Landforms* **26**, 1237–1248.

Bond, G.C., Showers, W., Elliot, M., Evans, M., Lotti, R., Hajdas, I., Bonani, G., Johnson, S., 1999. The North Atlantic's 1–2 kyr climate rhythm: relation to Heinrich Events, Dansgaard/Oeschger cycles and the Little Ice Age. In: Clark, P., Webb, R., Keigwin, L. (Eds.), Mechanisms of global climate change at millennial time scales. *Geophysical Monograph Series* **112**, American Geophysical Union, Washington, DC, 35–58.

Böttcher, C., Knobloch, T., Rühl, N.-P., Sternheim, J., Wichert, U., Wöhler, J., 2011. Munitionsbelastung der deutschen Meeresgewässer – Bestandsaufnahme und Empfehlungen. Sekretariat Bund/Länder-Messprogramm für die Meeresumwelt von Nord- und Ostsee (BLMP) im Bundesamt für Seeschifffahrt und Hydrographie (BSH), 174 p.

Böttcher, C., Knobloch, T., Sternheim, J., Weinberg, I., Wichert, U., Wöhler, J., 2017. Munitionsbelastung der deutschen Meeresgewässer – Entwicklungen und Fortschritt. Bund/Länder-Ausschuss Nord- und Ostsee (BLANO): Ministerium für Energiewende, Landwirtschaft, Umwelt, Natur und Digitalisierung des Landes Schleswig-Holstein, 48 p.

Brandt, H.T., 2018. Foraminifera as proxy for the palaeoenvironmental evolution of a historic polder on the Eiderstedt peninsula (German North Sea coast). Unpublished Master thesis, Institute for Geology, Universität Hamburg, 68 p.

Broeg, K., Köhler, A., Westernhagen, H.v., 2002. Disorder and recovery of environmental health monitored by means of lysosomal stability in liver of European flounder (*Platichthys flesus* L.). *Marine Environmental Research* **54**, 569–573.

Bromberg Gedan, K., Silliman, B.R., Bertness, M.D., 2009. Centuries of human-driven change in salt marsh ecosystems. *Annual Review of Marine Science* **1**, 117–141.

Brunner, C.A., Yeager, K.M., Hatch, R., Simpson, S., Keim, J., Briggs, K.B., Louchouarn, P., 2013. Effects of oil from the 2010 Macondo well blowout on marsh foraminifera of Mississippi and Louisiana, USA. *Environmental Science and Technology* **47**, 9115–9123.

Bryan, G.W., Langston, W.J., 1992. Bioavailability, accumulation and effects of heavy metals in sediments with special reference to United Kingdom estuaries: a review. *Environmental Pollution* **76**, 89–131.

Bungenstock, F., 2005. Das Küstenholozän der südlichen Nordsee – Archiv der Meeresspiegelbewegungen. In: Fransa, M. (Ed.), Kulturlandschaft Marsch – Natur, Geschichte, Gegenwart. *Schriftenreihe des Landesmuseums für Natur und Mensch* **33**, Isensee-Verlag Oldenburg, 37–51.

Bungenstock, F., Schäfer, A., 2009. The Holocene relative sea-level curve for the tidal basin of the barrier island Langeoog, German Bight, Southern North Sea. *Global and Planetary Change* **66**, 34–51.

Bungenstock, F., Weerts, H.J.T., 2010. The high-resolution Holocene sea-level curve for northwest Germany: global signals, local effects or data-artefacts? *International Journal of Earth Sciences* **99**, 1687–1706.

Bunzel, D., Milker, Y., Müller-Navarra, K., Arz, H.W., Friedrich, J., Lahajnar, N., Schmiedl, G., 2020. Integrated stratigraphy of foreland salt-marsh sediments of the south-eastern North Sea region. *Newsletters on Stratigraphy* **53**, 415–442.

Burr, G.S., Thomas, J.M., Reines, D., Jeffrey, D., Courtney, C., Jull, A.J.T., Lange, T., 2001. Sample preparation of dissolved organic carbon in groundwater for AMS ^{14}C analysis. In: Carmi, I., Boaretto, E. (Eds.), Proceedings of the 17th International Radiocarbon Conference June 18–23, 2000. *Radiocarbon* **43**, 183–190.

Callaway, J.C., DeLaune, R.D., Patrick Jr., W.H., 1996. Chernobyl ^{137}Cs used to determine sediment accretion rates at selected northern European coastal wetlands. *Limnology and Oceanography* **41**, 444–450.

Camphuysen, K., Vollaard, B., 2015. Oil pollution in the Dutch sector of the North Sea. In: Carpenter A. (Ed.), Oil pollution in the North Sea. *The Handbook of Environmental Chemistry* **41**, 117–140.

Chanton, J.P., Martens, C.S., Kipphut, G.W., 1983. Lead-210 sediment geochronology in a changing coastal environment. *Geochimica et Cosmochimica Acta* **47**, 1791–1804.

Chaumillon, E., Bertin, X., Fortunato, A.B., Bajo, M., Schneider, J.-L., Dezileau, L., Walsh, J.P., Michelot, A., Chauveau, E., Créach, A., Hénaff, A., Sauzeau, T., Waeles, B., Gervais, B., Jan, G., Baumann, J., Breilh, J.-F., Pedreros, R., 2017. Storm-induced marine flooding: lessons from a multidisciplinary approach. *Earth-Science Reviews* **165**, 151–184.

Chernorukov, N.G., Nipruk, O.V., Kostrova, E.L., 2015. Cesium Uranate $Cs_3U_{12}O_{31}(OH)_{13} \cdot 3H_2O$: synthesis and characterization. *Russian Journal of Inorganic Chemistry* **60**, 1329–1332.

Chirol, C., Gallop, S., Pontee, N., Haigh, I., Thompson, C., 2015. Creek networks: natural evolution and design choices for intertidal habitat recreation. Conference Paper, Conference: 'sea lines of communication: construction', Southampton, DOI: 10.13140/RG.2.1.1066.1841.

Church, J.A., White, N.J., Aarup, T., Wilson, W.S., Woodworth, P.L., Domingues, C.M., Hunter, J.R., Lambeck, K., 2008. Understanding

global sea levels: past, present and future. *Sustainability Science* **3**, 9–22.

Comans, R.N.J., Middelburg, J.J., Zonderhuis, J., Woittiez, J.R.W., De Lange, G.J., Das, H.A., Van Der Weijden, C.H., 1989. Mobilization of radiocaesium in pore water of lake sediments. *Nature* **339**, 367–369.

Comas-Bru, L., McDermott, F., 2014. Impacts of the EA and SCA patterns on the European twentieth century NAO-winter climate relationship. *Quaternary Journal of the Royal Meteorological Society* **140**, 354–363.

Coughlan, C., Stips, A., 2015. Modelling the tides on the North West European shelf. Joint Reseach Centre (JRC) technical report. European Commission, Institute for Environment and Sustainability, European Union, 27 p.

Craft, C., Clough, J., Ehman, J., Joye, S., Park, R., Pennings, S., Guo, H., Machmuller, M, 2009. Forecasting the effects of accelerated sea-level rise on tidal marsh ecosystem services. *Frontiers in Ecology and the Environment* **7**, 73–78.

Cundy, A.B., Croudace, I.W., 1995. Physical and chemical associations of radionuclides and trace metals in estuarine sediments: an example from Poole Harbour, Southern England. *Journal of Environmental Radioactivity* **29**, 191–211.

Cundy, A.B., Croudace, I.W., Warwick, P.E., Oh, J.-S., Haslett, S.K., 2002. Accumulation of COGEMA-La Hague-derived reprocessing wastes in French salt marsh sediments. *Environmental Science and Technology* **36**, 4990–4997.

CWSS, Common Wadden Sea Secretariat, 2009. Marencic, H., de Vlas, J. (Eds.), Quality Status Report 2009. Wadden Sea Ecosystem No. 25. Common Wadden Sea Secretariat, Trilateral Monitoring and Assessment Group, Wilhelmshaven, Germany, 597 p.

CWSS, Common Wadden Sea Secretariat, 2010. Wadden Sea Plan 2010. Eleventh Trilateral Governmental Conference on the Protection of the Wadden Sea. Common Wadden Sea Secretariat, Wilhelmshaven, Germany, 102 p.

Dahlmann, G., Timm, D., Averbeck, C., Camphuysen, C., Skov, H., Durinck, J., 1994. Oiled seabirds – comparative investigations on oiled seabirds and oiled beaches in the Netherlands, Denmark and Germany (1990–93). *Marine Pollution Bulletin* **28**, 305–310.

Dangendorf, S., Mudersbach, C., Wahl, T., Jensen, J., 2013a. Characteristics of intra-, inter-annual and decadal sea-level variability and the role of meteorological forcing: the long record of Cuxhaven. *Ocean Dynamics* **63**, 209–224.

Dangendorf, S. Mudersbach, C., Jensen, J., Anette, G., Heinrich, H., 2013b. Seasonal to decadal forcing of high water level percentiles in the German Bight throughout the last century. *Ocean Dynamics* **63**, 533–548.

Dangendorf, S., Müller-Navarra, S., Jensen, J., Schenk, F., Wahl, T., Weisse, R., 2014. North Sea storminess from a novel storm surge record since AD 1843. *Journal of Climate* **27**, 3582–3595.

Dangendorf, S., Hay, C., Calafat, F.M., Marcos, M., Piecuch, C.G., Berk, K., Jensen, J., 2019. Persistent acceleration in global sea-level rise since the 1960s. *Nature Climate Change* **9**, 705–710.

Davies, A.M., Jones, J.E., 1995. The influence of bottom and internal friction upon tidal currents: Taylor's problem in three dimensions. *Continental Shelf Research* **15**, 1251–1285.

Davy, A.J., Bakker, J.P., Figueroa, M.E., 2009. Human modification of European salt marshes. In: Silliman, B.R., Grosholz, E.D., Bertness, M.D. (Eds.), Human impacts on salt marshes – a global perspective. University of California Press, Berkeley, Los Angeles, London, 311–335.

de Groot, A.V., Veeneklaas, R.M., Bakker, J.P., 2011. Sand in the salt marsh: contribution of high-energy conditions to salt-marsh accretion. *Marine Geology* **282**, 240–254.

de Groot, A.V., van Duin, W., 2013. Best practices for creating new salt marshes in a saline estuarine setting, a literature study. IMARES report number C145/12, ecoshape: building with nature. Wageningen, 39 p.

de Jong, D.J., de Jong, Z., Mulder, J.P.M., 1994. Changes in area, geomorphology and sediment nature of salt marshes in the Oosterschelde estuary (SW Netherlands) due to tidal changes. *Hydrobiologia* **282/283**, 303–316.

De Rijk, S., 1995. Salinity control on the distribution of salt marsh foraminifera (Great Marshes, Massachusetts). *Journal of Foraminiferal Research* **25**, 156–166.

De Rijk, S., Troelstra, S.R., 1997. Salt marsh foraminifera from the Great Marshes, Massachusetts: environmental controls. *Palaeogeography, Palaeoclimatology, Palaeoecology* **130**, 81–112.

De Vos, W., Tarvainen, T., Salminen, R., Reeder, S., De Vivo, B., Demetriades, A., Pirc, S., Batista, M.J., Marsina, K., Ottesen, R.T., O'Connor, P.J., Bidovec, M., Lima, A., Siewers, U., Smith, B., Taylor, H., Shaw, R., Salpeteur, I., Gregorauskiene, V., Halamic, J., Slaninka, I., Lax, K., Gravesen, P., Birke, M., Breward, N., Ander, E.L., Jordan, G., Duris, M., Klein, P., Locutura, J., Bel-lan, A., Pasieczna, A., Lis, J., Mazreku, A., Gilucis, A., Heitzmann, P., Klaver, G., Petersell, V., 2006. Geochemical atlas of Europe. Part 2 – interpretation of geochemical maps, additional tables, figures, maps, and related publications. Geological Survey of Finland, Otamedia Oy, Espoo, 690 p.

Deek, A., 2011. Sources and sinks of reactive nitrogen in the German Bight. Doctoral dissertation, Institute for Geology, Universität Hamburg, 143 p.

Dijkema, K.S., 1987. Changes in salt-marsh area in the Netherlands Wadden Sea after 1600. In: Huiskes, A.H.L., Blom, C.W.P.M., Rozema, J. (Eds.), Vegetation between land and sea. Junk Publishers, Dordrecht, Boston, Lancaster, 42–49.

Donahue, D.J., Linick, T.W., Jull, A.J.T., 1990. Isotope-ratio and background corrections for accelerator mass spectrometry radiocarbon measurements. *Radiocarbon* **32**, 135–142.

Dong, B., Sutton, R.T., Woollings, T., Hodges, K., 2013. Variability of the North Atlantic summer storm track: mechanisms and impacts on European climate. *Environmental Research Letters* **8**, 034037.

Dunster, H.J., 1998. An historical perspective of radioactive effluents: discharges from Sellafield to the Irish Sea. *Radiation Protection Dosimetry* **75**, 15–21.

Dypvik, H., Harris, N.B., 2001. Geochemical facies analysis of fine-grained siliciclastics using Th/U, Zr/Rb and (Zr/Rb)/Sr ratios. *Chemical Geology* **181**, 131–146.

ECA, Economics of Climate Adaptation, 2009. Shaping climate-resilient development: a framework for decision-making. Climate Works Foundation, Global Environment Facility, European Commission, McKinsey & Company, Rockefeller Foundation, Standard Chartered Bank and Swiss Re, 164 p.

Ehlers, J., 1988. The morphodynamics of the Wadden Sea. Balkema A.A. Publishers, 320 p.

Ehlers, J., Nagorny, K., Schmidt, P., Stieve, B., Zietlow, K., 1993. Storm surge deposits in North Sea salt marshes dated by ^{134}Cs and ^{137}Cs determination. *Journal of Coastal Research* **9**, 698–701.

Eisma, D., 1981. Supply and deposition of suspended matter in the North Sea. In: Nio, S.-D., Schüttenhelm, R.T.E., van Weering, T.C.E. (Eds.), Holocene marine sedimentation in the North Sea basin. Blackwell Scientific Publications, Oxford, London, Edinburgh, Boston, Melbourne, 415–428.

Eisma, D., Kalf, J., 1987. Dispersal, concentration and deposition of suspended matter in the North Sea. *Journal of the Geological Society* **144**, 161–178.

Eisma, D., Irion, G., 1988. Suspended matter and sediment transport. In: Salomons, W., Bayne, B.L., Duursma, E.K., Förstner, U. (Eds.), Pollution of the North Sea – an assessment. Springer-Verlag, Berlin, Heidelberg, New York, London, Paris, Tokyo, 20–35.

Elshanawany, R., Ibrahim, M.I., Milker, Y., Schmiedl, G., Badr, N., Kholeif, S.E.A., Zonneveld, K.A.F., 2011. Anthropogenic impact on benthic foraminifera, Abu-Qir Bay, Alexandria, Egypt. *Journal of Foraminiferal Research* **41**, 326–348.

Enfield, D.B., Mestas-Nuñez, A.M., Trimble, P.J., 2001. The Atlantic multidecadal oscillation and its relation to rainfall and river flows in the continental U.S. *Geophysical Research Letters* **28**, 2077–2080.

Enfield, D., Cid-Serrano, L., 2010. Secular and multidecadal warmings in the North Atlantic and their relationships with major hurricane activity. *International Journal of Climatology* **30**, 174–184.

Enting, I.G., 1982. Nuclear weapons data for use in carbon cycle modelling. Division of Atmospheric Physics Technical Paper No. 44, Commonwealth Scientific and Industrial Research Organization, Australia, 18 p.

Erchinger, H.F., Coldewey, H.-G., Meyer, C., 1996. Interdisziplinäre Erforschung des Deichvorlandes im Forschungsvorhaben ‚Erosionsfestigkeit von Hellern'. *Die Küste* **58**, 1–45.

Esselink, P., Zijlstra, W., Dijkema, K.S., van Diggelen, R., 2000. The effects of decreased management on plant-species distribution patterns in a salt marsh nature reserve in the Wadden Sea. *Biological Conservation* **93**, 61–76.

Esselink, P., Petersen, J., Arens, S., Bakker, J.P., Bunje, J., Dijkema, K.S., Hecker, N., Hellwig, U., Jensen, A.-V., Kers, A.S., Körber, P., Lammerts, E.J., Stock, M., Veeneklaas, R.M., Vreeken, M., Wolters, M., 2009. Salt marshes. Thematic Report No. 8. In: Marencic, H., de Vlas, J. (Eds.), Quality Status Report 2009. Wadden Sea Ecosystem No. 25. Common Wadden Sea Secretariat, Trilateral Monitoring and Assessment Group, Wilhelmshaven, Germany, 54 p.

Esselink, P., van Duin, W.E., Bunje, J., Cremer, J., Folmer, E.O., Frikke, J., Glahn, M., de Groot, A.V., Hecker, N., Hellwig, U., Jensen, K., Körber, P., Petersen, J., Stock, M., 2017. Salt marshes. In: Kloepper, S. et al. (Eds.), Wadden Sea Quality Status Report 2017. Common Wadden Sea Secretariat, Trilateral Monitoring and Assessment Group, Wilhelmshaven, Germany, 41 p.

Ewing, R.C., 2008. Nuclear fuel cycle: environmental impact. *Materials Research Society (MRS) Bulletin* **33**, 338–340.

Fagherazzi, S., 2014. Strom-proofing with marshes. *Nature Geoscience* **7**, 701–702.

Fairbridge, R.W., Krebs Jr., O.A., 1961. Sea Level and the Southern Oscillation. *Geophysical Journal International* **6**, 532–545.

Familkhalili, R., Talke, S.A., 2016. The effect of channel deepening on tides and storm surge: a case study of Wilmington, NC. *Geophysical Research Letters* **43**, 9138–9147.

Fatela, F., Taborda, R., 2002. Confidence limits of species proportions in microfossil assemblages. *Marine Micropaleontology* **45**, 169–174.

Feagin, R.A., Lozada-Bernard, S.M., Ravens, T.M., Möller, I., Yeager, K.M., Baird, A.H., 2009. Does vegetation prevent wave erosion of salt marsh edges? *Proceedings of the National Academy of Sciences (PNAS)* **106**, 10109–10113.

Ferraro, F., Meyer-Roux, S., Muellenhoff, O., Pavliha, M., Svetak, J., Tarchi, D., Topouzelis, K., 2009. Long term monitoring of oil spills in European seas. *International Journal of Remote Sensing* **30**, 627–645.

Feyling-Hanssen, R.W., 1972. The foraminifer *Elphidium excavatum* (Terquem) and its variant forms. *Micropaleontology* **18**, 337–354.

Fickert, M., Strotmann, T., 2007. Hydronamische Entwicklung der Tideelbe. In: Gönnert, G., Pflüger, B., Bremer, J.-A. (Eds.), Von der Geoarchäologie über die Küstendynamik zum Küstenzonenmanagement. *Coastline Reports* **9**, 59–68.

Fischer, O., 1956. Das Wasserwesen an der schleswig-holsteinischen Nordseeküste, Eiderstedt. Dritter Teil: das Festland. Verlag von Dietrich Reimer, Berlin, 328 p.

Fischer, O., 1957. Das Wasserwesen an der schleswig-holsteinischen Nordseeküste, Dithmarschen. Dritter Teil: das Festland. Verlag von Dietrich Reimer, Berlin, 328 p.

Flather, R., Williams, J., 2000. Climate change effects on storm surges: methodologies and results. In: Beersma, J., Agnew, M., Viner, D., Hulme, M. (Eds.), Climate scenarios for water-related and coastal impact. ECLAT-2 workshop report no. 3, the Netherlands: KNMI, 66–78.

Fleet, D.M., Reineking, B., 2000. Have efforts to clean up the marine environment been successful? – German beached bird surveys provide an index for oil pollution levels in the southern North Sea. In: Brebbia, C.A., Rodriguez, G.R. (Eds.), Oil and hydrocarbon spills II: modelling, analysis and control. WIT Press, 117–126.

Flemming, B.W., Nyandwi, N., 1994. Land reclamation as a cause of fine-grained sediment depletion in backbarrier tidal flats (Southern North Sea). *Netherlands Journal of Aquatic Ecology* **28**, 299–307.

Fletcher, W.J., Zielhofer, C., 2013. Fragility of western Mediterranean landscapes during Holocene rapid climate changes. *Catena* **103**, 16–29.

Folk, R.L., Ward, W.C., 1957. Brazos River bar: a study in the significance of grain size parameters. *Journal of Sedimentary Petrology* **27**, 3–26.

Fralick, P.W., Kronberg, B.I., 1997. Geochemical discrimination of elastic sedimentary rock sources. *Sedimentary Geology* **113**, 111–124.

Francescangeli, F., Armynot du Chatelet, E., Billon, G., Trentesaux, A., Bouchet, V.M.P., 2016. Palaeo-ecological quality status based on foraminifera of Boulognesur-Mer harbour (Pas-de-Calais, Northeastern France) over the last 200 years. *Marine Environmental Research* **117**, 32–43.

Francescangeli, F., Bouchet, V.M.P., Trentesaux, A., Armynot du Chatelet, E., 2017. Does elevation matter? Living foraminiferal distribution in a hyper tidal salt marsh (Canche Estuary, Northern France). *Estuarine, Coastal and Shelf Science* **194**, 192–204.

Francescangeli, F., Portela, M., Armynot du Chatelet, E., Billon, G., Andersen, T.J., Bouchet, V.M.P., Trentesaux, A., 2018. Infilling of the Canche Estuary (eastern English Channel, France): insight from benthic foraminifera and historical pictures. *Marine Micropaleontology* **142**, 1–12.

French, J.R., 1993. Numerical simulation of vertical marsh growth and adjustment to accelerated sea-level rise, North Norfolk, UK. *Earth Surface Processes and Landforms* **18**, 63–81.

French, J., 2006. Tidal marsh sedimentation and resilience to environmental change: exploratory modelling of tidal, sea-level and sediment supply forcing in predominantly allochthonous systems. *Marine Geology* **235**, 119–136.

Freund, H., Streif, H., 2000. Natürliche Pegelmarken für Meeresspiegelschwankungen der letzten 2000 Jahre im Bereich der Insel Juist. *Petermanns Geographische Mitteilungen* **143**, 34–45.

Frontalini, F., Coccioni, R., 2008. Benthic foraminifera for heavy metal pollution monitoring: a case study from the central Adriatic Sea coast of Italy. *Estuarine, Coastal and Shelf Science* **76**, 404–417.

Frontalini, F., Buosi, C., Da Pelo, S., Coccioni, R., Cherchi, A., Bucci, C., 2009. Benthic foraminifera as bio-indicators of trace element pollution in the heavily contaminated Santa Gilla lagoon (Cagliari, Italy). *Marine Pollution Bulletin* **58**, 858–877.

Gallagher, D., McGee, E.J., Mitchell, P.I., Alfimov, V., Aldahan, A., Possnert, G., 2005. Retrospective search for evidence of the 1957 Windscale fire in NE Ireland using ^{129}I and other long-lived nuclides. *Environmental Science and Technology* **39**, 2927–2935.

Ganske, A., Fery, N., Gaslikova, L., Grabemann, I., Weisse, R., Tinz. B., 2018. Identification of extreme storm surges with high-impact potential along the German North Sea coastline. *Ocean Dynamics* **68**, 1371–1382.

Garwin, R.L., 2001. Can the world do without nuclear power? Can the world live with nuclear power? *Interdisciplinary Science Reviews* **26**, 265–271.

Gehrels, W.R., Newman, S.W.G., 2004. Salt-marsh foraminifera in Ho Bugt, western Denmark, and their use as sea-level indicators. *Geografisk Tidsskrift-Danish Journal of Geography* **104**, 97–106.

Gerber, M., Ganske, A., Müller-Navarra, S., Rosenhagen, G., 2016. Categorisation of meteorological conditions for storm tide episodes in the German Bight. *Meteorologische Zeitschrift* **25**, 447–462.

Geslin, E., Stouff, V., Debenay, J.-P., Lesourd, M., 2000. Environmental variation and foraminiferal test abnormalities. In: Martin, R.E. (Ed.), Environmental micropaleontology: the application of microfossils to environmental geology. Kluwer Academic/Plenum Publishers, New York, 191–215.

Geslin, E., Debenay, J.-P., Duleba, W., Bonetti, C., 2002. Morphological abnormalities of foraminiferal tests in Brazilian environments: comparison between polluted and non-polluted areas. *Marine Micropaleontology* **45**, 151–168.

Gönnert, G., Sossidi, K., 2011. A new approach to calculate extreme storm surges: analysing the interaction of storm surge components. Coastal Processes II, *Transactions on Ecology and the Environment* **149**, 139–150.

Gornitz, V., 2005. Storm Surge. In: Schwartz M.L. (Ed.), Encyclopedia of coastal science. Encyclopedia of Earth Science Series. Springer, Dordrecht. DOI: 10.1007/1-4020-3880-1_298, 912–914.

Gregory, J., Griffies, S., Hughes, C., Lowe, J., Church, J., Fukimori, I., Gomez, N., Kopp, R., Landerer, F., Le Cozannet, G., Ponte, R.M., Stammer, D., Tamisiea, M.E., van de Wal, R.S.W., 2019. Concepts and terminology for sea level: mean, variability and change, both local and global. *Surveys in Geophysics* **40**, 1251–1289.

Hadler, H., Vött, A., Newig, J., Emde, K., Finkler, C., Fischer, P., Willershäuser, T., 2018. Geoarchaeological evidence of marshland destruction in the area of Rungholt, present-day Wadden Sea around Hallig Südfall (North Frisia, Germany), by the Grote Mandrenke in 1362 AD. *Quaternary International* **473**, 37–54.

Haigh, I., Nicholls, R., Wells, N., 2010. Assessing changes in extreme sea levels: application to the English Channel, 1900–2006. *Continental Shelf Research* **30**, 1042–1055.

Hammer, Ø., Harper, D.A.T., Ryan, P.D., 2001. PAST: Paleontological Statistics software package for education and data analysis. *Palaeontologia Electronica* **4**, 1–9.

Haslett, S.K., Davies, P., Strawbridge, F., 1997. Reconstructing Holocene sea-level change in the Severn Estuary and Somerset Levels: the foraminifera connection. *Archaeology in the Severn Estuary* **8**, 29–40.

Hofstede, J.L.A., 2003. Integrated management of artificially created salt marshes in the Wadden Sea of Schleswig-Holstein, Germany. *Wetlands Ecology and Management* **11**, 183–194.

Hollebrandse, F.A.P., 2005. Temporal development of the tidal range in the southern North Sea. Doctoral dissertation, Faculty of Civil Engineering and Geoscience, Delft University of Technology, the Netherlands, 92 p.

Holm, E., Persson, R.B.R., 1978. Biophysical aspects of Am-241 and Pu-241 in the environment. *Radiation and Environmental Biophysics* **15**, 261–276.

Horsburgh, K.J., Wilson, C., 2007. Tide-surge interaction and its role in the distribution of surge residuals in the North Sea. *Journal of Geophysical Research* **112**, C08003.

Horton, B.P., 1999. The distribution of contemporary intertidal foraminifera at Cowpen Marsh, Tees Estuary, UK: implications for studies of Holocene sea-level changes. *Palaeogeography, Palaeoclimatology, Palaeoecology* **149**, 127–149.

Horton, B.P., Edwards, R.J., Lloyd, J.M., 1999. A foraminiferal-based transfer function: implications for sea-level studies. *Journal of Foraminiferal Research* **29**, 117–129.

Horton, B.P., Edwards, R.J., 2006. Quantifying Holocene sea-level change using intertidal foraminifera: lessons from the British Isles. *Cushman Foundation for Foraminiferal Research, Special Publication* **40**, 95 p.

Hoskin, P.W.O., Ireland, T.R., 2000. Rare earth element chemistry of zircon and its use as a provenance indicator. *Geology* **28**, 627–630.

Hua, Q., Barbetti, M., 2004. Review of tropospheric bomb ^{14}C data for carbon cycle modeling and age calibration purposes. *Radiocarbon* **46**, 1273–1298.

Hurrell, J.W., 1995. Decadal trends in the North Atlantic Oscillation: regional temperatures and precipitation. *Science* **269**, 676–679.

Hurrell, J.W., Kushnir, Y., Ottersen, G., Visbeck, M., 2003. An overview of the North Atlantic Oscillation. *Geophysical Monograph* **134**, DOI: 10.1029/134GM01.

Hylander, L.D., Meili, M., 2003. 500 years of mercury production: global annual inventory by region until 2000 and associated emissions. *The Science of the Total Environment* **304**, 13–27.

Ionita, M., Rimbu, N., Lohmann, G., 2011. Decadal variability of the Elbe river streamflow. *International Journal of Climatology* **31**, 22–30.

IPCC, Intergovernmental Panel on Climate Change, special report on the ocean and cryosphere in a changing climate, 2019. In: Pörtner, H.-O., Roberts, D. C., Masson-Delmotte, V., Zhai, P., Tignor, M., Poloczanska, E., Mintenbeck, K., Alegria, A., Nicolai, M., Okem, A., Petzold, J., Rama, B., Weyer, N. M. (Eds), Technical report, IPCC (in press).

Jacob, D., Podzun, R., 1997. Sensitivity studies with the regional climate model REMO. *Meteorology and Atmospheric Physics* **63**, 119–129.

Jarvis, S., Croudace, I.W., Rothwell, R.G., 2015. Parameter optimization for the ITRAX core scanner. In: Croudace, I.W., Rothwell, R.G. (Eds.), Micro-XRF studies of sediment cores: applications of a non-destructive tool for the environmental sciences. *Developments in Paleoenvironmental Research* **17**, Springer, Dordrecht, Heidelberg, New York, London, 535–562.

Jensen, J., Mudersbach, C., 2007. Zeitliche Veränderung in den Wasserstandszeitreihen an den Deutschen Küsten. In: Gönnert, G., Grassel, H., Kelletat, D., Kunz, H., Probst, B., von Storch, H., Sündermann, J. (Eds.), Klimaänderung und Küstenschutz. Berichte zur Deutschen Landeskunde, Bd. 81, 99–112.

Jungclaus, J., Fischer, N., Haak, H., Lohmann, K., Marotzke, J., Matei, D., Mikolajewicz, U., Notz, D., Storch, J., 2013. Characteristics of the ocean simulations in the Max Planck Institute Ocean Model (MPIOM) the ocean component of the MPI-Earth system model. *Journal of Advances in Modeling Earth Systems* **5**, 422–446.

Kabat, P., Bazelmans, J., van Dijk, J., Herman, P.M.J., van Oijen, T., Pejrup, M., Reise, K., Speelman, H., Wolff, W.J., 2012. The Wadden Sea region: towards a science for sustainable development. *Ocean and Coastal Management* **68**, 4–17.

Kathilankal, J.C., Mozdzer, T.J., Fuentes, J.D., D'Odorico, P., McGlathery K.J., Zieman, J.C., 2008. Tidal influences on carbon assimilation by a salt marsh. *Environmental Research Letters* **3**, 044010.

Kautsky, H., 1987. Investigations on the distribution of ^{137}Cs, ^{134}Cs and ^{90}Sr and the water mass transport times in the northern North Atlantic and the North Sea. *Deutsche Hydrografische Zeitschrift* **40**, 49–69.

Kelletat, D., 1992. Coastal erosion and protection measures at the German North Sea coast. *Journal of Coastal Research* **8**, 699–711.

Kemp, A.C., Horton, B.P., Culver, S.J., 2009. Distribution of modern salt-marsh foraminifera in the Albemarle-Pamlico estuarine system of North Carolina, USA: implications for sea-level research. *Marine Micropaleontology* **72**, 222–238.

Kemp, A.C., Nelson, A.R., Horton, B.P., 2013. Radiocarbon dating of plant macrofossils from tidal-marsh sediment. In: Shroder, J., Switzer, A.D., Kennedy, D.M. (Eds.), Treatise on geomorphology. Academic Press, San Diego, CA, *Methods in Geomorphology* **14**, 370–388.

Kiehl, K., Eischeid, I., Gettner, S., Walter, J., 1996. Impact of different sheep grazing intensities on salt marsh vegetation in northern Germany. *Journal of Vegetation Science* **7**, 99–106.

Kiesel, J., Schuerch, M., Christie, E.K., Möller, I., Spencer, T., Vafeidis, A.T., 2020. Effective design of managed realignment schemes can reduce coastal flood risks. *Estuarine, Coastal and Shelf Science* **242**, 106844.

Kirchner, G., 2011. ^{210}Pb as a tool for establishing sediment chronologies: examples of potentials and limitations of conventional dating models. *Journal of Environmental Radioactivity* **102**, 490–494.

Kirchner, G., Ehlers, H., 1998. Sediment geochronology in changing coastal environments: potentials and limitations of the ^{137}Cs and ^{210}Pb methods. *Journal of Coastal Research* **14**, 483–492.

Kirwan, M.L., Mudd, S.M., 2012. Response of salt-marsh carbon accumulation to climate change. *Nature* **489**, 550–553.

Kirwan, M.L., Megonigal, J.P., 2013. Tidal wetland stability in the face of human impacts and sea-level rise. *Nature* **504**, 53–60.

Kirwan, M.L., Temmerman, S., Skeehan, E.E., Guntenspergen, G.R., Fagherazzi, S., 2016. Overestimation of marsh vulnerability to sea level rise. *Nature Climate Change* **6**, 253–260.

Knight, J.R., Folland, C.K., Scaife, A.A., 2006. Climate impacts of the Atlantic Multidecadal Oscillation. *Geophysical Research Letters* **33**, L17706.

Krause, G., Wolter, R., 1970. Neuregelung der Wasserwirtschaft in Ostfriesland. *Die Küste* **19**, 186–212.

Lal, K.K., Bonetti, C., Woodroffe, C.D., Rogers, K., 2020. Contemporary distribution of benthic foraminiferal assemblages in coastal wetlands of south-eastern Australia. *Estuarine, Coastal and Shelf Science* **245**, 106949.

Lang, A., Mikolajewicz, U., 2019. The long-term variability of extreme sea levels in the German Bight. *Ocean Science* **15**, 651–668.

Lang, A., Mikolajewicz, U., 2020. Rising extreme sea levels in the German Bight under enhanced CO_2 levels: a regionalized large ensemble approach for the North Sea. *Climate Dynamics* **55**, 1829–1842.

Larsen, T., Yokoyama, Y., Fernandes, R., 2017. Radiocarbon in ecology: insights and perspectives from aquatic and terrestrial studies. *Methods in Ecology and Evolution* **9**, 181–190.

Lehmann, H.-A., Heinz, J., 2008. Tidal barriers at the North and Baltic Sea coast. *Die Küste* **74**, 212–232.

Leipe, T., Moros, M., Kotilainen, A., Vallius, H., Kabel, K., Endler, M., Kowalski, N., 2013. Mercury in Baltic Sea sediments – natural background and anthropogenic impact. *Chemie der Erde* **73**, 249–259.

Leonardi, N., Carnacina, I., Donatelli, C., Ganju, N.K., Plater, A.J., Schuerch, M., Temmerman, S., 2018. Dynamic interactions between coastal storms and salt marshes: a review. *Geomorphology* **301**, 92–107.

Lepland, A., Andersen, T.J., Lepland, A., Arp, H.P.H., Alve, E., Breedveld, G.D., Rindby, A., 2010. Sedimentation and chronology of heavy metal pollution in Oslo harbour, Norway. *Marine Pollution Bulletin* **60**, 1512–1522.

Libby, W.F., 1961. Radiocarbon dating. *Science* **133**, 621–629.

Lorenzen, J., 1960. 25 Jahr Forschung im Dienst des Küstenschutzes. *Die Küste* **8**, 7–28.

Lubis, A.A., 2006. Constant rate of supply (CRS) model for determining the sediment accumulation rate in the coastal area using ^{210}Pb. *Journal of Coastal Development* **10**, 9–18.

MacDonald, G.J.F., 1964. Tidal friction. *Reviews of Geophysics* **2**, 467–541.

Mariotti, G., Fagherazzi, S., 2010. A numerical model for the coupled long-term evolution of salt marshes and tidal flats. *Journal of Geophysical Research* **115**, F01004.

Marsland, S.J., Bindoff, N., Williams, G., Budd, W., 2004. Modeling water mass formation in the Mertz Glacier Polynya and Adélie Depression, east Antarctica. *Journal of Geophysical Research* **109**, C11003.

Martínez-Colón, M., Hallock, P., Green-Ruíz, C., 2009. Strategies for using shallow-water benthic foraminifers as bioindicators of potentially toxic elements: a review. *Journal of Foraminiferal Research* **39**, 278–299.

Martínez-Colón, M., Hallock, P., 2010. Preliminary survey on foraminiferal responses to pollutants in Torrecillas Lagoon Puerto Rico. *Caribbean Journal of Science* **46**, 1–6.

Martínez-Colón, M., Hallock, P., Green Ruíz, C., Smoak, J.M., 2018. Benthic foraminifera as bioindicators of potentially toxic element (PTE) pollution: Torrecillas lagoon (San Juan Bay Estuary), Puerto Rico. *Ecological Indicators* **89**, 516–527.

Martínez-Cortizas, A., Pontevedra-Pombal, X., García-Rodeja, E., Nóvoa-Muñoz, J.C., Shotyk, W., 1999. Mercury in a Spanish peat bog: archive of climate change and atmospheric metal deposition. *Science* **284**, 939–942.

Matulla, C., Schöner, W., Alexandersson, H., von Storch, H., Wang, X.L., 2008. European storminess: late nineteenth century to present. *Climate Dynamics* **31**, 125–130.

Mayer, L.M., Macko, S.A., Mook, W.H., Murray, S., 1981. The distribution of bromine in coastal sediments and its use as a source indicator for organic matter. *Organic Geochemistry* **3**, 37–42.

Mayer, L.M., Schick, L.L., Allison, M.A., Ruttenberg, K.C., Bentley, S.J., 2007. Marine vs. terrigenous organic matter in Louisiana coastal sediments: the uses of bromine:organic carbon ratios. *Marine Chemistry* **107**, 244–254.

Mayewski, P.A., Rohling, E.E., Stager, J.C., Karlén, W., Maasch, K.A., Meeker L.D., Meyerson, E.A., Gasse, F., van Kreveld, S., Holmgren, K., Lee-Thorp, J., Rosqvist, G., Rack, F., Staubwasser, M., Schneider, R.R., Steig, E.J., 2004. Holocene climate variability. *Quaternary Research* **62**, 243– 255.

McCarthy, G.D., Haigh, I.D., Hirschi, J.J.-M., Grist, J.P., Smeed, D.A., 2015. Ocean impact on decadal Atlantic climate variability revealed by sea-level observations. *Nature* **521**, 508–510.

Mcleod, E., Chmura, G.L., Bouillon, S., Salm, R., Björk, M., Duarte, C.M., Lovelock, C.E., Schlesinger, W.H., Silliman, B.R., 2011. A blueprint for blue carbon: toward an improved understanding of the role of vegetated coastal habitats in sequestering CO_2. *Frontiers in Ecology and the Environment* **9**, 552–560.

MELUND, Ministry of Energy, Agriculture, the Environment, Nature and Digitalization, 2014. Bewirtschaftungsplan für den 2. Bewirtschaftungszeitraum gemäß Artikel 13 der Richtlinie 2000/60/EG (§ 83 WHG) für die Flussgebietseinheit Eider. Ministerium für Energiewende, Landwirtschaft, Umwelt und ländliche Räume des Landes Schleswig-Holstein, 311 p.

MELUND, Ministry of Energy, Agriculture, the Environment, Nature and Digitalization, 2015a. Strategie für das Wattenmeer 2100. Ministerium für Energiewende, Landwirtschaft, Umwelt und ländliche Räume des Landes Schleswig-Holstein, 88 p.

MELUND, Ministry of Energy, Agriculture, the Environment, Nature and Digitalization, 2015b. Bewirtschaftungsplan (gemäß Artikel 13 EG-WRRL bzw. § 83 WHG) FGE Eider – 2. Bewirtschaftungszeitraum 2016-2021. Ministerium für Energiewende, Landwirtschaft, Umwelt und ländliche Räume des Landes Schleswig-Holstein, 314 p.

Meurer, R., 2000. Wasserbau und Wasserwirtschaft in Deutschland. Vergangenheit und Gegenwart. Parey Buchverlag Berlin, 371 p.

Mierwald, U., Romahn, K., 2006. Die Farn- und Blütepflanzen Schleswig-Holsteins, Rote Liste Band 1. Landesamt für Natur und Umwelt des Landes Schleswig-Holstein, Kiel, 122 p.

Milan, C.S., Swenson, E.M., Turner, R.E., Lee, J.M., 1995. Assessment of the ^{137}Cs method for estimating sediment accumulation rates: Louisiana salt marshes. *Journal of Coastal Research* **11**, 296–307.

Milker, Y., Horton, B.P., Nelson, A.R., Engelhart, S.E., Witter, R.C., 2015. Variability of intertidal foraminiferal assemblages in a salt marsh, Oregon, USA. *Marine Micropaleontology* **118**, 1–16.

Möller, I., Kudella, M., Rupprecht, F., Spencer, T., Paul, M., van Wesenbeeck, B.K., Wolters, G., Jensen, K., Bouma, T.J., Miranda-Lange, M., Schimmels, S., 2014. Wave attenuation over coastal salt marshes under storm surge conditions. *Nature Geoscience* **7**, 727–731.

Moros, M., Andersen, T.J., Schulz-Bull, D., Häusler, K., Bunke, D., Snowball, I., Kotilainen, A., Zillén, L., Jensen, J.B., Kabel, K., Hand, I., Leipe, T., Lougheed, B.C., Wagner, B., Arz, H.W., 2016. Towards an event stratigraphy for Baltic Sea sediments deposited since AD 1900: approaches and challenges. *Boreas* **46**, 129–142.

Morton, R.A., 1981. Formation of storm deposits by wind-forced currents in the Gulf of Mexico and the North Sea. In: Nio, S.-D., Schüttenhelm, R.T.E., van Weering, T.C.E. (Eds.), Holocene marine sedimentation in the North Sea basin. Blackwell Scientific Publications, Oxford, London, Edinburgh, Boston, Melbourne, 385–396.

Mudersbach, C., Wahl, T., Haigh, I.D., Jensen, J., 2013. Trends in high sea levels of German North Sea gauges compared to regional mean sea level changes. *Continental Shelf Research* **65**, 111–120.

Müller, P., Ladiges, N., Jack, A., Schmiedl, G., Kutzbach, L., Jensen, K., Nolte, S., 2019. Assessing the long-term carbon-sequestration potential of the semi-natural salt marshes in the European Wadden Sea. *Ecosphere* **10**, e02556.

Müller-Navarra, S.H., Giese, H., 1999. Improvements of an empirical model to forecast wind surge in the German Bight. *German Journal of Hydrography* **51**, 385–405.

Müller-Navarra, S.H., Lange, W., Dick, S., Soetje, K.C., 2003. Über die Verfahren der Wasserstands- und Sturmflutvorhersage; Hydrondynamisch-numerische Modelle der Nord- und Ostsee und ein

empirisch-statistisches Verfahren für die Deutsche Bucht. *Promet*, Jahrg. **29**, 117–124.

Müller-Navarra, K., Milker, Y., Schmiedl, G., 2016. Natural and anthropogenic influence on the distribution of salt marsh foraminifera in the Bay of Tümlau, German North Sea. *Journal of Foraminiferal Research* **46**, 61–74.

Müller-Navarra, K., Milker, Y., Schmiedl, G., 2017. Applicability of transfer functions for relative sea-level reconstructions in the southern North Sea coastal region based on salt-marsh foraminifera. *Marine Micropaleontology* **135**, 15–31.

Müller-Navarra, K., Milker, Y., Bunzel, D., Lindhorst, S., Friedrich, J., Arz, H.W., Schmiedl, G., 2019. Evolution of a ditched salt marsh in the southeastern North Sea region – anthropogenic and natural forcing. *Estuarine, Coastal and Shelf Science* **218**, 268–277.

NABU, Nature and Biodiversity Conservation Union, 2019. Jahresbericht 2019, Kreisgruppe Dithmarschen im Naturschutzbund Deutschland, Nr. 36, 35 p.

Nies, H., Goroncy, I., Herrmann, J., Michel, R., Daraoui, A., Gorny, M., Jakob, D., Sachse, R., Tosch, L., Nielsen, S.P., Dwadall, M., Rudjord, A.L., Gäfvert, T., Synal, H.-A., Stocker, M., Alfimov, V., 2009. Ressortforschungsberichte zur kerntechnischen Sicherheit und zum Strahlenschutz. Kartierung von Tc-99, I-129 und I-127 im Oberflächenwasser der Nordsee – Vorhaben StSch 4481. Bundesamt für Strahlenschutz (BfS), 204 p.

Nieuwhof, A., Vos, P.C., 2018. New data from terp excavations on sea-level index points and salt marsh sedimentation rates in the eastern part of the Dutch Wadden Sea. *Netherlands Journal of Geosciences* **97**, 31–43.

Nolte, S., Müller, F., Schuerch, M., Wanner, A., Esselink, P., Bakker, J.P., Jensen, K., 2013a. Does livestock grazing affect sediment deposition and accretion rates in salt marshes? *Estuarine, Coastal and Shelf Science* **135**, 296–305.

Nolte, S., Koppenaal, E.C., Esselink, P., Dijkema, K.S., Schuerch, M., De Groot, A.V., Bakker, J.P., Temmerman, S., 2013b. Measuring sedimentation in tidal marshes: a review on methods and their applicability in biogeomorphological studies. *Journal of Coastal Conservation* **17**, 301–325.

Norton, S.A., Evans, G.C., Kahl, J.S., 1997. Comparison of Hg and Pb fluxes to hummocks and hollows of ombrotrophic big heath bog and to nearby sergeant Mt. Pond, Maine, USA. *Water, Air, and Soil Pollution* **100**, 271–286.

Oldfield, F., Appleby, P.G., Battarbee, R.W., 1978. Alternative ^{210}Pb dating: results from the New Guinea Highlands and Lough Erne. *Nature* **271**, 339–342.

Pacyna, E.G., Pacyna, J.M., 2002. Global emission of mercury from anthropogenic sources in 1995. *Water, Air, and Soil Pollution* **137**, 149–165.

Paillard, D., Labeyrie, L., Yiou, P., 1996. Macintosh program performs time-series analysis. *Eos* **77**, 379.

Pedersen, J.B.T., Bartholdy, J., 2006. Budgets for fine-grained sediment in the Danish Wadden Sea. *Marine Geology* **235**, 101–117.

Pennington, W., Tutin, T.G., Cambray, R.S., Fisher, E.M., 1973. Observations on lake sediments using fallout ^{137}Cs as a tracer. *Nature* **242**, 324–326.

Pirrone, N., Cinnirella, S., Feng, X., Finkelman, R.B., Friedli, H.R., Leaner, J., Mason, R., Mukherjee, A.B., Stracher, G.B., Streets, D.G., Telmer, D.G., 2010. Global mercury emissions to the atmosphere from anthropogenic and natural sources. *Atmospheric Chemistry and Physics* **10**, 5951–5964.

Polovodova, I., Schönfeld, J., 2008. Foraminiferal test abnormalities in the western Baltic Sea. *Journal of Foraminiferal Research* **38**, 318–336.

Postma, H., 1981. Exchange of materials between the North Sea and the Wadden Sea. *Marine Geology* **40**, 199–213.

Pugh, D.T., 1987. Tides, surges, and mean sea level. John Wiley & Sons, Chichester, New York, Brisbane, Toronto, Singapore, 472 p.

Raspopov, O.M., Dergachev, V.A., Kolström, T., 2004. Hale cyclicity of solar activity and its relation to climate variability. *Solar Physics* **224**, 455–463.

Redfield, A.C., 1972. Development of a New England salt marsh. *Ecological Monographs* **42**, 201–237.

Reimer, P.J., Brown, T.A., Reimer, R.W., 2004. Discussion: reporting and calibration of post-bomb ^{14}C data. *Radiocarbon* **46**, 1299–1304.

Reimer, P.J., Bard, E., Bayliss, A., Beck, J.W., Blackwell, P.G., Ramsey, C.B., Buck, C.E., Cheng, H., Edwards, R.L., Friedrich, M., Grootes, P.M., Guilderson, T.P., Haflidason, H., Hajdas, I., Hatté, C., Heaton, T.J., Hoffmann, D.L., Hogg, A.G., Hughen, K.A., Kaiser, K.F., Kromer, B., Manning, S.W., Niu, M., Reimer, R.W., Richards, D.A., Scott, E.M., Southon, J.R., Staff, R.A., Turney, C.S.M., van der Plicht, J., 2013. IntCal13 and Marine13 radiocarbon age calibration curves 0–50 000 years cal. BP. *Radiocarbon* **55**, 1869–1887.

Reimer, R., Reimer, P., 2017. An online application for ΔR calculation. *Radiocarbon* **59**, 1623–1627.

Reineck, H.-E., 1982. Das Watt: Ablagerungs- und Lebensraum. Waldemar Kramer Verlag, Frankfurt am Main, 185 p.

Reineck, H.-E., Schäfer, W., 1956. Kleines Küsten-ABC für Binnenländer an der Nordsee. Berichte der Senckenbergischen Naturforschenden Gesellschaft zu Frankfurt am Main, Sonderdruck aus Natur und Volk 86, Heft 9, 261–284.

Reynaud, J.-Y., Dalrymple, R.W., 2012. Shallow-marine tidal deposits. In: Davis Jr., R.A., Dalrymple, R.W. (Eds.), Principles of tidal sedimentology. Springer, Dordrecht, 335–369.

Richter, T.O., van der Gaast, S., Koster, B., Vaars, A., Gieles, R., De Stigter, H.C., De Haas, H., van Weering, T.C.E., 2006. The Avaatech XRF core scanner: technical description and applications to NE Atlantic sediments. In: Rothwell, R.G. (Ed.), New techniques in sediment core analysis. *Geological Society, London, Special Publications* **267**, 39–50.

Röhrs, W., 1938. Der Dammbau zur Sicherung des Seedeiches an der Friedrichskoogspitze in Süderdithmarschen. *Westküste* **2**, 1–15.

Rothwell, R.G., Hoogakker, B., Thomson, J., Croudace, I.W., Frenz, M., 2006. Turbidite emplacement on the southern Balearic abyssal plain (western Mediterranean Sea) during marine isotope stages 1–3: an application of ITRAX XRF scanning of sediment cores to lithostratigraphic analysis. In: Rothwell, R.G. (Ed.), New techniques in sediment core analysis. *Geological Society, London, Special Publications* **267**, 79–98.

Rothwell, R.G., Croudace, I.W., 2015. Twenty years of XRF core scanning marine sediments: what do geochemical proxies tell us? In: Croudace, I.W., Rothwell, R.G. (Eds.), Micro-XRF studies of sediment cores: applications of a non-destructive tool for the environmental sciences. *Developments in Paleoenvironmental Research* **17**, Springer, Dordrecht, Heidelberg, New York, London, 25–102.

Scheder, J., Frenzel, P., Bungenstock, F., Engel, M., Brückner, H., Pint, A., 2019. Vertical and lateral distribution of foraminifera and ostracoda in the East Frisian Wadden Sea – developing a transfer function for relative sea-level change. *Geologica Belgica* **22**, 99–110.

Schmitz, H.P., 1965. Modellrechnungen zur *deep-water-surge*-Entwicklung – das *external surge problem*. Numerische Beiträge zur Meteoro-Hydrographie II, *Deutsche Hydrographische Zeitschrift*, Jahrg. **18**, 49–70.

Schönfeld, J., Alve, E., Geslin, E., Jorissen, F., Korsun, S., Spezzaferri, S., and members of the FOBIMO group, 2012. The FOBIMO (FOraminiferal BIo-MOnitoring) initiative – towards a standardized protocol for soft-bottom benthic foraminiferal monitoring studies. *Marine Micropaleontology* **94–95**, 1–13.

Schönfeld, J., 2018. Monitoring benthic foraminiferal dynamics at Bottsand coastal lagoon (western Baltic Sea). *Journal of Micropalaeontology* **37**, 383–393.

Schuerch, M., Rapaglia, J., Liebetrau, V., Vafeidis, A., Reise, K., 2012. Salt marsh accretion and storm tide variation: an example from a barrier island in the North Sea. *Estuaries and Coasts* **35**, 486–500.

Schuerch, M., Vafeidis, A., Slawig, T., Temmerman, S., 2013. Modeling the influence of changing storm patterns on the ability of a salt marsh to keep pace with sea level rise. *Journal of Geophysical Research: Earth Surface* **118**, 84–96.

Schuerch, M., Dolch, T., Reise, K., Vafeidis, A.T., 2014. Unravelling interactions between salt marsh evolution and sedimentary processes in the Wadden Sea (southeastern North Sea). *Progress in Physical Geography* **38**, 691–715.

Schuerch, M., Spencer, T., Temmerman, S., Kirwan, M.L., Wolff, C., Lincke, D., McOwen, C.J., Pickering, M.D., Reef, R., Vafeidis, A.T., Hinkel, J., Nicholls, R.J., Brown, S., 2018. Future response of global coastal wetlands to sea-level rise. *Nature* **561**, 231–234.

Schuerch, M., Spencer, T., Evans, B., 2019. Coupling between tidal mudflats and salt marshes affects marsh morphology. *Marine Geology* **412**, 95–106.

Schulz, M., Mudelsee, M., 2002. REDFIT: estimating red-noise spectra directly from unevenly spaced paleoclimatic time series. *Computers and Geosciences* **28**, 421–426.

Scott, D.B., Hermelin, J.O.R., 1993. A device for precision splitting of micropaleontological samples in liquid suspension. *Journal of Paleontology* **67**, 151–154.

Scott, D.S., Medioli, F.S., 1978. Vertical zonations of marsh foraminifera as accurate indicators of former sea levels. *Nature* **272**, 528–531.

Scourse, J.D., Wanamaker Jr., A.D., Weidman, C., Heinemeier, J., Reimer, P.J., Butler, P.G., Witbaard, R., Richardson, C.A., 2012. The marine radiocarbon bomb pulse across the temperate North Atlantic: a compilation of $\Delta^{14}C$ time histories from *Arctica islandica* growth increments. *Radiocarbon* **54**, 165–186.

SfEP, Science for Environment Policy, 2017. Tackling mercury pollution in the EU and worldwide. In-depth Report 15, European Commission, DG Environment by the Science Communication Unit, UWE, Bristol, 72 p.

Silvestri, S., Defina, A., Marani, M., 2005. Tidal regime, salinity and salt marsh plant zonation. *Estuarine, Coastal and Shelf Science* **62**, 119–130.

Simon, S.L., Bouville, A., Land, C.E., 2006. Fallout from nuclear weapons tests and cancer risks: exposures 50 years ago still have health implications today that will continue into the future. *American Scientist* **94**, 48–57.

Skogen, M.D., Svendsen, E., Berntsen, J., Aksnes, D., Ulvestad, K.B., 1995. Modelling the primary production in the North Sea using a coupled three-dimensional physical-chemical-biological ocean Model. *Estuarine, Coastal and Shelf Science* **41**, 545–565.

Small, C., Nicholls, R.J., 2003. A global analysis of human settlement in coastal zones. *Journal of Coastal Research* **19**, 584–599.

Stevenson, J.C., Kearney, M.S., 2009. Impacts of global climate change and sea-level rise on tidal wetlands. In: Silliman, B.R., Grosholz, E.D., Bertness, M.D. (Eds.), Human impacts on salt marshes _ A global perspective. University of California Press, Berkeley, Los Angeles, London, 171–206.

Stock, M., 2003. Salzwiesenschutz im schleswig-holsteinischen Wattenmeer. *Vogelkundliche Berichte aus Niedersachsen* **35**, 115–124.

Stock, M., Gettner, S., Hagge, M., Heinzel, K., Kohlus, J., Stumpe, H., 2005. Salzwiesen an der Westküste von Schleswig-Holstein 1988–2001. Schriftenreihe des Nationalparks Schleswig-Holsteinisches Wattenmeer, Heft 15, 239 p.

Stock, M., Maier, M., 2016. Salzwiesenschutz im Nationalpark Wattenmeer – ein Überblick. *Vogelkundliche Berichte aus Niedersachsen* **44**, 131–156.

Stouff, V., Geslin, E., Debenay, J.-P., Lesourd, M., 1999. Origin of morphological abnormalities in *Ammonia* (foraminifera): studies in laboratory and natural environments. *Journal of Foraminiferal Research* **29**, 152–170.

Streif, H., 1978. Zur Geologie der deutschen Nordseeküste. *Die Küste* **32**, 30–49.

Streif, H., 1989. Barrier islands, tidal flats, and coastal marshes resulting from a relative rise of sea level in East Frisia on the German North Sea coast. In: van der Linden, W.J.M., Cloetingh, S.A.P.L., Kaasschieter, J.P.K., van de Graaff, W.J.E., Vandenberghe, J., van der Gun, J.A.M. (Eds.), Coastal lowlands, geology and geotechnology – proceedings of the symposium on coastal lowlands organized by the Royal Geological and Mining Society of the Netherlands (KNGMG), Kluwer Academic Publishers, Dordrecht, 213–223.

Streif, H., 2004. Sedimentary record of Pleistocene and Holocene marine inundations along the North Sea coast of Lower Saxony, Germany. *Quaternary International* **112**, 3–28.

Stuiver, M., Polach, H.A., 1977. Discussion reporting of ^{14}C data. *Radiocarbon* **19**, 355–363.

Stuiver, M., Reimer, P.J., 1993. Extended ^{14}C database and revised CALIB 3.0 ^{14}C age calibration program. *Radiocarbon* **35**, 215–230.

Stumpf, R.P., 1983. The process of sedimentation on the surface of a salt marsh. *Estuarine, Coastal and Shelf Science* **17**, 495–508.

Suchrow, S., Pohlmann, N., Stock, M., Jensen, K., 2012. Long-term surface elevation changes in German North Sea salt marshes. *Estuarine, Coastal and Shelf Science* **98**, 71–83.

Sutton, R.T., Hodson, D.L.R., 2005. Atlantic Ocean forcing of North American and European summer climate. *Science* **309**, 115–118.

Sutton, R.T., Dong, B., 2012. Atlantic Ocean influence on a shift in European climate in the 1990s. *Nature Geoscience* **5**, 788–792.

Svensson, C., Jones, D.A., 2002. Dependence between extreme sea surge, river flow and precipitation in eastern Britain. *International Journal of Climatology* **22**, 1149–1168.

Swindles, G.T., Galloway, J.M., Macumber, A.L., Croudace, I.W., Emery, A.R., Woulds, C., Bateman, M.D., Parry, L., Jones, J.M., Selby, K., Rushby, G.T., Baird, A.J., Woodroffe, S.A., Barlow, N.L.M., 2018. Sedimentary records of coastal storm surges: evidence of the 1953 North Sea event. *Marine Geology* **403**, 262–270.

Temmerman, S., Govers, G., Meire, P., Wartel, S., 2003. Modelling long-term tidal marsh growth under changing tidal conditions and suspended sediment concentrations, Scheldt estuary, Belgium. *Marine Geology* **193**, 151–169.

Thomson, J., Croudace, I.W., Rothwell, R.G., 2006. A geochemical application of the ITRAX scanner to a sediment core containing eastern Mediterranean sapropel units. In: Rothwell, R.G. (Ed.), New Techniques in Sediment Core Analysis. Geological Society, London, *Special Publications* **267**, 65–77.

Travis, C.C., Hester, S.T., 1991. Global chemical pollution. *Environmental Science and Technology* **25**, 814–819.

Turner, R.K., Subak, S., Adger, W.N., 1996. Pressures, trends, and impacts in coastal interactions between socioeconomic and natural systems. *Environmental Management* **20**, 159–173.

Turner, R.E., Baustian, J.J., Swenson, E.M., Spicer, J.S., 2006. Wetland sedimentation from hurricanes Katrina and Rita. *Science* **314**, 449–452.

UNEP, United Nations Environment Programme, 2006. Marine and coastal ecosystems and human wellbeing: a synthesis report based on the findings of the Millennium Ecosystem Assessment. UNEP, 76 p.

van der Molen, J., 2002. The influence of tides, wind and waves on the net sand transport in the North Sea. *Continental Shelf Research* **22**, 2739–2762.

Van Weering, T.C.E., Berger, G.W., Kalf, J., 1987. Recent sediment accumulation in the Skagerrak, northeastern North Sea. *Netherlands Journal of Sea Research* **21**, 177–189.

Vink, A., Steffen, H., Reinhardt, L., Kaufmann, G., 2007. Holocene relative sea-level change, isostatic subsidence and the radial viscosity structure of the mantle of northwest Europe (Belgium, the Netherlands, Germany, southern North Sea). *Quaternary Science Reviews* **26**, 3249–3275.

von Lieberman, N., Matheja, A., Schwarze, H., Zimmermann, C., 1997. Schlußbericht zum Forschungsvorhaben MTK 0564, Optimierung von Küstensicherungsarbeiten im Küstenvorfeld der Nordseeküste, Teil 3: Wellenuntersuchungen in Modell-Lahnungen. Franziskus-Institut für Wasserbau und Küsteningenieurwesen, Universität Hannover, 335 p.

von Storch, H., Woth, K., 2008. Storm surges: perspectives and options. *Sustainability Science* **3**, 33–43.

von Storch, H., Gönnert, G., Meine, M., 2008. Storm surges – an option for Hamburg, Germany, to mitigate expected future aggravation of risk. *Environmental Science and Policy* **11**, 735–742.

Wahl, T., Jensen, J., Frank, T., Haigh, I.D., 2011. Improved estimates of mean sea level changes in the German Bight over the last 166 years. *Ocean Dynamics* **61**, 701–715.

Wakelin, S.L., Woodworth, P.L., Flather, R.A., Williams, J.A., 2003. Sea-level dependence on the NAO over the NW European continental shelf. *Geophysical Research Letters* **30**, 1403.

Wang, J., Baskaran, M., Niedermiller, J., 2017. Mobility of ^{137}Cs in freshwater lakes: a mass balance and diffusion study of Lake St. Clair, Southeast Michigan, USA. *Geochimica et Cosmochimica Acta* **218**, 323–342.

Weidman, C.R., 1995. Development and application of the mollusc *Arctica islandica* as a paleoceanographic tool for the North Atlantic Ocean. Doctoral dissertation, Massachusetts Institute of Technology, Woods Hole Oceanographic Institution, 207 p.

Weisse, R., von Storch, H., 2010. Marine climate and climate change – storms, wind waves and storm surges. Springer-Verlag, Berlin, Heidelberg, New York, 219 p.

Weisse, R., von Storch, H., Niemeyer, H.D., Knaack, H., 2012. Changing North Sea storm surge climate: an increasing hazard? *Ocean and Coastal Management* **68**, 58–68.

Weltje, G.J., Tjallingii, R., 2008. Calibration of XRF core scanners for quantitative geochemical logging of sediment cores: theory and application. *Earth and Planetary Science Letters* **274**, 423–438.

Wigeland, R.A., Bauer, T.H., Hill, R.N., Stillman, J.A., 2012. Impact on geologic repository usage from limited actinide recycle in pressurized light water reactors. *Journal of Nuclear Science and Technology* **44**, 415–422.

Wilken, R.-D., Hintelmann, H., 1991. Mercury and methylmercury in sediments and suspended particles from the river Elbe, North Germany. *Water, Air, and Soil Pollution* **56**, 427–437.

Winther, N.G., Johannessen, J.A., 2006. North Sea circulation: Atlantic inflow and its destination. *Journal of Geophysical Research* **111**, C12018.

Wolff, W.J., 2013. Ecology of the Wadden Sea: research in the past and challenges for the future. *Journal of Sea Research* **82**, 3–9.

Wolff W.J., Dankers N., Dijkema K.S., Reijnders P.J.H., Smit C.J., 1994. Biodiversity of the Wadden Sea (Denmark, Germany, the Netherlands): recent changes and future projections. In: Boyle T.J.B., Boyle C.E.B. (Eds.), Biodiversity, temperate ecosystems, and global change. NATO ASI series (series I: global environmental change), vol. 20., Springer, Berlin, Heidelberg, 337–355.

Wolff, W.J., Bakker, J.P., Laursen, K., Reise, K., 2010. The Wadden Sea quality status report – synthesis report 2010. Wadden Sea Ecosystem 29, Common Wadden Sea Secretariat, Wilhelmshaven, Germany, 25–74.

Wolfstein, K., Kies, L., 1999. Composition of suspended particulate matter in the Elbe estuary: implications for biological and transportation processes. *Deutsche Hydrographische Zeitschrift* **51**, 453–463.

Woolnough, S.J., Allen, J.R.L., Wood, W.L., 1995. An exploratory numerical model of sediment deposition over tidal salt marshes. *Estuarine, Coastal, and Shelf Science* **41**, 515–543.

Wright, A.J., Edwards, R.J., van de Plassche, O., 2011. Reassessing transfer-function performance in sea-level reconstruction based on benthic salt-marsh foraminifera from the Atlantic coast of NE North America. *Marine Micropaleontology* **81**, 43–62.

WSV, Federal Waterway and Shipping Administration, HPA, Hamburg Port Authority, 2011. Anpassung der Fahrrinne der Unter- und Außenelbe an die Containerschifffahrt, Bericht zur Beweissicherung 2000 bis 2010, Abschlussbericht 2011. Wasser- und Schifffahrtsamt Hamburg, 142 p.

Yanko, V., Ahmad, M., Kaminski, M., 1998. Morphological deformities of benthic foraminiferal tests in response to pollution by heavy metals: implications for pollution monitoring. *Journal of Foraminiferal Research* **28**, 177–200.

Zanchettin, D., Toniazzo, T., Taricco, C., Rubinetti, S., Rubino, A., Tartaglione, N., 2019. Atlantic origin of asynchronous European interdecadal hydroclimate variability. *Scientific Reports* **9**, 10998.

Ziegler, M., Jilbert, T., de Lang, G. J., Lourens, L.J., Reichart, G.-J., 2008. Bromine counts from XRF scanning as an estimate of the marine organic carbon content of sediment cores. *Geochemistry, Geophysics, Geosystems* **9**, Q05009.

Photo Credits

Front/back cover: B. Vennemann (upper photo), Pixabay.com (Creative Commons Zero, CC0; lower photo)
Page 17: B. Bunzel
Page 33: G. Schmiedl
Page 57: Pixabay.com (Creative Commons Zero, CC0)
Page 75: B. Vennemann
Page 89: C. Sievers
Page 105: C. Sievers
Page 109: D. Bunzel

Type set

The sans serif font used in parts of this doctoral thesis is: "TheSans UHH" / LucasFonts.

Web Sources

http://calib.org (accessed 29 October 2018)
https://oceanservice.noaa.gov/facts/stormsurge-stormtide.html (accessed 26 January 2021)
https://pixabay.com (accessed 3 February 2021)
https://www.marinespecies.org/index.php (accessed 19 January 2021)

APPENDICES

The following pages contain the compilation of all supplementary materials derived from the previously presented articles as well as the provision of additional information.

Appendix A

To: CHAPTER ONE | Unifying essay

The following supplementary material is intended to provide additional information to Chapter 1, and has not yet been published elswhere in this form.

A. In a nutshell: water-level components

Generally, the **mean sea level** (MSL) is defined as the average long-term state of the sea-surface height, which may vary by region, and does not consider short-term variations such as tides, storm surges, or waves (e.g., Wahl et al., 2011; Gregory et al., 2019). Local changes of the MSL rates that refer to a given local benchmark (e.g., the sea floor or land surface) are then defined as relative sea-level changes or relative mean sea level (RMSL), thus, the GMSL represents the global mean of the RMSL (Gregory et al., 2019). In principle, the GMSL is mainly controlled by slowly acting geophysical (e.g., land movements) and oceanographic (e.g., thermal expansion or melting of glaciers and ice-sheets) processes that affects the geomorphology of the ocean basins as well as the water volume on relatively long time scales (Weisse and von Storch, 2010; Weisse et al., 2012). On shorter time scales, however, the relative height of the sea surface at a given time and place is further driven by astronomical (tides) and meteorological (storm surges) forces (Pugh, 1987; Haigh et al., 2010; Weisse and von Storch, 2010).

Tidal oscillations arise because of dynamical changes in the earth's and moon's orbit around the sun, and the induced gravitational attractions between the earth and the moon that change periodically in relation to their relative position (MacDonald, 1964; Pugh, 1987). In large continental shelf seas, such as the North Sea, the semidiurnal propagating tidal currents (i.e., barotropic Kelvin waves) account for a regular sediment re-suspension and redistribution, specifically at the shallow near-shore areas (van der Molen, 2002; Reynaud and Dalrymple, 2012). There, the tidal amplitude can even equal the same order of magnitude as the local water depth, which is then referred to as *shallow-water tide* (Müller-Navarra and Giese, 1999). Within the North Sea, the characteristic anti-clockwise rotation of the surface waters is evoked by the amphidromic systems that are located around the British Isles, in the central part of the North Sea, and at the south Norwegian coast (Pugh, 1987; Reynaud and Dalrymple, 2012). These amphidromic systems act as nodes for the propagating tidal waves in a rotating reference system (Coughlan and Stips, 2015). Resulting tidal ranges owed by the amphidromic cell in the central part of the North Sea vary nowadays between 1 and 3 m according to the location, meaning that the tide amplitudes increase with increasing distance to the amphidromic cell (Coughlan and Stips, 2015; Nieuwhof and Vos, 2018). Accordingly, the position of an amphidromic cell and related tidal amplitudes strongly depend on bottom-friction forces, water depths and bathymetry (Davies and Jones, 1995; Fickert and Strotmann, 2007; Reynaud and Dalrymple, 2012; Coughlan and Stips, 2015). On this basis, if the water depth changes due to the current rise in sea level, the tidal range is also affected. This means, by implication, that natural climate variability and/or human influences can likewise exert on changes in the tidal range (Hollebrandse, 2005). In fact, Jensen and Mudersbach (2007) documented a pronounced increase in the mean tidal range along the North Sea coastline from the 1960s onwards. This finding is in line with the reconstructed GMSL that showed an acceleration in SLR since the 1960s (Dangendorf et al., 2019), suggesting impacts by global warming (Jensen and Mudersbach, 2007).

Interestingly, a similar trend also occurred for the meteorologically forced changes in sea level, showing a strengthening and enhanced frequency of **storm surges** in the North Sea from 1960 until 1990 CE (Matulla et al., 2008; Weisse et al., 2012). Basically, the North Sea coastline is exposed to annual storm surges (e.g., Gerber et al., 2016), while the flood risk itself further depends on the prevailing wind direction and strength during a storm surge. The so-called *storm surges* (also referred to it as *storm flood*, *storm tide*, *surge residual*, *non-tidal component*, *non-tidal residual* or *meteorological residual*) are defined as the temporal and spatial offshore elevation (or depression) of the sea surface initiated by storms (e.g., Pugh, 1987; Weisse et al., 2012; Gregory et al., 2019). This mainly involves three different meteorological processes, namely: (i) the *inverse barometric effect*, (ii) *wind stress*, and (iii) *external surges* (e.g., Schmitz, 1965; Müller-Navarra et al., 2003; von Storch and Woth, 2008). In case of a decline within the centre of an atmospheric low-pressure system (such as an extratropical cyclone), the vertical force that acts on the water column below the sea surface then likewise decreases, which in turn leads to a rise in sea level (and vice versa), referred to it as

the *inverse barometric effect* (Schmitz, 1965; Weisse et al., 2012). These strong atmospheric low-pressure centres are generally formed over the North Atlantic and then move as north-west storm tracks across the North Sea (Müller-Navarra and Giese, 1999; Gerber et al., 2016). In contrast, the direct *wind stress* is subject of the local wind strength and direction, which means that under these conditions the water is pushed towards the coast by westerly winds (Gornitz, 2005). *External surges* are provoked by pressure gradients of passing cyclones over the North-East Atlantic, that propagate as long-waves over the shelf edge into the shallow North Sea, thereby resembling common tidal waves (Schmitz, 1965; Gönnert and Sossidi, 2011; Ganske et al., 2018).

However, whether or not a storm surge finally occurs during severe wind conditions (storms) usually depends on additional factors, such as the tidal phase (von Storch and Woth, 2008). In fact, storm surges are preferably generated with rising tides (Horsburgh and Wilson, 2007), finally exceeding the mean high water (MHW) by ≥ 1.5 m (Müller-Navarra et al., 2003; Gerber et al., 2016). The wind fields that are required to generate sufficient storms must have wind forces of at least 7 Beaufort (Bft, which equals ≥ 50 km h^{-1}), with wind directions facing towards the coast (or away) to push the water onshore (or offshore) (Weisse and von Storch, 2010; Weisse et al., 2012; Gerber et al., 2016). If a storm is directly facing the coastline, pushing the water masses towards the coast and the local sea-surface height temporarily increases (Fig. A1), this is referred to as *positive surge*, while the opposite case is called a *negative surge* (Weisse and von Storch, 2010). Positive storm surges in particular pose a flood risk to the adjacent salt marshes, especially when they coincide with substantial high tides, such as high-water springs (Ehlers et al., 1993; Weisse and von Storch, 2010). The consequences can then be, as already described in Chapter 1.1, vertical marsh erosion and/or the introduction and deposition of allochthonous sediments on top of the marsh surfaces (Allen, 2000, and references therein).

When evaluating impacts by storm surges, the strong wind conditions should last for at least 6 hours, which is the average time duration between MHW (or high tide) and mean low water (MLW; or low tide), in order to take the different timing of MHW along the North Sea coast into account (Gerber et al., 2016). At the North Sea region, strongest wind fields tend to appear during wintertime (November to February), in which the initiated disturbances have greatest impacts on the shallow shelf areas, provoking specifically severe storm surges (Fig. 3; Pugh, 1987; Weisse and von Storch, 2010). On this basis, meteorologically forced changes in sea level are inversely related to the water depth, which means that storm surges are strongest when the meteorological processes involved acts on shallow water depths, such as found in the North Sea (Gornitz, 2005).

Appendix B

To: CHAPTER TWO | Integrated stratigraphy

The following supplementary material has been published in:

Bunzel, D., Milker, Y., Müller-Navarra, K., Arz, H.W., Friedrich, J., Lahajnar, N., Schmiedl, G., 2020. Integrated stratigraphy of foreland salt-marsh sediments of the south-eastern North Sea region. *Newsletters on Stratigraphy* **53**, 415–442, DOI: 10.1127/nos/2020/0540.

Raw data can be found at: https://doi.pangaea.de/10.1594/PANGAEA.905240.

B. Preliminary results

The following Figures of Appendix B provide an overview about the first sedimentological and geochemical results obtained from the four salt-marsh sequences studied (Fig. B1). Since the measured ^{210}Pb activities turned out to be rather problematic, as a clear down-core decrease was missing specifically with regard to the unsupported ^{210}Pb signal (Figs. B3, B4), ^{210}Pb-based age models (CRS, CIC) were generated only for sites TB13-1 and GeoHH-GIE (Fig. B5). Mean grain size and radionuclide data from TB13-1 were provided by Müller-Navarra et al. (2019).

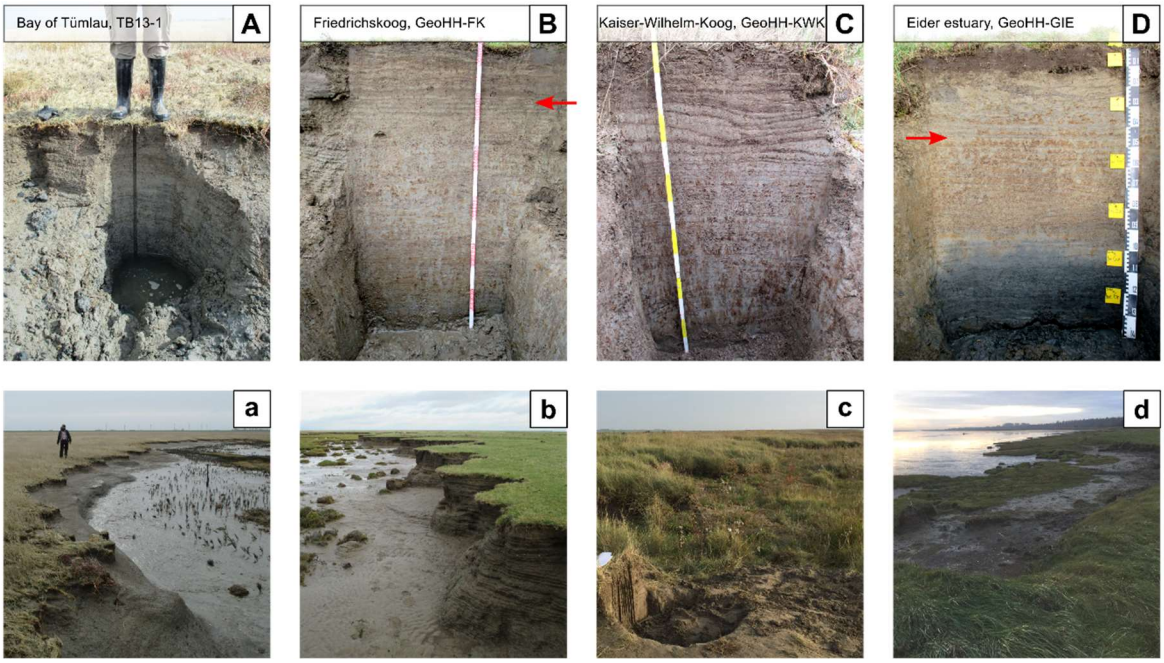

Fig. B1 | Overview of the salt-marsh sediment sequences at the erosional cliffs in the Bay of Tümlau (**a**), Friedrichskoog (**b**), Kaiser-Wilhelm-Koog (**c**), and Eider estuary (**d**) during low tide. Red arrows indicate distinct shell layers at around 24 cm depth at site GeoHH-FK (Friedrichskoog), and at 46 cm depth at site GeoHH-GIE (Eider estuary).

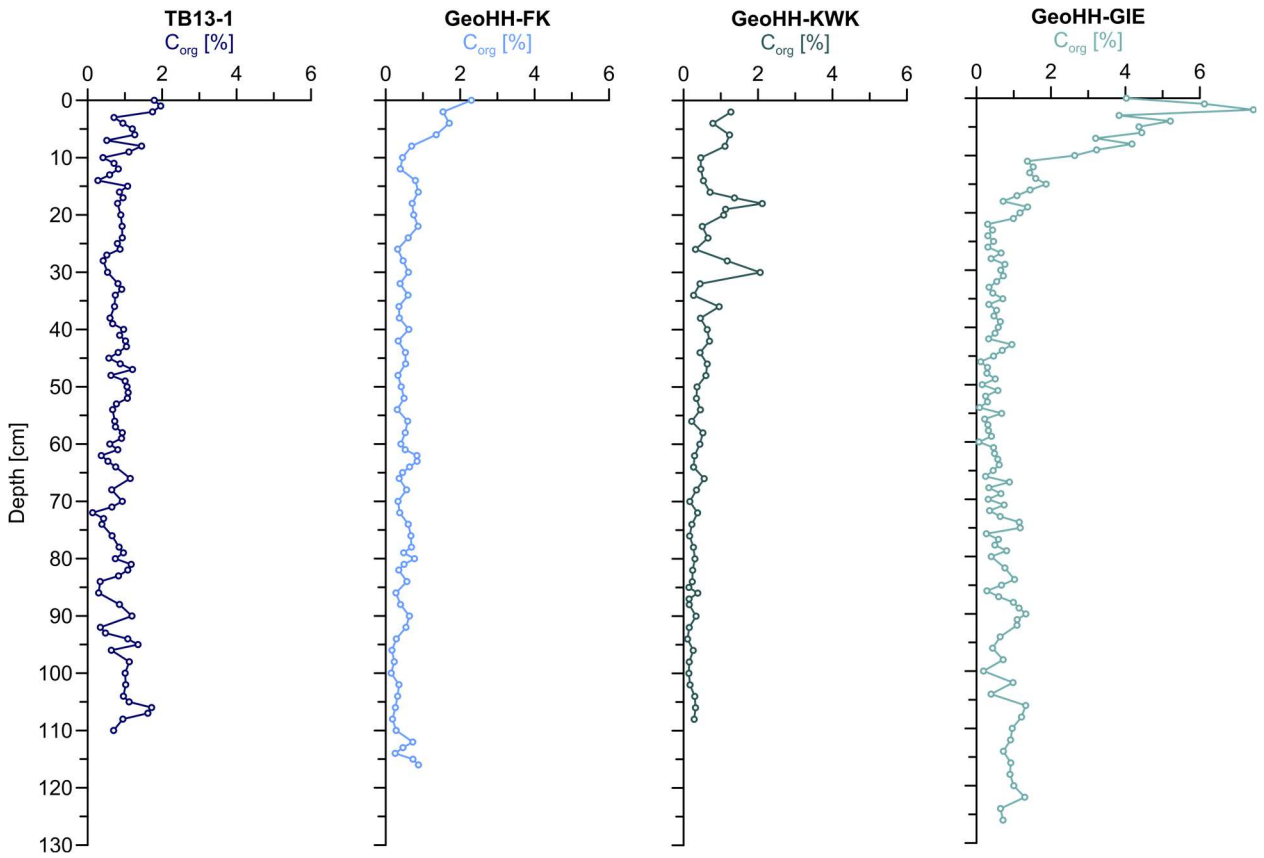

Fig. B2 | Down-core distribution of the organic carbon (C_{org}) content at the Bay of Tümlau (TB13-1, dark blue), Friedrichskoog (GeoHH-FK, light blue), Kaiser-Wilhelm-Koog (GeoHH-KWK, dark green), and Eider estuary (GeoHH-GIE, light green). High C_{org} levels around 18 cm and 30 cm depth at site GeoHH-KWK probably reflect its proximity to the Elbe estuary, since sediments within the Elbe estuary reveal highest C_{org} contents in comparison to open marine sediments in the German Bight (Deek 2011).

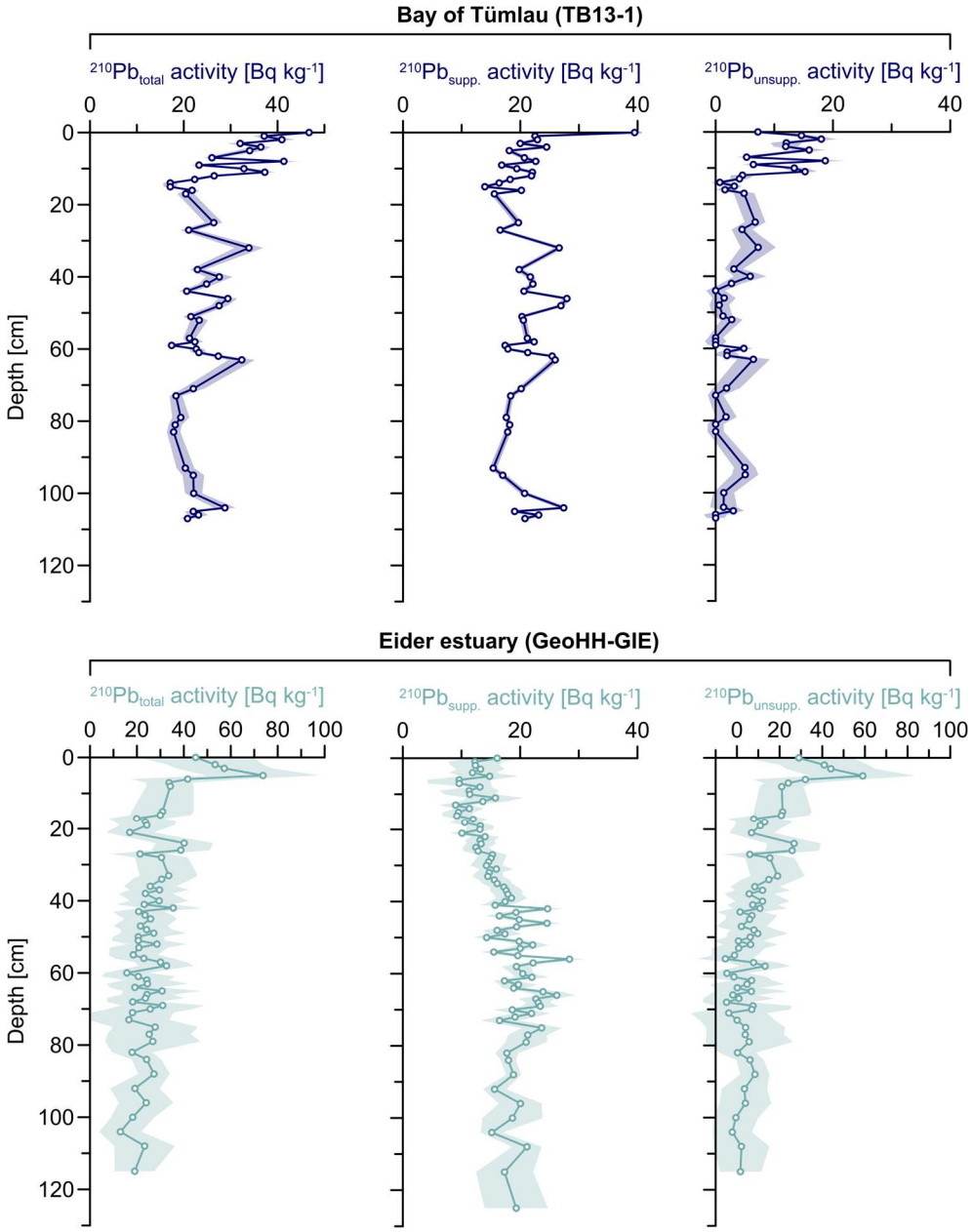

Fig. B3 | Decay-corrected activities (initial raw data) of the total ^{210}Pb, supported ^{210}Pb, and unsupported ^{210}Pb of sediment sequences TB13-1 (Bay of Tümlau, dark blue; Müller-Navarra et al. 2019) and GeoHH-GIE (Eider estuary, light green). Gaussian error-propagation estimates are expressed as shaded areas.

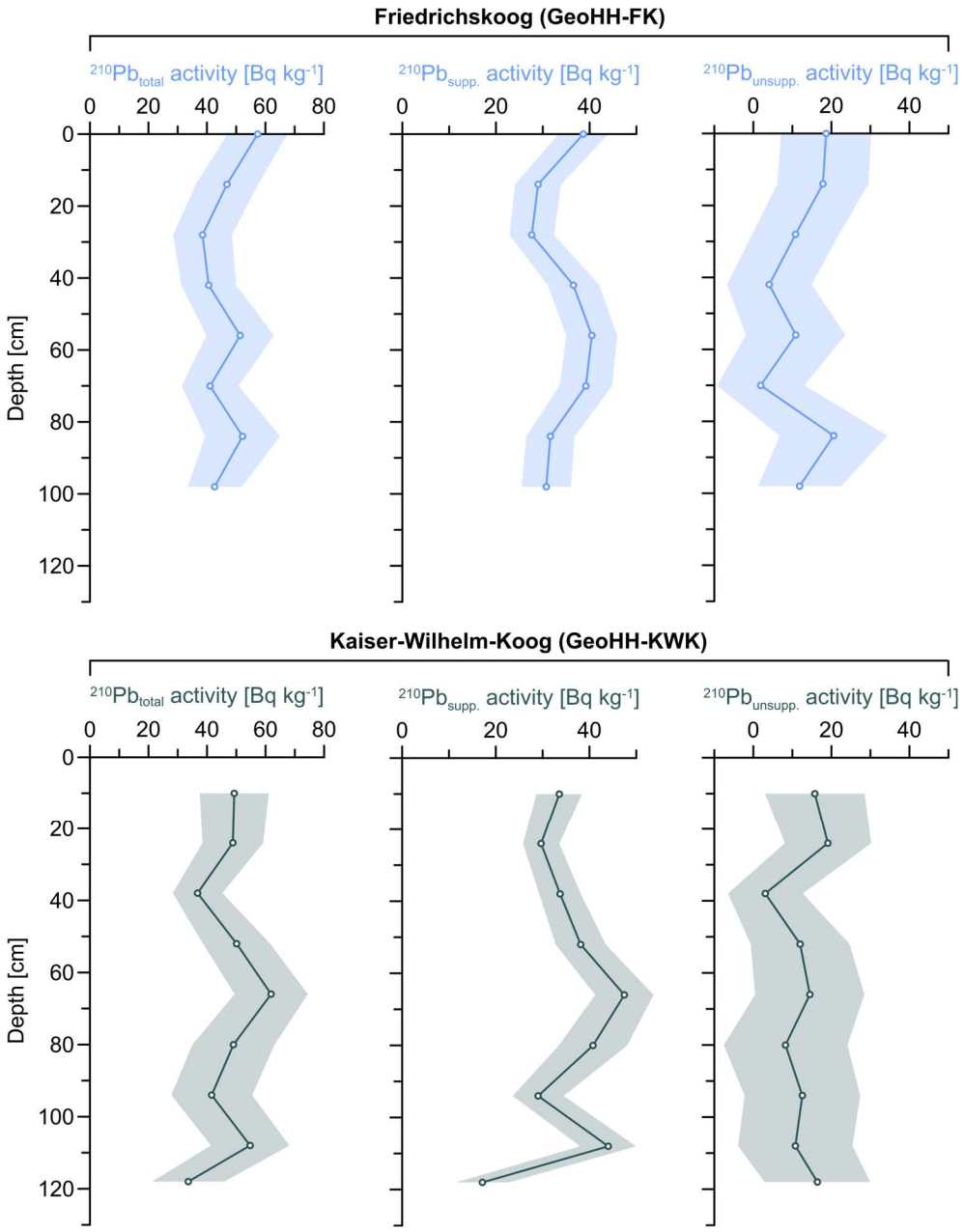

Fig. B4 | Decay-corrected activities (initial raw data) of the total ^{210}Pb, supported ^{210}Pb, and unsupported ^{210}Pb of sediment sequences GeoHH-FK (Friedrichskoog, light blue) and GeoHH-KWK (Kaiser-Wilhelm-Koog, dark green). Gaussian error-propagation estimates are expressed as shaded areas.

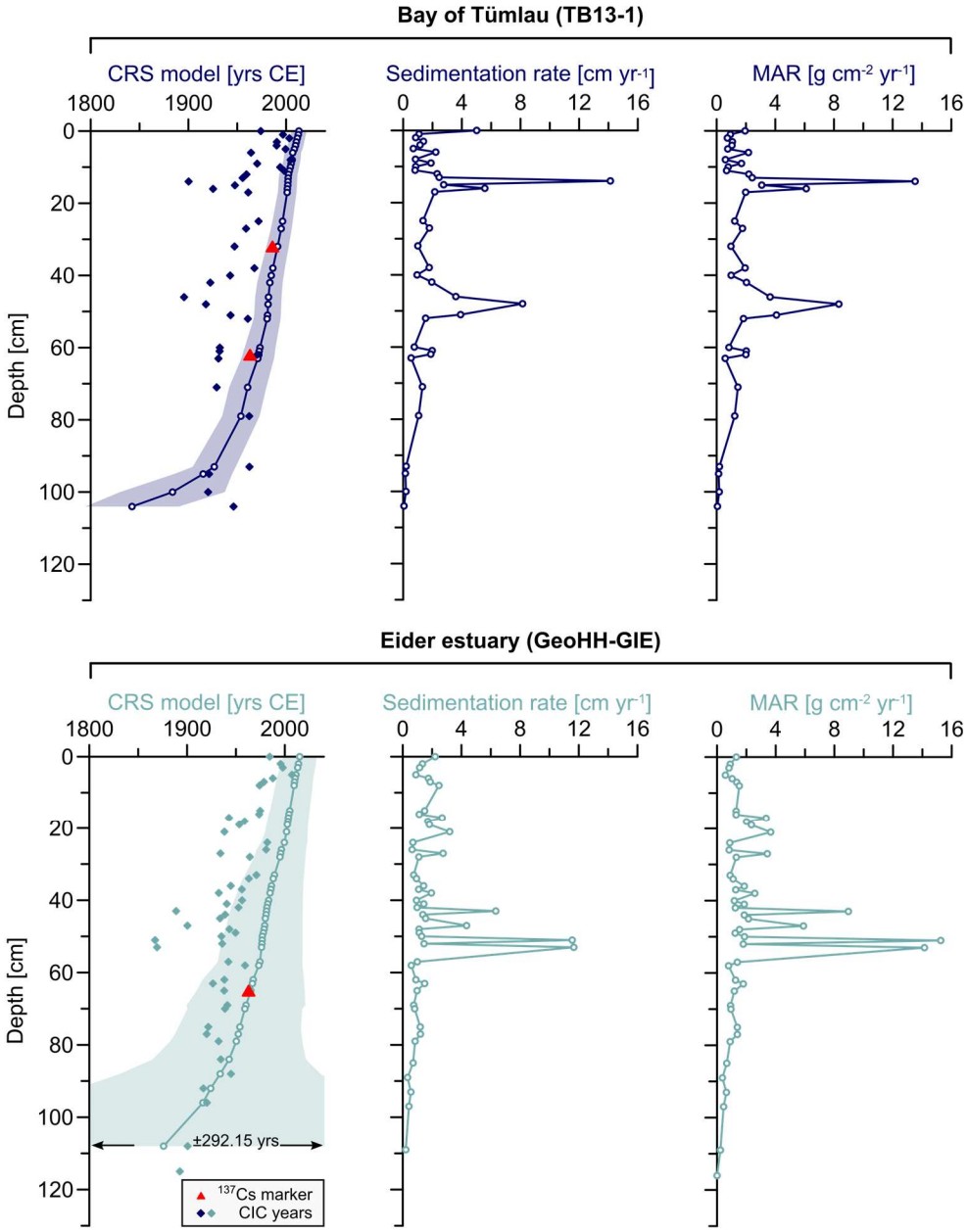

Fig. B5 | Constant rates of unsupported ^{210}Pb supplies (CRS), obtained sedimentation and mass accumulation rates (MAR), and constant initial ^{210}Pb concentration (CIC) in the Bay of Tümlau (TB13-1, dark blue, Müller-Navarra et al. 2019) and the Eider estuary (GeoHH-GIE, light green). Corresponding Gaussian error-propagation estimates are shown as shaded areas for the CRS models, highest uncertainties of ±292.15 yrs in 108 cm depth at site GeoHH-GIE are only indicated by arrows and not completely shown in here. Red symbols denote maximum concentrations in the ^{137}Cs activity at both sites. For the determination of sediment ages in the sediment sequence GeoHH-GIE, the CRS model was tested based on the assumption of different sediment supply. The ^{137}Cs peak at 65 cm depth marks the end of the nuclear bomb testing in 1963 CE, respectively, and was used for validating the ^{210}Pb age model. The CRS model reproduces the age of maximum bomb fallout signal in the mid-1960s.

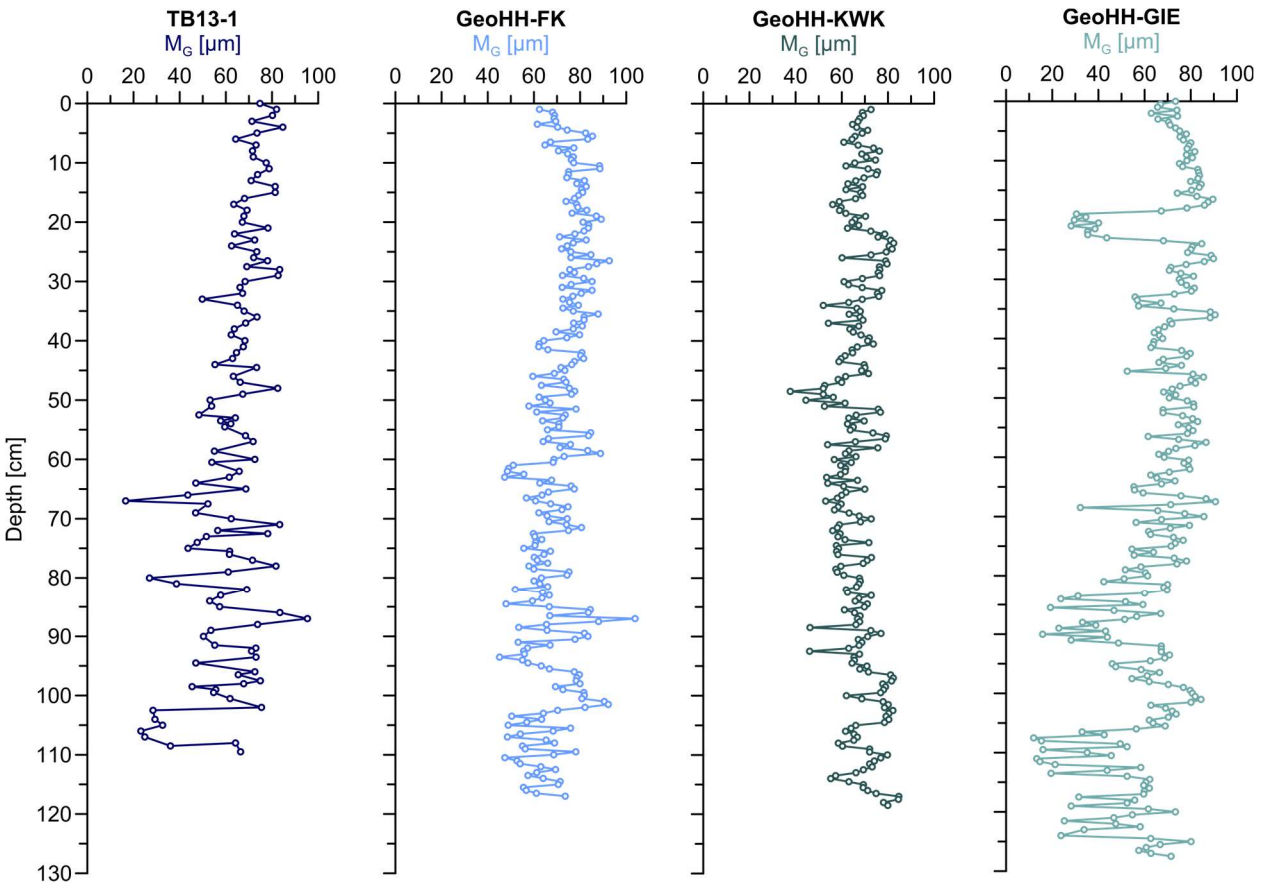

Fig. B6 | Mean grain-size (M_G) spectra of salt-marsh sediments in the Bay of Tümlau (TB13-1, dark blue, data were taken from Müller-Navarra et al. 2019), Friedrichskoog (GeoHH-FK, light blue), Kaiser-Wilhelm-Koog (GeoHH-KWK, dark green), and Eider estuary (GeoHH-GIE, light green).

Appendix C

To: CHAPTER THREE | Salt-marsh archives

The following supplementary material has been published in:

Bunzel, D., Milker, Y., Müller-Navarra, K., Arz, H.W., Schmiedl, G., 2021. North Sea salt-marsh archives trace past storminess and climate variability. *Global and Planetary Change* **198**, 103403, DOI: 10.1016/j.gloplacha.2020.103403.

Raw data can be found at: https://doi.pangaea.de/10.1594/PANGAEA.927307.

C. Stratigraphic framework

Salt-marsh accretion rates were reconstructed based on the establishment of an integrated stratigraphic framework for active foreland salt marshes along the south-eastern North Sea coast, which combines absolute and relative dating techniques commonly used for dating of modern sediments. This integrated approach allowed to obtain additional stratigraphic information, which proves particularly useful for dating salt-marsh sediment sequences usually containing a significant proportion of reworked material. Originally, required measurements were carried out on four different salt-marsh sediment sequences in total (see Chapter 2). For each of the four sediment sequence, mercury (Hg), ^{210}lead (^{210}Pb), and ^{137}caesium (^{137}Cs) have been measured. In addition, ^{241}americium (^{241}Am) was detected at the Bay of Tümlau. At this site, Müller-Navarra et al. (2019) carried out the ^{210}Pb, ^{137}Cs, and ^{241}Am analyses and provided the required radionuclide data for this study. As Chapter 3 only addresses the results of TB13-1 (Bay of Tümlau) and GeoHH-FK (Friedrichskoog), Figures C1 and C2 once again provide an overview of the corresponding local stratigraphy.

The commonly applied ^{210}Pb-based age models (constant initial ^{210}Pb concentration, CIC; constant rate of unsupported ^{210}Pb supply, CRS) appeared to be rather problematic at highly dynamical coastal systems such as the south-eastern North Sea. Due to strong fluctuations, the unsupported ^{210}Pb activity lacks a clear down-core decrease within the sediment sequence at Friedrichskoog, which would be required for reliable ^{210}Pb-based age-model calculations, and hence, the CIC and CRS models failed to provide plausible ages for this site (Fig. C1). Although not perfectly exponential, the expected unsupported ^{210}Pb decrease with increasing depth was moderately distinct at the Bay of Tümlau, and ^{210}Pb-based age models (CIC, CRS) were calculated in accordance. For this site, both CIC and CRS calculations were conducted and provided by Müller-Navarra et al. (2020). At highly dynamic coastal depositional settings, however, the ^{210}Pb-based models should be considered with caution, even though the CRS model approximately matches the ^{137}Cs-derived ages of 1963 CE and 1986 CE at the Bay of Tümlau. The observed down-core fluctuations within both unsupported ^{210}Pb records are likely owed by a frequent sediment reworking initiated by storm surges. Therefore, related age estimates for the CRS models are associated with high Gaussian error-propagation estimates (purple shaded area in Fig. C1). Consequently, the unsupported ^{210}Pb data (and related CIC or CRS model calculations) should be rather used as general stratigraphic orientation. In contrast, this study builds on the more accurate age information provided by distinct ^{137}Cs peaks owed by the onset and maximum of atmospheric fallout of nuclear weapon tests around 1954 and 1963 CE, and the Chernobyl nuclear power plant accident in 1986 CE. Additional stratigraphic information was extracted by high mercury (Hg) concentrations in the salt-marsh sediments, which can be linked to the World War II aftermaths (around 1945 CE), and the European industrial pollution maximum (between 1960 and 1970 CE). After foundation of the Wadden Sea National Park, the evolution of a high salt-marsh vegetation in the Bay of Tümlau is accompanied by the occurrence of the foraminiferal high-marsh marker species *Balticammina pseudomacrescens* since around 2001 CE (Stock et al., 2005; Müller-Navarra et al., 2019). Supplementary inter-correlation of the salt-marsh sequences were based on the ln(Zr/Rb) ratio at the Bay of Tümlau and Friedrichskoog, in which both records show similar appearing variability likely owed by comparable natural and human influences. To conclude, each site has its individual stratigraphy based on the integration of different age information (see also Fig. C2).

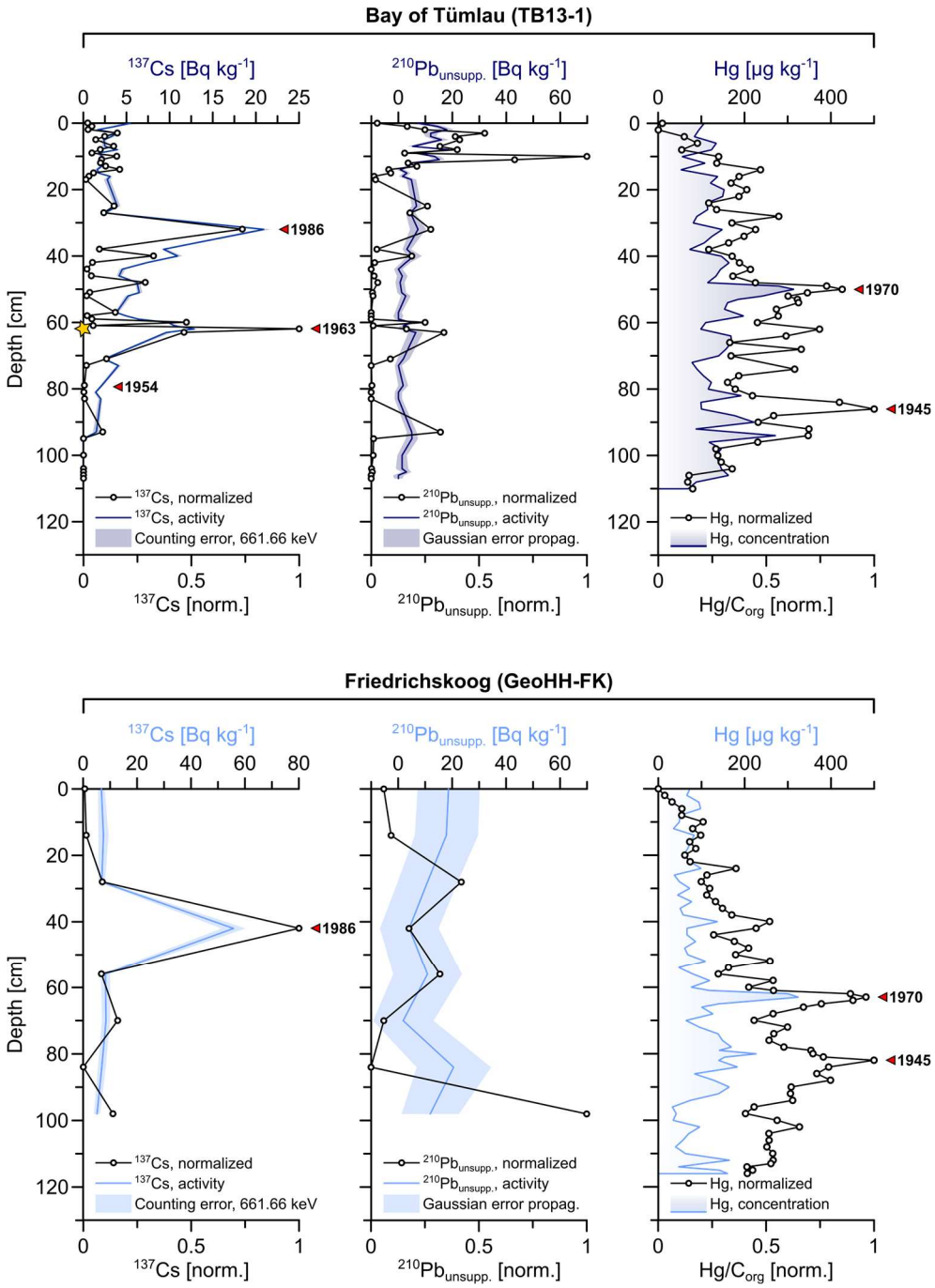

Fig. C1 | Natural and artificial down-core radionuclide (^{137}Cs, unsupported ^{210}Pb) activities, as well as mercury (Hg) concentrations of the evaluated sediment sequences at the Bay of Tümlau (TB13-1) and Friedrichskoog (GeoHH-FK). Areas shaded in blue denote the counting errors on energy line 661.66 keV (^{137}Cs activities), ranging between ±0.17 Bq kg^{-1} and ±0.99 Bq kg^{-1} at the Bay of Tümlau, and between ±1.15 Bq kg^{-1} and ±4.48 Bq kg^{-1} at Friedrichskoog. Uncertainties that were obtained from Gaussian error-propagation calculations (unsupported ^{210}Pb activities) range between ±1.26 Bq kg^{-1} and ±4.49 Bq kg^{-1} at the Bay of Tümlau, and between ±10.61 Bq kg^{-1} and ±13.77 Bq kg^{-1} at Friedrichskoog (also shaded in blue). Black lines describe the data normalized to the sum of organic carbon (C_{org}) and the < 20 µm sediment fraction, which applies to ^{137}Cs and the unsupported ^{210}Pb, while Hg has been corrected to the organic carbon content only. The yellow star symbol, which is in line with the maximum ^{137}Cs activity at the Bay of Tümlau denotes the exclusive ^{241}Am spike at this site. Age markers are given in years CE, representing the aftermaths of World War II (1945 CE), the onset of nuclear weapon tests (1954 CE), the maximum fallout from nuclear weapon testing (1963 CE), the industrial pollution maximum (1970 CE), and the nuclear power plant accident in Chernobyl (1986 CE). Data of the uncorrected ^{241}Am, ^{137}Cs, and unsupported ^{210}Pb activities were provided by Müller-Navarra et al. (2019), all further analyses were carried out by Bunzel et al. (2020).

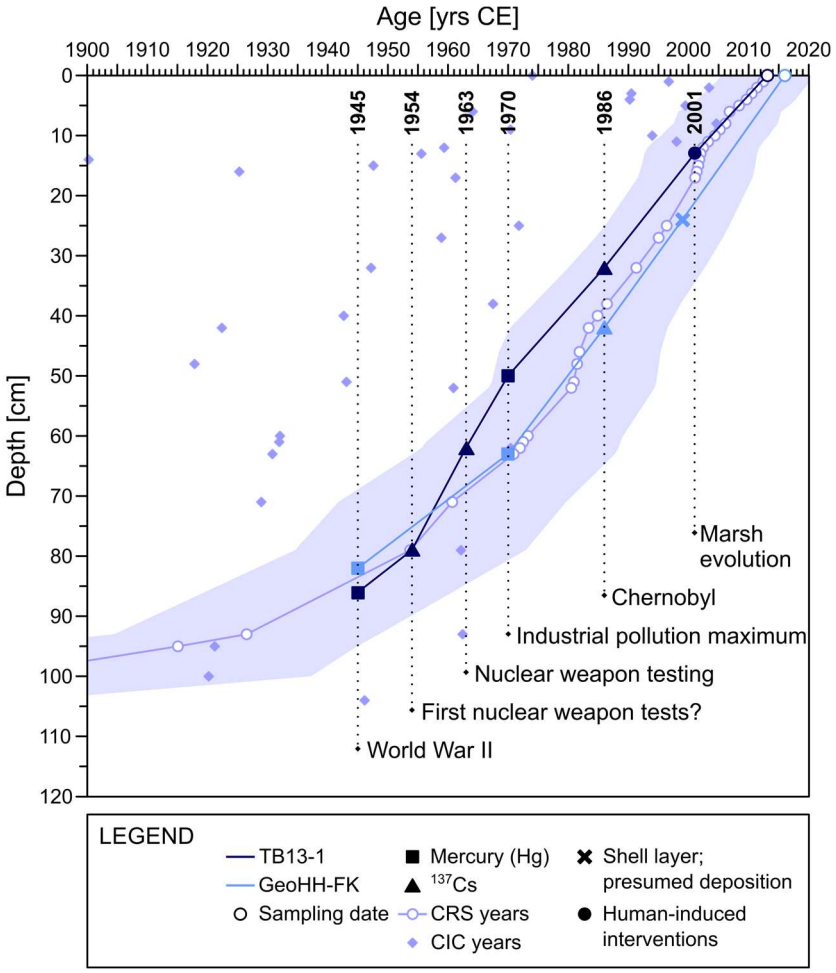

Fig. C2 | Age-depth models for sediment successions TB13-1 (Bay of Tümlau; dark blue) and GeoHH-FK (Friedrichskoog; light blue). At each site, the individual stratigraphy integrates various time markers, mainly based on the artificial radionuclide activity (^{137}Cs) and mercury (Hg) pollution history. The ^{210}Pb-based age-model calculations (CIC, CRS; purple) are only concerning site TB13-1 (data were taken from Müller-Navarra et al., 2019), and are rather used as orientation for the general stratigraphy and not for obtaining precise age values for the calculation of sedimentation rates. Shaded purple areas denote the Gaussian-error propagation estimates for the CRS model belonging to sediment sequence TB13-1.

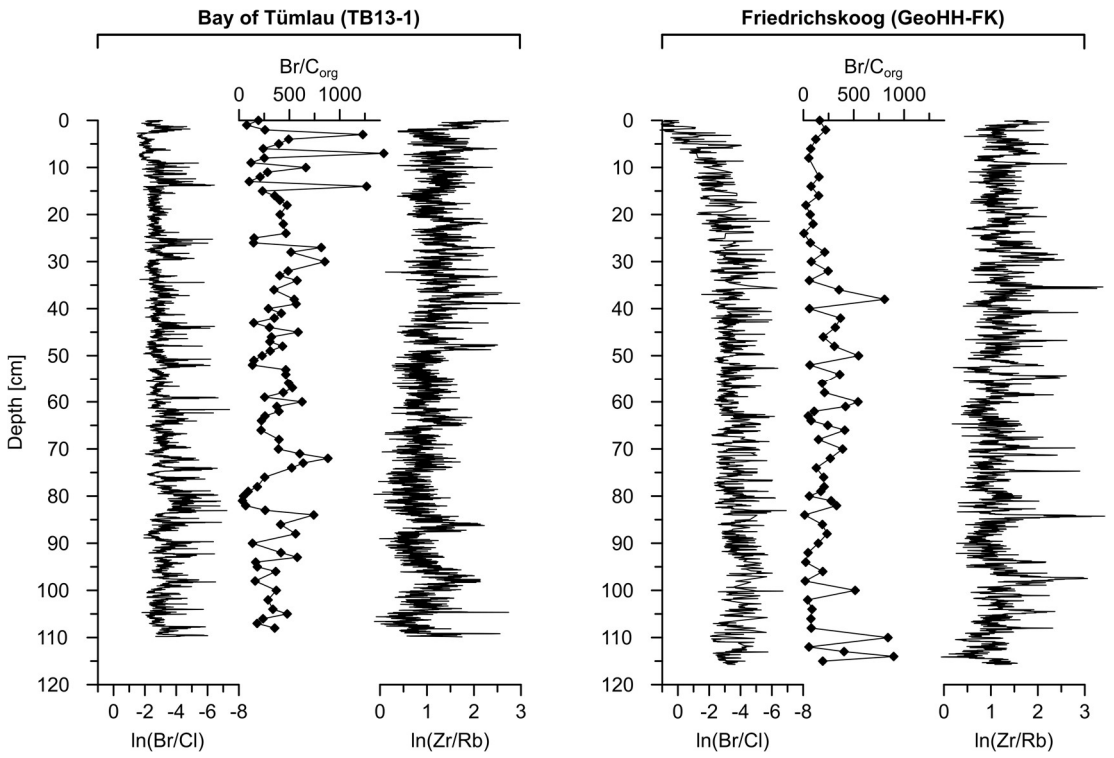

Fig. C3 | Down-core distribution of the ln(Br/Cl), ln(Zr/Rb), and Br/C_{org} ratios, each represented as full-resolution data at the Bay of Tümlau (TB13-1) and Friedrichskoog (GeoHH-FK).

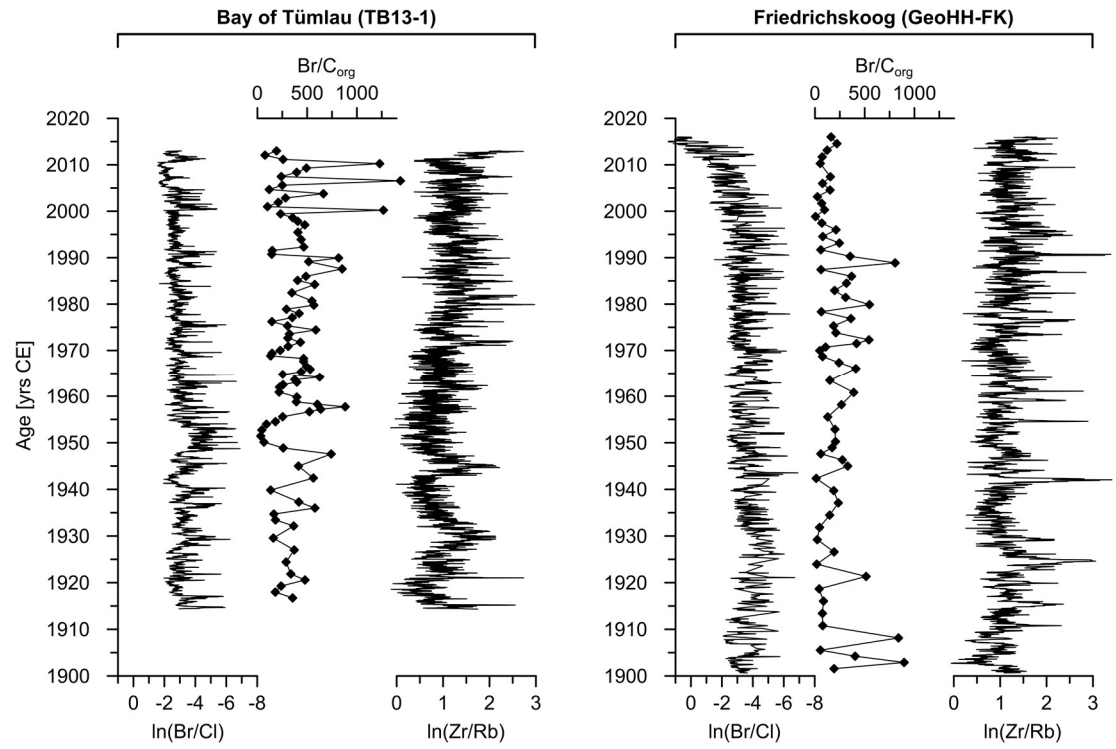

Fig. C4 | Overview of the variability of ratios ln(Br/Cl), ln(Zr/Rb), and Br/C_{org} at the Bay of Tümlau (TB13-1) and Friedrichskoog (GeoHH-FK) during the last century.

Appendix D

To: CHAPTER FOUR | Deformed marsh foraminifera

The following supplementary material is intended to provide additional information to Chapter 4, and has not yet been published nor submitted elswhere in this form.

Raw data of the foraminiferal census counts from Friedrichskoog (sediment sequence GeoHH-FK), which are discussed in Chapter 4 (Bunzel et al., 2020, under review), can be found at: https://doi.pangaea.de/10.1594/PANGAEA.927336.

D. Benthic foraminiferal taxonomy

In order to provide an overview of the benthic foraminifera investigated within sediment sequences from the south-eastern North Sea region, high-resolution images were generated showing most of the taxa mentioned in Chapter 4. The benthic foraminiferal genera and species were mainly classified following the descriptions given by Feyling-Hanssen (1972), Wright et al. (2011), Milker et al. (2015), Müller-Navarra et al. (2016), and Schönfeld (2018). The taxonomic correctness of the names was additionally verified using the World Register of Marine Species (WoRMS). The coloured images were created by using a Keyence VHX-6000 microscope and on samples originating from the Bay of Tümlau (TB13-1; Müller-Navarra et al., 2019), Friedrichskoog (GeoHH-FK), and the Eider estuary (GeoHH-GIE). Although Chapter 4 focused only on the salt marshes in the Bay of Tümlau and Friedrichskoog, a few samples and images from the Eider estuary were also included for Appendix D in order to provide as complete a taxonomic overview as possible in here.

Plate 1 represents an overview about selected calcareous benthic foraminiferal taxa that preferably inhabit the tidal flats to low marsh zones (e.g., Francescangeli et al., 2016, 2017; Müller-Navarra et al., 2016), and which were most often identified in the sediment samples examined. **Plate 2** provides a coverage for the most abundant agglutinated salt-marsh foraminifera found at the south-eastern North Sea coast, as well as few more rare species (such as *Miliammina petila*) and conspicuous irregularities in the test morphology of the locally dominant salt-marsh indicator species *Entzia macrescens*, accordingly referred to it as *E. macrescens*$_{\text{irregular}}$. Also included in Plate 2 is an overview of individuals often found to be poorly preserved and likely reworked, some of which belonging to an extinct group of cretaceous species (planktonic taxa such as *Planoheterohelix* and *Hedbergella*). As a result, taxonomic identification up to species level often failed, leaving the corresponding individuals grouped by genera.

Plate 1

Ammoniidae, Bolivinitidae, Buliminellidae, Elphidiidae, Hauerinidae, Haynesinidae, Rosalinidae

---

1–4 ***Ammonia* spp.**
1: GeoHH-FK (65 cm; spiral view); 2–3: TB13-1 (surface; spiral view);
4: TB13-1 (surface; umbilical view)

5–6 ***Rosalina* sp.**
5: TB13-1 (surface; spiral view); 6: TB13-1 (surface; umbilical view)

7–8 ***Cribroelphidium selseyense*** (Heron-Allen and Earland, 1911)
7: GeoHH-FK (63 cm; side view); 8: TB13-1 (surface; side view)

9–10 ***Elphidium excavatum subsp. clavatum*** Cushman, 1930
9: GeoHH-FK (63 cm; side view); 10: TB13-1 (surface; side view)

11 ***Cribroelphidium incertum*** (Williamson, 1858)
TB13-1 (surface; side view)

12 ***Cribroelphidium gunteri*** (Cole, 1931)
TB13-1 (surface; side view)

13–15 ***Cribroelphidium williamsoni*** (Haynes, 1973)
13: TB13-1 (surface; side view); 14: GeoHH-FK (94 cm; side view);
15: GeoHH-FK (63 cm; side view)

16–17 ***Haynesina depressula*** (Walker and Jacob, 1798)
16: GeoHH-FK (63 cm; side view); 17: TB13-1 (surface; side view)

18–20 ***Haynesina germanica*** (Ehrenberg, 1840)
18: GeoHH-FK (96 cm; side view); 19–20: TB13-1 (surface; side view)

21–22 ***Bolivina variabilis*** (Williamson, 1858)
21: GeoHH-FK (95 cm; side view); 22: TB13-1 (surface; side view)

23–24 ***Buliminella elegantissima*** (d'Orbigny, 1839)
23: GeoHH-FK (65 cm; apertural view); 24: GeoHH-FK (101 cm; side view)

25 ***Quinqueloculina* sp.**
GeoHH-FK (113 cm; side view)

Plate 1

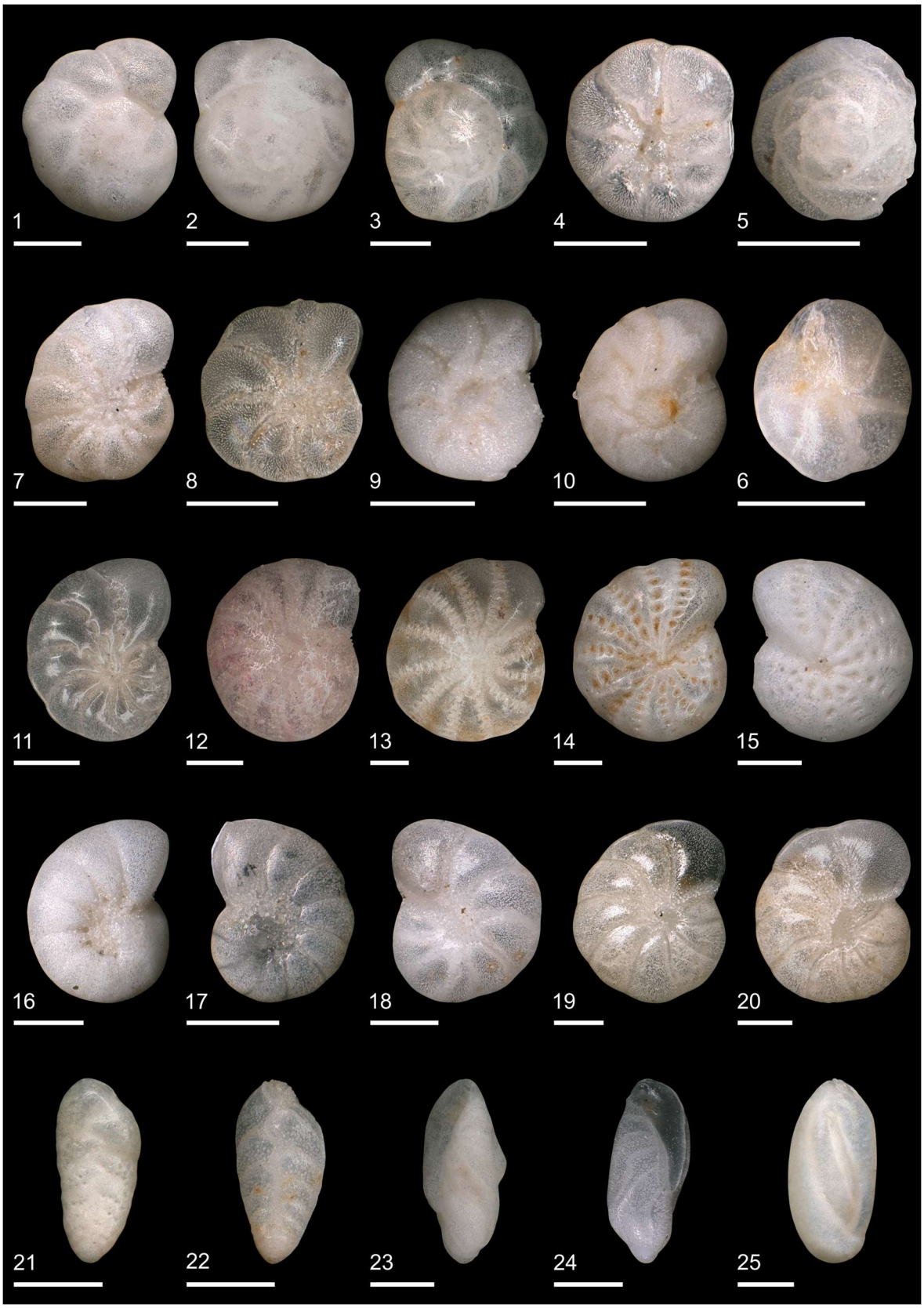

Scale bars = 100 µm

Plate 2

Buliminidae, Cibicididae, Hedbergellidae, Heterohelicidae, Miliamminidae, Trochamminidae, Uvigerinidae

---

1–2 ***Entzia macrescens*** (Brady, 1870)
1: TB13-1 (surface; spiral view); 2: TB13-1 (surface; umbilical view)

3–4 ***Trochammina inflata*** (Montagu, 1808)
3: GeoHH-FK (90 cm; spiral view); 4: GeoHH-FK (90 cm; umbilical view)

5–9 ***Entzia macrescens*$_{\text{irregular}}$**
5: GeoHH-FK (53 cm; spiral view); 6: GeoHH-FK (25 cm; spiral view);
7: GeoHH-FK (44 cm; spiral view); 8: GeoHH-FK (24 cm; spiral view);
9: GeoHH-FK (41 cm; undefined view)

10 ***Miliammina petila*** Saunders, 1958
GeoHH-GIE (112.5 cm; side view)

11 ***Miliammina fusca*** (Brady, 1870)
GeoHH-GIE (120 cm; side view)

12 ***Lepidodeuterammina ochracea*** (Williamson, 1858)
GeoHH-GIE (117.5 cm; spiral view)

13–14 ***Planoheterohelix* sp. †**
13: GeoHH-FK (95 cm; side view); 14: GeoHH-FK (96 cm; side view)

15–16 ***Hedbergella* sp. †**
15: GeoHH-FK (96 cm; umbilical view); 16: TB13-1 (surface; spiral view)

17–18 ***Bulimina* sp.**
17: GeoHH-GIE (85 cm; apertural view); 18: GeoHH-GIE (95 cm; apertural view)

19 ***Cibicides* sp.**
GeoHH-GIE (95 cm; spiral view)

20 ***Trifarina angulosa*** (Williamson, 1858)
GeoHH-GIE (105 cm; side view)

Plate 2

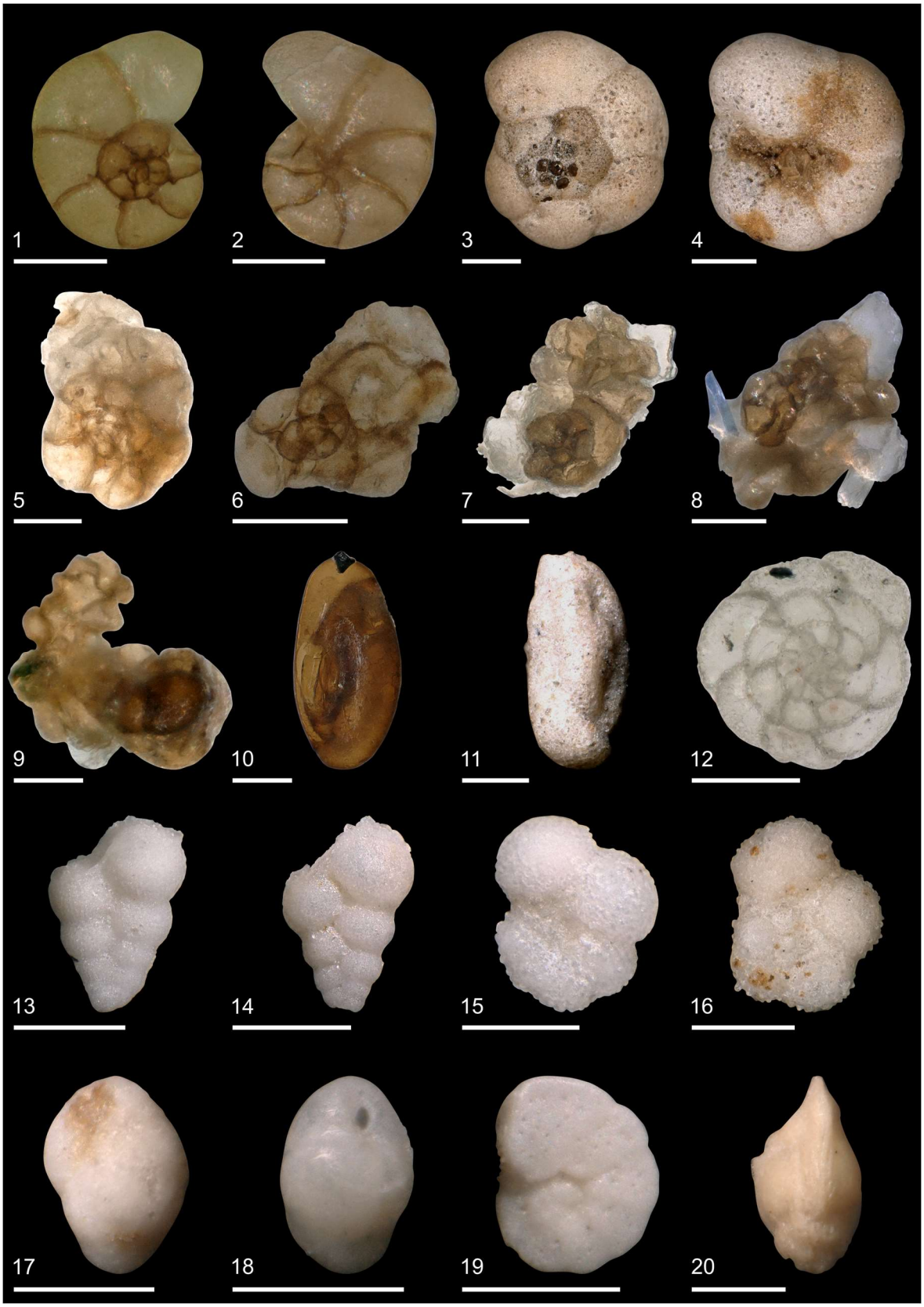

Scale bars = 100 µm

ACKNOWLEDGEMENTS

First and foremost, my most sincere thanks go to my Ph.D. supervisor Gerhard Schmiedl for his constant assistance and valuable support of my research over the last years. I am very grateful that he gave me the freedom to work independently and always encouraged my own ideas and goals in science. Many thanks also to Christian Betzler and Lars Kutzbach for co-supervision and fruitful discussions during the advisory panel meetings. Very special thanks go to Yvonne Milker for all the scientific and non-scientific assistance, many discussions, tough fieldwork projects and necessary sediment-sample preparation measures in the most unusual places. I would also like to acknowledge Gerhard Schmiedl, Sebastian Lindhorst, Christian Betzler, and Yvonne Milker (Universität Hamburg), as well as Uwe Mikolajewicz and Johann Jungclaus (MPI-M, Hamburg) for proposing and contributing to our very interesting and interdisciplinary SEASTORM project. In this context, I also want to acknowledge the German Research Foundation (DFG) for providing financial support through grants SCHM1180/19 and MI1508/4 as part of the Priority Program (SPP-1889). A big thank also to my SEASTORM-comrades Amalie Cordua and Andreas Lang for the positive company and support at meetings, workshops and conferences, and of course for the always good collaboration in our project. For the many lecture opportunities and scientific network, I would like to thank the School of Integrated Climate System Sciences (SICSS).

Furthermore, I would like to thank my former and current office mates J. Reolid, K. Müller-Navarra, M. Bartels, and F. Francescangeli for valuable coffee breaks, good conversations and the always good atmosphere. Special thanks also go to M. Sabino and P. Göllner, who always helped me with advice and company in the final phase of the Ph.D. Last but not least, I'm very grateful to the entire micropaleontological working group in Hamburg, specifically H. Campos, P. Kowalski, V. Kümmerer, M. Theodor, C. Sievers, and H.A. Winkelbauer, who always supported my fieldwork, sediment sampling, and laboratory analyses with their substantial help – thank you, guys! Finally, my sincere thanks go to B. Vennemann, M.C. Vallée, L. Schiebel, and J. Schuh for simply always believing in me.

EIDESSTATTLICHE VERSICHERUNG

Hiermit versichere ich an Eides statt, dass ich die vorliegende Dissertation mit dem Titel: *„North Sea salt marshes and their response to changing storm-climate conditions over the last century“* selbstständig verfasst und keine anderen als die angegebenen Hilfsmittel – insbesondere keine im Quellenverzeichnis nicht benannten Internet-Quellen – benutzt habe. Alle Stellen, die wörtlich oder sinngemäß aus Veröffentlichungen entnommen wurden, sind als solche kenntlich gemacht. Ich versichere weiterhin, dass ich die Dissertation oder Teile davon vorher weder im In- noch im Ausland in einem anderen Prüfungsverfahren eingereicht habe und die eingereichte schriftliche Fassung der auf dem elektronischen Speichermedium entspricht.

DECLARATION ON OATH

I hereby declare an oath that I have written the present dissertation on my own with the title: *"North Sea salt marshes and their response to changing storm-climate conditions over the last century"* and have not used other than the acknowledge resources and aids. All passages taken literally or analogously from other publications are identified as such. I further declare that this thesis has not been submitted to any other German or foreign examination board and that the submitted written version corresponds to that on the electronic repository.

Hamburg, 8 February 2021

Dorothea Bunzel

Gutachter:
Prof. Dr. Gerhard Schmiedl
Prof. Dr. Christian Betzler

Vorsitzender des Fachpromotionsausschusses:
Prof. Dr. Dirk Gajewski

Dekan der MIN-Fakultät:
Prof. Dr. Heinrich Graener